Imperial College London

Impacts of climate, CO_2 levels and human activity on the spatial distribution of global fire regimes

Olivia Michele Mira Haas

January 2024

Imperial College London

Department of Life Sciences

Submitted in part fulfilment of the requirements for the degree of

Doctor of Philosophy (PhD) of Imperial College London

Statement of Originality

The work presented in this thesis is original and is my own. When this is not the case, the authors are appropriately referenced, and the original sources are available in the bibliography. This thesis constitutes work which has been previously published in the following articles:

Haas, O., Prentice, I. C., and Harrison, S. P., Global environmental controls on wildfire burnt area, size, and intensity. *Environmental Research Letters* **17** 065004, https://doi.org/10.1088/1748-9326/ac6a69, (2022).

Haas, O., Prentice, I. C., and Harrison, S. P., The response of fire regimes to Last Glacial Maximum carbon dioxide and climate. *Biogeosciences* **20**, 3981–3995, https://doi.org/10.5194/bg-20-3981-2023, (2023).

It also contains work which has been recently submitted to *Science* under the title “Wildfires on a changing planet”.

Copyright Declaration

Acknowledgements

First and foremost, I would like to thank my supervisors Colin Prentice and Sandy P. Harrison. Their insights, guidance, and patience have been invaluable to this work and without their support and expertise this thesis would not have been possible. I must also thank Adriana Ford and Natalie Sanders for their continued guidance and support throughout this PhD.

I would also like to acknowledge my colleagues at the Leverhulme Wildfires Centre, some of whom have become dear friends.

My partner and best friend, Oisin Donnelly, has been a rock for me over past few years, and I could not be more grateful to him for his unconditional support to my childlike curiosity. I also must thank my parents who have continually championed and believed in me.

I am thankful for the financial support from the NERC Centre for Doctoral Training in Quantitative and Modelling Skills in Ecology and Evolution (QMEE) and from the Leverhulme Wildfires Centre.

Finally, this PhD thesis is dedicated to the hills and people of the Massif du petit Luberon. Watching those hills burn nearly twenty years ago inspired in me a curiosity for vegetation and fire which I have had the privilege to nurture and explore over the last few years. With every return, I cast a glance in their direction. As the rock and the vegetation reclaim their place, the stain of red fire retardant on those hills is now only visible to those who remember it was once there. And though the traces of that burnt have all but completely faded, my love for that land has just begun.

Abstract

Wildfires are fundamental to the distribution of vegetation on Earth. Wildfires vary in size, frequency, and intensity and are controlled by climate, vegetation, and human activity. A fire regime refers to the long-term, repeated patterns of wildfires under a given set of conditions. Shifts in global fire regimes in response to changing environmental conditions are a growing concern. Many global vegetation models include wildfire but struggle to predict fire properties beyond the first-order patterns of burnt area and disagree on its environmental responses and historical trends. This thesis develops robust empirical models of burnt area, fire size and a measure of intensity and uses them to explore the global sensitivity of fire regimes to changes in climate, atmospheric CO_2 and human activity. Simulation of fire regimes under the very different conditions of the Last Glacial Maximum predicts reduced fire activity consistent with evidence from sedimentary charcoal records, while allowing for the separation of CO_2 and climate change effects (both significant). Simulation of future fire regimes under low- and high-mitigation scenarios indicates a global shift in wildfire patterns by 2100 CE with burning reduced in tropical regions but larger and more intense wildfires in extra-tropical regions. Under low mitigation, increases in burnt area worldwide overwhelm the current human-driven declining trend, with fire size and intensity increasingly limited by dryness and vegetation fragmentation. These model experiments highlight the distinct controls of different fire properties. Whilst burnt area is driven by fuel availability and dryness, fire intensity is limited by fuel build-up, and fire size by fuel continuity. This decoupling occurs because of the different temporal and spatial scales on which the controls of burnt area, fire size and fire intensity operate. These findings have immediate implications for the improvement of process-based fire models, which currently do not take these distinctions into account.

Table of Contents

List of Figures and Tables

Figure 9. Latitudinal distribution of the LGM-MOD climate anomalies for MPI.ESM1.2 (orange), AWI-ESM1.2 (pink) and CESM1.2 (brown) for (a) the mean number of dry days, (b) the seasonality of dry days, (c) maximum monthly VPD, (d) maximum monthly DTR, (e) maximum monthly mean wind speeds, (f) mean monthly temperature and (g) mean monthly total precipitation. The zero-intercept line represents no change between LGM and MOD climate, with negative values representing lower values at the LGM and positive values representing higher values at the LGM.

Figure 10. Experiments for BA, FS and FI for MPI-ESM1.2 LGM scenario (MOD 395 ppm and LGM 185 ppm represent the realistic modern-day simulation and LGM simulation, whilst MOD 185 ppm and LGM 395 ppm represent the CO_2 and climate sensitivity experiments respectively. The ice is shown in grey). (The other experiments can be found in S3)

Figure 11. Boxplots showing relative importance of each predictor (GPP: gross primary production, GPP.s.: GPP seasonality, tree; tree cover, shrub; shrub cover, grass; grass cover, DD: dry days, DD.s.: dry days seasonality, VPD: vapour pressure deficit, DTR: diurnal temperature range, wind: wind speed) in driving the BA, FS or FI anomaly between the MOD 395 ppm and LGM 185 ppm experiment. For each grid cell common to both experiments (on modern-day continental shelves and masking the LGM ice sheets), the predictor which caused the largest change in the anomaly between the two experiments when it was excluded from the GLM model was retained, it is the change in anomaly that is shown here. This was taken as an indicator of relative importance of that predictor in driving the observed change for (a) the AWIESM1 LGM scenario, (b) the MPI-ESM-1.2 LGM scenario and (c) the CESM1.2 LGM scenario. A positive anomaly indicates the variable caused an increase in BA, FS or FI at the LGM and a negative anomaly indicates the variable caused a decrease in BA, FS or FI at the LGM.

Figure 12. Map showing selection of four variables (GPP in green, DD in red, VPD in orange and wind in grey) responsible for some of the most important grid-cell drivers in reducing BA, increasing FS and FI for (a) AWIESM1 LGM scenario, (b) MPI-ESM1.2 LGM scenario and (c) CESM1.2 LGM scenario. Maps of most important grid-cell drivers for all variables and all experiments can be found in S3.

Figure 13. Comparison of BA anomalies between the experiment outputs from the MPI-ESM1.2 LGM scenario with charcoal records from the Reading Palaeofire Database (RPD) for (a) the realistic LGM experiment (b) the LGM climate/MOD CO_2 sensitivity experiment and (c) the MOD climate/LGM CO_2 sensitivity experiment The modelled positive LGM-MOD anomalies are shown in red and LGM-MOD negative anomalies in blue. Dotted red (positive anomaly) and blue (negative anomaly) points show the location of the RPD records for the LGM. The LGM ice sheets are shown in dark blue.

Figure 14. Regions of change in burnt area (BA), fire size (FS) and fire intensity (FI) under the high mitigation scenario (left) and the low mitigation scenario (right). Regions where all three properties increase are shown in red, regions where all three properties decrease are shown in dark blue.

Figure 15. Percentage change in burnt area (BA), fire size (FS) and fire intensity (FI) per biome for (a) the high mitigation scenario and (b) the low mitigation scenario. See Supplementary Chapter 4 for more detail.

Figure 16. Predictors responsible for driving changes in burnt area (BA), fire size (FS) and fire intensity (FI) respectively of (a) the high mitigation scenario and (b) the low mitigation scenario. The top row shows predictors driving increases and the bottom row shows predictors driving decreases in the fire properties.

Figure 17. Importance of four switches for burnt area (BA), fire size (FS) and fire intensity (FI) for each statistical model (shown by t-values) with darker red being more important. White values are not significant at the significance threshold used. Fuel availability (gross primary production: GPP, GPP seasonality, tree, grass, shrub) and fuel continuity (cropland, road density, topography) are separated out here. The arrows above show whether changes in climate, CO_2-induced changes in vegetation or human activity influence the different drivers in simulations of the past and future.

Figure 18. Latitudinal distribution of normalized median FRP values derived from MCD14ML (Giglio et al., 2006) (red) and the intensity metric used in this analysis (blue). The asymmetry can be observed in the median FRP values between the latitudes 0-25°S (with a rapidly increasing slope) and 0-25°N (with a much flatter slope that only increases after 25°N.

Figure 19. Global distribution of observed median FRP values (in $W.km^{-2}$) (left) and the fire intensity metric used in this analysis (in $W.km^{-1}$) (right)

Figure 20. Percentage change in global total BA, median FS, and median FI between the modern, low mitigation 2100CE, high mitigation 2100CE and LGM experiments for the climate only sensitivity experiment.

Figure 21. Global distribution of modelled burnt area (BA) in km^2, fire size (FS) in km^2, and fire intensity (FI) in $W.km^{-1}$ for the original model (including human activity) (top) and for the sensitivity analysis in which all human predictors are set to zero (excluding human activity) (bottom)

Figure 22. Breakdown per biome of total annual burnt area (in km^2), mean fire size (in km^2) and mean fire intensity ($W.km^{-1}$) for the modelled values with and without human presence

Figure S1. Partials residual plots for burnt area, fire size and fire intensity as functions of (GPP) gross primary production, (GPP (s)) seasonality of GPP, (shrub) shrubland cover, (grass) grassland cover, (tree) tree cover, (roads) road density, (crop) cropland, (VRM) vector ruggedness measure, (TPI) topographic position index, (DD) dry days, (DD (s)) dry days seasonality, (VPD) vapour pressure deficit, (DTR) diurnal temperature range, (wind) wind speed, (popd) population density and (light) lightning ground-strikes . Green represents vegetation and land cover predictors; purple represents fragmentation predictors; red represents climate predictors; blue represents ignition source predictors.

Figure S2. Partial residual plots for burnt area, fire size and fire intensity as functions of (GPP) gross primary production, (GPP (s)) seasonality of GPP, (shrub) shrubland cover, (grass) grassland cover, (tree) tree cove (crop) cropland, (VRM) vector ruggedness measure, (TPI) topographic position index, (DD) dry days, (DD (s)) dry days seasonality, (VPD) vapour pressure deficit, (DTR) diurnal temperature range, (wind) wind speed, (popd) population density and (light) lightning ground-strikes . Green represents vegetation and land cover predictors; purple represents fragmentation predictors; red represents climate predictors; blue represents ignition source predictors.

Figure S3. Partial residual plots for burnt area, fire size and fire intensity as functions of (GPP) gross primary production, (GPP (s)) seasonality of GPP, (shrub) shrubland cover, (grass) grassland cover, (tree) tree cover, (roads) road density, (crop) cropland, (VRM) vector ruggedness measure, (TPI) topographic position index, (DD) dry days, (DD (s)) dry days seasonality, (VPD) vapour pressure deficit, (DTR) diurnal temperature range, (wind) wind speed, and (light) lightning ground-strikes . Green represents vegetation and land cover predictors; purple represents fragmentation predictors; red represents climate predictors; blue represents ignition source predictors.

Figure S4. Figure 1. Partial residual plots for burnt area, fire size and fire intensity as functions of (GPP) gross primary production, (GPP (s)) seasonality of GPP, (shrub) shrubland cover, (grass) grassland cover, (tree) tree cover, (crop) cropland, (VRM) vector ruggedness measure, (TPI) topographic position index, (DD) dry days, (DD (s)) dry days seasonality, (DTR) diurnal temperature range, (wind) wind speed, (popd) population density and (light) lightning ground-strikes . Green represents vegetation and land cover predictors; purple represents fragmentation predictors; red represents climate predictors; blue represents ignition source predictors.

Figure S5. Partial residual plots for burnt area, fire size and fire intensity as functions of (GPP) gross primary production, (shrub) shrubland cover, (grass) grassland cover, (tree) tree cover, (roads) road density, (crop) cropland, (VRM) vector ruggedness measure, (TPI) topographic position index, (DD) dry days, (DD (s)) dry days seasonality, (VPD) vapour pressure deficit, (DTR) diurnal temperature range, (wind) wind speed, (popd) population density and (light) lightning ground-strikes . Green represents vegetation and land cover predictors; purple represents fragmentation predictors; red represents climate predictors; blue represents ignition source predictors.

Figure S6. Histograms showing the distribution of the fitted values by the GLM BA model when observed BA values are 0 in the 2010-2015 climatology for (a) the whole range and (b) the range up to the 95^{th} percentile. The red line shows the median value, and the black lines show the 10^{th} and 90^{th} percentile values.

Figure S.7 Maps of BA ignition mask (where no burning is assumed to occur) under modern-day conditions (2010-2015 climatology) showing in red (a) where the observational BA values are 0 and (b) where the fitted BA values are equal or lower to 0.0011.

Figure S8. Changes in burnt area (BA), fire size (FS) and fire intensity (FI) using modern day climate (MOD) or Last Glacial Maximum (LGM) climate from the MPI-ESM1.2 simulation with either modern (395 ppm) or LGM (185 ppm) CO_2.

Figure S9. Changes in burnt area (BA), fire size (FS) and fire intensity (FI) using modern day climate (MOD) or Last Glacial Maximum (LGM) climate from the AWIESM1 simulation with either modern (395 ppm) or LGM (185 ppm) CO_2.

Figure S10. Changes in burnt area (BA), fire size (FS) and fire intensity (FI) using modern day climate (MOD) or Last Glacial Maximum (LGM) climate CESM1.2 simulation with either modern (395 ppm) or LGM (185 ppm) CO_2.

Figure S10. Changes in burnt area (BA), fire size (FS) and fire intensity (FI) using modern day climate (MOD) or Last Glacial Maximum (LGM) climate CESM1.2 simulation with either modern (395 ppm) or LGM (185 ppm) CO_2.

Figure S11. Map showing which model variable was responsible for some of the most important grid-cell changes between the realistic modern-day climate (MOD) 395 ppm experiment and the realistic Last Glacial Maximum (LGM) 190 ppm scenarios for BA, FS and FI for (a) the AWIESM1 LGM scenario, (b) the MPI-ESM1.2 LGM scenario and (c) the CESM1.2 LGM scenarios. Faded colors represent that the effect was a negative one, leading to a decrease in the wildfire property at the LGM whilst full colors represent an increase in the wildfire property at the LGM.

Figure S12. Map showing which model variable was responsible for some of the most important grid-cell changes between the MOD 395 ppm and LGM 395 ppm experiment (LGM climate/MOD CO_2) for BA, FS and FI for (a) the AWIESM1 LGM scenario, (b) the MPI-ESM1.2 LGM scenario and (c) the CESM1.2 LGM scenarios. Faded colors represent that the effect was a negative one, leading to a decrease in the wildfire property at the LGM whilst full colors represent an increase in the wildfire property at the LGM.

Figure S13. Boxplots showing relative importance of each predictor (GPP; gross primary production, GPP.s.; GPP seasonality, tree; tree cover, shrub; shrub cover, grass; grass cover, DD; dry days, DD.s.; dry days seasonality, VPD; vapour pressure deficit, DTR; diurnal temperature range, wind; wind speed) in driving the anomaly between the MOD 395 ppm and LGM 395 ppm experiment. For each grid cell common to both experiments (on modern-day continental shelves and masking the LGM ice sheets), the predictor which cause the largest change in the anomaly between the two experiments when it was excluded from the GLM model was retained, it is the change in anomaly that is shown here. This was taken as an indicator of relative importance of that predictor in driving the observed change for (a) the AWIESM1 LGM scenario, (b) the MPI-ESM-1.2 LGM scenario and (c) the CESM1.2 LGM scenario. A positive anomaly represents the variable driving an increase in BA, FS or FI at the LGM and a negative anomaly represents the variable driving a decrease in BA, FS or FI at the LGM.

Figure S14. Map showing which model variable was responsible for some of the most important grid-cell changes between the realistic MOD 395 ppm and MOD 190 ppm experiment (MOD climate/LGM CO_2) for BA, FS and FI for (a) the AWIESM1 LGM scenario, (b) the MPI-ESM1.2 LGM scenario and (c) the CESM1.2 LGM scenarios. Faded colors represent that the effect was a negative one, leading to a decrease in the wildfire property at the LGM whilst full colors represent an increase in the wildfire property at the LGM.

Figure S15. Boxplots showing relative importance of each predictor (GPP; gross primary production, GPP.s.; GPP seasonality, tree; tree cover, shrub; shrub cover, grass; grass cover, DD; dry days, DD.s.; dry days seasonality, VPD; vapour pressure deficit, DTR; diurnal temperature range, wind; wind speed) in driving the anomaly between the MOD 395 ppm and MOD 190 ppm experiment. For each grid cell common to both experiments (on modern-day continental shelves and masking the LGM ice sheets), the predictor which cause the largest change in the anomaly between the two experiments when it was excluded from the GLM model was retained, it is the change in anomaly that is shown here. This was taken as an indicator of relative importance of that predictor in driving the observed change for (a) the AWIESM1 LGM scenario, (b) the MPI-ESM-1.2 LGM scenario and (c) the CESM1.2 LGM scenario. A positive anomaly represents the variable driving an increase in BA, FS or FI at the LGM and a negative anomaly represents the variable driving a decrease in BA, FS or FI at the LGM.

Figure S16. Comparison of anomalies between the experiment outputs from the MPI-ESM1.2 LGM scenario with charcoal records from the Reading Palaeofire Database (RPD) for (a) the relatistic BA LGM experiment (b) the BA LGM climate/MOD CO_2 sensitivity experiment and (c) the BA MOD climate/LGM CO_2 sensitivity experiment (d) the relatistic FS LGM experiment (e) the FS LGM climate/MOD CO_2 sensitivity experiment and (f) the FS MOD, (g) the relatistic FI LGM experiment (h) the FI LGM climate/MOD CO_2 sensitivity experiment and (i) the FI MOD climate/LGM CO_2 sensitivity experiment climate/LGM CO_2 sensitivity experiment. The modeled positive LGM-MOD anomalies are shown in red and LGM-MOD negative anomalies in blue. Dotted red (positive anomaly) and blue (negative anomaly) points show the location of the RPD records for the LGM. The LGM ice sheets are shown in dark blue.

Figure S17. Comparison of anomalies between the experiment outputs from the AWIESM1 LGM scenario with charcoal records from the Reading Palaeofire Database (RPD) for (a) the relatistic BA LGM experiment (b) the BA LGM climate/MOD CO_2 sensitivity experiment and (c) the BA MOD climate/LGM CO_2 sensitivity experiment (d) the relatistic FS LGM experiment (e) the FS LGM climate/MOD CO_2 sensitivity experiment and (f) the FS MOD, (g) the relatistic FI LGM experiment (h) the FI LGM climate/MOD CO_2 sensitivity experiment and (i) the FI MOD climate/LGM CO_2 sensitivity experiment climate/LGM CO_2 sensitivity experiment. The modeled positive LGM-MOD anomalies are shown in red and LGM-MOD negative anomalies in blue. Dotted red (positive anomaly) and blue (negative anomaly) points show the location of the RPD records for the LGM. The LGM ice sheets are shown in dark blue.

Figure S18. Comparison of anomalies between the experiment outputs from the CESM1.2 LGM scenario with charcoal records from the Reading Palaeofire Database (RPD) for (a) the relatistic BA LGM experiment (b) the BA LGM climate/MOD CO_2 sensitivity experiment and (c) the BA MOD climate/LGM CO_2 sensitivity experiment (d) the relatistic FS LGM experiment (e) the FS LGM climate/MOD CO_2 sensitivity experiment and (f) the FS MOD, (g) the relatistic FI LGM experiment (h) the FI LGM climate/MOD CO_2 sensitivity experiment and (i) the FI MOD climate/LGM CO_2 sensitivity experiment climate/LGM CO_2 sensitivity experiment. The modeled positive LGM-MOD anomalies are shown in red and LGM-MOD negative anomalies in blue. Dotted red (positive anomaly) and blue (negative anomaly) points show the location of the RPD records for the LGM. The LGM ice sheets are shown in dark blue.

Figure S19. Global 10-year trend in burnt area (BA) from 2006-2015 in Mha from the model (red), GFED4(s) (light green) and GFED5 (dark green).

Figure S20. Global 10-year trend in burnt area (BA) for the (A) northern hemisphere, (B) southern hemisphere, (C) above 60°N, (D) Africa, (E) northern hemisphere America and (F) southern hemisphere America from the model (in red), GFED4(s) (in light green) and GFED5 (in dark green)

Figure S21. Anomalies for burnt area (BA), fire size (FS) and fire intensity (FI) between the modern-day experiment and the high mitigation experiment (top) and low mitigation experiment (bottom) for the mean of the experiments driven by the outputs of all four climate models in which CO_2 levels are 424ppm and 651ppm respectively and human activity follows a SSP2 trajectory. Red represents an increase in the fire property by the end of the century and blue represents a decrease.

Figure S22. Percentage change for all three fire properties between realistic modern-day conditions and the realistic future experiments broken down by biome type. The mean is across all four of the climate model experiments for each scenario.

Figure S23. Map showing which GLM model variable was responsible for the most important grid-cell changes between the realistic modern-day experiment and the realistic future high mitigation (left) and low mitigation (right) experiment for the GFDL-ESM2M climate model outputs. Muted colours show that the effect was negative, leading to a decrease in the wildfire property at under future conditions, whilst full colours represent an increase in the wildfire property under future conditions.

Figure S24. Map showing which GLM model variable was responsible for the most important grid-cell changes between the realistic modern-day experiment and realistic future high mitigation (left) and low mitigation (right) experiments for the IPSL-CM5A-LR climate model outputs. Muted colours show that the effect was negative, leading to a decrease in the wildfire property at under future conditions, whilst full colours represent an increase in the wildfire property under future conditions.

Figure S25. Map showing which GLM model variable was responsible for the most important grid-cell changes between the realistic modern-day experiment realistic future high mitigation (left) and low mitigation (right) experiment for the HadGEM2-ES climate model outputs. Muted colours show that the effect was negative, leading to a decrease in the wildfire property at under future conditions, whilst full colours represent an increase in the wildfire property under future conditions.

Figure S26. Map showing which GLM model variable was responsible for the most important grid-cell changes between the realistic modern-day experiment realistic future high mitigation (left) and low mitigation (right) experiment for the MIROC5 climate model outputs. Muted colours show that the effect was negative, leading to a decrease in the wildfire property at under future conditions, whilst full colours represent an increase in the wildfire property under future conditions.

Figure S27. Regions of change in burnt area (BA), fire size (FS) and fire intensity (FI) under the high mitigation scenario (left) and the low mitigation scenario (right) where CO_2 levels and human activity were held constant. Regions where all three properties increase are shown in red, regions where all three properties decrease are shown in dark blue.

Figure S28. Anomalies for burnt area (BA), fire size (FS) and fire intensity (FI) between the modern-day experiment and the high mitigation experiment (top) and low mitigation experiment (bottom) for the mean of the experiments driven by the outputs of all four climate models in which CO_2 levels are held constant at 395ppm and human activity is held constant at the 2010-2015 baseline. Red represents an increase in the fire property by the end of the century and blue represents a decrease.

Figure S29. Percentage change for all three fire properties between realistic modern-day conditions and the climate only future experiments broken down by biome type. The mean is taken across all four climate-model experiments for each scenario.

Figure S30. Regions of change in burnt area (BA), fire size (FS) and fire intensity (FI) under the high mitigation scenario (left) and the low mitigation scenario (right) where climate and human activity were held constant. Regions where all three properties increase are shown in red, regions where all three properties decrease are shown in dark blue.

Figure S31. Anomalies for burnt area (BA), fire size (FS) and fire intensity (FI) between the modern-day experiment and the high mitigation experiment (top) and low mitigation experiment (bottom) for the mean of the experiments driven by the outputs of all four climate models in which CO_2 levels are 424ppm and 651ppm respectively and climate human activity are held constant at the 2010-2015 baseline. Red represents an increase in the fire property by the end of the century and blue represents a decrease.

Figure S32. Percentage change for all three fire properties between realistic modern-day conditions and the CO_2 only future experiments broken down by biome type. The mean is taken across all four climate-model experiments for each scenario.

Figure S33. Regions of change in burnt area (BA), fire size (FS) and fire intensity (FI) under the high mitigation scenario (left) and the low mitigation scenario (right) where human activity were held constant. Regions where all three properties increase are shown in red, regions where all three properties decrease are shown in dark blue.

Figure S34. Anomalies for burnt area (BA), fire size (FS) and fire intensity (FI) between the modern-day experiment and the high mitigation experiment (top) and low mitigation experiment (bottom) for the mean of the experiments driven by the outputs of all four climate models in which

CO_2 levels are 424ppm and 651ppm respectively and human activity are held constant at the 2010-2015 baseline. Red represents an increase in the fire property by the end of the century and blue represents a decrease.

Figure S35. Percentage change for all three fire properties between realistic modern-day conditions and the climate and CO_2 only future experiments broken down by biome type. The mean is taken across all four climate-model experiments for each scenario.

Figure S36. Regions of change in burnt area (BA), fire size (FS) and fire intensity (FI) under the high mitigation scenario (left) and the low mitigation scenario (right) where climate and CO_2 were held constant. Regions where all three properties increase are shown in red, regions where all three properties decrease are shown in dark blue.

Figure S37. Anomalies for burnt area (BA), fire size (FS) and fire intensity (FI) between the modern-day experiment and the high mitigation experiment (top) and low mitigation experiment (bottom) for the mean of the experiments driven by the outputs of all four climate models in which only human activity changes (SSP2 scenario) and in which climate and CO_2 levels are held constant at the 2010-2015 baseline. Red represents an increase in the fire property by the end of the century and blue represents a decrease.

Figure S38. Percentage change for all three fire properties between realistic modern-day conditions and the human activity only future experiments broken down by biome type. The mean is taken across all four climate-model experiments for each scenario.

s**Table 1.** Summary of the models included in the first FireMIP phase

Table 2. Summary of the remotely sensed satellite products available

Table 3. Summary of predictor and fire response variables

Table 4. Summary statistics with regression coefficients, *t*-values, and variance inflation factors (VIF) for each of the final models. Predictors included were all significant at $t > 4.5$ ($p < 10^{-5}$).

Table 5. Total annual gross primary production (GPP) (in PgC) estimates for each scenario.

Table 6. Comparison of signs in BA anomalies (between the MOD climate/MOD CO_2 experiment and other three experiments respectively) at the location of each RDP charcoal-based reconstruction record. A positive anomaly represents increased biomass burning, and a negative anomaly represents decreased biomass burning. Successful identification means that the sign of the experiment anomaly and the sign of the RPD charcoal-based reconstructions are the same.

Table 7. Summary of modern and future realistic experiments and the associated counterfactual tests. Additional information on the source and availability of the data for each experiment can be found in the Supplementary Chapter 4 Materials.

Table 8. Total burnt area per biome under modern, high, and low mitigation scenarios

Table S1. Inputs used for the calculation of GPP in the p-model (Wang et al., 2017; Stocker et al., 2020)

Table S2. Summary table of results of for all three models when all predictors are included with regression coefficients (where *** ($p<0.001$), ** ($p<0.01$), * ($p<0.05$),**.** ($p<0.1$) and results in brackets represent ($p\geq0.05$)), t-values and variance inflation factors (VIF).

Table S3 Summary table of results of for all three models when all predictors are included with regression coefficients (where *** ($p<0.001$), ** ($p<0.01$), * ($p<0.05$). ($p<0.1$) and results in brackets represent ($p\geq0.05$)), t-values and variance inflation factors (VIF).

Table S4 Summary table of results of for all three models when all predictors are included with regression coefficients (where *** ($p<0.001$), ** ($p<0.01$), * ($p<0.05$)**.** ($p<0.1$) and results in brackets represent ($p\geq0.05$)), t-values and variance inflation factors (VIF).

Table S5 Summary table of results of for all three models when all predictors are included with regression coefficients (where *** ($p<0.001$), ** ($p<0.01$), * ($p<0.05$). ($p<0.1$) and results in brackets represent ($p\geq0.05$)), t-values and variance inflation factors (VIF).

Table S6. Summary table of results of for all three models when all predictors are included with regression coefficients (where *** ($p<0.001$), ** ($p<0.01$), * ($p<0.05$). ($p<0.1$) and results in brackets represent ($p\geq0.05$)), t-values and variance inflation factors (VIF).

Table S7. Statistics for the fitted BA distribution when observed BA is 0 for the 2010-2015 climatology.

Table S8. Comparison of sign in BA anomalies (between the MOD climate/MOD CO_2 experiment and other three experiments respectively) at the location of each RDP (Harrison et al., 2022) charcoal-based reconstructions record. A positive anomaly represents increased biomass burning, and a negative anomaly represents decreased biomass burning. Successful identification means that the sign of the experiment anomaly and the sign of the RPD charcoal-based reconstructions are the same.

Table S9. Comparison of sign in FS anomalies (between the MOD climate/MOD CO_2 experiment and other three experiments respectively) at the location of each RDP (Harrison et al., 2022) charcoal-based reconstructions record. A positive anomaly represents increased biomass burning, and a negative anomaly represents decreased biomass burning. Successful identification means that the sign of the experiment anomaly and the sign of the RPD charcoal-based reconstructions are the same.

Table S10. Comparison of sign in FI anomalies (between the MOD climate/MOD CO_2 experiment and other three experiments respectively) at the location of each RDP (Harrison et al., 2022) charcoal-based reconstructions record. A positive anomaly represents increased biomass burning, and a negative anomaly represents decreased biomass burning. Successful identification means that the sign of the experiment anomaly and the sign of the RPD charcoal-based reconstructions are the same.

Table S11. Burnt area correlations and benchmarking scores of modelled burnt area and the global fire models included in the first Fire Modeling Intercomparaison Project (FireMIP) compared to GFED4(s) and GFED5. The normalized mean error (NME) scores for the spatial patterns (Kelley et al., 2013; Hantson et al., 2020) are for the overlapping period (2006-2013). A perfect score is 0, and a score below 1 is better than the mean model. The mean value and the range (in brackets) are given for the FireMIP models.

Table S12. Global annual burnt area (BA), mean fire size (FS) and mean fire intensity (FI) values for the realistic experiments.

Table S13. Global for annual burnt area (BA), mean fire size (FS) and mean fire intensity (FI) values for the climate only experiments.

Table S14. Global annual burnt area (BA), mean fire size (FS) and mean fire intensity (FI) values for the CO_2 only experiments.

Table S15. Global annual burnt area (BA), mean fire size (FS) and mean fire intensity (FI) values for the climate and CO_2 only experiments.

List of Acronyms

BA	Burnt Area
FS	Fire Size
FI	Fire Intensity
FRP	Fire Radiative Power
DD	Dry Days
DTR	Diurnal Temperature Range
VPD	Vapor Pressure Deficit
GPP	Gross Primary Production
fAPAR	Fraction of absorbed photosynthetically active radiation
ppfd	Photosynthetic Photon Flux Density
huss	Specific Humidity
cld	Fractional Cloud Cover
rsds	Downward Shortwave Radiation
GFED	Global Fire Emissions Database
GRIP	Global Roads Inventory Project
RPD	Reading Palaeofire Database
VIIRS	Visible Infrared Imaging Radiometer Suite
MODIS	Moderate-Resolution Imaging Spectroradiometer
ESA	European Space Agency
GPWG	Global Palaeofire Working Group
CMIP	Coupled Model Intercomparison Project
ISIMIP	Inter Sectoral Impact Model Intercomparison Project
FireMIP	Fire Model Intercomparison Project
PMIP	Palaeoclimate Modelling Intercomparison Project
DGVM	Dynamic Global Vegetation Model
IBIS	Integrated Biosphere Simulator
LPX	Land Processes and eXchanges
LPJ-GUESS	Lund-Potsdam-Jena General Ecosystem Simulator

JULES	Joint UK Land Environment Simulator
MPI-ESM1.2	Max Planck Institute for Meteorology Earth System Model version 1.2
AWI-ESM1.2	AWI Earth System Model version 1.2
CESM1.2	Community Earth System Model version 1.2
Glob-FIRM	Fire module Global FIRe Model
INFERNO	INteractive Fire and Emission algoRithm for Natural envirOnments
SMIFIRE-BLAZE	SIMple FIRE model, Blaze-Induced Land-Atmosphere Flux Estimator
Reg-FIRM	The Regional Fire Model
SPITFIRE	SPread and InTensity of FIRE
CLM	Community Land Model
CTEM	Canadian Terrestrial Ecosystem Model
GFDL-ESM2M	Geophysical Fluid Dynamics Laboratory Earth System Model
HadGEM2-ES	Met Office Hadley Centre Earth System Model
IPSL-CM5A-LR	Institut Pierre Simon Laplace Earth System Model
MIROC5	Model for Interdisciplinary Research On Climate
PFT	Plant Functional Type
GLM	Generalized Linear Model
NME	Normalized Mean Error
RoS	Rate of Spread
PI	Pre-industrial
LGM	Last Glacial Maximum
MOD	Modern
SSP	Shared Socioeconomic Pathways
RCP	Representative Concentration Pathway

Code availability

The work in this thesis relied heavily on computer code. The code and data for each chapter can be found in the following *figshare* projects:

Chapter 2: https://figshare.com/account/home#/projects/131081

Chapter 3: https://figshare.com/account/home#/projects/162328

Chapter 4: https://figshare.com/account/home#/projects/188589

All analysis for this thesis was conducted in R using the raster, stats, car, benchmarkMetrics, visreg, caret, lubricate, ggplot2, reshape2, formattable, GeoInterpolation and tidyverse packages.

Chapter 1: Introduction and literature review

Wildfires have gained significant attention in the recent decades both in academic and larger societal settings. Whilst fundamental to the distribution of vegetation on Earth (Bond et al., 2005; Pausas & Keeley, 2009; Harrison et al., 2010; Pausas & Ribeiro, 2017; Mucina, 2019) they can also be a destructive force and the response of wildfires to changing climate and land cover is a growing concern (Pausas and Keeley et al., 2021; Jones et al., 2022; UNEP, 2022). Different properties of wildfires, such as size or intensity, also influence the impact of a given wildfire, notably on vegetation and people. Wildfires are explicitly included in many global vegetation models. However, the formulation of these models varies greatly in complexity, and they struggle to predict the dynamics of wildfires beyond the broad geographic and temporal patterns of burnt area (Hantson et al., 2016; Hantson et al., 2020). As such, there is a pressing need to provide better tools to address the growing concern of wildfire regimes in a changing climate.

Wildfires are controlled by vegetation, climate, and human activity (Rabin et al., 2017) and there is a growing understanding of how these factors influence wildfires at a global scale (Bistinas et al., 2014; Knorr et al., 2014; Forkel et al., 2019a, Forkel et al., 2019b; Kelley et al., 2019). However, a lot of this knowledge, specifically related to vegetation and human activity has not made its way into global fire models (Forkel et al., 2019a). As such, many of these models do not capture the underlying properties controlling burning on Earth adequately (Forkel et al., 2019a). The sensitivity of these wildfire models to changing conditions also vary greatly (Teckentrup et al., 2019) which means there is large uncertainty as to how wildfires will respond to changing climate, vegetation, and human activity. Although vegetation is a key driver of wildfires, there has been little consideration of how the impact of changing atmospheric CO_2 levels on vegetation productivity and hence fuel loads will influence wildfires. It is not just the increasing wildfire frequency, but also increasing size and intensity in some regions has led to renewed concern over future trajectories (e.g. Mueller et al., 2019; Abatzoglou et al., 2019; Duane et al 2021; Mansoor et al., 2022; Jones et al., 2022). Nevertheless, there is also limited knowledge of global controls of distinct aspects of wildfires, such as wildfire size or intensity on a global scale (Forkel et al., 2019a; Hantson et al., 2020). Developing a better understanding of how climate, vegetation and human activities influence different fire properties, and using this understanding to create better fire models, is a research priority.

This thesis aims to make use of newly available datasets and vegetation models to develop empirical models of different fire properties, including burnt area, individual fire size and fire intensity and then to use these models to study the sensitivity of distinct aspects of global fire regimes to changes in climate, atmospheric CO_2 levels and human activity. In this first chapter, I review the current understanding of fire regimes on Earth drawing attention to a focus on burnt area, which has resulted in modelling efforts that struggle to reproduce other fire properties. I discuss the opportunities offered by other datasets to go beyond modelling burnt area. I then turn my attention to model validation and show that evidence from the past can provide tools in which to build more robust models for the future. I highlight ways in which we can also make use of the past to explore the sensitivity of different fire regimes to changing conditions. Finally, I present a coupled biogeography biogeochemistry model and a first-principle, vegetation model which provide a way to decouple the effect of changes in climate from the effect changes in CO_2 on vegetation. As such, this review is broken into the following sections: (a) Fire regimes as a fundamental component of the Earth System (b) Wildfire controls: A focus on burnt area, (c) Wildfire controls: Moving beyond burnt area, (d) Current global wildfire modelling efforts, (e) Mapping global wildfire regimes, (f) Global change and fire regimes: evidence from the past, (g)

Global change and fire regimes: looking to the future and (h) Sensitivity analysis as a tool to explore the impact of changing conditions on fire regimes. Following this review, I present the three research questions which motivate my thesis. These research questions are addressed in following three chapters, which are based on two published (Chapter 2 and Chapter 3) and one submitted paper (Chapter 4). The closing chapter (Chapter 5) provides a discussion of my findings, their limitations and future research directions.

Fire regimes as a fundamental component of the Earth System

There is no single interpretation of the term wildfire, with varying definitions offered both within and between disciplines (Tedim and Leone, 2020). In this thesis, a wildfire refers to the unplanned, free burning of vegetation caused by an ignition source, which could be natural or anthropogenic. Fossil records show that wildfires appeared on Earth soon after the establishment of terrestrial plants, around 420 million years ago (Scott et al., 2006; Harrison et al., 2010). Today, they occur on all continents except Antarctica, with around 4-6% of global vegetated area on Earth burning each year (Giglio et al., 2013; Van Der Werf et al., 2017; Chen et al., 2023). Though most ecosystems have conditions favourable to wildfires at some point in the year, wildfire properties differ greatly across ecosystems, offering a rich variety of burning patterns on Earth (Archibald et al., 2013). As such, wildfires are viewed as a fundamental ecological control of global vegetation composition and distribution with a long ecological history (Bond et al., 2005; Pausas and Keeley, 2009; Bowman et al., 2009; Harrison et al., 2010; He et al., 2019; McLauchlan et al., 2020; Harrison et al., 2021). The recognition of the key role of wildfires by ecologists has led to a recent paradigm shift, with fire managers as well as general society increasingly moving away from wildfires being viewed as a solely destructive force to a fundamental ecological one (Pausas and Keeley, 2023).

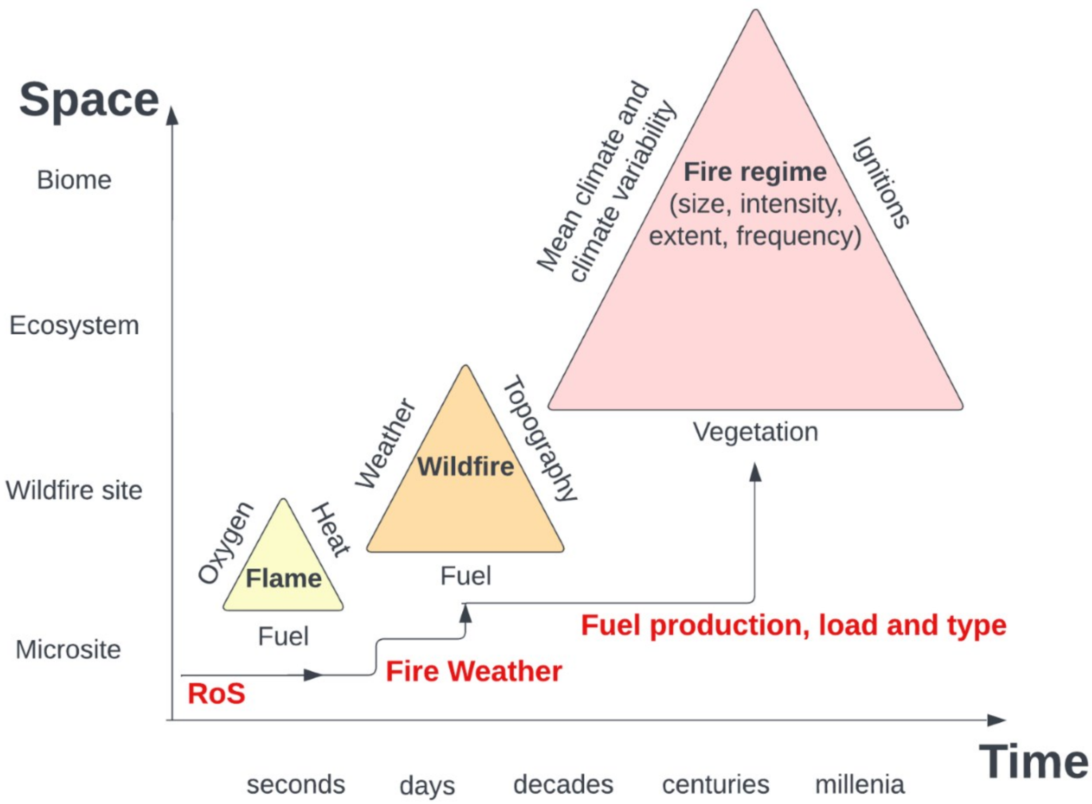

Figure 1. Controls influencing wildfires on different temporal and spatial scales based on the 'fire triangle' (Countryman et al., 1972; Pyne et al., 1996) and adapted from Moritz et al. (2005). Arrows have been added below the triangles to represent the different ways in which the controls of fire spread are conceptualized (and modelled) on different scales.

A fire regime can be understood as the long-term, repeated patterns, and properties of wildfires under specific spatial and temporal conditions (Lavorel et al., 2007; Archibald et al., 2018). However, as exemplified by Krebs et al. (2010), the way in which the term fire regime is employed varies in complexity. Its definition can encompass everything from the "spatial-temporal unit in the fire distribution" to describing single binary variables such as the presence or not of wildfires, depending on the availability of information (Krebs et al., 2010). Commonly cited properties of fire regimes are fire size, seasonality, intensity, extent, and frequency (Harrison et al., 2010; Krebs et al., 2010; Archibald et al., 2018). It has been suggested that established fire regimes, known as “pyromes,” act as a key global control of vegetation (Archibald et al., 2013). Some ecosystems rely on frequent wildfires for the establishment of dominant plant-types, whilst others can only support infrequent burning (Archibald et al., 2013; Archibald et al., 2018; Harrison et al., 2021; Foster et al., 2018; Simpson et al., 2021; Shen et al., 2023). For example, feedback between fire and the C_4 grasses allows for the maintenance of savanna ecosystems, which are the most frequently burnt ecosystem in the world (Beerling and Osborne, 2006). C_4 grasses utilize a different photosynthetic pathway to C_3 grasses and has a competitive advantage over the latter under low CO_2 conditions, high temperatures and water deficit conditions. This gives it an advantage in post-fire conditions due to its ability to accumulate fuel fast due to higher photosynthetic capacity and water-use efficiency (Edwards et al., 2010). Fire occurrence prevents the encroachment of trees which in turn favours the establishment of flammable C_4 grasses (Bond et al., 2005; Keeley and Rundel, 2005). Furthermore, the same fire regime can be found in different biomes and different fire regimes within the same biome (Archibald et al., 2018). An example of this is the boreal forests in North America and Eurasia, where crown fires, which spread through the tree canopies, and surface fires, which spread along the surface below the canopy, are respectively dominant. This is a factor that is thought to be due in part to differences in dominant tree species and plant traits (Wooster & Zhang, 2004; Wirth, 2005; Sitnov & Mokhov, 2018). For example, in North America the dominance of black spruce *(Picea mariana)* contributes to crown fires whereas in Eurasia, established Scots Pine *(Pinus Sylvestris)* and larch drive ground fires (Rogers et al., 2015).

Multiple plant traits can be considered adaptations to particular fire regimes (Kelley and Pausas, 2011; Kelley and Pausas, 2022). North American conifers have thick bark which protects them from damage during low-intensity surface fire whereas in higher latitudes, trees exposed to infrequent, high-intensity stand-replacing fires have thin bark but serotinous cones (Pausas, 2015; Pausas, 2017; Lamont et al., 2020). Serotiny and resprouting capacities after fire are also common plant traits found in fire prone regions, such as the Mediterranean (Keeley et al., 2011; Enright et al., 2014; Lamont et al., 2020). These traits are not adaptations to fire, but rather reflects the established fire regime, as they favour survival under specific fire conditions (Keeley et al., 2011; Harrison et al., 2021; Lamont et al., 2022). The established fire regime in a particular location influences long-term vegetation distribution and traits, and these traits enable the persistence of that same fire regime in that location (Archibald et al., 2018; Foster et al., 2018; Lamont et al., 2022).

Wildfire controls: A focus on burnt area

Wildfires on EEarth are controlled and maintained by interactions between climate, vegetation, and human activity (Bowman et al., 2009; Harrison et al., 2010; Bowman et al., 2011). At a global scale, the most studied wildfire property is fractional burnt area (BA), which represents the fractional amount of burnt vegetation in a given area over a given period and is often used to represent wildfire occurrence. The global controls of burnt area are relatively well understood compared to other wildfire properties (e.g. Bistinas et al., 2013; Bistinas et al., 2014; Knorr et al., 2014; Forkel et al., 2019a; Forkel et al., 2019b; Kuhn-Régnier et al., 2021). The "four switches" framework is a useful way of conceptualizing the controls of burnt area. Four conditions must be met for an ignition and a resulting wildfire to occur. There must be sufficient fuel; it must be dry and therefore flammable; weather conditions must be suitable (fire weather); and there must be an ignition source (Bradstock, 2010). Only when all four switches are "on" can an ignition and a wildfire occur. Climate, vegetation, and human activity have the potential to influence each of these four switches independently and through their interactions.

Climate affects burnt area on multiple time scales. On longer timescales (months to years), temperature and precipitation influence the distribution of burnt area through their control on vegetation productivity and type, which controls the availability and continuity of fuels (e.g. Falk et al., 2007). On shorter timescales (days to hours), in addition to temperature and precipitation, other climatic variables such as wind speed and atmospheric moisture affect the flammability of fuels and the probability of fire spread. Combinations of these climate conditions favourable to fire ignition and spread are known as fire weather, with indexes such as the Canadian Fire Weather Index (FWI) or the hot-dry-windy index used by many practitioners to determine the risk of wildfire occurrence on a given day (van Wagner et al., 1974; Stocks et al., 1989; Srock et al., 2018). Whilst there is a lot of focus on fire weather as a driver of current and future wildfire activity globally (e.g. Field et al., 2015; Abatzoglou et al., 2019; Vitolo et al., 2019) vegetation also controls the distribution of burnt area, independently and through its interaction with climate.

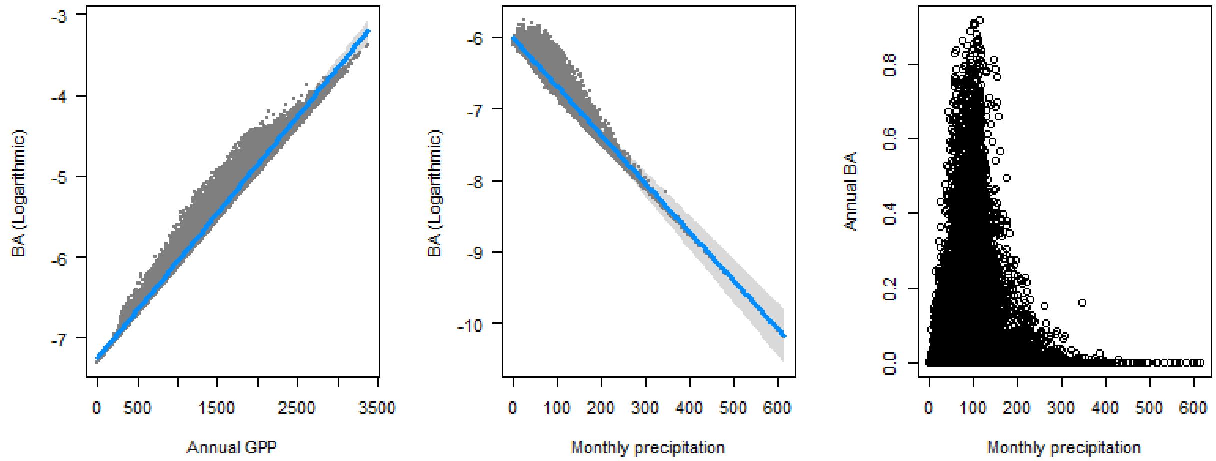

Figure 2. These plots were produced using climate data from the WFDE5 ERA5 dataset (Cucchi et al., 2020), GPP outputs are from the p model (Wang et al., 2017; Stocker et al., 2020) burnt area data from GFED4 (Randerson et al., 2018). A generalized linear model was fitted between GPP, precipitation and BA and the plots above are the resulting underlying and emergent relationships. On the left, the monotonically positive partial residual relationship fitted between annual GPP (annual mean from 2010-2015) and BA (annual mean from 2010-2015) when precipitation is held constant, in the middle the monotonically negative partial residual relationship fitted between monthly precipitation (monthly mean from 2010-2015) and BA when GPP is held constant, and on the right emergent relationship between monthly precipitation and BA.

A key emergent property from these vegetation-climate interactions is the humped relationship between burnt area and precipitation. This emergent relationship can be explained by the underlying relationships between burnt area, primary production, and precipitation respectively (Bistinas et al., 2014). The relationship between burnt and primary production can be explained in its simplest form as a positive linear relationship, with increasing primary production promoting fuel availability and thus likelihood of burning. On the other hand, precipitation has a negative linear relationship with burnt area, as increased moisture decreases fuel dryness and thus the likelihood of burning. The spatial interaction of these two linear relationships with burnt area leads to the emergent humped relationship with precipitation and burnt area to be highest at intermediate levels of productivity (van der Werf et al., 2008; Harrison et al., 2010; Prentice et al., 2011; Pausas and Ribeiro, 2013; Bistinas et al., 2014). It also causes two domains to emerge: regions in which burnt area is fuel-limited and regions in which it is aridity-limited. In very dry environments fuel is limited and more discontinuous preventing ignition and spread. In very wet environments on the other hand, fuel is abundant but too wet to burn (Harrison et al., 2010; Boer et al., 2021). In fuel-limited regions, burnt area has been shown to be sensitive to antecedent vegetation conditions responsible for the build-up of fuel, whilst in moisture-limited regions the current weather conditions which cause fuel drying are more important (e.g. Kuhn-Régnier et al., 2021).

Though vegetation availability and type are controlled by climate, they are also influenced by independent factors such as atmospheric CO_2 concentrations. CO_2 acts as a substrate for photosynthesis (Farquhar et al., 1982). Changes in the concentration of atmospheric CO_2 directly affect photosynthesis, with rising levels enhancing photosynthesis through the 'CO_2 fertilization effect' (Ruehr et al., 2023). As such, atmospheric CO_2 levels play an indirect role on global wildfire activity through its effect on vegetation productivity and load (Martin Calvo et al., 2014; Knorr et al., 2016). Studies have shown that reduced atmospheric CO_2 levels may have been in part responsible for reduced burning activity in the geologic past, for example at the Last Glacial Maximum, ca 21,000 years ago (Martin Calvo et al., 2014; Martin Calvo et al., 2015; Sato et al., 2021). However, it is difficult to disentangle the effect of changes in CO_2 on wildfires from that of climate from observations alone due the fact both affect vegetation and are temporally correlated. There has been limited research exploring the impact of changes in CO_2 on fire regimes, though it has been suggested as an area of future research (Hantson et al., 2020)

In addition to climate and vegetation, human activity also affects burnt area. Capturing the underlying relationships between human activity and burnt area on a global scale has proved difficult, and the sensitivity of wildfires to human activity is a heavily debated topic (Pechony and

Shindell, 2010; Scott et al., 2016; Riley et al., 2019; Bowman et al., 2020; Harrison et al., 2021). This challenge is in part due to a prevailing but erroneous perception that humans are responsible for increasing wildfire ignitions on Earth (Santin and Doerr, 2016). There is a wide range of reasons for human-ignited fires, ranging from deliberate ignitions for crop preparation and residue burning, vegetation clearance or pasture management for example, to accidental ignitions (Millington et al., 2022). An emergent humped relationship between population density and burnt area has been observed and explained by the interaction of a positive relationship between population density and fire ignition (dominant under low population densities) and a negative relationship between population density and fire spread (dominant under high population densities) (Pechony and Shindell, 2010; Lasslop and Kloster, 2017). However, empirical studies (e.g. Bistinas et al., 2014; Knorr et al., 2014; 2016) have shown that globally, the relationship between burnt area and population density is negative when accounting for climate and vegetation. In addition, analysis of past fire regimes through sedimentary charcoal records and ice cores (Marlon et al., 2008; Marlon et al., 2013; Harrison et al 2010, Wang et al., 2010; Power et al., 2008; Calder et al., 2019; Marlon, 2020) show no universal trend of increasing wildfire activity with increasing human population, with a period of high wildfire activity in the pre-industrial era, attributed to land clearance for agriculture especially in North America, followed by decreasing fire activity with increasing population during the 20th century (Marlon et al., 2008). The shape of the emergent relationship can also be explained through interactions with climate and vegetation: low vegetation productivity due to dry or cold conditions limits human population, whereas high vegetation productivity favours large population densities (Hantson et al., 2016). Although there is a perception that humans are causing increases in wildfire activity globally through fuel accumulation, increased ignitions and anthropogenic climate change (Running et al., 2006; North et al., 2015; Doerr and Satin, 2016; Balch et al., 2017), remote-sensing data shows there has been a decline in recent decades, which has specifically been attributed to agricultural expansion and intensification in grasslands and savannas (Andela and Van Der Werf, 2014; Andela et al., 2017). The magnitude of this change is dependent on the data set and the specific interval considered, and changes in climate and vegetation also explain some of the trend (Forkel et al., 2019b). Nevertheless, the evidence that human activity is reducing the incidence of wildfire in many regions is compelling. This negative effect comes about because fire spread is restricted by the clearance of natural vegetation and landscape fragmentation in many ecosystems (Harrison et al., 2021) and there is active fire suppression in regions of large human settlement or permeant agricultural. This conceptualization of humans as actors of landscape fragmentation explains the global negative correlation between population density and burnt area (Harrison et al., 2021). The only regions in which a positive correlation is observed between burnt area and human population is in densely forested such as the tropical forests of Borneo and areas of the Amazon (Armenteras et al., 2017; Harrison et al., 2021). In these regions, increased human activity through deforestation, logging and road building increases the likelihood of both natural and anthropogenic ignitions through increased human presence as well increased wind and fuel drying because of vegetation clearing (Pausas & Keeley, 2021; Harrison et al., 2021). Additionally, the presence of humans in fire-free ecosystems such as temperate or boreal forests may greatly increase the chances of ignition (Balch et al., 2017). These areas also correlate with low burnt area, suggesting different relationships between human activity and burnt area in fire-prone and fire-free regions (Harrison et al., 2021).

Wildfire controls: Moving beyond burnt area

Beyond burnt area, the properties of global fire regimes are much less constrained with only a few studies attempting to identify their distribution (Ichoku et al., 2008; Chuvieco et al., 2008; Archibald et al., 2013; Luo et al., 2013; Luo et al., 2017; Hantson et al., 2015). Authors have suggested that the distribution of global wildfire size can be approximated by a power-law (Drossel et al., 1993; Malamud et al. 1999). As such, power-laws have been fitted to global burnt area data (e.g. Archibald et al., 2013; Hantson et al., 2015; Andela et al., 2017). One study (Hantson et al., 2015) made use of generalized additive models to establish the relationship between fire size (obtained from a power-law) and climatic and human drivers. The analysis fitted a negative linear relationship between cropland cover and fire size, levelling off at high precipitation values. For population density, the fitted relationship was humped, with fire size peaking at intermediate levels of population densities. Another study, making use of similar assumptions, suggested that expansion of agricultural activity is a key driver in decreasing fire size over the last decade especially in northern Africa (Andela et al., 2017), though this agricultural expansion has a smaller influence on reducing fire sizes than it does on reducing wildfire numbers globally.

Studies have also focused on describing different aspects of fire regimes (e.g. size, frequency, intensity) in relation to each other. Such work has led to the establishment of the intermediate fire occurrence-intensity (IFOI) hypothesis, which proposes a humped relationship between fire frequency and fire intensity globally (Luo et al., 2017). Hypothesized explanations for these humped relationships include the effect of previous burns on landscape fragmentation and fuel availability. As the fire season progresses, previous burns fragment the landscape and limit the spread of wildfires, thus restricting fire size (Laurent et al., 2019). Additionally, frequent burns limit the amount of available fuel, thus limiting wildfire intensity (Luo et al., 2017) and season length (Archibald et al., 2013). Using fire radiative power (FRP) to represent fire intensity and a power-law to represent fire size, Archibald et al. (2013) identified a set of five distinct "pyromes", characterised by specific combinations of fire properties, specifically burnt area, fire return intervals, fire intensity, fire size and the length of the fire season. They argue, for example, that high intensity fires cannot be frequent or have long fire seasons, as too much biomass is consumed by early, intense fires to sustain this (Archibald et al., 2013). They identify four combinations of "natural" pyromes, frequent intense and large (FIL), frequent cool and small (FCS), rare, intense, and large (RIL), rare, cool, and small (RCS). They also identify a pyrome driven by human activity, the intermediate, cool, and small (ICS) fire regime. However, there are some surprising results in this analysis, since the RIL pyrome, characteristic of crown fires, are found inland in southwestern Australia where there is very little vegetation such as in the Gibson desert. A similar relationship was established between fire size and fire intensity by Laurent et al., (2019). They showed that the two fire properties have a humped relationship globally, with fire size peaking at intermediate levels of intensity. This result suggests that the positive relationship between the fire line intensity and fire spread of an individual fire, described by the Rothermel rate of spread (RoS) equations (1972), does not scale up to describe fire size globally. They hypothesized that the decrease in fire size with higher fire intensities is a consequence of the increasing landscape fragmentation as the fire season progresses, and thus controlled by fuel connectivity. This is in line with previous work showing that fire spread is limited by the connectivity of fuels (Archibald et al., 2012).

Current global wildfire modelling efforts

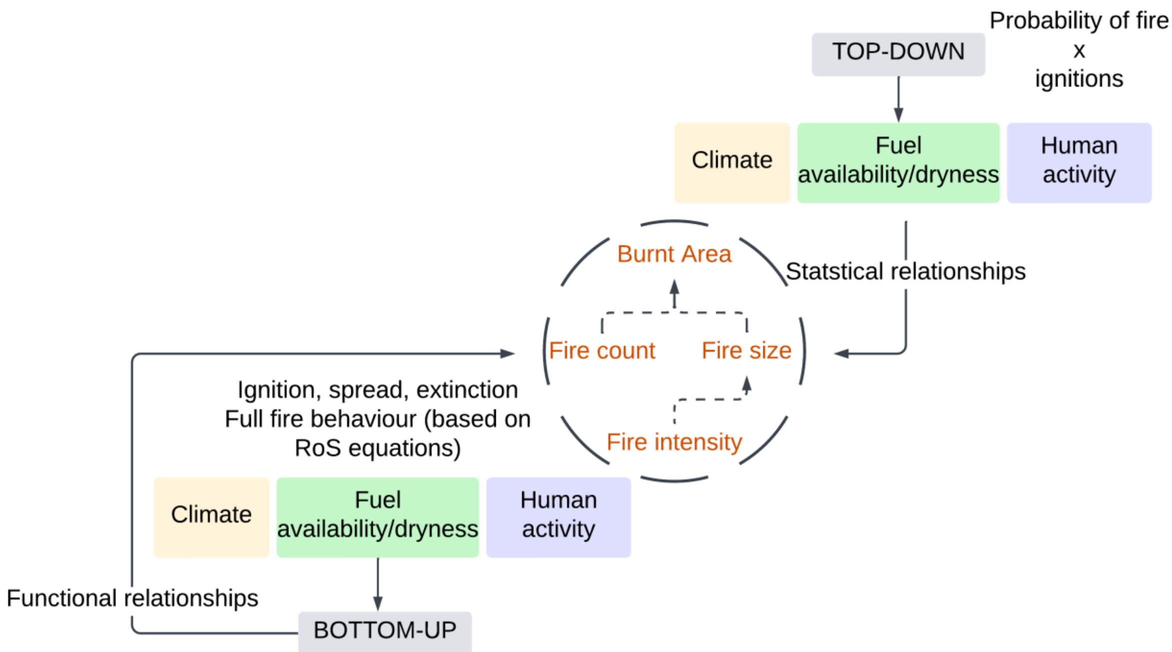

Figure 3. "Bottom up" and "top down" approaches to global fire modelling.

Wildfires are explicitly included in most dynamic global vegetation models (DGVMs) through coupled fire modules. The first DGVM to be published was developed in 1996 (IBIS; Foley et al., 1996) and the first model to explicitly include fire disturbance (MC-FIRE Lenihan and Neilson, 1998) followed soon after. The aim of these early coupled vegetation-fire models was to dynamically simulate global vegetation patterns and their associated fluxes and provide a way on incorporating vegetation dynamics into atmospheric models more accurately. These new modelling tools also provided a way in which to test theoretical ecological assumptions, by comparing modelled outputs to observations, as well as coming up with new hypotheses. Over the last two decades, the development of numerous global fire modules, for coupling with DGVMs, have developed alongside each other, and used varying approaches which can be loosely divided into empirical and process-based approaches (Hantson et al., 2016).

Empirical fire models rely on statistical relationships between grid-cell level climate, vegetation, land use, and ignition sources to simulate burnt area. They do not simulate individual fire sizes or intensities at a sub-grid cell resolution and have been referred to as “top down” modelling approach (Hantson et al., 2016). There are many different approaches to empirical fire modelling. For example, Glob-FIRM (Thonickle et al., 2001) was the first semi-empirical fire model and simulates burnt area as a scaling product based on regional published estimates of burning, and an estimated fire season length. JULES-INFERNO (Mangeon et al., 2016) makes use of a set of climatic factors and a reworked versions of the Pechony and Shindell (2009) fire parametrization algorithm. This algorithm simulates the humped relationship between human population and burnt area. It assumes a linear increase in the number of ignitions per km^2 with population density and a linear increase in fire suppression with increasing population density. LPJ-GUESS-SIMFIRE-BLAZE uses an alternative approach, based on optimizing a simple function for fire frequency using non-linear parameter estimations (Knorr et al., 2014).

Process-based fire models explicitly simulate full small-scale fire behaviour through theoretical equations (based on rate of spread (RoS) equations) and then scale up to grid-cell burnt area, providing outputs of different complexity levels (e.g. spread and fire sizes as well as burnt area). For this reason, they have been referred to as “bottom up” modelling approaches (Hantson et al., 2016). Using a rate-of-spread (RoS) model, based on the Rothermel (1972) equations, MC-FIRE was the first attempt to explicitly simulate fire spread. The framework has inspired many other process-based models with different levels of complexity. The Regional Fire Model (Reg-FIRM: Venevsky et al., 2002) took a different approach which is now also widely used of simulating burnt area as the product of number of fires and average fire size (Hantson et al., 2016). SPITFIRE (Thonickle et al., 2010) takes the Reg-FIRM approach but explicitly considers ignition rates and then simulates fire spread as a two-step process. It determines is there is sufficient and flammable fuel present. Then it simulates fire spread, explicitly simulating fire intensity and only allows fires to spread if a sufficient surface fire intensity is reached and if the resulting fire has sufficient height to reach the crowns (Thonickle et al., 2010).

Table 1. Summary of the models included in the first FireMIP phase.

Fire module	Coupled DGVM	Modelling approach	Reference
GlobFIRM	LPJ-GUESS	Empirical	Smith et al., 2014
SIMFIRE-BLAZE	LPJ-GUESS	Empirical	Knorr et al., 2014
INFERNO	JULES	Empirical	Mangeon et al., 2016
MC2		Process-based	Bachelet et al., 2015
SPITFIRE	LPJ-GUESS	Process-based	Lehsten et al, 2009
CLM		Process-based	Li et al., 2013
SPITFIRE	ORCHIDEE	Process-based	Yue et al., 2014
SPITFIRE	JSBACH	Process-based	Lasslop et al., 2014
CTEM	CLASS	Process-based	Melton and Arora 2016

An attempt to systematically compare the performance of different global fire models began in 2014, with the first Fire Model Intercomparison Project (FireMIP) (Hantson et al., 2016; Rabin et al., 2017). The first round of FireMIP included nine fire models, three of which were empirical models and six of which were process-based. Excluding the two oldest models (LPJ-GUESS-GlobFIRM and MC2) all FireMIP models were able to spatially reproduce the patterns of burnt area, the annual total burnt area (345-468 Mha) as well as its seasonality relatively well (Hantson et al., 2020). However, models disagree on historical trends over the last century, leading to low confidence in their ability to project future trends (Teckentrup et al., 2019; Jones et al., 2022). FireMIP ran a set of transient sensitivity analysis to determine the sensitivity of the different fire models to atmospheric CO_2 levels, population density, land-use change, lightning, and climate to determine what may be causing the divergence in trends between models. The largest differences were driven by differences in the representation of anthropogenic activity and the effect of land use on vegetation and fire. All the fireMIP models showed a significant trend associated with changes in CO_2 levels, but they disagreed in the direction of this trend. Conversely, they showed no significant trend to changes in climate, though it showed a strong control on the inter-annual variability of burnt area for all models (Teckentrup et al., 2019). The models show a consistent trend in burnt area in response to population density changes (especially since 1921), with fire suppressed under high population densities (Teckentrup et al., 2019). All models struggled with simulating the length of the fire season and interannual variability (Hantson et al., 2020). This underperformance has been attributed in part to the underestimation and misrepresentation of the importance of previous-season leaf area index, plant productivity and the effect of climate on fuel moisture. Indeed, satellite-derived relationships have shown that these factors have strong controls of interannual variability on burnt area (Forkel et al, 2019b). Only the SPITFIRE (Thonicke et al., 2010) fire module explicitly simulated fire size and count as output variables. Although it was coupled with three different DGVMs, none were able to outperform the null model, which assumes a mean value everywhere. However, the DGVMs coupled with SPITFIRE did simulate the number of fires reasonably well (Hantson et al., 2020).

Despite added complexity, process-based models did not outperform the empirical ones (Hantson et al., 2020). The poor performance of process-based models in simulating global fire properties beyond burnt area (specifically fire size) suggest that the current “bottom up” approaches, based on simulating individual fire behaviour, do not capture the global distribution of these properties. This poor performance may be because of incomplete understanding on the controls of individual fire properties (Forkel et al., 2019a), and the fact that RoS equations may not scale up globally. Another issue is the varying spatial and temporal scales on which these assumptions operate. An example of this can be found in the way process-based models’ make use of the rate of spread (RoS) equations. Derived from the theoretical Rothermel (1972) equations, which represent the energy released from a flaming front, or the fire line intensity, the RoS equation assumes the larger the fire line intensity, the faster the fire spread and thus the larger the resulting fire. Burnt area is then often derived from the product of mean simulated fire sizes and simulated ignitions. As such, these parametrizations assume linear relationships between fire intensity, fire size, and burnt area and rely heavily on ignition counts. Furthermore, they assume that fire size is completely driven by environmental and vegetation controls. Nevertheless, several studies suggest that many of these relationships between fire intensity, ignitions and fire size saturate globally as the season progresses (e.g. Luo et al., 2017; Laurent et al., 2019) and that human activity influences fire size in addition to climate and vegetation (Hantson et al., 2015). Furthermore, RoS equations require many parameters the values of which are poorly known, and it is computationally very difficult to calibrate RoS equations within a global process-based model.

Recent work has shown that different fire properties have independent and contrasting global controls, but they are yet to be modelled independently from each other (Forkel et al., 2019a; Hantson et al., 2020). The findings of FireMIP also highlight areas of opportunity. The ability of empirical models to reproduce the spatial patterns of burnt area based on statistical relationships derived from data suggests that they could also be used to explore the controls on other aspects of the fire regime, such as fire intensity or fire size, given the available data.

Mapping global wildfire regimes

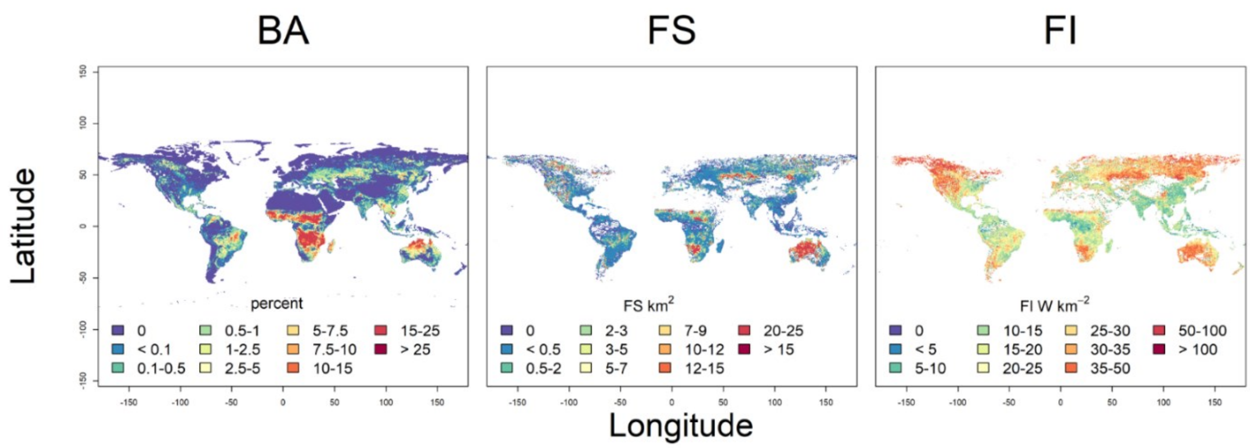

Figure 4. Global fire regimes from 2010-2015. Burnt area from GFED4 (Randerson et al., 2018) on the left, fire size from the Global Fire Atlas (Andela et al., 2019) in the middle and fire intensity, represented by median FRP derived from MCD14ML (Giglio et al., 2006). The unit for fire intensity here is W.km^2 as FRP represents the energy released from the active fire integrated over a whole pixel. Issues that arise from this representation of fire intensity are discussed later in the chapter.

Much of the current knowledge on the controls of wildfire regime and the subsequent development of global fire models has been made possible thanks to the recent emergence of remotely sensed active fire (AF) products which provide long-term quality data from regional to global scales and with a variety of temporal resolutions (e.g. Landsat, MODIS, Sentinel, VIIRS). Active fire pixels identify the location, timing, and fire radiative powerpower (FRP) of fires at the time of the satellite overpass (Wooster et al., 2021; Chuveico et al., 2019). Algorithms then convert active fire information into burnt area data, determining the fraction of vegetation burnt at a particular location in a given time period (Hantson et al., 2013; Chuveico et al., 2019; Wooster et al., 2021). Although these burnt area products were originally developed to provide information on fire emissions, they are now widely used for a variety of purposes, including modelling and regional fire management (Mouillot et al., 2014). In the past decade, the quality of burnt area datasets derived from AF pixels has improved. The most recent product, GFED5 (Chen et al., 2023) provides improvements in adjusting for biases associated with small fires and unburned islands (Chen et al., 2023). GFED5 represents a 93% increase in global burnt area compared to MCD64A1 and a 61% compared to GFED4. This large increase compared to previous datasets is due primarily to the inclusion of small fires which are difficult to detect and as such omitted from previous products (Randerson et al., 2012).

Most global studies on wildfires use these burnt area products as a proxy for wildfire activity. However, burnt area does not provide information on global fire regimes beyond wildfire occurrence, extent, and frequency, which is often understood as the inverse of burnt area (Knorr et al., 2014; 2016; Bistinas et al., 2014; Kelley et al., 2019; Shen et al., 2023). Within a given BA grid cell, a variety of different fire sizes and intensities are possible. For example, the same burnt area could represent a grid cell with multiple small and high-intensity wildfires or a very large, low-intensity wildfire. Fire radiative power (FRP), which represents the rate at which fires are emitting thermal energy, is provided with active fire pixels and has been used as a proxy for fire intensity (e.g. Smith and Wooster, 2005; Ichoku et al., 2008; Chuvieco et al., 2008; Archibald et al., 2013; Heward et al., 2013), However, it is not a direct measure of fire intensity as it is integrated over the whole pixel, whereas fire line intensity only represents the energy released at the flaming front (Giglio et al., 2006). As such, caution should be taken when using FRP to represent fire intensity, and it cannot be used as a direct proxy (Wooster et al., 2021; Giglio et al., 2006). Some of the highest FRP values are detected over areas with very low vegetation cover, notably in deserted regions of southwestern Australia. Without accounting for this, misleading conclusions about global fire intensity can be drawn such as Archibald et al., (2013) assigning the rare, intense, and large fires (RIL) pyrome (crown fires) in regions of southern Australia were there is very little tree cover.

One way around this would be to obtain FRP values for the flaming fronts of individual fires. However, obtaining individual fire properties such as size from active fire products is also not a straightforward endeavour (Hantson et al., 2013; Mouillot et al., 2014; Andela et al., 2019). Characterizing individual fire scars is a crucial step towards this, and one that has been highlighted as an important aim (Mouillot et al., 2014). The recent publication of three datasets of individual fire properties, the FRY database (Laurent et al., 2018), the Global Fire Atlas (Andela et al., 2019), and the GlobFire database (Artés et al., 2019) is a big step forward and provides new opportunities to explore the individual drivers of fire regimes beyond burnt area.

Table 2. Summary of the remotely sensed satellite products available

	Time span	Temporal resolution	Reference
	Global BA products		
GLOBSCAR	>2000	Monthly	Simon et al. (2004)
GBA2000	2000	Monthly	Tansey et al. (2004)
GBS	1982–1999	Weekly	Carmona-Moreno et al. (2005)
GLOBCARBON	1998–2007	Monthly	Plummer et al., 2006
MCD45A1C51	2000-2017	Monthly	Roy et al. (2006)
	Global fire patch products		
FRY	2005-2011	Individual fires	Laurent et al 2018
GLOBFIRE	2001-2017	Individual fires	Artés et al., 2019
GLOBAL FIRE ATAS	2003-2016	Individual fires	Andela et al., 2019

Global change and fire regimes: evidence from the past

Many of the recent advances in global wildfire modelling have relied on the information derived from the study of present-day fire regimes, which itself relies heavily on satellite data. However, this data only covers the last few decades in which anthropogenic climate change and increasing CO_2 concentrations were already occurring. The study of palaeo-fires provides a way to document fire history on decadal to millennial scales, giving us a picture of how wildfires have changed throughout history (Marlon et al., 2020). Changes in past fire regimes have been documented through tree-ring scars, fire-related biomarkers in sediments and ice cores, as well as charcoal preserved in lake and bog sediments and soils. Charcoal data are the most common source of information about wildfires before the last few centuries (Marlon et al., 2020). The Global Palaeofire Working Group (GPWG), established in 2006, has provided global compilations of charcoal data covering much of the Late Quaternary (Power et al., 2008, 2010; Daniau et al., 2012; Blarquez et al., 2014; Marlon et al., 2016). The most recent compilation of such data is the Reading Palaeofire Database (RPD) (Harrison et al., 2022). The recently published RDP is a 128% increase in the number of records compared to previous versions.

Trends in fire regimes over thousands of years have been attributed in the most part to changes in climate (Daniau et al., 2010; Marlon et al., 2009; Daniau et al., 2012; Power et al., 2013; Marlon et al., 2020). Indeed, fire regime shifts have been observed on glacial-interglacial timescales as well as during rapid warming associated with Dansgaard-Oeschger (D-O) events during the last glacial interval. Global fire history seems to suggest the lowest fire activity during the coldest periods and the highest under warm periods (Daniau et al., 2010; Power et al., 2008). Analyses of the charcoal data have shown that during the height of the LG Maximum (LGM) LGMthere were very low levels of biomass burning compared to the present (Power et al., 2008). Since then, records show increasing wildfire activity, this through until the Holocene, although these increases were spatially heterogeneous (Power et al., 2008). In addition to climate, the role of vegetation is also hypothesized to be key in explaining past fire regimes, in some cases overriding the climate signal (Higuera et al., 2009). Vegetation records show that vegetation productivity and forest cover were reduced at the LGM compared to present (Harrison and Prentice, 2003; Kaplan et al., 2016) and this reduction was driven by changes in atmospheric CO_2 levels as well as climate (Bragg et al., 2013). This reduction in vegetation was a crucial factor in the low levels of biomass burning at the time (Martin Calvo, 2015). Model experiments demonstrate the importance of productivity in shaping fire regimes in the past (Bond et al., 2005; Martin Calvo et al., 2014; Martin Calvo et al., 2015). There is evidence that humans made use of fire throughout the Holocene (Bowman et al., 2009; Bowman et al., 2020). Analysis of palaeorecords from the last two millennia show a decline in global biomass burning from 1 CE to around 1750 CE. From 1750 CE, the records then show a sharp increase in biomass burning for about a hundred years, followed by a sharp decline until the present (Marlon et al., 2008). From 1750 CE, the sharp rise in fire activity on Earth is decoupled from climate and vegetation changes, and this spike has been attributed to humans (Marlon et al., 2008). The following decrease, from now until present has also been largely attributed to humans and is understood as a response to increased landscape fragmentation and fire management (Marlon et al., 2008), with the current trend in satellite data being understood as a continuation of this fragmentation (Jones et al., 2022; Andela et al., 2017).

In contrast to current wildfire information, which describe the characteristics of wildfires over a relatively short (days to years) period in a well-defined region (identifiable in order of km), the study of past wildfires does not offer the same precision. Nevertheless, these long-term datasets provide information about wildfire regimes under dramatically different conditions than today. Not only do they allow us to document how wildfires have responded to large-scale changes in climate and CO_2 levels, but they also provide insights into burning on Earth before humans became a major influence. Importantly, simulating past wildfire regimes during periods of radically different conditions provides a way of simulating the past but also as a test for our climate models (Kageyama et al., 2018). By testing the ability of models to simulate realistic reconstructions of the past outside of the range of values on which the models were trained (known as an out-of-sample experiment) we can evaluate how robust and sensitive models are to dramatically different conditions (Burls et al., 2022). Given that conditions by the end of the 21st century are expected to be radically different than today, the only way to ensure confidence in our ability to project future changes is to rely on such out-of-sample experiments for model evaluation.

Global change and fire regimes: looking to the future

Recent increases in wildfire activity globally (Mueller et al., 2019; Jones et al., 2022; Mansoor et al., 2022; Jones et al., 2022, Abatzoglou et al., 2019; Duane et al 2021) have led to concerns that, under climate change, these trends may continue. Increasing temperatures and dryness are often cited as the key drivers of projected increases in fire activity (Pausas & Keeley, 2021; Jones et al., 2022; Williams et al., 2019; Goss et al., 2020, UNEP, 2022). Studies focusing on fire weather conditions have shown widespread increases across much of the world under future conditions (Flannigan et al., 2009; Lui et al., 2009; Jones et al., 2022), especially in boreal regions, with more than a doubling in FWI expected in parts of Canada (Lund et al., 2023) but also large increases across Africa, Central Asia, southern hemisphere South America (Jones et al., 2022) and southern Europe (Dupuy et al., 2020). Though these increases vary in magnitude, future trends in fire weather are spatially homogenous, with practically no regions in which decreases are predicted.

However, whilst the effect of climate change on temperature and precipitation has the potential to increase flammability through accelerated drying rates and drought conditions, the drivers of wildfire activity are not limited to climatic factors. The sensitivity of global fire regimes to changes in human pressures, land use, productivity and fuel load under higher CO_2 levels are still all relatively unknown however their impact will vary spatially and temporally and have contrasting effects (Forkel et al., 2019a; McLauchan et al., 2020; Tang et al., 2021; Chuvieco et al., 2021). Despite increasing trends in FWI over the last decades (Jones et al., 2022) a global decreasing trend in burnt area has been observed over the same period (Andela et al., 72017). This observed decline in burnt area has been attributed to agricultural intensification and population growth (Andela et al., 2017). Human activities strongly control both fuel continuity and fuel load and will most likely have one of the largest impacts on future global fire regimes (UNEP, 2022). Fire suppression policies in some regions are also known to have altered established fire regimes (Harrison et al., 2021). Another, often overlooked part of how fire regimes will respond to change, will depend on their sensitivity to CO_2-enduced changes to vegetation productivity and structure. Atmospheric CO_2 levels directly affect productivity through its control on photosynthesis, but also on plant growth and structure (Grossiord et al., 2020; Park Williams et al., 2013; Martin Calvo & Prentice, 2015). Net primary production has been estimated to have decreased by 25% under low CO_2 levels during the Last Glacial Maximum (Bond et al., 2005; Martin Calvo & Prentice, 2015). The positive feedback between changes in productivity as a response to CO_2 changes and wildfires has been shown to be strongest in the tropical regions as well as dryer regions (Bond et al., 2005; Martin Calvo & Prentice, 2015). Observed increases of woody species in savannas over the last few decades have been attributed to increasing CO_2 levels, with changes in land use also playing a role (Bond et al., 2000; Buitenwerf et al., 2012; Stevens et al., 2017; Venter et al., 2018). In addition, greening has been observed in the tropics as a response to high CO_2 and increased precipitation amongst other factors (Cai et al., 2023). These changes in vegetation as a response to CO_2 level changes and land use changes will influence fire regimes and may have an opposing effect to that expected from changes in climate alone.

The fact that fire weather is expected to increase globally under climate change but that future simulations identify regions of decreasing fire activity also highlights the importance of considering factors beyond climate. Future global simulations of wildfire activity agree somewhat on the broad geographic trends, with increased burnt area by the end of the century especially present in the mid to northern latitudes and decreases observed in the tropics (Krawchuk et al., 2009, Power et al., 2013; Moritz et al., 2012; Huang et al., 2015; Knorr et al., 2016; Kloster et al., 2016; Wu et al. 2021) However, regional trends in these projections differ, especially in the Amazon with some studies projecting decreases in fire activity (Krawchuk et al., 2009; Moritz et al., 2012) and others projecting increases (Huang et al., 2015; Knorr et al., 2016; Wu et al., 2021, UNEP, 2022). In the northern latitudes, some studies show decreasing fire activity across northern Russia (Krawchuk et al., 2009; Wu et al., 2021) whilst other show significant increases (Moritz et al., 2012; UNEP, 2022). There is also disagreement over the sign of the global trend in burnt area under high-emission scenarios, with some studies showing an increasing trend (UNEP, 2022; Moritz et al., 2012), some no significant trend (Krawchuk et al., 2009) and some a decreasing trend (Knorr et al., 2016; Wu et al., 2021; Kloster et al., 2017). The differences in the magnitude of these trends can be explained by model sensitivities to climate, CO_2 and human activity, with very few of the studies accounting directly for the effect of CO_2-enduced changes on vegetation. Knorr et al., (2016) simulated future fire regimes on a global scale and accounted for the direct effect of CO_2- fertilization on vegetation. The authors found opposing effects of climate and CO_2 on both burnt area and fuel loads. Whereas climate change decreased fuel load (through increased decomposition rates), increasing CO_2 increased fuel loads (through CO_2–fertilization). However, whereas climate change increased global burnt area (through fire weather increases), increasing CO_2 had a negative trend on global burnt area due to woody thickening in tropical savannas (Knorr et al., 2016). These results contrast that of previous work (Kloster and Lasslop, 2017) which did not observe the decreasing trend in burnt area. Large divergences in projected regional trends means that large uncertainties remain surrounding how fire regimes may respond to global change. Nevertheless, given that the performance of these models has not been systematically tested in dramatically different climate and CO_2 conditions, it is difficult to assess their ability to accurately predict the response of fire regimes to large-scale global change and as such to determine which trends are most realistic.

Sensitivity analysis as a tool to explore the impact of changing conditions on fire regimes

When conceptualizing the global controls of fire regimes, the "four-switches" (Bradstock et al., 2010) are useful for a few reasons. Firstly, they provide a conceptual framework through which to determine the critical 'switch' under different conditions. By focusing on which switch is limiting wildfire occurrence instead of trying to simulate the individual behaviours of wildfires, simple but robust boundaries can be established between varying global controls of wildfire occurrence. This approach provides a way in which to further our understanding of the underlying controls and distribution of wildfire occurrence globally. This is the methodology Boer et al., (2021) used to establish a hydroclimatic model which simulated the global distribution of fire potential and was able to establish fuel-limited and dryness-limited regions respectively simply but robustly. Their analysis showed that 80% of the global variation in the 99^{th} quantile of the observed mean annual fractional burned area could be explained from a combination of mean annual precipitation and potential evapotranspiration (Boer et al., 2021). Although the model explored differences between biomes, similar approaches could be used to investigate the effects of human activity through changes in ignition regimes or manipulation of vegetation, as well as the effects of changing climate. This framework can also help us think about how the critical constraints of different properties of fire regimes may differ. Indeed, wildfire occurrence is conditional on ignition, and therefore, relies on all four switches being met. However, once ignition has occurred, the other three switches become more important in determining whether a wildfire spreads, how rapidly, and how intense it will be (Archibald et al., 2013). We may expect that fuel load and fuel continuity will greatly influence the size and intensity of resulting fires and will not necessarily have the same constraints as ignition. Indeed, as with burnt area, global fire size is thought to be controlled by precipitation, with larger fires occurring at greater levels of aridity (Hantson et al., 2015). However, lack of precipitation and atmospheric dryness limits fuel build-up and plant growth (Keeley & Syphard, 2021; Fu et al., 2022; Valdez et al., 2017; Kuhn-Régnier et al., 2021). Thus, we might expect that intense fires, which require large fuel loads, may be negatively related to dryness (Kuhn-Régnier et al., 2021; Forkel et al., 2019). Even if we can identify the key drivers of different aspects of global fire regimes, the challenge becomes how to determine the sensitivity of these drivers to change. However, this is crucial if we want to address uncertainties about future trends in fire regimes.

A major limitation to exploring this question is the short time frame of remotely sensed products (~40 years). Many fire regimes may have fire return intervals of over a hundred years, meaning that they are not captured in the satellite data record (Giglio et al., 2020). There have been some attempts to remedy this with reconstructions of relatively recent fire history (e.g. Mouillot et al., 2005; Yang et al., 2014). However, these reconstructions either rely on models themselves, or on historical fire data which is not always available. An alternative approach is to make use of models themselves by exploring the sensitivity of outputs to the varying inputs (Harrison et al., 2023). Such sensitivity analysis allows us to run models in hypothesis-testing mode and determine influential drivers. This kind of analysis also allows us to explore the output of conditions that cannot observed, either because they are counterfactual due to temporal or spatial correlations (for example atmospheric CO_2 levels and climate), or because it is impractical (for example studying systems with or without human presence). An empirical burnt area model, SOFIA (Forkel et al., 2019b) was used to investigate the impact of people on fire return intervals by running two simulations, one with all variables and one in the effect of the human variable (population density) was removed. The results showed that in some biomes, wildfires would be more frequent without humans, whereas in others it would remain unchanged or be less frequent (Harrison et al., 2021). Studies have also used sensitivity analysis when projecting future fire regimes to determine key drivers (Moritz et al., 2012; Knorr et al., 2016). Running models in hypothesis-testing mode can also allow us to make use of our knowledge of past climates, by simulating wildfires under past climates with varying conditions and comparing the outputs to palaeorecords. An example of this methodology is the work of Bond et al., (2005) and more recently Lasslop et al., (2020) in which the authors ran fire-enabled a DGVM to simulate vegetation in a world with and without fire. Their simulations allowed them to determine that without fire, the extent of forested ecosystems on earth has the potential to double would increase, with a global increase of 10% [3-25%] in the most recent study (Lasslop et al., 2020). This increase in forest cover would occur primarily at the expense of C_4 vegetation. Their study also showed that the spread of C_4 plants, driven by wildfire activity, occurred before the presence of humans, adding to the body of literature that argues wildfires were an important ecological force long before humans could manipulate fire regimes. A similar methodology was used by Martin Calvo et al., (2015). By running experiments on a DGVM of "fire on" vs "fire off" they showed that the removal of fire caused a global expansion of forest. They also applied counter factual combinations of climate and atmospheric CO_2 levels to show that CO_2 at the last glacial maximum was a strong driver in the low levels of net primary production. Their study suggests that CO_2 (through its control on photosynthesis) along with fire (through its control on biome distribution) are important drivers of vegetation. Another study by the same group (Martin Calvo et al., 2014) inferred that the increases in biomass burning that we have observed since the LGMLGM can be attributed to increasing CO_2 concentrations and its effect on vegetation productivity. This analysis was particularly interesting because of the difficulty of studying the effect of CO_2 levels on wildfire-vegetation interactions.

An added complication of using models to run sensitivity analysis in out-of-sample experiments is that estimations of vegetation type and productivity often rely on prescribed parameter values for plant functional type (PFTs) based on the classical biome's distribution (Stocker et al., 2020; Wang et al., 2017). Nevertheless, we know these PFTs may not be appropriate to predict vegetation's response to fire regimes, since traits specific to fire may play a significant role (Archibald et al., 2018). Additionally, these parameters are fixed, making the effect of changing conditions difficult to observe. Here as well, empirically developed models provide opportunities to deal with these limitations. BIOME4 is a coupled biogeography-biogeochemistry model that simulates potential natural vegetation types solely from information on latitude, CO_2 levels, climate, and soils. It simulates competition between different vegetation types as a function of productivity and has been used as a diagnostic tool as well as to simulate palaeo-vegetation patterns (Kaplan et al., 2003). Furthermore, the P model (Wang et al., 2017; Stocker et al., 2020) is a data-driven vegetation model which provides robust gross primary production (GPP) estimates in a PFT and biome independent way. Both these vegetation models may provide significant new opportunities to explore the interaction of CO_2-enduced changes on vegetation and fire regimes.

By using an optimality-based approach that focuses on predicting the ratio of leaf-internal to pressure and ambient CO_2 concentrations, the P model also reduces the number of prescribed values. In addition, it uses a first-principles model of GPP which allows continuous acclimation of photosynthetic parameters to environmental variations in space and time, allowing it to account directly for the effect of CO_2 on vegetation (Wang et al., 2017; Stocker et al. 2020). Previous models such as LPJ (Stich et al., 2000; Stich et al., 2003) have considered the effect of acclimation, however this response remains constant and PFT-specific. By focusing solely on the need of plants to maintain long-term average photosynthetic capacity (Vcmax) in the most efficient way, the P model makes abstraction from these PFT-specific parameters, providing a flexible way to explore the effect of GPP under changing climate. This approach means that changes in CO_2 levels can be observed directly under past and future conditions, providing a new way to test the response of fire regimes-vegetation dynamics to changing conditions. Combining the use of sensitivity analysis of empirical wildfire models based on wildfire constraints, out-of-sample experiments and an optimality-based vegetation model provides a real opportunity to assess the impact of climate, CO_2 levels and human activity on fire regimes in a novel way.

Research questions

This PhD thesis aims to adds to the existing body of knowledge presented above by exploring the impacts of changes in climate, atmospheric CO_2 levels and human activity on the spatial distribution of global burnt area, fire size and fire intensity. As a first step, I develop statistical models that represent these three wildfire properties independently (Chapter 2). In addition to validating the performance of these models under modern conditions (Chapter 2), I also evaluate their performance in an out-of-sample experiment, the Last Glacial Maximum (Chapter 3). The Last Glacial Maximum is a time when the change in climate forcing was as large, albeit in the opposite direction, as that projected change in climate forcing by the end of the 21st century under low climate change mitigation scenarios. I then use a set of sensitivity experiment to explore the response of fire regimes to large-scale changes in climate, CO_2 levels and human activities at the Last Glacial Maximum (Chapter 3). Finally, I explore the impacts of changes in climate, CO_2 levels and human activity on the spatial distribution of global fire regimes by the end of the 21st century under different climate change mitigation scenarios (Chapter 4). The associated published work and my role in this work is briefly described below.

RQ1: How do the global spatial controls of burnt area, fire size, fire intensity differ?

This work was published in *Environmental Research Letters* in May 2022 under the title "Global environmental controls on wildfire burnt area, size, and intensity". I was entirely responsible for the data curation, processing, and analysis, as well as producing all the associated graphics and tables. I shared the responsibility for the development of the concepts, strategy, and interpretation of the results with my co-authors. I wrote the first draft of the paper and my co-authors contributed to the final draft.

Haas, O., Prentice, I. C., and Harrison, S. P., Global environmental controls on wildfire burnt area, size, and intensity. *Environmental Research Letters* **17** 065004, https://doi.org/10.1088/1748-9326/ac6a69, (2022).

RQ2: Were low atmospheric CO_2 levels' impact on vegetation, cooler climate, or a combination of both responsible for limiting wildfire activity at the Last Glacial Maximum and what were the effects on the distribution of global fire regimes?

This work was published in *Biogeosciences* in September 2023 under the title "The response of fire regimes to Last Glacial Maximum carbon dioxide and climate". I was entirely responsible for the data curation, processing, and analysis, as well as producing all the associated graphics and tables. I shared the responsibility for the development of the concepts, strategy, and interpretation of the results with my co-authors. I wrote the first draft of the paper and my co-authors contributed to the final draft.

Haas, O., Prentice, I. C., and Harrison, S. P., The response of fire regimes to Last Glacial Maximum carbon dioxide and climate. *Biogeosciences* **20**, 3981–3995, https://doi.org/10.5194/bg-20-3981-2023, (2023).

RQ3: How do we expect global fire regimes to respond to 21st century CO_2 levels and climate conditions when also accounting for demographic and land use changes?

This work was submitted to *Science* in December 2023 under the title "Global wildfires on a changing planet". I was entirely responsible for the data curation, processing, and analysis, as well as producing all the associated graphics and tables. I shared the responsibility for the development of the concepts, strategy, and interpretation of the results with my co-authors. I wrote the first draft of the paper and my co-authors contributed to the final draft.

Chapter 2: Global controls on the spatial distribution of wildfire burnt area, size, and intensity

The aim of this chapter is to address the question of how the global spatial controls of burnt area, fire size, fire intensity differ (**RQ1**). It is structured as a paper, with an introduction, followed by a description of the methodology, a presentation of the results and finally a discussion. This work was published in *Environmental Research Letters* in May 2022 under the title "Global environmental controls on wildfire burnt area, size, and intensity" and has been reworded in some parts, however the methodology, results and discussion remain unchanged.

Introduction

Fire is a necessary component of some ecosystems, but a destructive influence in others (Keeley et al., 2011; Archibald et al., 2018; Harrison et al., 2021). In both cases, however, it represents a major influence on vegetation structure and composition. Recent changes in wildfire regimes, especially the incidence of exceptionally large fires in some regions, have raised serious concerns about how they will develop in response to projected future changes in climate and land use (Bond et al., 2005; Pausas and Keeley, 2009; Pausas and Ribeiro, 2017a).

Wildfire regimes are characterized as combinations of specific fire properties (Krebs et al., 2010; Archibald et al., 2018, 2013), of which the most cited are total burnt area and the sizes and intensities of individual fires. Although all these properties are understood to be jointly controlled by climatic, vegetation and land-cover conditions (Archibald et al., 2013; Rogers et al., 2020; Kelley et al., 2019; Archibald et al., 2018), the specifics remain unclear. This is manifested in the poor performance of process-based models designed to predict wildfire and its interactions with vegetation. Fire-enabled dynamic global vegetation models (DGVMs) have been used to simulate fire during the historical period (e.g. Teckentrup et al., 2019), and to predict how fire regimes might change in future (Kloster et al., 2012; Sheehan et al, 2015; Wu et al., 2021). However, the Fire Model Intercomparison Project (FireMIP: Hantson et al., 2016; Rabin et al., 2017) showed that process-based models performed no better than empirical models in predicting burnt area (Forkel et al., 2019a; Hantson et al., 2020). Furthermore, no fire-enabled DGVM could predict global patterns in fire size better than a null model that assumed the same mean size everywhere (Hantson et al., 2020). This failure has been attributed to inadequate understanding, and therefore incomplete or incorrect representation, of the key processes and their relationship to environmental factors (Forkel et al., 2019a; Hantson et al., 2020) in process-based models.

Several empirical studies have investigated the relationships between environmental factors and remotely sensed burnt area (e.g. Bistinas et al., 2014, 2013; Knorr et al., 2016; Knorr et al., 2014; Andela et al., 2017; Forkel et al., 2019b, 2017; Kuhn-Régnier et al., 2021). Global fire size has been shown to vary along precipitation gradients, with greater aridity linked to larger fires (Hantson et al., 2015). Human activity on the other hand strongly restricts fire size through landscape fragmentation, which limits fire spread (Laurent et al., 2019; Hantson et al., 2015; Andela et al., 2017). Intensity depends on fire type, with crown fires generally more intense than ground fires (Sugihara et al., 2006; Keeley, 2009; Archibald et al., 2018). However, research into the controls of the geographic patterns in fire size and fire intensity has been limited, mainly due to the lack of observations (Bowman, 2018). Novel products from newly available satellite data sets (eg Laurent et al., 2018; Andela et al., 2019; Artés et al., 2019) provide new opportunities to investigate these controls.

Four conditions must be met for a fire to start. There must be sufficient fuel; it must be dry, and therefore flammable; weather conditions must be suitable; and there must be an ignition source (Bradstock, 2010). Once ignition occurs, however, other factors may influence whether the fire spreads, how rapidly it spreads, and how intense it is (Archibald et al., 2013). In fire-enabled DGVMs, burnt area is sometimes derived as the product of the number of fires started and a mean fire size. This concept intrinsically links ignition frequency to the total amount of burning, an assumption that has been challenged (Bistinas et al., 2014; Harrison et al., 2021). Globally, fire intensity has been observed to increase with fire occurrence up to a threshold, also known as the intermediate fire occurrence-intensity (IFOI) hypothesis (Pausas & Ribeiro, 2013; Luo et al., 2017). In process-based models fire size is often dependent on fire intensity, defined as the amount of energy released by a wildfire, through rate-of-spread equations (Yue et al., 2014; Hantson et al., 2016). Indeed, as a key component of the Rothermel equation (Rothermel, 1972), greater fire intensity is assumed to increase the speed of fire spread, thus producing larger fires. However, this relationship has been shown to saturate in much of the world (Laurent et al., 2019).

In this chapter, we explored the causal relationships between environmental factors and geographic variation in fractional burnt area, fire size and fire intensity. These underlying relationships may differ from the emergent relationships with individual drivers. We develop generalized linear models (GLM) for each fire property, using a common set of quantitative predictors representing vegetation, land cover, climate, and ignition sources. We explore the direction and power of the linear relationships fitted between each predictor and each fire property, when all other variables are held constant, to identify significant drivers and constraints for different aspects of the fire regime and assess their (differing) relative importance.

Data and methods

Fire Data

Burnt area (BA) data were derived from monthly mean fractional burnt area from the Global Fire Emissions Database (GFEDv4; Randerson et al., 2018). This provides monthly burnt area at 0.25 × 0.25° resolution for the period from June 1995 to December 2016. Fire size (FS) was represented by median monthly fire size from the Global Fire Atlas (Andela et al., 2019). This provides global vector shapefiles gridded at 500 m with the timing and location of each individual fire, along with its key properties, from 2003 to 2016. The median was used to account for the highly skewed distribution of fire size. Fire intensity (FI) was approximated by a metric based on the median monthly fire radiative power (FRP) in the MCD14ML dataset (Giglio et al., 2006). This provides geographic coordinates of active ~ 1 km × 1 km fire pixels detected by the MODIS sensor onboard the Terra and Aqua satellites, from 2000 to 2017. FRP in MW is provided for each pixel. Only type 0 pixels (presumed vegetation fires) and with confidence > 50% were retained. We divided the monthly median values by the square root of monthly median fire size in the Global Fire Atlas. Although FRP has been used directly to indicate fire intensity (Wooster and Zhang, 2004; Wooster et al., 2005), it is a measure of the instantaneous energy emission over the whole pixel. Normalizing by the square root of median fire size provides a measure (in units of $W\ m^{-1}$) more closely related to the fire line intensity of any given fire (Supplementary Chapter 2).

Predictor variables

A set of predictors representing vegetation, landcover, climate and ignition sources was identified from previous research on the drivers of wildfire regimes globally (Forkel et al., 2019b, 2018; Bistinas et al., 2014).

Vegetation, land cover and landscape fragmentation.

Mean annual gross primary production (GPP) obtained from monthly outputs of the P-model (Stocker et al., 2020), a first-principles model of GPP that allows continuous acclimation of photosynthetic parameters to environmental variations in space and time (Supplementary Chapter 2), was used as an index of vegetation productivity. Land cover categories were used to represent vegetation types. Annual fractional shrubland, grassland and tree cover were obtained by converting the land cover types from the European Space Agency (ESA) Climate Change Initiative (CCI) Land Cover dataset, which provides annual maps from 1992 to 2015 (Li et al., 2018), to fractional cover following Poulter (2015) using the conversion table in Forkel et al. (2017). Landscape fragmentation was represented by cropland cover, two landscape heterogeneity indexes and road density. This categorization is by no means exhaustive, however all three of these factors have been shown to influence fire activity and spread (Pfeiffer et al., 2013; Andela et al., 2017; Povak et al., 2018; Kelley et al., 2019; Harrison et al., 2021; Pausas and Keeley, 2021). Vector ruggedness measure (VRM) and topographic position index (TPI) were used to represent topographic controls (Sappington et al., 2007). VRM captures variability in slope and aspect into a single measure, providing a measure for terrain heterogeneity, whilst TPI provides information on valleys (negative values) and ridges (positive values). We obtained 50km aggregated information for these variables, derived from the digital elevation model products of global 250 m GMTED2010 and near-global 90 m SRTM4.1dev (Amatulli et al., 2018). Although the data layers only cover 2010, it was assumed that there would be no significant changes in VRM or TPI from 2010 to 2015 at this resolution. Fractional annual cropland cover was taken from version 3.2 of the HistorY Database of the global Environment (HYDE 3.2: Klein Goldewijk et al., 2017) database, which provides annual data from 2000 to 2017 at 0.25 × 0.25° resolution. Road density was obtained from the Global Roads Inventory Project (GRIP) database (Meijer et al., 2018), which provides average road density from 1979-2015 (although >50% of the data is from 2010 or later) at 0.5 × 0.5° resolution.

Climate

We calculated the total monthly number of dry days (DD), monthly mean daily vapour pressure deficit (VPD), monthly mean daily diurnal temperature range (DTR) and monthly mean wind speed from the WFDE5 bias-adjusted ERA5 dataset (Cucchi et al., 2020) (Supplementary Chapter 2). This provides hourly data from 1979 to 2018 at 0.5 × 0.5° resolution.

Ignition sources

Annual values of population density, representing the potential for human ignitions, were taken from HYDE3.2. Mean monthly lightning ground-strike density, representing potential natural ignitions, was obtained from the Worldwide Lightning Location Network (WWLLN) Global Lightning Climatology (WGLC) dataset (Kaplan & Lau, 2021). This contains global monthly gridded data at 0.5 × 0.5° resolution from 2010 to 2020.

Data processing

A seasonal climatology over the common 6-year period from 2010 to 2015 was constructed for all variables with monthly data, eliminating inter-annual variability. This was the only common period for all the variables but, given the strong spatial patterns involved, we assume this is sufficiently long for our purpose. Annual variables were averaged over the six years. For monthly data, a single global layer was constructed from the seasonal climatology. For each grid cell, the value of the month with (on average) the largest DTR, and the highest VPD and mean number of dry days were selected. Wind speed value was taken from the hottest month of the year (determined from the WFDE5 2 m air temperature (Cucchi et al., 2020)). For lightning, the mean value over the seasonal climatology was selected.

Additionally, we included two seasonality predictors to account for periods of high vs low productivity (seasonality of GPP) and wet vs dry seasons (seasonality of DD). These seasonality predictors were constructed from the GPP and DD climatology, respectively. To capture the seasonality of GPP, we divided the range of monthly values from the seasonal climatology by the mean value of all 12-months. The same was done to capture the seasonality of DD. For road density and the vector ruggedness measure, no additional processing was performed. This provided a set of 16 predictors (Table 3). For the fire variables, the mean value over the seasonal climatology was selected. All variables were re-gridded to a 0.5 x 0.5 ° resolution grid to order to be compatible with the lowest resolution datasets and all analysis were conducted at this scale.

Table 3. Summary of predictor and fire response variables

Predictors	**Data source**	**Abbreviation**	**Transformation**
Vegetation, land cover and landscape fragmentation			
Annual gross primary production (g C m^{-2} a^{-1})	P-model (Stocker et al., 2020)	GPP	logarithmic
Gross primary production seasonality (unitless)	P-model (Stocker et al., 2020)	GPP_seasonality	Logarithmic
Fractional shrubland cover	ESA CCI Landcover	Shrub	none
Fractional grassland cover	ESA CCI Landcover	Grass	none
Fractional tree cover	ESA CCI Landcover	Tree	none
Road Density (km^{-2})	GRIP (Meijer et al., 2018)	Roads	square root
Fractional cropland cover	HYDE 3.2 (Klein Goldewijk et al., 2017)	Crop	none
Vector Ruggedness Measure	(Amatulli et al., 2018)	VRM	none
Topographic Position Index	(Amatulli et al., 2018)	TPI	none
Climate			
Mean monthly number of dry days	WFDE5 (Cucchi et al., 2020)	DD	logarithmic
Seasonality of monthly number of dry days (unitless)	WFDE5 (Cucchi et al., 2020)	DD_seasonality	logarithmic
Maximum mean monthly vapour pressure deficit (Pa)	WFDE5 (Cucchi et al., 2020)	VPD	logarithmic
Maximum mean monthly diurnal temperature range (K)	WFDE5 (Cucchi et al., 2020)	DTR	logarithmic
Mean wind speed of the hottest month (m s^{-1})	WFDE5 (Cucchi et al., 2020)	Wind	logarithmic
Ignition sources			
Population density (km^{-2})	HYDE 3.2 (Klein Goldewijk et al., 2017)	Popd	square-root
Mean monthly lightning ground-strikes (km^{-2})	WGLC WWLLN (Kaplan et al., 2019)	Light	square-root
Fire variables			
Monthly mean burnt area (fraction)	GFEDv4 (Randerson et al., 2018)	BA	none (logit link function)
Monthly median fire size (km^2)	Global Fire Atlas (Andela et al., 2019)	FS	min-max normalized (log link function)
Monthly median fire intensity (W. km^{-1})	MCD14ML (Giglio et al., 2006)	FI	Median FRP divided by square root of median fire size, min-max normalized (log link function)

Predictor variables were transformed appropriately (Table 3) to reduce differences in scale and improve interpretability (Schielzeth, 2010). GPP was the only predictor with zero values. We applied logarithmic transformation to GPP, ignoring zero values in the model. Since we assume no fire occurs where GPP was zero, the missing values were re-coded as zero afterwards. Square root transformation was applied to predictors representing densities, for which zero values were assumed to be meaningful. To reduce distortion introduced by a few (extremely rare) very large values, fire size and intensity were transformed to *z*-scores:

$$z_i = (x_i - \mu_i)/\sigma_i \qquad (1)$$

where μ_i is the mean and σ_i is the standard deviation of the variable x_i, and values of x_i yielding *z*-scores > 3 or < –3 were excluded (Shiffler, 1988). The remaining values were scaled using the min-max transformation:

$$x_{ni} = [x_i - \min(x_i)]/[\max(x_i) - \min\,(x_i) \qquad (2)$$

to confine the range of the transformed (x_{ni}) values to the interval (0, 1). This scaling helps interpretability but does not interfere with the statistical distribution of values (Juszczak et al., 2002).

Statistical modelling

Generalized linear models (GLMs) have previously been used to model burnt area (Bistinas et al., 2014; Lehsten et al., 2010) because they provide highly interpretable results (Nelder & Wedderburn, 1972; McCullagh & Nelder, 1989). GLMs are useful because they (a) handle response variables with highly non-Gaussian error distributions without the problems introduced e.g. by log-transformation of response variables, (b) are embedded in a well-established (multiple regression) framework, which allows quantification of the independent effects of multiple predictors even if they are partially correlated with one another, and (c) generate partial residual plots showing the effect of each predictor while the others are held constant (Larsen & McCleary, 1972). The relative importance of each predictor was assessed using absolute t-values (the fitted regression coefficient of each predictor divided by its standard error) calculated with the package caret in R. These t-values are unitless and scale-invariant, and in addition to providing a simple measure of the importance of each predictor (Grömping, 2015), are directly related to the coefficient of determination (R^2): the squared t-value of each predictor x_i represents the reduction in R^2 that occurs when that predictor is removed from the model (Bring, 1996; Darlington, 1968). Thus, the larger the t-value of a predictor, the more variance it explains. Variance inflation factors (VIF) were examined to evaluate multicollinearity among predictors. A VIF of 1 indicates no collinearity; we eliminated predictors with VIF values > 5 (O'Brien, 2007). We used normalized mean error (NME) to evaluate the performance of the models, following Kelley et al., (2013). NME is a standard metric to assess global fire model performances, allowing direct comparison with these other models (Boer et al., 2019; Kelley et al., 2019; Hantson et al., 2020). NME is defined as $NME = \frac{\sum A_i |obs_i - sim_i|}{\sum A_i |obs_i - \overline{obs}|}$ (3)

where the difference between observations (obs) and simulation (sim) are summed over all cells (i) weighted by cell area (Ai) and normalized by the average distance from the mean of the observations (obs). An NME score has no upper limit, but smaller values signify better performance with a 0-value meaning perfect fit between observed and simulated values. All analysis was conducted in R using the stats, car, benchmarkMetrics and visreg packages.

Fractional BA was equated with the probability of burning, ranging between 0 and 1. We assumed this probability to follow a quasi-binomial distribution, and applied the logit link function. The distribution of fire size and intensity is hypothesized to follow a power law (Kumar et al., 2011;

Hantson et al., 2016a, 2016b). We assumed a quasi-Poisson distribution for both variables (due to their large overdispersion, with many very small values) and applied the log link function.

All three models were initially constructed using all 16 predictors (Supplementary Chapter 2). Population density has been hypothesized to indicate landscape fragmentation (Bistinas et al., 2014; Knorr et al., 2014) but is highly correlated with road density (r=0.31). Therefore, we made two additional model runs, with all predictor variables excluding either population density or road density, to assess how much of the variance was explained by these predictors when the other is not present (Supplementary Chapter 2). VPD, the absolute difference in water vapor content of the air and the water holding capacity of the atmosphere, influences long-term plant growth and photosynthesis (Williams et al., 2013; Abatzoglou et al., 2016; Grossiord, et al., 2020) but GPP seasonality is correlated with VPD (r=0.71). We therefore made two separate model runs, using all predictors but excluding either GPP seasonality or VPD (Supplementary Chapter 2) From these runs, we present the best model for each fire property. Only predictors with p $<10^{-5}$ were retained, resulting in three final models that includes only predictors with substantial explanatory power.

Results

All 16 predictors showed significant relationships with BA (Table S2). GPP (t = 63.00), DD (t = 70.23) and DD seasonality (t = 59.26), grassland cover (t = 52.91), and VPD (t = 39.11) showed strong positive relationships with BA. Shrubland cover (t = 26.35), DTR (t = 19.82) and TPI (t = 18.86) also showed positive relationships with BA. Lightning (t = 12.35) and population density (t = 10.64) showed positive relationships with BA (the relationship with population density however became negative when road density was excluded). Road density (t = −37.32), VRM (t =

−21.39), tree cover (t = −18.74), cropland (t = −10.05) and wind (t = −6.80) and showed negative relationships with BA (Figure 5).

Eleven of the original 16 predictors were retained in the final fire size model (Table 4). GPP, grassland cover, TPI and population density were statistically insignificant, and seasonality of DD did not meet the t-value threshold (Table S2). DTR (t = 14.46), and wind speed (t = 14.41), followed in importance by DD (t = 11.16), shrubland cover (t = 7.61), lightning (t = 5.50) GPP seasonality (t = 5.18) and VPD (t = 5.12) all showed positive relations with fire size (Figure 5). Cropland cover (t = −22.42), road density (t = −16.47), VRM (t = 5.78) and tree cover (t = −5.25) showed negative relationships with fire size (Figure 5).

Only nine of the original 16 predictors were retained in the final model for fire intensity (Table 4). DTR, wind speed cropland cover and TPI were statistically insignificant and VRM and seasonality of GPP did not meet the t-value threshold (Supplementary Chapter 2). Tree cover (t = 9.08) and road density (t = 8.58) showed positive relationships with FI, whereas VPD (t = −47.55), GPP (t = −18.47), DD (t = −16.18) and DD seasonality (t = −14.27) population density (t = −13.49) and lightning (t = −7.15) all showed negative relationships (Figure 5).

Excluding population density did not change the significance or sign of any relationship with burnt area, fire size or fire intensity. Excluding road density led to a weak (p = 0.05) negative relationship between population density and BA, a highly significant negative relationship with FS, but no change for FI (Table S3). Excluding VPD lead the seasonality of GPP to become insignificant with BA and to show a weak (p=0.06) positive relationship with FS. For FI, the exclusion of VPD lead to a large increase in the strength of the seasonality of GPP (from t = 3.32 to t = 27.67) (Table S4).

Table 4. Summary statistics with regression coefficients, *t*-values, and variance inflation factors (VIF) for each of the final models. Predictors included were all significant at $t > 4.5$ ($p < 10^{-5}$).

Predictors	Burnt area			Fire size			Fire intensity		
	Coefficient	*t*-value	VIF	Coefficient	*t*-value	VIF	Coefficient	*t*-value	VIF
(intercept)	-48.25	-103.6		-13.09	-25.75		6.43	44.85	
Gross primary production (g C m^{-2} a^{-1})	1.76	63.00	4.13	–	–	–	-0.21	-18.47	3.04
Seasonality of gross primary production	0.59	14.78	2.43	0.30	5.18	3.29	–	–	–
Fractional tree cover	-0.93	-18.74	2.92	-0.42	-5.25	2.19	0.19	9.08	2.20
Fractional shrubland cover	1.39	26.35	1.70	0.64	7.61	1.29	–	–	–
Fractional grassland cover	2.93	52.91	1.56	–	–	–	-0.35	-11.91	1.18
Road density (km^{-2})	-0.05	-37.32	1.44	-0.04	-16.47	1.40	0.00	8.58	1.80
Fractional cropland cover	-0.79	-10.05	2.15	-3.51	-22.42	1.42	–	–	–
Vector Ruggedness Measure	-188.70	-21.39	1.55	-62.28	-5.78	1.50	–	–	–
Topographic Position Index	0.43	18.86	1.33	–	–	–	–	–	–
Mean monthly number of dry days	4.54	70.23	2.89	1.14	11.16	2.30	-0.31	-14.27	1.95
Seasonality of monthly number of dry days	1.33	59.26	2.57	–	–	–	-0.15	-16.18	1.97
Maximum mean monthly vapour pressure deficit (Pa)	1.35	39.11	1.78	0.31	5.12	3.72	-0.66	-47.55	2.03
Maximum mean monthly diurnal temperature range (K)	0.87	19.82	1.78	1.24	14.46	1.91	–	–	–
Mean wind speed of the hottest month (m s^{-1})	-0.20	-6.80	1.93	0.80	14.41	2.20	–	–	–
Mean monthly lightning ground-strikes (km^{-2})	0.94	12.35	1.66	0.83	5.50	2.06	-0.30	-7.15	2.11
Population density (km^{-2})	0.02	10.64	1.71	–	–	–	-0.01	-13.49	1.56
R^2 (McFadden, 1974)	0.69			0.29			0.27		

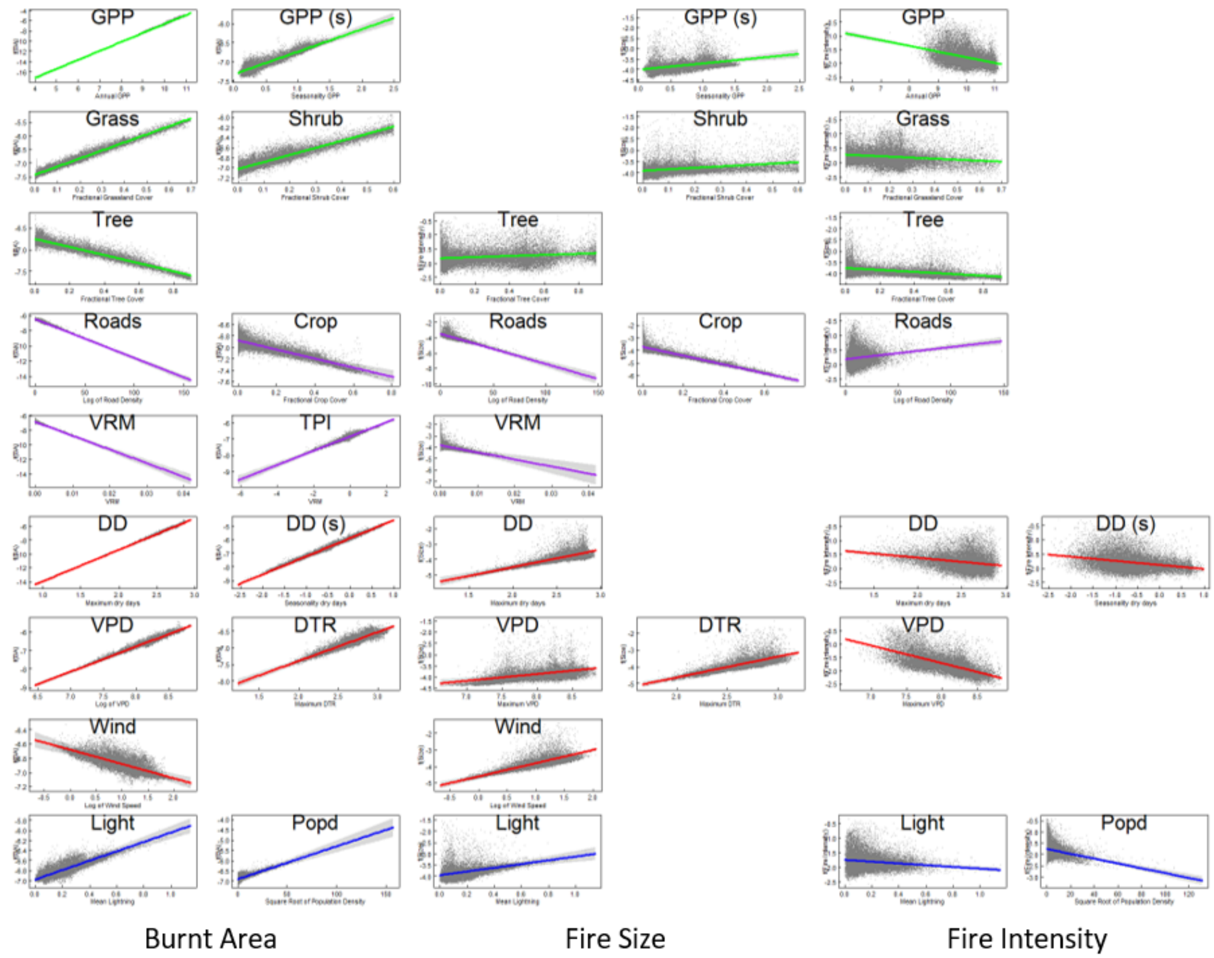

Figure 5. Partial residual plots for burnt area, fire size and fire intensity as functions of (GPP) gross primary production, (GPP (s)) seasonality of GPP, (shrub) shrubland cover, (grass) grassland cover, (tree) tree cover, (roads) road density, (crop) cropland, (VRM) vector ruggedness measure, (TPI) topographic position index, (DD) dry days, (DD (s)) dry days seasonality, (VPD) vapour pressure deficit, (DTR) diurnal temperature range, (wind) wind speed, (popd) population density and (light) lightning ground-strikes . Green represents vegetation and land cover predictors; purple represents fragmentation predictors; red represents climate predictors; blue represents ignition source predictors.

The strongest relationships differed between models. BA was driven above all by variables related to fuel availability (GPP and grass cover: positive relationships) and dryness (DD and the seasonality of DD: positive relationships) (Figure 6). Cropland cover and road density (negative relationships) were the two strongest drivers of FS (positive relationships), followed closely by

DTR and wind speed (positive relationships) (Figure 6). VPD and GPP showed the strongest relationships with FI (Figure 6), both being negative relationships.

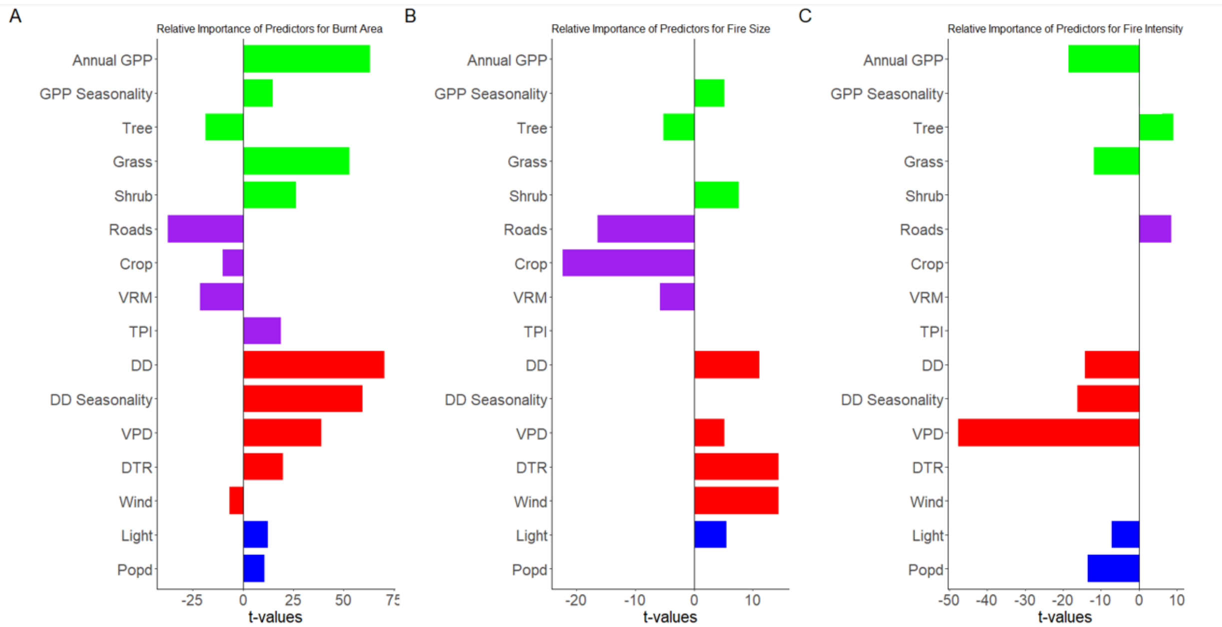

Figure 6. *t*-values for each predictor included in the final burnt area (A), fire size (B) and fire intensity models (C) showing relative importance of each predictor. The larger the absolute *t*-values of a predictor within a model, the more variance that individual predictor explains in that model. Green represents vegetation and land cover predictors; purple represents fragmentation predictors; red represents climate predictors; blue represents ignition source predictors.

The predictive power of the BA model ($R^2 = 0.69$) was substantially greater than that for FS ($R^2 = 0.29$) or FI ($R^2 = 0.27$), suggesting these last two properties are influenced by factors not included in the analysis. Despite modest R^2 values, however, all three models capture the broad geographic patterns of the observations (Figure 7). We obtained NME scores of 0.51, 0.86 and 0.86 for the burnt area, fire size and fire intensity models, respectively. Our burnt area and fire size models outperformed all models included in the Fire Intercomparison Project, which had NME scores ranging from 0.60 to 1.10 for burnt area and 0.96 to 0.98 for fire size (Hantson et al., 2020).

Although no direct comparison with the Fire Model Intercomparison Project (FireMIP) models is possible for fire intensity, this model performed as well as the fire size model. All three models perform better than a null mean model, which assumes the observational mean globally and produces an NME score of 1. All three GLMs tend to compress the reconstructed range of values, leading to apparent over- (under-) prediction at the low (high) extremes. However, the partial residual plots (Figure 5) do not show systematic biases suggesting that the apparent compression may simply reflect the highly stochastic nature of wildfire. The fitted models represent an estimate of the most probable outcome, whereas the observations are what actually happened – including some exceptionally large and/or intense fires, but also many grid cells where no fires were detected. The observations also have a systematic low-end bias, as fires smaller than a certain size are not detected by MODIS (Ramo et al., 2021; Roteta et al., 2019).

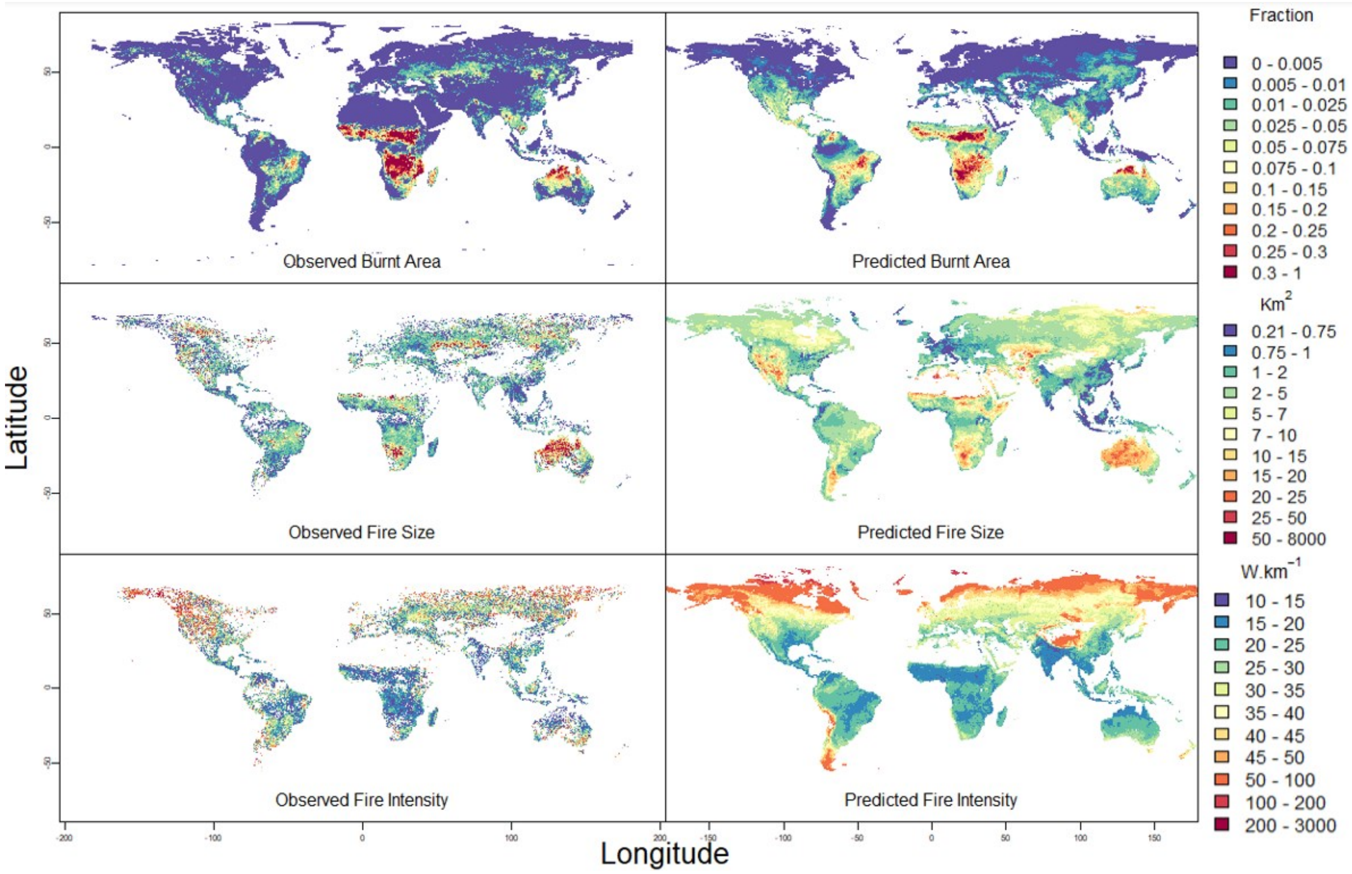

Figure 7. Observed (left) and predicted (right) annual burnt area (fraction), monthly median fire size (km^2) and monthly median fire intensity (W km^{-1}).

Discussion

We have shown that the environmental controls on geographic patterns of burnt area, fire size and fire intensity are different. Here we discuss these differences, how they might be interpreted, and their implications for improving predictive models.

Burnt area was shown to be primarily driven by fuel availability (represented by GPP and grass cover) and dryness (particularly DD, but also VPD and DTR) and constrained by road density. These results are consistent with previous research (Bistinas et al., 2014; Andela et al., 2017; Forkel et al., 2019a, b; Kelley et al., 2019; Kuhn-Régnier et al., 2021) and with the global fire-productivity hypothesis that the main drivers of fire activity are fuel availability and fire weather, varying in importance globally along the productivity gradient (Pausas and Ribeiro, 2013). In addition, both lightning and population density positively influence burnt area. The apparent fire-suppressing effect of population density (noted by Bistinas et al., 2014 and Knorr et al., 2014, among others) is represented in our analysis by road density. Roads provide barriers to fire spread, hence the negative relationship of BA to road density. When this effect is accounted for, population density relates positively to BA. The positive relationship with TPI suggests that fractional burnt area increases as we move from valleys to ridges, and that ridges do not constrain burnt area. This result is in line with previous research suggesting that ridges do not necessary provide fire breaks, and that valleys, characterized by higher soil moisture, lower insolation, and higher terrain shading show stronger control on fire spread (Povak et al., 2018). Terrain heterogeneity (VRM) however, strongly constrains burnt area. Although wind speed promotes fire spread, wind speed was negatively related to burnt area, in line with previous research showing the limited effect of wind speeds on burnt area at a coarse global scale (Lasslop et al., 2015).

Factors promoting fire spread, namely wind speed and dryness (particularly DTR, but also VPD) were shown to be the primary drivers of *fire size* while cropland cover, road density, and terrain heterogeneity (VRM), all agents of landscape fragmentation, strongly constrain fire size. The effect of wind speed was significant for fire size. TPI was not statistically significant, suggesting that the presence of steep slopes and ridges do not necessarily control fire spread (Povak et al., 2018). This is consistent with research suggesting fuel continuity is important for FS (Hantson et al., 2015; Laurent et al., 2019; Viedma et al., 2009). In contrast with BA, FS showed no significant relationship to GPP or grassland cover – indicating fuel availability is less important for FS than burnt area, and that large fires tend not to occur in highly productive environments.

The *fire intensity* metric was shown to be positively influenced by tree cover and road density and constrained by dryness (particularly VPD, and also DD). Lack of precipitation has been shown to limit fuel build-up (Keeley and Syphard, 2017; Pausas and Keeley, 2021, Kuhn-Régnier et al., 2021) and high atmospheric dryness (VPD) limits plant growth (Fu et al., 2022). The negative relationship with dryness is therefore not surprising since we expect fuel load to be an important driver of fire intensity. Although GPP is negatively related to the fire intensity measure, when VPD was excluded, the seasonality of GPP became the strongest driver of the FI model, an effect that did not translate into the other two models. This would suggest that sufficient atmospheric moisture along with seasonal changes in productivity, provide the dense fuel loads necessary for intense fires. These dense fuel loads are mostly restricted to areas with high tree cover, explaining the negative relationship with grassland and shrubland cover (Archibald et al., 2018, 2013; Luo et al., 2017). The overall negative relationship with GPP could therefore be explained by intense fires mainly occurring in regions with a seasonal variation in productivity, more characteristic of the high latitude forests than the more productive, tropical ones. A plausible reason for the positive relationship between FI and road density is the correlation between intense deforestation fires and the access roads required in remote forest areas. The observed negative relationship between lightning and FI is expected since frequent fire limits fuel build-up (Luo et al., 2017; Pausas and Ribeiro, 2013). Similarly, the negative relationship between population density and FI can be interpreted as a trade-off between the frequency and intensity of fires, probably compounded by active fire suppression in densely populated regions.

The FI metric shared few strong predictors with either of the other models. It was not limited by landscape fragmentation; wind speed and DTR were insignificant, and it showed an opposite relationship with dryness to the other models. This implies that the widely assumed positive relationship between fire intensity and fire size does not hold generally. Saturation of this relationship in fire-prone ecosystems (Laurent et al., 2019) has been attributed to feedback between burnt area and fuel connectivity, with landscape fragmentation increasing through the fire season due to previous burns, thus limiting fire size. Our results are consistent with this but suggest additional factors may influence the relationship between fire size and intensity. The limiting effect of dryness on FI suggests fuel loads are important, consistent with previous research (Kuhn-Régnier et al., 2021; Forkel et al., 2019a). Antecedent conditions and current dryness may promote fine and flammable fuels that favour large but cooler fires, while limiting build-up of the larger, more dense fuels required for intense fires (Hantson et al., 2015; Kuhn-Régnier et al., 2021).

Some of the original 16 predictors proved unimportant for the FS and FI models. Although all predictors included in the final models were highly significant ($p < 10^{-5}$) the partial residual plots suggest that there may be cases where the relationship is not linear (e.g. GPP), although in no case did the inclusion of a non-linear (polynomial) term in the models improve predictability. Together with the relatively low level of predictability of these two models, this suggests that other factors need to be investigated. There is growing evidence of fire regimes differing in similar biomes, as well as different biomes showing similar fire regimes – phenomena that cannot be explained without consideration of fire-adaptive plant traits (Archibald et al., 2018; Pausas et al., 2016; Pausas and Ribeiro, 2017b; Pausas, 2015; Hollingsworth et al., 2013). The boreal forests in North America and Eurasia are a case in point, where crown and surface fires respectively are dominant (Wooster & Zhang, 2004; Wirth, 2005; Sitnov & Mokhov, 2018). The distribution of fire-adaptive plant traits may be crucial to understand fire size and intensity (Harrison et al., 2021). Unfortunately, although there is information about fire-adaptive traits for some regions, including southern Europe and eastern Australia (Tavşanoğlu & Pausas, 2018; Falster et al., 2021), such information is limited elsewhere; this is a key data gap.

The results of this Chapter have implications for fire modelling. Process-based models generally rely on the product of fire counts and fire size to simulate burnt area. Our results suggest that the controls on burnt area, fire size and fire intensity should be modelled separately. Our results also add to the growing literature suggesting the use of population density to determine number of ignitions should be reviewed (Bistinas et al 2014, Knorr et al 2014, 2016, Andela et al 2017). Our results suggest it would be better to include landscape fragmentation explicitly as a control on fire spread. Population density apparently has a globally negative effect on burnt area unless an alternative measure of landscape fragmentation, such as road density, is included (Table S3). Thus, population density as used in current models is a surrogate for human fire suppression and landscape fragmentation (Harrison et al., 2021; Knorr et al., 2014; Knorr et al., 2016; Bistinas et al., 2013); any positive impact of population on ignitions will only be captured when fragmentation is explicitly considered. Some process-based models account for the emergent relationship between population and fire properties (Harrison et al., 2021), whereby increasing population density leads to increased ignitions up to a threshold and further increases lead to suppression (Rabin et al., 2017). We have shown that some elements of landscape fragmentation show strong spatial control on fire spread that can be modelled at a global scale. In addition to factors of landscape fragmentation considered here, additional features such as deforestation, non-flammable land cover and previous burns can all fragment the landscape and thus effect fuel continuity (Laurent et al., 2019; Harrison et al., 2021; Pausas and Keeley, 2021). There is a pressing need to investigate how each of these features of landscape fragmentation influence different aspects of the fire regime and integrate them to global wildfire modelling explicitly. Although lightning showed a positive relationship with BA and fire size, the relationship was not particularly strong. Lightning also constrained fire intensity, possibly via a trade-off between intensity and frequency. Process-based models may therefore have overestimated the importance of ignition sources generally. Indeed, fire-enabled DGVMs struggle to simulate fire starts accurately (Forkel et al., 2019).

We have represented fire size using data from the Global Fire Atlas and intensity with FRP values from MCD14ML dataset. The Global Fire Atlas relies on the MODIS sensor, so the minimum size of a recorded fire is one MODIS pixel (0.21 km^2) and thus our data does not include fires smaller than this. However, the environmental drivers of small fires are not expected to differ from those of larger fires. Although FRP has been used as a measure of fire intensity, it represents the radiative energy emitted and does not account for convection and conduction. Fire intensity in the Rothermel equation represents the intensity of the flaming front of an individual fire, whereas retrieved FRP values from MCD14ML integrate radiative energy over a 1 km × 1 km pixel. The normalization introduced here provides a partial solution to this problem and accurately highlights the regions of high fire intensity. However, work is required to derive fireline intensity more reliably from remotely sensed products.

This analysis did not account for any inter-annual variability, such as changes in the length of the fire season or the departure of the established fire regime within a given year. Though these factors have been shown to influence the different aspects of the fire regime (Pausas, 2004; Pausas and Keeley, 2021), we were interested in the underlying climatic, land cover and ignition spatial controls when the effect inter-annual variability was removed. Understanding these controls for different aspects of the fire regime is a first and crucial step to predicting how they will respond to different conditions between years and in the future. The timeframe of this analysis was relatively short, though like timeframes used in previous empirical analyses due to similar data availability issues. The strong spatial patterns displayed both by the fire variables and the predictors meant that key relationships could nonetheless be established. Each model reproduces the spatial patterns of regions of high burnt area, large fire size and high fire intensity, allowing useful conclusions to be drawn.

Chapter 3: The response of global wildfire regimes to Last Glacial Maximum carbon dioxide and climate

The previous chapter established the key global controls of burnt area, fire size and fire intensity by developing three standalone GLM models. Making use of these models, the aim of this chapter is to address the question of whether low atmospheric CO_2 levels and their impact on vegetation, cooler climate, or a combination of both were responsible for limiting wildfire activity and the distribution of global fire regimes at the Last Glacial Maximum (**RQ2**). It is structured as a paper, with an introduction, followed by a description of the methodology, a presentation of the results and finally a discussion. This work was published in *Biogeosciences* in September 2023 under the title "The response of fire regimes to Last Glacial Maximum carbon dioxide and climate" and has been reworded in some parts, however the methodology, results and discussion remain unchanged.

Introduction

Climate influences the occurrence of wildfires both through fire weather, which affects the probability of wildfire start and spread, and the long-term establishment of vegetation which is strongly controlled by temperature and precipitation (Bradstock, 2010; Pausas & Ribeiro, 2013). It has been suggested that current climate change, driven by increasing atmospheric CO_2 levels, will increase wildfire risk in many regions through increased fuel dryness whilst potentially reducing wildfire risk in some regions due to decreasing fuel availability (e.g. Abatzoglou et al., 2019a; Bowman et al., 2020; Harrison et al., 2021; Rogers et al., 2020). However, atmospheric CO_2 levels also affect fuel loads independently of climate through physiological effects on photosynthesis which cascade into plant growth rates (Bond et al., 2003; Bond & Midgley, 2012;

Kgope et al., 2010). Much emphasis has been placed on recent and future changes in fire weather (see e.g. Abatzoglou et al., 2019; Betts et al., 2015; Flannigan et al., 2013; Jolly et al., 2015). However, increases in atmospheric CO_2 concentrations promote vegetation productivity, thus altering fuel availability and loads, as well as affecting fuel types through e.g. woody thickening (Buitenwerf et al., 2012; Donohue et al., 2013; Knorr et al., 2016; Martin Calvo et al., 2014; Martin Calvo & Prentice, 2015; Pausas, 2015). Fuel properties have different effects on different aspects of the fire regime, with fire size strongly constrained by fuel continuity and fire intensity limited by fuel loads as demonstrated in Chapter 2. Thus, CO_2-induced changes in vegetation properties will most likely affect these aspects of wildfire regimes differently.

One reason the impact of CO_2 on wildfires is poorly constrained is the difficulty of isolating it based on observations alone. Satellite records only span ~25 years, a relatively short period to monitor the effect of changing CO_2 levels on the vegetation properties that influence wildfires. Furthermore, changes in atmospheric CO_2 levels and climate are temporally correlated, and since both affect vegetation, it is difficult to attribute changes in observations to one or the other. An alternative approach is to use process-based fire-enabled vegetation models which explicitly account for the physiological effects of CO_2 and can be used to examine the temporal and spatial patterns of wildfires under different conditions. Process-based models have been used to examine the impact of climate and atmospheric CO_2 changes on both vegetation and wildfire at the last glacial maximum (LGM; 21,000 years ago) (Martin Calvo et al., 2014; Martin Calvo & Prentice, 2015). The LGM is a useful out-of-sample experiment since the climate forcing is of similar magnitude as the change expected by the end of the century in high-end scenarios, though of opposite sign (Kageyama et al., 2021). The LGM had a generally colder and drier climate than today, with CO_2 levels ~ 185 ppm. Palaeorecords show reduced vegetation productivity and forest cover (Harrison & Prentice, 2003; Kaplan et al., 2016; Moreno et al., 2018), and ice core and sedimentary charcoal records indicate reduced biomass burning globally (Albani et al., 2018; Harrison et al., 2022; Marlon et al., 2016; Rubino et al., 2016). Although this reduction could reflect the colder and drier conditions, model experiments suggest that low CO_2 also played a crucial role. Experiments using the coupled biogeography and biogeochemistry model BIOME4 (Kaplan et al., 2003) showed that it was necessary to include the direct effect of CO_2 to simulate observed global and regional reduction in forest cover during the glacial (Bragg et al., 2013; Harrison & Prentice, 2003). Similarly, Martin Calvo et al. (2015) showed that low CO_2 was necessary to simulate the observed reduction of biomass burning in LGM experiments using the LPX fire-enabled vegetation model.

In this analysis, we use the three empirical models developed in Chapter 2 to explore the relative importance of climate and of CO_2 on the global spatial patterns of burnt area, fire size and fire intensity. We performed two experiments under realistic modern CO_2 and climate conditions (MOD climate/MOD CO_2 and LGM climate/LGM CO_2). We also performed two counterfactual sensitivity experiments to quantify the sensitivity of each wildfire property to climate and CO_2 independently (MOD climate/LGM CO_2 and LGM climate/MOD CO_2). Comparisons to LGM charcoal records from the Reading Palaeofire Database (RPD) (Harrison et al., 2022) were used to examine which experiments provided the most realistic spatial patterns.

Data and Methods

Experimental Design

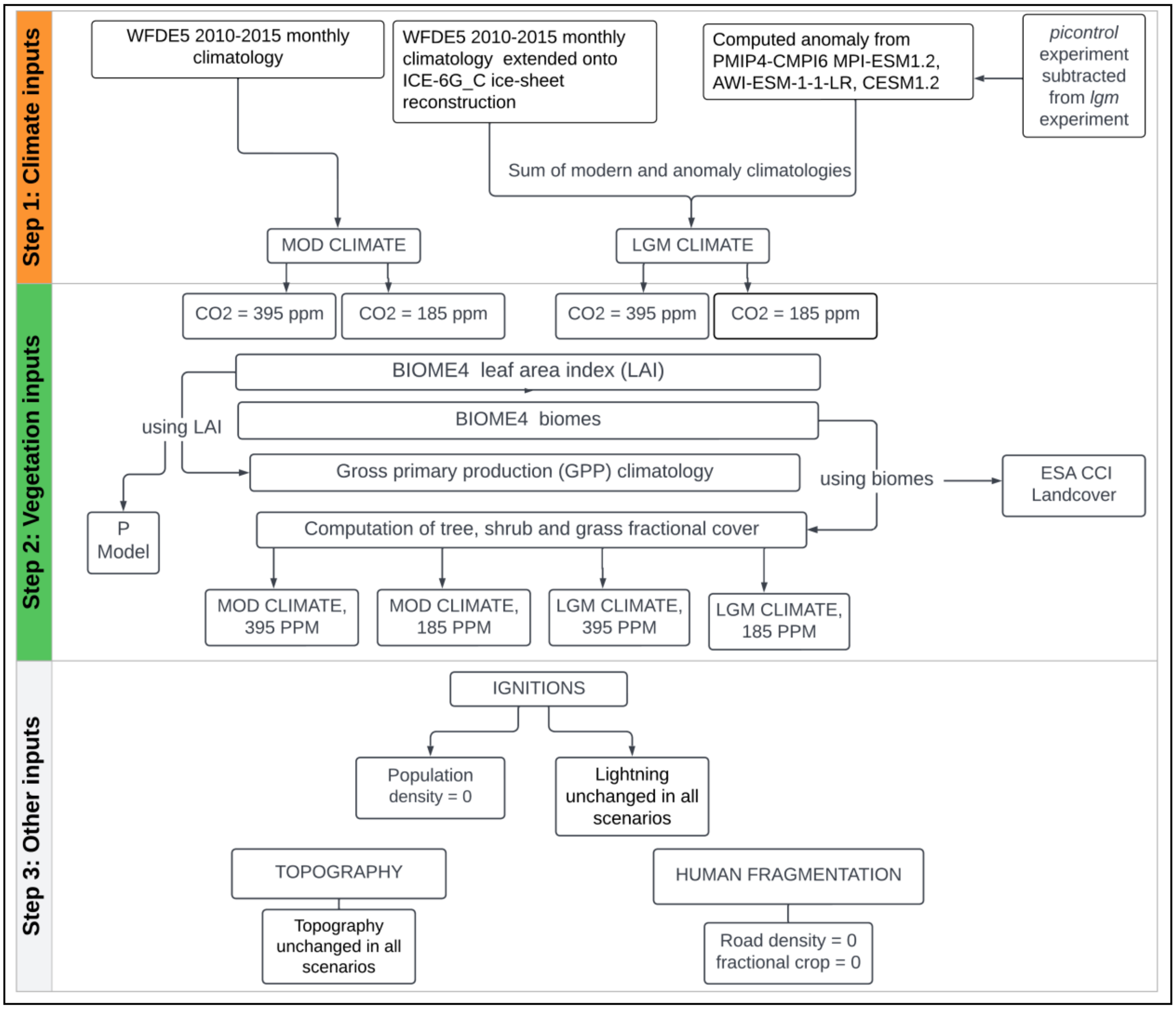

Figure 8. Flowchart of the method to obtain each of the four scenarios: MOD climate and MOD CO_2, LGM climate and LGM CO_2, MOD climate and LGM CO_2 and LGM climate and LGM CO_2.

In chapter 2, we developed empirical models of the global spatial patterns of burnt area (BA), fire size (FS) and fire intensity (FI) using generalized linear modelling (GLM) of modern observations. Here we use these models to simulate the global spatial patterns of burnt area (BA), fire size (FS) and fire intensity (FI) under four climate/ CO_2 scenarios (Figure 8). We used two realistic scenarios: (a) MOD climate and CO_2 conditions and (b) LGM climate and CO_2. We ran two sensitivity experiments (a) combining MOD climate and LGM CO_2 and (b) combining LGM climate and MOD CO_2 levels. The empirical models use climate, vegetation, topography, lightning ignitions, land cover, road density and human population density as predictors to represent the environmental controls on each of the wildfire properties.

Data collection and processing

Modern (MOD) climate data (daily temperature (T), daily precipitation (P), photosynthetic photon flux density (PPFD), monthly wind speeds (wind), vapour pressure deficit (VPD), monthly specific humidity (huss), cloud cover (cld), monthly pressure (Pa)) were obtained from the WFDE5 bias-adjusted ERA5 database (Cucchi et al., 2020) for 2010 to 2015. The number of monthly dry days (DD) (days with ≤ 1mm of precipitation), monthly diurnal temperature range (DTR) (daily maximum temperature – daily minimum temperature) and monthly vapour pressure deficit (VPD), a function of specific humidity, temperature and pressure were all calculated following the methodology in Chapter 2. Seasonal climatologies were derived for all variables eliminating inter-annual variability. For each grid cell, values from the month with (on average) the mean number of DD, the largest DTR, and the highest VPD were selected. Wind speed value was taken from the hottest month of the year (determined from the WFDE5 2 m air temperature (Cucchi et al., 2020)). For lightning, the mean value over the seasonal climatology was selected. A seasonality predictor to account for wet vs dry seasons was constructed by dividing the range of monthly values from the seasonal DD climatology by the mean value of all 12 months. Expanded ice sheets in North America, Fennoscandia, Greenland, and Antarctica resulted in global sea levels ~ 120 m lower than today at the LGM. The modern climate data were extrapolated out onto the exposed shelves using the ICE-6G_C (Peltier et al., 2015) boundary conditions and a nearest neighbour approach from the GeoInterpolation package in R.

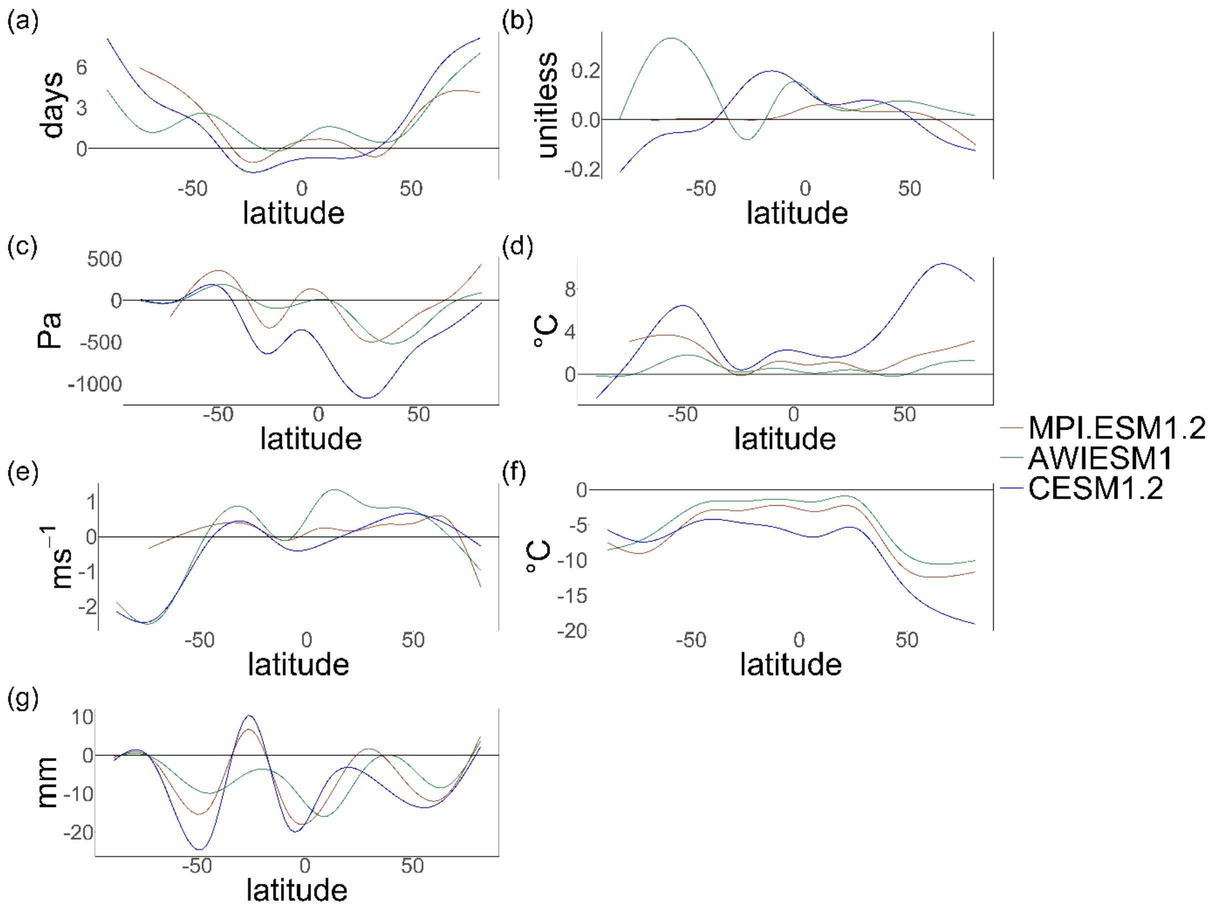

Figure 9. Latitudinal distribution of the LGM-MOD climate anomalies for MPI.ESM1.2 (orange), AWI-ESM1.2 (pink) and CESM1.2 (brown) for (a) the mean number of dry days, (b) the seasonality of dry days, (c) maximum monthly VPD, (d) maximum monthly DTR, (e) maximum monthly mean wind speeds, (f) mean monthly temperature and (g) mean monthly total precipitation. The zero-intercept line represents no change between LGM and MOD climate, with negative values representing lower values at the LGM and positive values representing higher values at the LGM.

LGM climate data were obtained from three models participating in the Palaeoclimate Modelling Intercomparison Project (PMIP) contribution to the sixth phase of the Coupled Model Intercomparison Project (CMIP6), AWI-ESM-1-1-LR (short name: AWIESM1) (Lohmann et al., 2020; Sidorenko et al., 2015), MPI_ESM1.2 (Mauritsen et al., 2019), CESM1.2 (F. Li et al., 2013;

Tierney et al., 2020) to represent a range of LGM climates (Figure 9). A seasonal climatology was derived for each climate variable from the PMIP *picontrol* experiment (pre-industrial conditions, PI) and the PMIP *lgm* experiment of the PMIP4-CMIP6 simulations. The difference between the PI and LGM values (LGM-PI climate anomalies) were calculated and added to the MOD climatology (LGM-MOD climate anomalies) (Figure 8). In the case of negative values which did not make physical sense (for example precipitation), these values were set to zero. We use the term climate anomalies to refer to the difference between the MOD climatology for each climate variable and the computed bias-adjusted LGM climatology for the same variable, consistent with the PMIP4 protocol (Kageyama et al., 2017). The use of anomalies is designed to minimize the impact of systematic model biases on the derived climate. This approach provided three LGM climate scenarios, resulting in twelve experiments for burnt area, fire size and fire intensity respectively.

We obtained MOD and LGM vegetation and gross primary production (GPP) using the coupled biogeography and biogeochemistry model BIOME4 (Kaplan et al., 2003) and a simple optimality-based model of GPP, the P Model (Wang et al., 2017; Stocker et al., 2020). BIOME4 was used to simulate biome distribution with modern day climate data (T, P, cld) setting CO_2 levels to 395 ppm (the annual mean from 2010-2015) and 185 ppm in turn. LGM biome distributions were simulated using the three different LGM scenarios, again setting CO_2 levels to 395 ppm and 185 ppm respectively. We derived mean fractional tree, shrub, and grass cover for each of these twelve experiments using the mean values for each biome from ESA CCI Landcover (W. Li et al., 2018). We also calculated fAPAR for each experiment from the leaf area index (LAI) computed by BIOME4 and obtained fractional cover of C_4 plants (Supplementary Chapter 3). We computed global monthly C_3 and C_4 photosynthesis using the P model using appropriate combinations of climate (T, VPD, ppfd and Pa), BIOME4-derived fAPAR and CO_2 concentration for the MOD and LGM scenarios (Figure 8). Total GPP was calculated as:

$$GPP_{monthly} = GPP_{c3}\left(1 - C4_{fraction}\right) + GPP_{c4}C4_{fraction} \,, \quad (4)$$

with GPP_{c3} and GPP_{c4} representing monthly C_3 and C_4 GPP values from the P Model and $C4_{fraction}$ representing the fractional C4 cover from BIOME4 (Table 5).

Table 5. Total annual gross primary production (GPP) (in PgC) estimates for each scenario.

Scenario	Modern climate	MPI_ESM1.2	AWIESM1	CESM1.2
Modern CO_2 (395 ppm)	149.37	106.63	112.06	88.44
LGM CO_2 (185 ppm)	66.54	55.49	69.61	50.37

This approach led to estimates of total burnt area, median fire size, and median fire intensity under modern conditions of a similar magnitude to the original GLM models and other global estimates (Andela et al., 2019; Humber et al., 2019) (Supplementary Chapter 3).

Topographic and lightning variables were assumed not to change between the LGM and the present day. We used modern values, extrapolated out onto the exposed shelves, for the LGM experiments. The GLMs developed in Chapter 2 include predictors associated with human activity, specifically human population density, road density and cropland cover. Population density is used as a measure of potential human ignitions and road density and cropland cover as measures of landscape fragmentation. As shown in Chapter 2, including these anthropogenic predictors in the GLM models was found to be essential to capture the global drivers of the observed spatial patterns of wildfires. This is because modern fire regimes are influenced by human activity on a global scale (e.g. Marlon et al., 2008; Bowman et al., 2020; Harrison et al., 2021). However, although the practice of foraging for plants by some hunter-gatherer communities at the LGM has been shown (Liu et al., 2013), we presume that there was no large-scale agriculture (or road networks) at the LGM. Additionally, information about pre-agricultural population sizes is limited and highly uncertain (see e.g. Williams et al., 2013; Gautney & Holliday, 2015) and though some regional models of human population do exist (Tallavaara et al., 2015), a reliable global product is not yet available. To avoid confounding effects due to the high uncertainty of human impacts on global wildfire regimes, we decided to exclude these anthropogenic predictors in all the experiments by setting them to zero. This ensured that differences between the experiments were driven solely by climate and CO_2. We performed sensitivity analysis to examine the impact of setting human predictors to zero under modern and LGM conditions (Supplementary Chapter 3). Whilst burnt area and fire size increase in the modern sensitivity analyses (especially in areas with high road density and cropland density such as Europe and India) the effect was negligible for fire intensity, highlighting the sensitivity of burnt area and fire size to human activity. Under LGM conditions, the effect of including human population was negligible for all three fire properties. This reflects the slight and localized human impact on the natural landscape at the LGM (Black et al, 2007; Fuller et al., 2014; Portenga et al., 2016).

When modelled GPP values were 0, burnt area, fire size and fire intensity were automatically set to 0. Modelled burnt area values smaller than 0.001 were assumed to imply no burning, thus under these conditions fire size and fire intensity were also assumed to be 0 since both GLM models were trained on data of existing fires (Supplementary Chapter 3).

The resulting burnt area, fire size and fire intensity anomalies refer to the difference between the MOD climate/MOD CO_2 experiment and the three other experiments since each experiment is considered to represent the long-term average spatial pattern for each fire property under the set experimental conditions. We used the sensitivity experiments to quantify the separate effects of CO_2 and climate on burnt area, fire size and fire intensity independently. We then used the realistic experiments to identify which predictors were driving the largest change between MOD and the three LGM scenarios by excluding one predictor at a time from the GLM models, re-running the LGM experiments and identifying which excluded variable caused the greatest change in the Burnt area, fire size and fire intensity MOD-LGM anomalies in each grid-cell. Comparing these results to the burnt area, fire size and fire intensity MOD-LGM anomalies of the full GLM models allowed us to determine if the predictor was responsible for an increase or a decrease in burnt area, fire size and fire intensity.

We also compared the spatial patterns of burnt area, fire size and fire intensity with sedimentary charcoal data from the Reading Palaeofire Database (RPD; Harrison et al., 2022). Sedimentary charcoal records provide a record of fire activity but may reflect changes in both burnt area or completeness of combustion (Power et al., 2008) so this comparison allowed us firstly to establish which of the fire regimes properties was most closely reflected in these records and secondly which of the scenarios produced the most realistic patterns of burning. Model outputs and the charcoal records were re-gridded to the coarsest resolution of the three climate models (2.5° x 1.875° resolution). We calculated the number of correctly predicted burnt area, fire size and fire intensity anomalies (same sign within a given grid-cell), separating positive and negative burnt area, fire size and fire intensity anomalies to assess the rate of false positives as well as false negatives for each scenario and each LGM climate scenario.

Results

Global burnt area was substantially reduced compared to the realistic MOD scenario under all three realistic LGM scenarios, decreasing by 72% for the coldest CESM1.2 LGM scenario, 62% for the MPI-ESM1.2 LGM scenario and 41% for the warmest AWIESM1 LGM scenario. The largest decreases were observed in sub-Saharan Africa (excluding the tropical regions) as well as northern Australia and the Indian subcontinent (MPI-ESM1.2 and CESM1.2 LGM scenarios). Some increases in BA were observed in Alaska (MPI-ESM1.2 and AWIESM1 LGM scenarios) as well as south-East Asia, Indonesia, Papua-New-Guinea, and the northern tip of Australia. Increases in Somalia and Central America were also observed (MPI-ESM1.2 and AWIESM1 LGM scenarios). The number of grid cells (excluding ice covered cells) in which no burning occurred was 3 times higher in the MPI-ESM1.2 and AWIESM1 LGM scenarios and 4 times higher in the CESM1.2 LGM scenario compared to the realistic MOD scenario. This was driven by the expansion of desert and tundra biomes at the LGM. The Arabian plate, Middle East, inland China and Australia, and the tips of South America and Africa saw burning reduced to zero. Nearly all burning above 60°N was excluded, except for Alaska under the MPI-ESM1.2 and AWIESM1 LGM scenarios, with the exclusion extending down to 50°N for the CESM1.2 LGM scenario (Supplementary Chapter 3).

Globally, there was a large decrease in global median fire size and fire intensity when considering all grid-cells (not covered in ice) because of overall global reduction in burning. Under all three LGM scenarios, global median fire size and fire intensity were reduced to 0 compared to ~5km^2 for FS and 40W.km^2 for fire intensity. However, when excluding grid-cells in which no burning occurred, both global median fire size increased compared to the realistic MOD scenario (by ~16% under the two less conservative scenarios (MPI-ESM1.2 and AWIESM1) and by 12%

under the CESM1.2 LGM scenario). The main increases in fire size occurred in the Central America, Amazonia, tropical Africa as well as the Indian Subcontinent and Europe and Asia between 30°N and 60°N (except for CESM1.2 which had very few positive fire size anomalies). The largest reductions were observed North America, southern Australia, Middle East, and the rest of Eurasia. Global median fire intensity also increased in regions that were burning under two of the LGM scenarios, by 11% under the CESM1.2 LGM scenario and by 4% for MPI.ESM1.2 LGM scenario. Under the AWIESM1 LGM scenario global median fire intensity decreased by 2% even when excluding grid-cells that were not burning. Despite this, changes in fire intensity were spatially consistent across all three LGM scenarios, with increases in fire intensity occurring primarily across the American and African continents, as well as the Mediterranean Basin and Europe and decreases occurring in Asia and inland Australia.

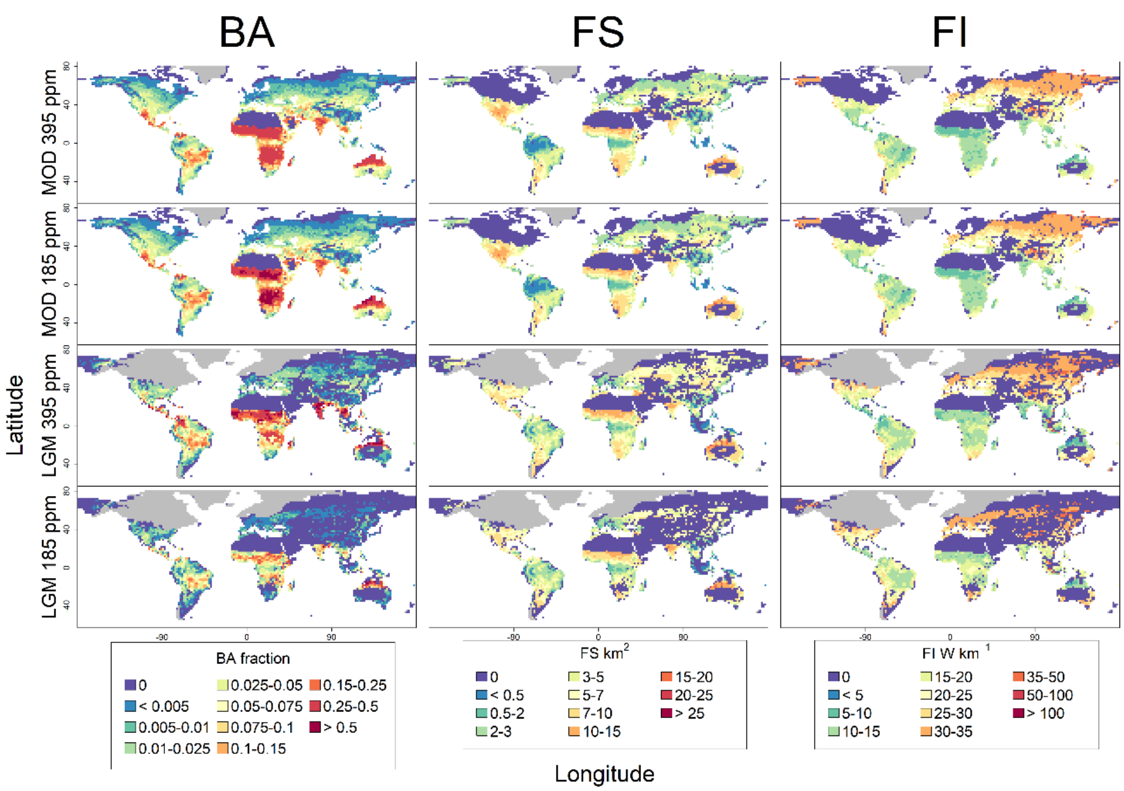

Figure 10. Experiments for BA, FS and FI for MPI-ESM1.2 LGM scenario (MOD 395 ppm and LGM 185 ppm represent the realistic modern-day simulation and LGM simulation, whilst MOD

185 ppm and LGM 395 ppm represent the CO_2 and climate sensitivity experiments respectively. The ice is shown in grey). (The other experiments can be found in S3)

Under low CO_2 levels with MOD climate (MOD climate/LGM CO_2) global burnt area decreased by ~ 70% under all three LGM scenarios (72% for CESM1.2 and AWIESM1, 73% for MPI-ESM1.2). Despite larger global decreased burnt area compared to the realistic LGM scenarios, the number of grid cells in which no burning occurred was only 1.7 times higher for MPI-ESM1.2 and AWIESM1 LGM scenarios and 1.5 times CESM1.2 LGM scenario compared to the realistic MOD scenario. The spatial pattern was consistent across all three LGM scenarios, with very few grid-points showing a positive burnt area anomaly relative to the MOD experiment. Though fire size increased slightly under this sensitivity experiment when burning did occur, this increase was concentrated in the tropical regions of South America and Africa (mainly Amazonia), (except for AWIESM1 where increases were observed across Eurasia). In burning grid-cells, global median fire intensity increased by ~ 15-18% in this sensitivity experiment (18% for MPI-ESM1.2 and CESM1.2, and 15% for AWIESM1). This spatial pattern was also consistent as with burnt area, with very few negative fire intensity anomalies, except for regions ~ 20-30°N and ~20-30°S.

Under MOD CO_2 and LGM climate, burnt area decreased by 41% compared to the MOD experiment for the CESM1.2 LGM scenario and by 4% for the MPI-ESM1.2 LGM scenario but increased by 48% for the AWIESM1 LGM scenario, showing a strong sensitivity to climate. The number of grid cells in which no burning occurred was of similar amplitude to the previous sensitivity experiment for the MPI-ESM1.2 and AWIESM1 LGM scenarios (~1.8 times higher compared to the realistic MOD scenario) but was much higher for the CESM1.2 LGM scenario (~3.5 increase). When burning occurred, the global median fire size increased under all LGM scenarios by 17% for CESM1.2, 25% for MPI-ESM1.2 and 23% for AWIESM1. These increases were concentrated in tropical Africa, central America, and Russia, with decreases shown in North America and South Africa. Global median fire intensity also increased under this sensitivity experiment by 2-3% for AWIESM1 and MPI-ESM1.2 but decreased by 5% for CESM1.2 LGM scenario, with decreases concentrated in Eurasia and North America.

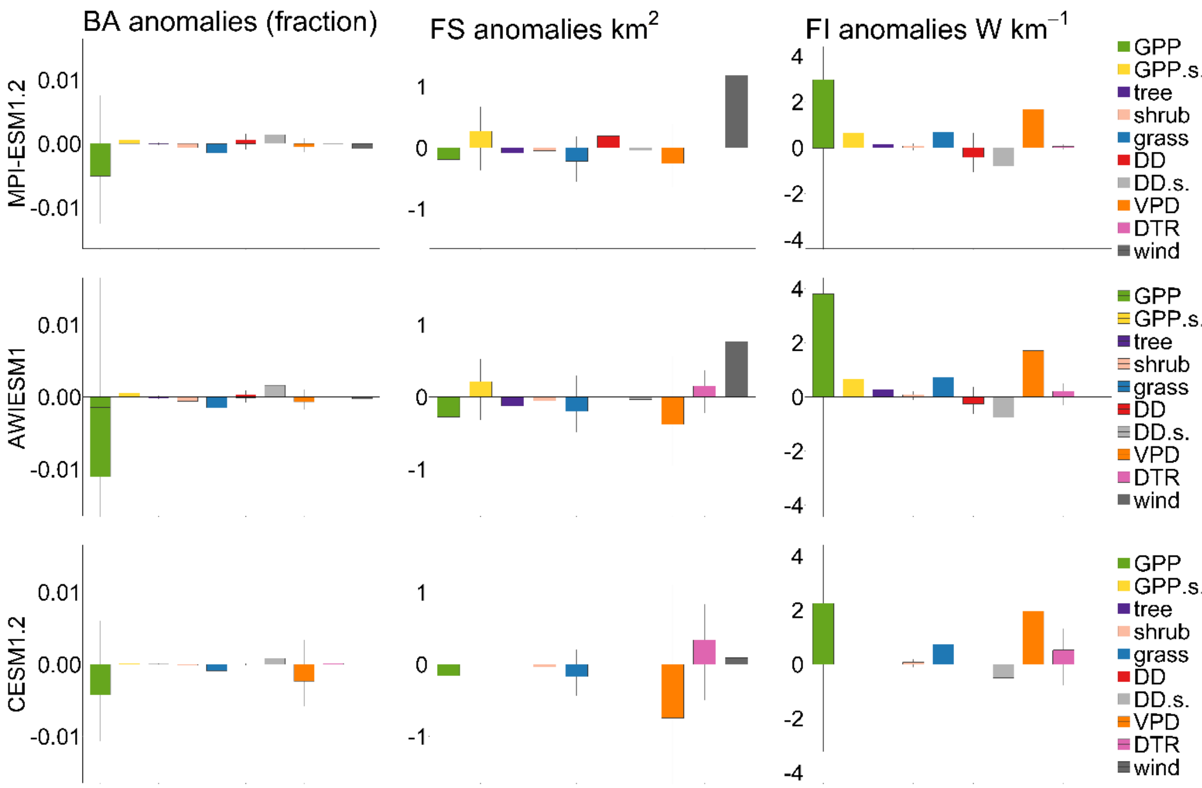

Figure 11. Boxplots showing relative importance of each predictor (GPP: gross primary production, GPP.s.: GPP seasonality, tree; tree cover, shrub; shrub cover, grass; grass cover, DD: dry days, DD.s.: dry days seasonality, VPD: vapour pressure deficit, DTR: diurnal temperature range, wind: wind speed) in driving the BA, FS or FI anomaly between the MOD 395 ppm and LGM 185 ppm experiment. For each grid cell common to both experiments (on modern-day continental shelves and masking the LGM ice sheets), the predictor which caused the largest change in the anomaly between the two experiments when it was excluded from the GLM model was retained, it is the change in anomaly that is shown here. This was taken as an indicator of relative importance of that predictor in driving the observed change for (a) the AWIESM1 LGM scenario, (b) the MPI-ESM-1.2 LGM scenario and (c) the CESM1.2 LGM scenario. A positive anomaly indicates the variable caused an increase in BA, FS or FI at the LGM and a negative anomaly indicates the variable caused a decrease in BA, FS or FI at the LGM.

Reductions in burnt area between the MOD and LGM scenarios were driven primarily by changes in GPP, grass cover, vapuor pressure deficit (VPD) and to a lesser extent dryness (dry days (DD) and dry-day seasonality (DD.s). Changes in fire intensity were driven by changes in GPP as well as VPD, with changes in GPP seasonality also leading to increased fire intensity in inland regions, reflecting both changes in climate and CO_2 levels for burnt area and fire intensity. Increased fire sie was largely driven by increased wind speeds, as well as DD and diurnal temperature range (DTR) reflecting a strong climate effect as well as GPP seasonality. Decreases in fire size were driven by changes in GPP and grass cover, as well as VPD under the CESM1.2 LGM scenario and DTR under the AWIESM1 LGM scenario (Figure 11). Changes in GPP and grass cover were responsible for the largest reductions in burning, with these vegetation effects concentrated across Africa and much of Eurasia (Figure 12). In Amazonia, changes in DD were the most important factor, reducing burnt area and fire size (except for MPI-ESM1.2 which saw increased fire size driven by DD). Increased burnt area in western Alaska was driven by GPP in the MPI-ESM-1.2 and AWIESM1 LGM scenarios. Increased burnt area in tropical regions were driven by grass cover, GPP and DD changes. Changes in VPD across the northern latitudes, especially of north America and Europe, led to decreased burnt area in the most conservative CESM1.2 LGM scenario. FS decreased across the Americas and Eurasia in the CESM1.2 LGM scenario because of low VPD values which reduced the occurrence of burning and offset the increases caused by wind speed and DTR in the other two LGM scenarios. Low values of VPD drove increases in fire intensity across eastern North America, South America, western Africa, and South-East Asia.

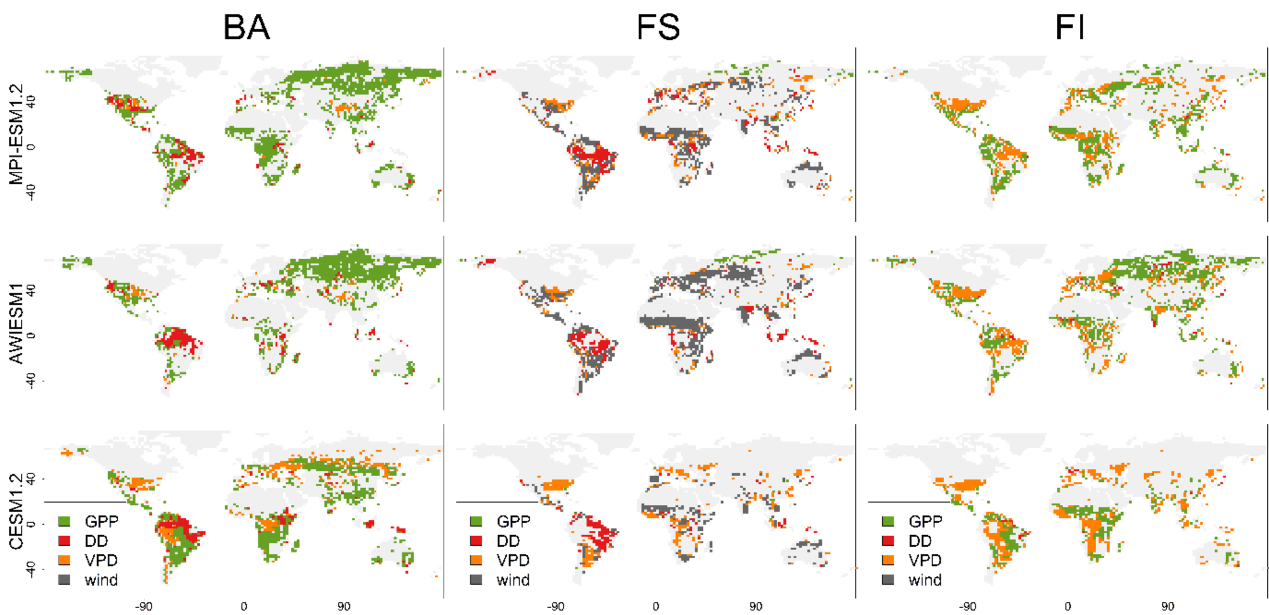

Figure 12. Map showing selection of four variables (GPP in green, DD in red, VPD in orange and wind in grey) responsible for some of the most important grid-cell drivers in reducing BA, increasing FS and FI for (a) AWIESM1 LGM scenario, (b) MPI-ESM1.2 LGM scenario and (c) CESM1.2 LGM scenario. Maps of most important grid-cell drivers for all variables and all experiments can be found in S3.

Comparing the spatial patterns of the simulated burnt area anomalies with charcoal-based reconstructions of the sign of changes in biomass burning (RPD; Harrison et al., 2022) showed that the best overall match occurred when both the climate and CO_2 effect were considered, with a success rate of ~ 39-45% depending on the climate scenario. The MPI-ESM1.2 and AWIESM1 LGM scenarios produced the best overall matches. None of the MOD climate/LGM CO_2 experiments identified any of the positive BA anomalies shown by the charcoal records. The LGM climate/MOD CO_2 experiments identified around half (~ 10-17%) of the negative burnt area anomalies identified by the realistic experiment (17-20%) and the MOD climate/LGM CO_2 sensitivity experiment, and only performed marginally better than the realistic experiment in identifying the positive burnt area anomalies (Table 6). Thus, although this sensitivity experiment produced a similar overall agreement with the reconstructions as LGM climate/LGM CO_2 simulations, only the realistic scenarios produced similar success rates for both the negative and positive burnt area anomalies. Climate change alone produced too few negative anomalies matches; CO_2 changes alone resulted in no positive anomaly matches.

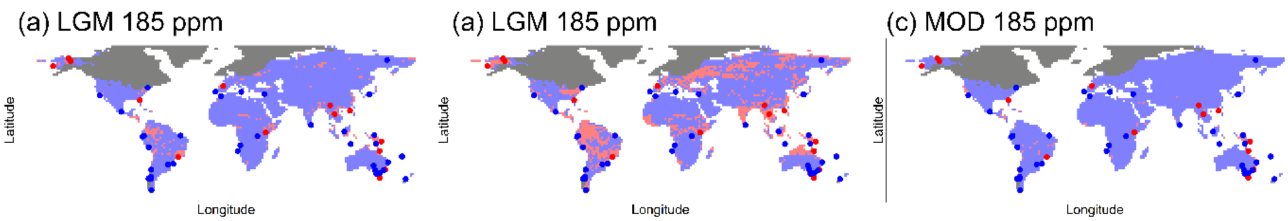

Figure 13. Comparison of BA anomalies between the experiment outputs from the MPI-ESM1.2 LGM scenario with charcoal records from the Reading Palaeofire Database (RPD) for (a) the realistic LGM experiment (b) the LGM climate/MOD CO_2 sensitivity experiment and (c) the MOD climate/LGM CO_2 sensitivity experiment The modelled positive LGM-MOD anomalies are shown in red and LGM-MOD negative anomalies in blue. Dotted red (positive anomaly) and blue (negative anomaly) points show the location of the RPD records for the LGM. The LGM ice sheets are shown in dark blue.

Table 6. Comparison of the sign in BA anomalies (between the MOD climate/MOD CO_2 experiment and other three experiments respectively) at the location of each RDP charcoal-based reconstruction record. A positive anomaly represents increased biomass burning, and a negative anomaly represents decreased biomass burning. Successful identification means that the sign of the experiment anomaly and the sign of the RPD charcoal-based reconstructions are the same.

BA experiments		**MPI_ESM1.2**			**AWIESM1**			**CESM1.2 LGM**		
Scenario	RPD	LGM 190	MOD 190	LGM 395	LGM 190	MOD 190	LGM 395	LGM 190	MOD 190	LGM 395
Negative RPD anomalies										
Number of records	35	20	21	13	17	21	10	20	20	17
Successful identification (percentage)		57	60	37	49	60	29	57	57	49
Positive RPD anomalies										
Number of records	16	3	0	8	6	0	5	0	0	3
Successful identification (percentage)		19	0	50	38	0	31	0	0	19
Total RPD anomalies										
Number of records	51	23	21	21	23	21	15	20	20	20
Successful identification (percentage)		45	41	41	45	41	29	39	39	39

The sign of the charcoal records could reflect changes in fire size or fire intensity as well as burnt area. However, the success rates in predicting the sign of the charcoal anomalies (both positive and negative) were not as good for FS (27-31%) and FI (24-30%) than those obtained for BA for the realistic LGM experiment. Furthermore, both FS and FI did not perform any better than BA under any experiment, with the sensitivity experiments matching the charcoal anomalies slightly better for FS and FI than the realistic LGM experiment (Supplementary Chapter 3).

Discussion

Our simulations show a global reduction in burning at the LGM but increased median fire size and intensity when burning did occur. Burnt area, fire size and fire intensity were all sensitive to changes in vegetation driven directly by CO_2 levels alone. BA and FI were most sensitive to this effect, with the climate effect dampening the effect of CO_2 alone when both are included. The largest reductions in burning occurred when only the CO_2 effect was considered although this experiment had fewer regions in which burning was excluded completely. This suggests that the reduction in burning was more spatially consistent and widespread under these conditions than when both effects were accounted for. The sensitivity of BA to CO_2 is explained by the reduction in fuel availability under low CO_2, a strong constraint on burnt area. For FI, including a CO_2 effect also amplified the overall global signal. This CO_2 effect is most likely driven by the negative relationship between GPP and FI fitted by the empirical model. Whilst this relationship might seem counter-intuitive, it has a sound basis. The most intense fires occur in regions with a seasonal variation in productivity rather than the most productive environments such as tropical forests (Archibald et al., 2013). High productivity can (under some climate conditions) increase the frequency of burning, which also reduces fuel loads (Rodrigues et al., 2019). Under appropriate climate conditions, there can be long-term fuel build-up in areas of low productivity that is not offset by frequent burning. All these factors help to explain why FI is not reduced at the LGM when burning occurs even though BA is. Low CO_2 decreased FS except for tropical regions and reduced the impact of climate in the realistic scenarios. We hypothesize this is because of decreased productivity leading to patchier vegetation, and hence reduced fuel continuity, which is a factor limiting wildfire spread (Dial et al., 2022; Schertzer et al., 2015).

Changes in climate alone also affected all three modelled wildfire properties. The climate effect was larger than the CO_2 effect across all models for FS, with increases in wind, DD and DTR driving the change. BA was particularly sensitive to the amplitude of climate change: climate change alone greatly reduced BA under the coldest LGM scenario (CESM1.2), had a limited effect in the intermediate LGM scenario (MPI-ESM1.2) and increased BA in the warmest LGM scenario (AWIESM1). The amplitude of change in VPD, a measure of atmospheric moisture, relative to other climate variables was especially important in influencing overall trends. In the case of BA, large decreases in VPD under the CESM1.2 climate scenario led to much more substantial reductions, most likely due to an increase in fuel moisture. Additionally, though stronger winds and increased DTR were the main drivers of larger wildfires at the LGM, low VPD values in CESM1.2 severely limited FS and FI in the northern latitudes. VPD has been shown to influence wildfire ignition and wildfire spread (Sedano & Randerson, 2014), and our results suggest high atmospheric moisture can inhibit fire spread. When vegetation was sufficiently abundant however, low VPD values were key in driving intensity. Although vegetation productivity was lower at the LGM, decreased VPD may have contributed to larger fuel build-ups, thus increasing fuel loads. This highlights the sensitivity of the fire regime not just to overall climate change but the relative amplitude of change in individual climate variables.

Our model results reproduce the global reduction of biomass burning at the LGM observed from ice cores and sedimentary charcoal records (Daniau et al., 2012; Harrison et al., 2022; Power et al., 2008; Rubino et al., 2016). Some studies have indicated the occurrence of high-intensity wildfires on the Palaeo-Agulhas Plain of South Africa, tropical regions, northern Australia, and central China at the LGM (Kraaij et al., 2020; Power et al., 2008; Rowe et al., 2021; Ruan et al., 2020; M. Song et al., 2023). Our results are consistent with the trends in these regions. The LGM simulations of BA that account for both climate and CO_2 appear to fit the charcoal records best. The spatial patterns of BA at the LGM were more consistent with the patterns shown by sedimentary charcoal records than FS and FI, consistent with the assumption that charcoal abundance can be used as a measure of biomass burning. The FS and FI anomaly patterns were less consistent than that of BA, suggesting a regime of less burning but larger and more intense wildfires at the LGM could be consistent with the charcoal records. Whilst FI has been reconstructed from charcoal (e.g. Duffin, 2008; Snitker, 2018) there are currently no comparable measures that record FS or FI changes globally. Charcoal records are not available from some regions, further limiting our ability to evaluate the models, particularly in Eurasia and inland South America where low CO_2 leads to large reductions in BA that are not observed when only climate is considered.

Our results are based on simple empirical models for Burnt area, fire size and fire intensity. However, the inferred changes in BA are like those of Martin Calvo et al. (2015) who used the Land surface Processes and eXchanges (LPX) dynamic global vegetation model. Empirical models have been shown to perform as well as more complex process-based models in simulating burned area under modern-day conditions (Hantson et al., 2020). Thus, our conclusions about the relative impact of climate and CO_2 changes on fire properties are unlikely to be adversely affected by the relative simplicity of the models used. Their simplicity facilitates running multiple scenarios and diagnosis of the factors influencing changes in wildfire properties.

The effect of human activity was not considered in this analysis and as such no conclusions can be drawn on how human activity may affect these trends. Although this is a limitation, we believe it is unlikely that human activity would substantially impact the response of wildfire regimes to the changes in climate and CO_2 observed here. Pre-agricultural hunter-gatherer populations used fire for land management, for example to facilitate hunting and to promote the local abundance of food plants (Bowman, 1998; Gott, 2005), although recent work indicates that the burning regimes, they practiced tended to reduce fire overall compared to the natural state (see e.g. Constantine IV et al., 2023). However, the areas suitable for hunter-gatherer populations was much reduced at the LGM by generally colder and drier climates and hunter-gatherer populations were confined to climatically suitable refugia (see e.g. Williams et al., 2013; Blinkhorn et al., 2022). Furthermore, although the estimates of population density are highly uncertain, the LGM population of Australia was less than 5% of the modern population and the reduction in Africa was even larger (Gautney and Holliday, 2015). Palaeoecological evidence from Australia suggests that the use of fire by pre-agricultural hunter-gatherers had a low impact on the environment before the late Holocene (e.g. Black et al., 2007; Fuller et al., 2014; Portenga et al., 2016). Thus, it is unlikely that human activities during the LGM would have substantially increased fire or offset the impact of the changes in climate and CO_2 on fire regimes. Previous studies show a weak influence of population and land-use change on driving global wildfire trends prior to the 18th century (e.g Pechony and Shindell, 2010; Bowman et al., 2020) and a sharp human-driven decline in wildfire activity since the mid-ninetieth century (e.g. Marlon et al., 2008; Wang et al., 2010). This recent reduction in global biomass burning was most likely driven by population growth and land-use change leading to increased landscape fragmentation, which tends to suppress fire spread (e.g. Knorr et al., 2014; Andela et al., 2016; Harrison et al., 2021).

These results add to a growing body of literature highlighting the importance of considering not only changes in wildfire weather but also vegetation properties in projections of future wildfire regimes (e.g. Harrison et al., 2021; Kuhn-Régnier et al., 2021; Pausas & Keeley, 2021). The impact of rising CO_2 levels will most likely enhance vegetation growth and litter accumulation, which are important controls on fuel availability, continuity, and load. However, climate and specifically VPD may have opposing effects to that of rising CO_2 levels. Since VPD controls plant growth, increasing VPD can limit ecosystem productivity and tree growth, in turn reducing fuel loads (Williams et al. 2013). Nevertheless, VPD has also been shown to increase litter fall, thus increasing available dead fuel (Resco de Dios 2020, De Faria et al. 2017). As such, it is important to consider how temporal and spatial scales affect the response of vegetation to changing VPD (Grossiord et al., 2020). Although the trade-offs between future increases in CO_2 and reductions in productivity due to higher temperatures and atmospheric dryness are not fully understood, this work highlights the importance of considering both. These effects will most likely not be evenly distributed across the globe (Gonsamo et al., 2021; Piao et al., 2020; van der Sleen et al., 2015) and CO_2 effects may be more important in some regions than others. In fuel-limited ecosystems, CO_2 fertilization could increase fuel loads and fuel continuity, increasing overall burnt area but also the potential for larger and more intense wildfires. This is particularly worrying in regions with anticipated decreases in atmospheric moisture, especially since evidence suggests rising VPD may only counteract a small proportion of CO_2-induced plant growth (Y. Song et al., 2022). Increased woody thickening, for example in tropical South Asia (Kumar et al., 2021; Scheiter et al., 2020), may also alter fuel loads in regions that are likely to be vulnerable to ignition under a drier and warmer atmosphere (Clarke et al., 2022). Whilst climate variables such as DD and DTR have also shown to be strong controls of global wildfires regimes (e.g. Bistinas et al., 2014; Forkel et al., 2019; Kuhn-Régnier et al., 2021), this study highlights the importance of VPD relative to other climate variables in driving spatial patterns of Burnt area, fire size and fire intensity. This is in line with previous studies that have highlighted the important role of VPD in promoting fuel loads and fire spread (e.g. Diffenbaugh et al., 2021; Grillakis et al., 2022; Duane et al., 2021; Balch et al., 2022). Correctly projecting changes in fuels in the next century will require considering both the effect of VPD and effects of CO_2 on plant growth and fuel loads.

Our results stress the importance of accounting for the effects of CO_2 on vegetation when considering how future fire regimes may evolve. Different aspects of the fire regime respond differently to changes in fuel properties. Without accounting for this crucial effect, our understanding of future risks will remain limited.

Chapter 4: Future global wildfire regimes under a high and low climate change mitigation scenario

The previous two chapters established the global controls of burnt area, fire size and fire intensity (Chapter 2) and showed that the models were able to perform in an out-of-sample experiment (Chapter 3). The aim of this chapter is to address the question of how we expect global fire regimes to respond to 21st century CO_2 levels and climate conditions when also accounting for demographic and land use changes (**RQ3**). It is structured as a paper, with an introduction, followed by a description of the methodology, a presentation of the results and finally a discussion. This work was submitted to *Science* in December 2023 under the title "Wildfires on a changing planet" and has been reworded in some parts, however the methodology, results and discussion remain unchanged.

Introduction

There is growing concern that recent increasing trends in wildfire occurrence and intensity in many regions will persist into the future (Abatzoglou et al., 2019; Mueller et al., 2020; Duane et al., 2021; Jones et al., 2022; Mansoor et al., 2022). Nevertheless, satellite observations show that area burnt has declined globally over the last two decades, most notably in the tropical savannas of South America and Africa and grasslands across the Asian steppe (Andela et al., 2017; Forkel et al., 2019b). Most of this decline has been associated with human activities such as cropland expansion, although climate and CO_2 changes may also have played a role (Forkel et al., 2019b; Pausas et al., 2021). Weather conditions promoting fire, as measured by fire danger indices, consistently increase in future climate-change projections (Wotton et al., 2017; Abatzoglou et al., 2019; Dupuy et al., 2020) — contributing to the concern raised by recent megafires. However, these physical indices do not take account of the potential for changes in vegetation to moderate the effect of future climate changes: warmer and drier conditions increase the incidence of fire weather, for example, but reduce fuel loads and fuel continuity, decreasing fire risk (Hang et al., 2015; Syphard et al., 2018; Kuhn-Régnier et al., 2021, Harrison et al., 2021; Pausas et al., 2021). Nor do they take account of the potential for human activities to mitigate wildfire risk (Syphard et al., 2017). While process-based global fire models that do take account of vegetation and human impacts on fire risk are being used in the Inter-Sectoral Impact Model Intercomparison Project (ISIMIP) to assess potential future wildfire regimes under climate change (UNEP, 2022), these models differ considerably in their predictions of historic trends (Teckentrup et al., 2019) and do not skillfully capture wildfire seasonality and interannual variability (Hantson et al., 2020). Given the impact of wildfires on natural resources and human well-being (UNEP, 2022), a better understanding of potential future wildfire trajectories is needed to devise appropriate management strategies and mitigate risks.

In this chapter we used the models developed in Chapter 2 to examine the consequences of two scenarios: one where global warming by the end of the century is kept under 2°C and another with a global warming of 3-4°C by 2100 CE, both assuming a 'middle of the road' socioeconomic pathway, as run by four state-of-the-art Earth System models. The models have been shown to capture both modern spatial patterns in fire properties (Chapter 2) and the impact of large changes in climate on these properties in a realistic way (Chapter 3). We also ran a series of counterfactual tests in which a set of factors (climate, CO_2, climate and CO_2, human activities) were allowed to change while others were held constant, to diagnose the causes of observed changes in fire properties under each scenario (Table 7).

Data and Methods

Experimental design

Modern burnt area inter-annual variability performance and trends

We ran the burnt area GLM model for the 10-year period from 2006-2015, with lightning held constant to be consistent with the future scenario experiment. The same roads model was also used for consistency. We set burnt area fractional values lower than 0.0011 to zero and we also excluded burning is regions where the ESA CCI land cover bare soil fraction > 95%. We compared the simulated BA trend with both the observations (van der Werf et al., 2017; Chen et al., 2023) and simulated burnt area fraction from the Fire Model Intercomparison Project (FireMIP) models (CLM: Li et al., 2013, CLASS–CTEM: Melton and Arora, 2016, JULES–INFERNO: Mangeon et al., 2016, JSBACH–SPITFIRE: Lasslop et al., 2014, LPJ–GUESS–SIMFIRE–BLAZE: Knorr et al., 2016, LPJ-GUESS-SPITFIRE: Lehsten et al., 2009, LPJ–GUESS–GlobFIRM: Smith et al., 2014, ORCHIDEE–SPITFIRE: Yue et al., 2014). We did not include the MC2 model, as there were only 3 years overlapping. We used normalized mean error (step 3) to assess performance (Kelley et al., 2013; Hantson et al., 2020)

Future scenario selection

The choice of future scenarios was motivated by the future wildfire simulations conducted by the Inter-Sectoral Impact Model Intercomparison Project (ISIMIP) for the United Nations Environment Programme (UNEP, 2022). Climate and human activity data from the ISMIP2b protocol were selected, providing the high mitigation scenario (RCP 2.6) and the low mitigation scenario (RCP 6.0). 'Middle of the road' socioeconomic activity (SSP2) was assumed in both scenarios. This allowed comparisons between the general spatial trends with the outputs from the ISIMIP projections (UNEP, 2022). We conducted five experiments for both scenarios, a realistic experiment, which assumed changes in climate, CO_2 levels and human impacts, and four sensitivity experiments (see Table 1). This was done using the climate projections from four different climate models which participated in the ISIMIP simulations, IPSL-CM5A-LR, GFDL-ESM2M and MIROC5, and HadGEM2-ES (Lange and Büchner, 2017). We downloaded all the data from the ISIMIP repository: https://data.isimip.org/search/simulation_round/ISIMIP2b/product/InputData/climate_forcing/gfdl-esm2m/subcategory/atmosphere/. This provided 40 experiments, the spatial patterns of which were compared with a modern-day simulation, based on the 2010-2015 period. We explored which predictors were driving changes between each experiment and the modern-day simulation by excluding one predictor at a time from the GLM models, re-running all the experiments, and identifying which excluded variable caused the greatest change in the burnt area, fire size, and fire intensity respectively when comparing to the modern-day simulation in each grid cell. By comparing these results to the burnt area, fire size, and fire intensity observed changes between the experiments and the modern-day simulation with the full GLM models we could determine whether the predictor was responsible for an increase of decrease in the given fire property.

Table 7. Summary of modern and future realistic experiments and the associated counterfactual tests. Additional information on the source and availability of the data for each experiment can be found in the Supplementary Chapter 4.

Experiments	
Realistic modern	2010-2015 WFDE5 climate (Cucchi et al., 2020) 2010-2015 annual global average CO_2 (gml.noaa.gov/ccgg/trends/) HYDE 3.2 population density and cropland (Goldewkuijk et al., 2017) GRIP4 road density (Meijer et al., 2018)
Realistic future	2090-2100 climate from GFDL-ESM2M, HadGEM2-ES, IPSL-CM5A-LR, and MIROC5 for RCP2.6 and RCP6.0 (Lange et al., 2017) 2090-2100 average CO_2 for RCP2.6 and RCP6.0 SSP2 socioeconomic pathway, average 2090-2100
Counterfactual experiments	
Climate change only	2090-2100 climate from GFDL-ESM2M, HadGEM2-ES, IPSL-CM5A-LR, and MIROC5 for RCP2.6 and RCP6.0 (Lange et al., 2017) *CO_2 and human factors held constant at modern levels*
CO_2 change only	2090-2100 average CO_2 for RCP2.6 and RCP6.0. *Climate and human factors held constant at modern levels*
CO2 and climate change only	2090-2100 climate from GFDL-ESM2M, HadGEM2-ES, IPSL-CM5A-LR, MIROC5 for RCP2.6 and RCP6.0 (Lange et al., 2017) 2090-2100 average CO_2 for RCP2.6 and RCP6.0. *Human factors held constant at modern levels*
Human activity change only	SSP2 socioeconomic pathway, average 2090-2100 *Climate and CO_2 factors held constant at modern levels*

Data collection and processing

Climate and human activity data from the ISMIP2b protocol were used, providing the high mitigation scenario (SSP2-2.6) and the low mitigation scenario (SSP2-6.0). 'Middle of the road' socioeconomic activity (SSP2) was assumed in both scenarios. A detailed description of the data collection and processing is provided below.

Climate inputs

For the modern-day simulation we used the same climate data (vapour pressure deficit, monthly dry days, dry day seasonality, diurnal temperature range and wind speed as used to construct the original GLM model from WFDE5 (Cucchi et al., 2020). A seasonal climatology was constructed for all variables based on daily data from 2010-2015. For the future experiments, we obtained the climate outputs (daily mean temperature: tas, daily minimum temperature: tmin, daily maximum temperature: tmax, monthly specific humidity: huss, monthly shortwave radiation: rsds, monthly sea level atmospheric pressure: psl, monthly surface wind speed: sfcWind, and daily precipitation: pr) on a daily timestep for the 2090-2100 period for all four climate models from the ISIMIP repository: https://data.isimip.org/. We then computed a monthly climatology for mean daily temperature (from tas), diurnal temperature range (from tasmin and tasmax), monthly number of dry days (from daily pr) wind speed (from tas and sfcWind) and vapour pressure deficit (from tas, huss and psl). We followed the methodology in Chapter 2 to summarize the climate data to obtain the single layer variable for each input.

Vegetation inputs

To design counterfactual experiments which disaggregated the temporal correlation between climate and atmospheric CO_2 levels, we used the methodology developed in Chapter 3 and summarized below. We obtained modern and future vegetation (tree, shrub, grass) and gross primary production (GPP) using the coupled biogeography and biogeochemistry model BIOME4 (Kaplan et al., 2003) and a simple optimality-based model of GPP, the P Model (Wang et al., 2017; Stocker et al., 2020). BIOME4 simulates biome distribution given a set of climates (temperature, precipitation, cloud cover) and CO_2 conditions and outputs biome classification, fraction of C4 photosynthesis and leaf area index (LAI). We obtained the temperature and pressure inputs from the climate inputs (described above). We obtained cloud cover for the future climate scenarios from shortwave radiation. We fitted a linear model between mean monthly global shortwave radiation (from 2010-2015) and mean monthly global fractional cloud cover (from 2010-2015) and then multiplied the future monthly shortwave radiation from all four climate models by the slope of the fitted model and adding the intercept.

Tree, grassland and shrubland cover

We derived mean fractional tree, shrub, and grass cover for each of these experiments using the mean values of tree, grass and shrub cover from ESA CCI (Climate Change Initiative) Land Cover (Li et al., 2018) for each biome simulated by BIOME4 under modern day conditions and applying that value to the same biome simulated by BIOME4 for each experiment. We also used the biome classification to examine the characteristics of burning within each biome between different experiments.

Gross primary production

The first step for obtaining the gross primary production was to run the BIOME4 model to obtain LAI for each experiment. We then obtained fAPAR (fraction of absorbed photosynthetically active radiation) using the Beer Lambert law:

$$fAPAR = 1 - e^{(-k.LAI)} \qquad (5)$$

where k ≈ 0.5, a constant extinction coefficient (Saitoh et al., 2012). BIOME4 tends to overestimate fAPAR when compared the NASA/GIMMS3g values which were used to calculate GPP in the original GLM models. We rescaled fAPAR for each experiment by the ratio between the monthly NASA/GIMMS3g fAPAR averaged from 2010-2015 and the simulated BIOME fAPAR for the same period as was done in Chapter 3. The second step was to compute global monthly C_3 and C_4 photosynthesis using climate inputs (temperature, vapour pressure deficit, photosynthetic photon flux density: PPFD, and atmospheric pressure) as input to the P Model (Wang et al., 2017; Stocker et al., 2020). We derived PPFD from shortwave radiation:

$$PPFD = 60 * 60 * 24 * 10 - 6 * \mathrm{kEC} * rsds \qquad (6),$$

where = 2.04 μmol J^{-1} (Meek et al., 1984) We used BIOME4-derived fAPAR, and CO_2 levels appropriate to each experiment. Total GPP was then calculated as follows:

$$GPP_{monthly} = GPP_{C3}\ (1 - C4_{fraction}) + GPP_{C4}C4_{fraction} \qquad (7),$$

with GPP_{C3} and GPP_{C4} representing monthly C3 and C4 GPP values from the P model and $C4_{fraction}$ representing the fractional C4 cover from BIOME4.

Human activity inputs

Human activity is represented in the GLM models by three input parameters: population density, cropland density, and road density.

Population density

Gridded annual global population data at 0.5°x0.5° resolution used in the ISIMIP2b protocol and based on the national SSP2 population projections (Samir and Lutz, 2014) for 2010 to 2015 and

2090 to 2100 was obtained from the ISIMIP data repository. These data were averaged to obtain mean gridded population density for the modern period and the end-of-the-century period.

Cropland density

Gridded global cropland fraction at 0.5°x0.5° resolution was obtained from the ISIMIP data repository. The ISIMIP2b protocol used transient land-use patterns based on patterns generated by the land-use model MAgPIE according to the SSP2 scenario of economic development and population growth. This model also accounts for climate and atmospheric CO_2 fertilization effects, forced with data associated with RCP2.6 and RCP6.0 respectively. We downloaded outputs for 2010 to 2015 and 2090 to 2100 from MagPIE/REMIND based on IPSL-CM4A-LR, MagPIE/REMIND based on GFDL-ESM2M MagPIE/REMIND based on MIROC5, and MagPIE/REMIND based on HadGEM2-ES. These outputs were averaged to obtain gridded population density for the modern period and the end-of-the-century period.

Road density

Gridded future road density was derived using the method discussed in Meijer et al. (2018) and using the predictors identified by the Global Roads Inventory Project specifically gridded population density and gridded gross domestic product (GDP). Gridded GDP data, obtained from downscaling country level estimates using ISIMIP2b gridded population density, for 2010 to 2015 and 2090 to 2100 was downloaded from the ISMIP repository at 0.5°x0.5° resolution. Total GDP per grid cell was divided by population density data to obtain GDP per capita. The yearly data were average to provide mean values for each time period.

A linear model was developed using the population density for 2010-2015, the GDP for 2010-2015, OECD membership (yes/no) (Meijer et al. 2018) and total area (in km^2) (obtained with the area function in the R raster package) to simulate the spatial pattern of road density. The summary of the model is presented below. The model performs less well than the country level model developed from the GRIP dataset (23; adjusted-R^2 = 0.90) but this is to be expected. It has a good correlation with the GRIP dataset (r = 0.68).

Table S2. Summary of linear model for road density.

Predictors	***Coefficient***	***Standard error***	***t-value***	***p-value***
(Intercept)	0.15	0.42	3.60	0.004
Population density (log-transformed)	0.65	0.00	171.51	< 0.001
GDP per capita (log-transformed)	0.20	0.00	80.09	< 0.001
OECD (yes/no)	0.65	0.02	38.27	< 0.001
Area (km^2)	0.00	0.00	18.85	< 0.001
R^2 /Adjusted-R^2	0.47/0.47			

We then use this model to predict road density under the SSP2 scenario, using the population density and GDP per capita data for the mean 2090-2100 period.

To minimize uncertainty related to changes in human activity and to account for potential biases with the models, we use the same approach as with the climate variables. We compute the anomalies between the modern day-period population density, cropland cover and road density and then add the anomalies to the original modern-day data used to build the GLM models.

Lightning and topographic inputs

Lightning ignitions were kept constant at the 2010-2015 WGLC WWLLN background rate (Kaplan et al., 2021) in all experiments, following the ISIMIP2b protocol in which lightning is prescribed. Topographic position index (TPI) and vector ruggedness measure (VRM) were held constant.

Results

Modelled mean annual burnt area from 2006-2015 was 623 Mha, intermediate between the values of 450 Mha for the GFED4s (van der Werf et al., 2017) and 764 Mha for the GFED5 (Chen et al., 2023) burnt area data products. The model captured the observed year-to-year variability in global burnt area reasonably well, and regional differences in trends (Supplementary Chapter 4). Model performance in predicting global patterns of burnt area comfortably exceeds that of "process-based" models participating in the Fire Modelling Intercomparison Project (FireMIP); modelled interannual variability of global burnt area is also better estimated than in the majority of FireMIP models, especially when compared to the most recent global estimates of burnt area (GFED5; Chen et al., 2023). In latitudes above 60°N, where warming will be strongest according to the IPCC (Hoegh-Guldberg et al., 2018), the model outperformed all FireMIP models for the recent trend. Over Africa, where the most significant decreasing trend has been observed (Andela et al., 2017), the model is also one of the best performing.

A global (17%-22%) decline in burnt area was shown under the high-mitigation scenario with three of the four climate models, reducing annual burnt area from 406 Mha a year today to 316-335 Mha by the end of the century. The fourth model showed a negligible global decrease (0.04%) because simulated drier conditions caused increases in fire activity in Amazonia and northern Australia not seen in the other models (Figure 14 and Supplementary Chapter 4). The modelled reduction in burnt area for all four models was largest in tropical regions, which account for 83% of global burnt area under modern conditions but only 77-81% at the end of the 21st century (Table 8 and Figure 15). The key driver of the reduction in burnt area in the tropics, particularly in Africa, India, and South-East Asia was increased human activity, as measured by road density and cropland cover. Climate changes, for example in Central America and the Amazon basin (primarily increasing dry days and decreasing dry-day seasonality), and vegetation changes (decreasing GPP and grass cover), drove a reduction in wetter tropical regions of South America (Figure 16). However, there are differences between tropical regions, with increases in burnt area in much of South America, especially in drier tropical biomes, driven by increasing dryness and gross primary production. Increases were also observed in the inland tropical savannas of Southern Africa (Figure 14). There was no modelled global decline in burnt area when socioeconomic changes were held constant, although there was a decline in burnt area in tropical grasslands, xerophytic shrublands, evergreen and semi-deciduous forests in this sensitivity experiment because of increasing dryness (Supplementary Chapter 4). This decrease was 17-20% for three of the models, and 1% for the fourth model, compared to 30-34% for the same three models (and 15% for the fourth model) when human activity was included. These results highlight the importance of human activities in reducing burnt area in future climates.

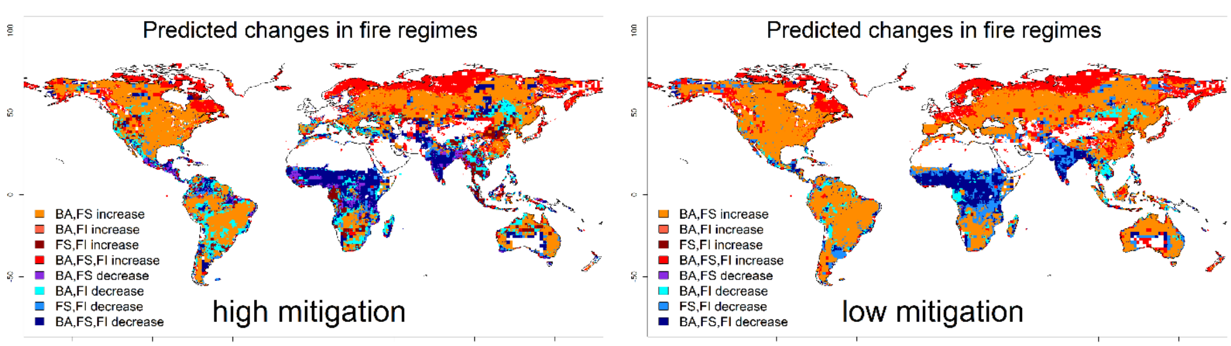

Figure 14. Regions of change in burnt area (BA), fire size (FS) and fire intensity (FI) under the high mitigation scenario (left) and the low mitigation scenario (right). Regions where all three properties increase are shown in red, regions where all three properties decrease are shown in dark blue.

Although there was an overall decrease in modelled burnt area under the ambitious mitigation scenario, increasing burnt area was shown for some northern extratropical regions (Figure 14 and Figure 15). Increases in burnt area in temperate and boreal forests, and in tundra (Figure 16) were driven by decreased precipitation (as reflected by an increase in the number of dry days) and increased atmospheric dryness (VPD). This was observed in both the climate-only and the CO_2-only experiments (Supplementary). These regional increases were not sufficient to counteract the impact of reductions in the tropics on the global decline in burnt area (Figure 15, Table 8).

Under the ambitious mitigation scenario, mean global fire size (23-36%) and mean global fire intensity (2-5%) increased and this pattern was robust across all climate models. The global increase in fire size and fire intensity primarily reflects increases in the northern extra-tropics (Figure 14) and was driven by changes in climate factors (increasing wind strength and dryness) and by human activities. The largest increases in fire intensity occurred in boreal forests and shrub tundra north of 60°N (Figure 15 and Figure 16). Modelled increases in fire intensity in these regions were driven by increased GPP and increased dryness. The number of grid cells in which wildfires occurred was 27-30% greater globally by the end of the 21st century than under modern conditions, and most (87-88%) of this increase occurred in the northern extra-tropics. Model results show global increases in fire size and fire intensity in extra-tropical regions that experience wildfires today, as well as the occurrence of wildfires in new areas.

Changes in fire size and fire intensity across the tropics are less coherent. The modelled decrease in burnt area in the tropics is accompanied by an increase in fire size but a decrease in fire intensity (Figure 16). This signal is primarily driven by increases in fire size in South America, with larger fires being driven by increased dryness in the tropical rainforests and increased cropland and increasing wind in drier, tropical savannas. Modelled decreases in fire size and fire intensity in tropical Africa are primarily driven by changes in human activity. Increased dryness, which led to an increase in vegetation fragmentation, also caused a reduction in both fire size and fire intensity in these regions (Figure 15 and 16). Even in those tropical savanna regions where burnt area increased, fire size and fire intensity decreased because of increased atmospheric dryness and increasing population density (Figure 16 and Supplementary).

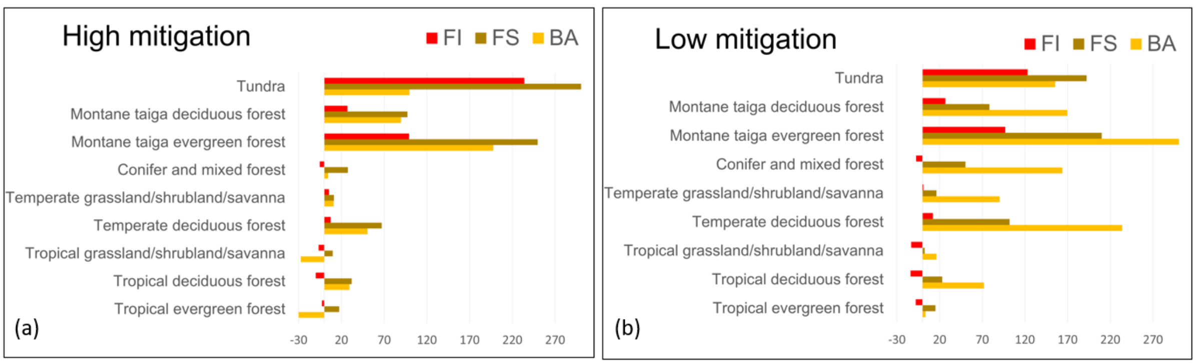

Figure 15. Percentage change in burnt area (BA), fire size (FS) and fire intensity (FI) per biome for (a) the high mitigation scenario and (b) the low mitigation scenario. See Supplementary Chapter 4 for more detail.

In stark contrast to the high mitigation scenario, there is a global increase (18-60%) in burnt area under the low mitigation scenario. Increased burning is seen across all vegetation types, even in the tropics (Figure 15). Human-driven reductions in tropical regions are offset by the combined effects of changes in climate and CO_2. The role of CO_2 is important, as the increases in burnt area do not occur in response to changes in climate alone. When only socio-economic changes are considered, we model large decreases in burnt area in tropical regions of Africa and India, but much smaller reductions in South America and South-East Asia. This probably reflects deforestation fires in the Amazon and Indonesia which, though reduced under the future socio-economic scenario, still occur (deforestation fires are captured through cropland cover and population density in the models). In temperate regions, vegetation types that had an increase in modelled burning under the high mitigation scenario had a much larger increase under the low mitigation scenario (Figure 15 and Table 8). Changes in climate are more important than changes in vegetation in driving burnt area increases in the low mitigation scenario, although vegetation changes still contribute to increasing burnt area in sub-Saharan Africa (Angola, Zambia, Malawi, Mozambique) (Figure 16 and ss Chapter 4). Increases in dryness and grass cover drove an increase in burnt area in North America and increases in GPP drove an increase over much of Eurasia. Increased road density in previously fire-free regions also lead to increases in burnt area in Europe and the east coast of the United States across all four models. This effect does not occur under the high mitigation scenario.

Both fire size and fire intensity are reduced globally under the low mitigation scenario compared to a high mitigation scenario. The global mean fire size increased 19-32% compared to modern while the global mean fire intensity decreased by 1-12% compared to modern. The largest increases in fire intensity and fire size compared to modern were concentrated in boreal forests and shrub tundra above 60°N (Figure 14 and Figure 15). The increase in fire size was substantially higher than in the high-mitigation scenario across all northern biomes including temperate forests (50% increase). Increased fire size in these northern regions was driven by increasing dryness and DTR. However, the increase in fire intensity was somewhat smaller than in the high-mitigation scenario overall, with large decreases in temperate grasslands and forests as well as conifer forests compared to the high-mitigation scenario (80% decrease). Whereas increased GPP was the major cause of increased fire intensity in the high-mitigation scenario, changes in precipitation (as reflected in the number and seasonality of dry days) and increased atmospheric dryness were the most important causes of increased fire intensity in the low-mitigation scenario (Figure 16 and

Supplementary Chapter 4) and this shift is likely the cause of the reduction in fire intensity compared to the high-mitigation scenario.

In contrast to the increases in fire size and fire intensity in the extra-tropics, both fire size and fire intensity decreased in tropical regions. The overall modelled decrease in fire intensity is twice as large (49%) as in the high-mitigation scenario except for tropical grasslands, where fire intensity increased (Figure 15 and Supplementary Chapter 4). Nevertheless, the changes in the tropics are insufficient to offset the impact of the large increases in fire size and fire intensity in the extra-topics on the global signal.

Table 8. Total burnt area per biome under modern, high, and low mitigation scenarios

Biome	Modern day		High mitigation		Low mitigation	
	burnt area (km^2)	global percentage	burnt area (km^2)	global percentage	burnt area (km^2)	global percentage
Tropical evergreen forest	817,813	20.14	842,705	24.20	1,317,980	21.56
Tropical deciduous forest	604,130	14.88	558,277	16.03	766,776	12.54
Tropical grassland/shrubland/savanna	2,010,784	49.52	1,372,585	39.42	2,281,542	37.31
Temperate deciduous forest	44,004	1.08	4,9132	1.41	121,593	1.99
Temperate grassland/shrubland/savanna	135,381	3.33	219,644	6.31	259,302	4.24
Conifer and mixed forest	395,355	9.74	394,149	11.32	1,284,318	21.0
Montane taiga evergreen forest	12,337	0.30	23,794	0.68	36,973	0.60
Montane taiga deciduous forest	38,160	0.94	19,254	0.55	31,589	0.52
Tundra	2,795	0.07	2,413	0.07	14,355	0.23
Global total	4059702		3481953		6114430	

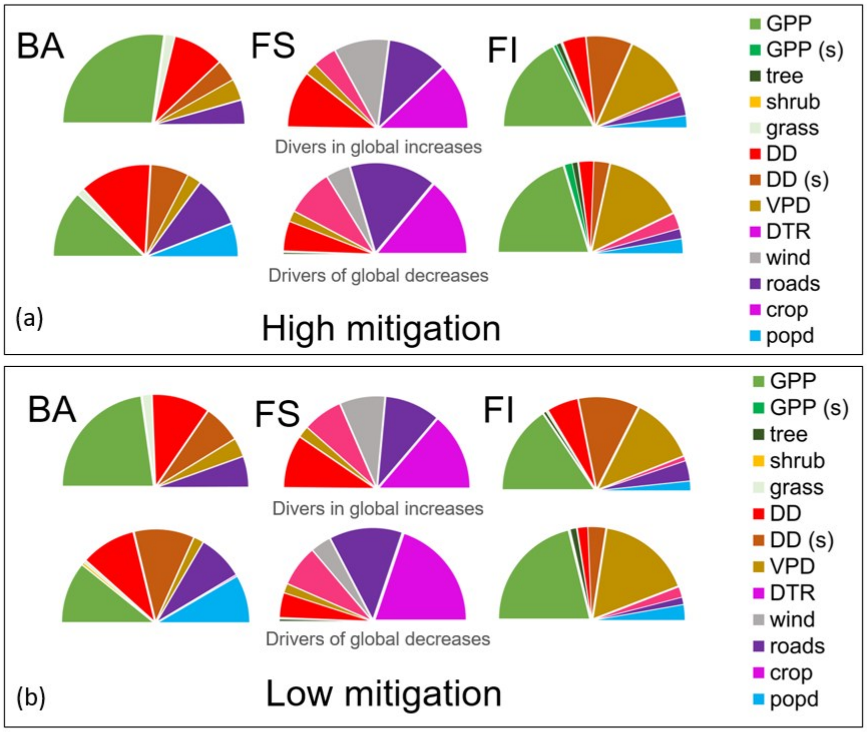

Figure 16. Predictors responsible for driving changes in burnt area (BA), fire size (FS) and fire intensity (FI) respectively of (a) the high mitigation scenario and (b) the low mitigation scenario. The top row shows predictors driving increases and the bottom row shows predictors driving decreases in the fire properties.

Discussion

Model simulations show major changes in the geographic patterns of wildfire occurrence by the end of the 21st century, under both high- and low-mitigation scenarios. Both scenarios show a reduction in burning in the tropics but increased burning elsewhere. Our results suggest a general trend towards larger and more intense wildfires in northern latitudes, under both high-mitigation and low-mitigation scenarios. The current global trend of decreasing burnt area may continue under high-mitigation efforts but is unlikely to continue under low-mitigation efforts where changes in climate promoting wildfires overwhelm the effects of human activities in reducing wildfires, particularly in the tropics. Differences in trajectories between the tropical regions can be partly explained as reflecting differing human impacts on wildfire regimes, for example in South

America deforestation fires are much more prominent than in Africa where the impact of human activity on wildfire activity is related to cropland expansion (Millington et al., 2022). Our conclusions are in line with previous studies (UNEP, 2022, Krawchuk et al., 2009; Moritz et al., 2012; Knorr et al., 2016; Kloster et al., 2018; Wu et al., 2021) in showing a redistribution of global wildfires under future conditions. Our projected increase in the global burnt area under the low-mitigation scenario is of similar magnitude to previous estimates (UNEP, 2022; Moritz et al., 2012). However, there are differences in the regional trends, especially in the Amazon (UNEP et al., 2022; Moritz et al., 2012) and northern latitudes where some studies show regions of decreasing fire activity despite an overall increasing trend (UNEP et al., 2022; Krawchuk et al., 2009; Moritz et al., 2012; Wu et al., 2021). There is disagreement in previous studies over the sign of the global trend in burnt area under high-mitigation scenarios, with some showing an increasing trend (UNEP, 2022; Moritz et al., 2012), some no trend (Krawchuk et al., 2009) and some a decreasing trend (Knorr et al., 2016; Kloster et al., 2018; Wu et al., 2021). Our analysis provides new insights into key regions in which global fire regimes are sensitive to changing conditions and suggests distinct trajectories for different climate change mitigation scenarios.

We have not considered the potential impact of changes in lightning frequency, and therefore lightning-caused ignitions, on future wildfire trajectories because there are large uncertainties in future lightning projections, even in terms of the sign of the global trend (Krause et al., 2014; Murray et al., 2018). Increased lightning frequency would be expected to lead to even larger increases in burning (Janssen et al., 2023), especially in high-latitude regions since drier fuels in boreal forest ecosystems would increase lightning ignition efficiency (Hessilt et al., 2022; Chen et al., 2023; Pérez-Invernón et al., 2023).

Our analysis highlights the sensitivity of future fire regimes to human activities. However, there are many assumptions and large uncertainties associated with the socioeconomic scenarios used in these analyses. The effect of human activities on fire is complex and cannot be captured by simple metrics such as population density (Bistinas et al., 2013; Knorr et al., 2014; Harrison et al., 2021). The use of road density as a measure of landscape fragmentation provides useful additional information but future estimates of road density are largely based on estimates of population changes and economic growth. However, the largest uncertainty in future scenarios is how policy changes will affect human activities, including landscape and wildfire management (Bukovsky et al., 2021).

Shifts in wildfire occurrence, as seen in both low- and high-mitigation scenarios, will have large ecological and human impacts. There are signs that these are already happening (UNEP, 2022, Jones et al., 2022). Given the widely differing trajectories of wildfire regimes in different regions, contrasting management strategies are likely to be required (Dwomoh et al., 2017). Better understanding of how human activity influences wildfire regimes is needed to implement any successful management strategy (Bowman et al., 2011; Gillson et al., 2019; Ford et al., 2021). One potential consequence of the predicted decrease in burnt area, fire size and fire intensity in the tropics is woody encroachment, which impacts biodiversity, the carbon cycle, and land-atmosphere interactions and has consequences for local economies, livestock production, tourism, and pastoralism. High-intensity fires have been used to limit woody encroachment, but with limited evidence of success (Luvuno et al., 2018; Morford et al., 2022). Integrated fire management strategies that include local knowledge and communities are likely to provide the greatest resilience (Eloy et al., 2019; Mistry et al., 2021; Scholtz et al., 2022; Strydom et al., 2023). In the extra-tropics and other regions where burnt area, fire size and fire intensity are predicted to increase, increased risks to life, property, and commercial activities are a major concern (UNEP, 2022, Humphrey et al., 2021). In currently fire-prone regions such as Mediterranean ecosystems, the viability of fire suppression policies needs to be reassessed (Moreira et al., 2020; European Commission, 2021; Commission, E & Centre, 2023). Furthermore, management practices may not be well defined in regions where wildfires have been infrequent in the past (Moreira et al., 2020; European Commission, 2021; Commission, E & Centre, 2023). In the northern latitudes, the most intense wildfires occur under the high mitigation scenario, and it is under these conditions that successful fuel load management and increased preparedness in the wildland urban interface will be most needed (Ingalsbee et al., 2017; Iglesias et al., 2022; Regos et al., 2023; Essen et al., 2023). Larger increases in burnt area in these regions under a low mitigation scenario will require moving beyond fire-suppression measures and towards adaptive ones in which communities learn to live with fire (European Commission, 2021; Commission, E & Centre, 2023) as they will be more common, though less destructive, than under a high mitigation scenario. Forest planting and restoration projects have received much attention as climate change mitigation tools (Fady et al., 2021; Basuki et al., 2022; Fucks & Noebel, 2022; Seddon et al., 2022; Kobayashi et al., 2023) but there has been limited consideration of the effect of wildfires on such projects. Wildfire management will need to be incorporated into the design of afforestation schemes, given that our simulations show substantial changes in fire regimes in the future in most regions of the world, including the tropics under the low mitigation scenario. Indeed, changes in wildfire regimes may preclude implementation of afforestation schemes in some areas (Lindenmayer et al., 2018; Hermoso et al., 2021) and wildfire management often conflicts with retaining native ecosystems, cultural landscapes, and local communities (Holl et al., 2020; Brancalion et al., 2020).

Chapter 5: Discussion and conclusions

The goal of this thesis was to explore the impacts of changes in factors that influence wildfires including climate, atmospheric CO_2 levels on vegetation properties and human activity. Addressing this goal involved developing new empirical models of three critical properties of wildfire regimes, specifically burnt area, fire size and fire intensity (Chapter 2), testing these models both under modern conditions (Chapter 2) and under a radically changed climate (Chapter 3) and then applying them to simulate the response of wildfires to plausible future scenarios (Chapter 4). These three steps have been presented in three separate papers, each with their own separate discussion. In this chapter, the overall implications of the research are discussed under four integrative themes: (1) empirical modelling and drivers of global fire regimes, (2) using the past to ensure robust understanding of the future, (3) mapping global fire intensity, (4) wildfire regimes and global change, specifically climate impacts, CO_2 impacts, and human impacts.

Empirical modelling and drivers of global fire regimes

Much of the recent discussion about changes in wildfire regimes has focussed on burnt area but new and novel wildfires, such as the recent megafires in California, have highlighted the need to consider different properties beyond fractional burning. Burnt area provides an estimate of area burnt but does not provide information about the average intensity or size of wildfire events, or how they may change in the future. Efforts to map global fire regimes (Chuvieco et al., 2008; Archibald et al., 2013; Garcia et al., 2020) have provided some information about the distribution of different fire regimes, however, they do not explicitly determine the global controls of each fire property separately. Consequently, whilst we can identify behavioural clusters, we do not know which underlying properties are leading to their emergence. Furthermore, whilst studying different fire properties in relation to each other provides insights into constraints and feedback (Luo et al., 2013; Luo et al., 2017; Laurent et al., 2019), it does not provide a way in which to identify the emergence of novel fire regimes which may not operate under current constraints.

A key aim of this thesis was to explore how the spatial controls of global burnt area, fire size and fire intensity might differ independently of each other. This was done by developing statistical models from a common set of sixteen predictors to represent each of the three properties separately. Since only the most significant predictors were retained for each model, I was able to determine which of the controls had the biggest influence on a specific wildfire property. Several statistical models have already been developed for the controls of burnt area (e.g. Bistinas et al., 2014; Knorr et al., 2014; Kelley et al., 2019) and thus the most important controls have been identified. I made use of this knowledge in choosing predictors for my burnt area model, and this is reflected in the performance of that model in which all the predictors were significant. Hantson et al. (2015) have made a statistical model for fire size, but the focus there was on determining the distribution of fire size rather than the global controls. Nevertheless, this research did show that the distribution of fire size changed over aridity gradients (Hantson et al., 2015). My research explicitly focused on the environmental controls of fire size. The model for fire intensity presented in this thesis is, to my knowledge, the first empirical stand-alone global model of fire intensity.

The three models were developed starting from a common set of predictors representative of controls related to climate factors, topography, ignitions, land cover and fragmentation, and vegetation productivity. My work shows that burnt area, fire size and fire intensity are influenced by different subsets of these factors. Burnt area was primarily limited by fuel availability and dryness, fire intensity was limited by fuel load and density and fire size by fuel continuity and factors promoting spread.

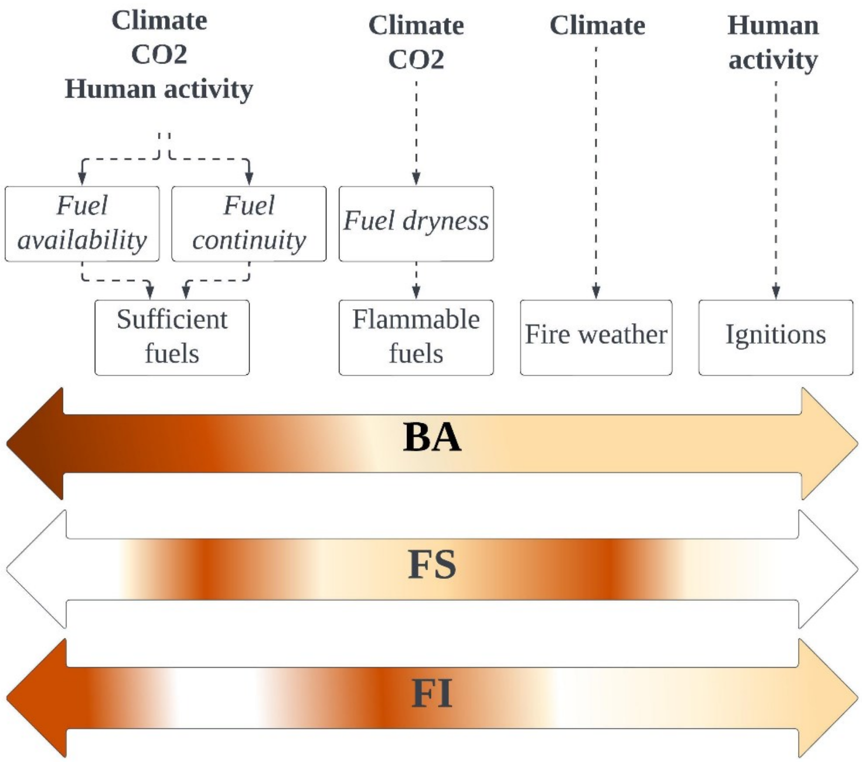

Figure 17. Importance of four switches for burnt area (BA), fire size (FS) and fire intensity (FI) for each statistical model (shown by t-values) with darker red being more important. White values are not significant at the significance threshold used. Fuel availability (gross primary production: GPP, GPP seasonality, tree, grass, shrub) and fuel continuity (cropland, road density, topography) are separated out here. The arrows above show whether changes in climate, CO_2-induced changes in vegetation or human activity influence the different drivers in simulations of the past and future.

The implications of these findings can be discussed through the framework of Bradstock's (2010) four switches, which postulates that wildfire occurrence requires sufficient fuel, flammable fuel, fire weather and ignitions. My results suggest (1) that different switches are limiting for different fire properties of the wildfire regime and (2) that the time scales on which these switches operate vary between the different fire properties. The sufficient fuel switch, when applied to properties other than burnt area, needs to be considered as two separate switches: sufficient fuel load and sufficient fuel continuity. The requirement for sufficient fuel is limiting for burnt area, fire intensity and fire size over much of the world, but the underlying reasons are different. For fire size, there must be sufficient fuel for fires to spread (and get larger) and this is limited primarily by landscape fragmentation driven by human activity (through croplands and road density) but also patchy fuels under dry and low CO_2 conditions. For fire intensity, there must also be sufficient fuel, but the main barrier is not the fuel's continuity but its load (as demonstrated by insignificant relationship to cropland and positive relationship to road density). Dry atmospheric conditions (as measured by vapour pressure deficit: VPD) and dryness seasonality limits plant growth and fuel build up which inhibits the most intense wildfires, and this is expressed by the negative relationships between VPD, dryness and fire intensity. Burnt area requires both a minimum fuel load and a level of fuel continuity. However, since it does not represent an individual fire property but rather the fractional amount of burning under given conditions, it is less sensitive to both. This property of burnt area is demonstrated by the strong relationship between gross primary production (GPP) and burnt area which is not present in the other two models, and which is in line with the intermediate productivity hypothesis, which states that the most biomass burning occurs at intermediate levels of productivity (Pausas and Bradstock, 2007; van der Werf et al., 2008; Pausas and Ribeiro, 2013). This emergent relationship occurs because of the interaction of a positive relationship between fire activity and productivity under low productivity which becomes negative at some point due to increasing precipitation needed to maintain high productivity.

Bradstock (2010) postulated that the first switch (1), available fuel, operates on months to years, the second switch (2), dry fuel, operates on weeks to months, the third switch (3), fire weather, operates on hours to days and the final switch (4), ignitions, is instantaneous. instantaneous. However, based on my work, I hypothesize that the timeframes on which the switches operate may be different for different fire properties and there may be feedback between them. Although the work in this thesis does not show this directly, I hypothesize that the reason we see opposing relationships between burnt area and fire intensity is due to the differences in the effect of seasonality on these two fire properties. Fuel availability is affected by dryness, through the control of VPD and dry day (DD) seasonality on plant growth. For fire intensity, this dryness can have a strong limiting effect, with the strongest (negative) relationships being with VPD and dryness. However, my work suggests that the timeframes on which the switches operate may be different for different fire properties and there may be feedback between them. Fuel availability is affected by dryness, through the control of VPD and dry day (DD) seasonality on plant growth. For fire intensity, this seasonal cycle can have a strong limiting effect, with the strongest (negative) relationships being with VPD and dryness. This effect also appears for fire size in future simulations, with increased dryness in the northern hemisphere reducing fire size. This is in line with previous work highlighting the importance of antecedent conditions on burning in dryness-limited ecosystems (Forkel et al., 2019a; Kuhn-Régnier et al., 2021) and shows that the switches operate on different seasonal timescales with long-term fuel availability requiring lower fuel dryness in the shorter-term. The ignition switch was only limiting for burnt area, consistent with the fact that both fire size and fire intensity are properties which implicitly assume that ignition has already occurred.

The intermediate fire occurrence-intensity (IFOI) hypothesis proposes a humped relationship between fire frequency and fire intensity globally (Luo et al., 2017). This hypothesis builds on the assumptions of the global intermediate productivity hypothesis. Luo et al. (2017) showed a humped relationship between burnt area and fire intensity. This humped relationship is explained by the fact that under low fire intensity, increasing fire intensity correlated with more fire-prone weather conditions and fuel conditions (switch 2 and 3), leading to a positive relationship between occurrence-intensity. Under high fire intensity, increasing fire intensity means less available fuel (switch 1) leading to a negative relationship between occurrence-intensity (Luo et al., 2017). My results are in line with the IFOI hypothesis and provide further explanation. They show that the humped relationship emerges from the controls of burnt area and fire intensity operating on different seasonal timescales as well as feedback between them. Burnt area requires high GPP, to produce available fuel as well as high dryness seasonality to provide drying out of those fuels. Indeed, there must first be a productive phase for fuel accumulation and then a dry phase in which this fuel is able to dry out. The highest fire intensity on the other hand, occurs at low GPP, high GPP seasonality but high GPP seasonality as well as low dryness seasonality. These conditions are essential to provide adequate fuel build-up over multiple years, and therefore, productivity must be continuous without the limitation of dryness. Thus, I postulate that burnt area and fire intensity both have an emergent humped relationship with precipitation but from opposite directions. These conditions are essential to provide adequate fuel build-up. Large burnt area on the other hand requires high dryness seasonality to provide drying out of fuels. Thus, burnt area and fire intensity both have an emergent humped relationship with precipitation but from opposite directions. Fire intensity monotonically decreases with dryness (as its long-term effect on fuel-build up dominates) whereas burnt area monotonically increases with dryness (as its short-term effect on fuel flammability dominates), leading to fire intensity and burnt area peaking at different values of precipitation. My results show that burnt area and fire intensity have similar controls (longer-term climate and CO2 levels playing an important role) but operate on different timeframes, that of drying and of biomass production.

The difference in the timeframes on which burnt area and fire intensity controls operate does not mean that their interaction is fixed. Burnt area was reduced at the LGM but fire intensity was increased, whereas both increased in future simulations, suggesting their controls (climate and vegetation) are decoupled. The negative relationship between fire intensity and ignitions fitted in the fire intensity model suggests a long-term limitation of fire frequency on fuel build-up, providing a feedback which relates to switch (1). In contrast, fire size has different fundamental controls to both fire intensity and burnt area, with a greater sensitivity to human activity and fire weather. Given the importance of fire weather, the timeframes on which fire size operates are much shorter. The fire weather switch (3) is most important for fire size, in line with the hypothesis that it is most useful in simulating individual fire properties (Boer, 2021). Laurent et al. (2019) found a humped relationship between fire size and fire intensity. This relationship emerges from increased fragmentation as season progresses which suggests that connectivity of fuels is a limiting factor for fire spread (Archibald et al., 2012). Whereas fire size shows a strong sensitivity to landscape fragmentation in my results, fire intensity does not. The different sensitivity of fire size and fire intensity to fuel continuity and fuel load respectively provides an explanation for the emergent humped relationship between fire intensity and burnt area, and between fire intensity and fire size. A fuel load switch for fire intensity and a fuel continuity switch for fire size emerge from these results.

There are large uncertainties in projections of some of the essential controls of wildfire into the future. My results show that road density is a crucial variable in estimating future trends in wildfire. The GRIP dataset (Meijer et al., 2018) provides future estimates of road density at country level, but gridded data are required for global modelling. To account for this, I derived gridded estimates of road density using population and GDP for my projections, but these projections are highly uncertain. Predicting future human activity is very difficult in general as it relies on many assumptions about future socioeconomic decisions (Bukovsky et al., 2021). There is also uncertainty associated with lightning estimates. In my work I have assumed no change in lightning ignitions because studies disagree on the sign of the global trend of lightning throughout the next century (Finney et al., 2018; Murray, 2018). However, some recent studies have projected increases in lightning-driven ignitions during the 21st century. Boreal regions would be especially vulnerable to such increases (Chen et al., 2021; Hessilt et al., 2022; Janssen et al., 2023). Given the importance of both these predictors in driving different wildfire properties, more attention needs to be given to generate high quality and reliable products for future simulations.

My research has focused on the external drivers of wildfire properties but, from a modelling perspective, it would be useful in future to consider the interactions between fire regimes and vegetation. One aspect that is not included in this analysis is the response of fire regimes to different plant traits (fire adaptive or traits promoting fire resilience and resistance). The presence of these traits depends on the established fire regime and but also help maintain that fire regime (Harrison et al., 2021). This feedback is because the presence of different plant traits influences fuel properties, which in turn influence fire regimes. For example, resprouting can lead to dramatically different recovery times between ecosystems after fire, affecting fuel continuity (Shen et al., 2023). The variation in fire regimes across savannas has been shown to depend on traits in grassy species (Simpson et al., 2022). Fire regimes also explain global variability of bark thickness, which in turn affects fuel load (Pausas, 2015). The inclusion of resprouting and adaptive bark thickness in the fire-enabled Land surface Processes and eXchanges dynamic global vegetation model (LPX-Mv1) led to large improvements, suggesting they are important in explaining variability of global fire regimes (Kelley et al., 2014). Nevertheless, this model was developed and tested only for Australia, and no global fire model currently accounts for such traitstraits. The absence of trait information in global models is because much of the knowledge on the presence of fire-related traits and their relationship to wildfires remains qualitative (Clarke et al., 2015; Keeley and Pausas, 2022). Semi-quantitative relationships have been drawn between fire frequency and intensity and the resprouting capabilities in plants regionally (Harrison et al., 2021; Shen et al., 2023), however quantitative global relationships are yet to be drawn. Such relationships would provide a way to explore how important these traits are in driving differences in the distribution of fire regimes and could be worked into future modelling efforts. Furthermore, the impact of changes in either vegetation (and thus traits) or fire regimes (through suppression efforts for example) on the feedback between the two could be quantified. Increasing our understanding of vegetation flammability as a vegetation property more generally (Pausas et al., 2017; Popović et al., 2021; Dickman et al., 2022) could also greatly improve the modelling of fire regimes.

The three empirical models presented here perform better than existing process-based fire models. The burnt area model outperforms all the fire-enabled models included in the Fire Model Intercomparison Project (FireMIP) in terms of spatial distribution (Hantson et al., 2020). The fire size model also performs better than the limited number of FireMIP models that explicitly simulate fire size. Although comparisons of fire intensity are not possible, my fire intensity model also performs reasonably well spatially. These empirical models are simple and fast and thus can be used to perform many sensitivity experiments, proving a useful explanatory tool. Thus, my results have large implications for the fire modelling community. Many of the important drivers in these models are not included in fire-enabled vegetation models. The strong relationship demonstrated with road density, as well as the importance of seasonality in dryness and vegetation productivity, is in line with previous research highlighting the need to move towards including measures of landscape fragmentation (Harrison et al., 2021) and antecedent conditions (Kuhn-Régnier et al., 2021, Forkel et al., 2019a) in global modelling efforts. Furthermore, my work provides an additional argument that these fire properties can and should be modelled separately, particularly because they are influenced by different factors and can become decoupled when climate changes are large. Empirical global fire models currently do not simulate fire properties beyond burnt area. Furthermore, although process-based models that do simulate fire properties such as intensity and size, they still rely on rate of spread equations, which indirectly couple burnt area, fire size and fire intensity. For example, the fire model SPITFIRE (Thonicke et al., 2010) relies on a product of number of fires and fire spread to determine burnt area. Coupled with JSBACH (Lasslop et al., 2014) LPJ-GUESS (Lehsten et al., 2009) and ORCHIDEE (Yue et al., 2014), SPITFIRE also derives fire size from fire spread. Finally, it derives fire intensity from a product of fire spread and fuel consumption. Thus, although SPITFIRE can obtain all three fire properties separately, therethey are all still proportional to fire spread, a complex process, which requires heavy parametrization and may not be appropriate at a 0.5-degree global scale. The empirical models provided in this thesis provide a way to explore how each individual predictor influences each fire property, independently of each other.

Using the past to ensure robust understanding of the future.

One novel feature of my thesis is testing the wildfire models at the Last Glacial Maximum. This was motivated by the fact that using global wildfire models to project future changes requires a demonstration of their ability to respond correctly to conditions outside the modern range was used to build and calibrate them. The Palaeoclimate Modelling Intercomparison Project (PMIP) was set up in part to assess how well state-of-the-art climate models perform under dramatically different conditions in the past (Joussaume et al., 1999; Braconnot et al., 2007; Harrison et al., 2015; Kageyama et al., 2018; Brierley et al., 2020), otherwise known as out-of-sample conditions (Kageyama et al., 2018; Kageyama et al., 2021). There have been calls for palaeoclimate simulations to be used alongside palaeo data to evaluate model performance as well as study model responses to large changes in forcing. This has been done for some individual Earth System Models (ESMs), for example the Community Earth System Model 2 (CESM2) adjusted its climate sensitivity because of an out-of-sample experiment simulating Last Glacial Maximum conditions (Zhu et al., 2022). However, beyond an overall evaluation of ESMs, the testing process has not been systematically extended to individual model components, despite calls to do so (Burls et al., 2022). Palaeo data has also been used to provide a constraint equilibrium climate sensitivity, ice sheet stability, and sea level rise (Tierney et al., 2020) and greenhouse gas feedback to climate (Liu et al., 2022).

However, little attention has been given to using palaeo-data to evaluate models of fire. Although the use of past climate to assess model performance was discussed in the first phase of FireMIP (Rabin et al., 2017), this has not been done yet. Most current state-of-the-art fire models have been developed using information from recent satellite data, which only covers the last forty years at best. Although these models agree on the spatial patterns of burnt area today, there is large disagreement between them onon the global trend over the historical era (i.e. the period from 1850 CE onwards) (Teckentrup et al., 2019) suggesting that the modelled underlying relationships and their sensitivity to changing conditions are different. Sensitivity experiments over this historical period do provide a better understanding of the sensitivity of different models to CO_2 levels, climate, population density, land use, and lightning (Teckentrup et al., 2019) however there is no way of verifying which model is right with such a short timeframe. This is a real concern for the robustness of future projections. In contrast, the models developed in this thesis were evaluated in an out-of-sample experiment and the simulated burnt area was evaluated against sedimentary charcoal data.

Charcoal records have been generally interpretated as an indicator of "biomass burning", which is related to burnt area (Power et al., 2008: Marlon et al., 2008; Daniau et al., 2012; Marlon et al., 2013). My comparison showed a good agreement of the sign of change in biomass burning with the simulated burnt area. The comparison with fire size and fire intensity was less good, confirming that the charcoal records are indicative of overall burnt area rather than some other aspect of the fire regime. However, there are ways of extracting additional information from charcoal data. For example, the software CharAnalysis (Higuera et al., 2009) allows both peak fire intensity and fire frequency to be extracted from these records and has been used to study past trends in these variables at a regional scale (e.g. Higuera et al., 2014; Meng et al., 2023). In future work, it could be useful to use CharAnalysis or other such software to validate the trends in other fire properties at a global scale. However, a limitation to the use of charcoal data for model evaluation is that the coverage is sparse during some time intervals and the patterns are geographically heterogenous. For example, there are large areas of Eurasia which show strong sensitivity to climate and CO_2 changes in my model simulations, but these changes cannot be validated due to a lack of records in this region. It would be useful to target areas for the collection of additional palaeo data based on these model experiments. Charcoal is not the only source of information about past fire regimes; organic biomarkers such as levoglucosan and benzene polycarboxylic acids are increasingly being used to identify pyrogenic carbon in soils and sediments (e.g. Elias et al., 2001; D'Anjou et al., 2012; Denis et al., 2012; Lehndorff et al., 2014). Combining multiple data sources would be useful for evaluating out-of-sample experiments. This thesis clearly demonstrates the utility of testing global fire models under out-of-sample conditions and recommends that the FireMIP community adopt such practices. Such efforts should not be limited to the Last Glacial Maximum; there are opportunities to evaluate the response to rapid climate warming in the past on a scale comparable to that of future climate warming (e.g. Malmierca-Vallet et al., 2022) and to examine the response to climate change and increasing human activities during the Holocene on fire regimes (e.g. Sweeney et al., 2022). Encouraging more exchange between the model development community and the palaeo fire community, through out-of-sample simulations, evaluation of models and palaeo simulations will also encourage more resources to be invested in obtaining high quality palaeo data, which in turn will help improve models and our confidence in them.

Mapping global fire intensity

Part of the difficulty with modelling global fire intensity is ensuring that what is recorded in the training observations is the energy released at the flaming front of a wildfire, which is the definition of fire intensity generally used. Active fire products, such as the MODIS collection 6 provide fire radiative power (FRP) measures (Giglio et al., 2006; Giglio et al., 2016) which represents instantaneous energy emitted by fire over the whole 1km x 1km MODIS pixel. Low FRP values (~15 MW) are attributed to cropland fires as well as very moist tropical and subtropical regions. In grassland fires, mean FRP values are around ~40 MW, and in boreal regions, with high tree cover and fuel loads, mean FRP values are around ~80 MW. These northern latitude wildfires are crown fires (Giglio et al., 2006). However, although FRP has been used as a measure for fire intensity (Wooster et al., 2004, 2013; Ichoku et al., 2008; Barrett and Kasischke, 2013; Archibald et al., 2013; Luo et al., 2017; Laurent et al., 2019) it cannot get at the energy emitted at the flaming front directly, meaning there is no direct way of distinguishing woody and crown high-intensity fires from surface or smouldering fires, directly from FRP (Kauffman et al., 2003; Wooster et al., 2004). Since FRP values from the MCD14ML dataset represent the energy emitted at the flaming front integrated over the whole pixel, it is expressed in W m^{-2}. This contrasts to the measure of fire line intensity in the Rothermel equations (1972), which is expressed per unit length of the fire line, in W m^{-1} (Byram, 1959).

Another limitation with using FRP values to represent intensity, is that the value in a pixel depends not only on the number of active fires (which can be obtained from active fire products) but also the individual sizes of each fire (which cannot). Not accounting for the average size of wildfires within a given grid-cell has led to unexpected results in the analysis of global FRP trends, an asymmetry exists between the Northern and the Southern hemispheres when mapping mean FRP values. This asymmetry has been attributed to very high values in the Southern hemisphere, notably Australia and South Africa (Giglio et al., 2006). Indeed, the highest global FRP values are found in Australian grasslands which are clearly not woody crown fires but large surface fires. These very large values lead to unrealistic conclusions in analyses, for example the presence of rare, intense wildfires in regions with no tree cover (in western Australia, Southern America, and Southern Africa) (Archibald et al., 2013). Even when weighting FRP values by fire counts (Luo et al., 2017) or when spatial-temporal matching between fire patches and FRP values is performed (Laurent et al., 2019) this issue does not disappear, and the highest values are still found in southwestern Australia.

To overcome these problems and take into consideration the effect of large fires on FRP values, I developed a metric for fire intensity that was more representative of intense wildfires, driven by high woody fuel loads. The square root of median fire size in a grid cell provides a rough estimate of median fire perimeter, which represents the fire line. Thus, dividing the FRP value in a grid cell by the square root of the median fire size in the same grid cell produces a metric for median fire line intensity and provides a way for the metric and its unit to be more consistent with an estimation of fire line intensity (W m^{-1}). This weighting allowed for a way to account for the effect that very large fire, primarily concentrated in grasslands, had on increasing FRP values in grid cells. The weighting is relatively simple but provides a big change in the global distribution of values, eliminating the asymmetry between the Northern and the Southern hemisphere. In addition, when looking at the spatial correlations, whereas median FRP values had a negative correlation with tree cover in tropical forests and much of Australia, this negative correlation disappears when weighing by the square root of median fire size. Median FRP values also correlated positively with grass cover in much of the world, which is inconsistent with large, woody fuel loads necessary for the most intense wildfires. On the other hand, the fire intensity metric correlates negatively with grass cover across much of the world, suggesting it is a better representation of woody-fueled wildfires.

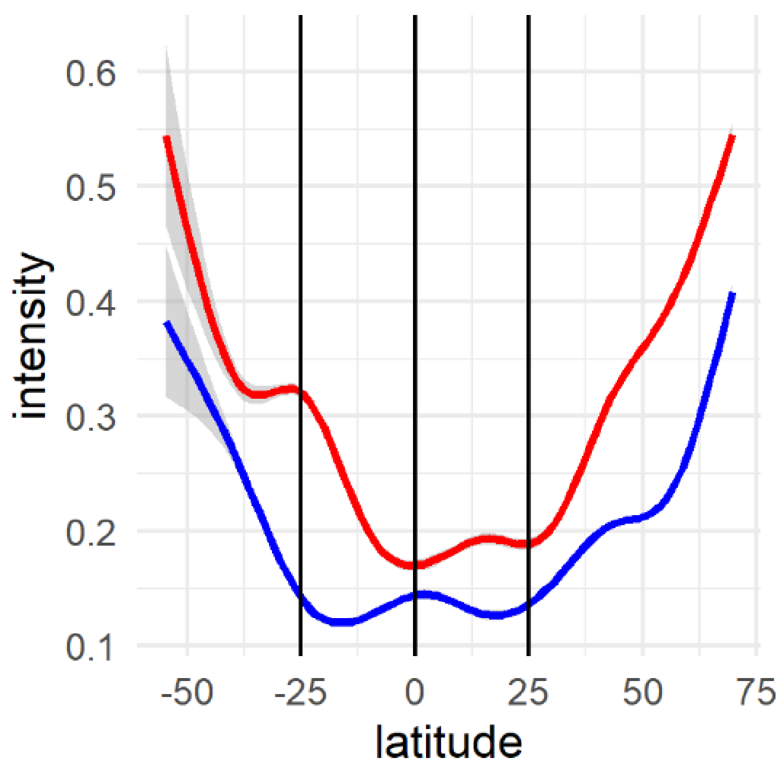

Figure 18. Latitudinal distribution of normalized median FRP values derived from MCD14ML (Giglio et al., 2006) (red) and the intensity metric used in this analysis (blue). The asymmetry can be observed in the median FRP values between the latitudes 0-25°S (with a rapidly increasing slope) and 0-25°N (with a much flatter slope that only increases after 25°N.

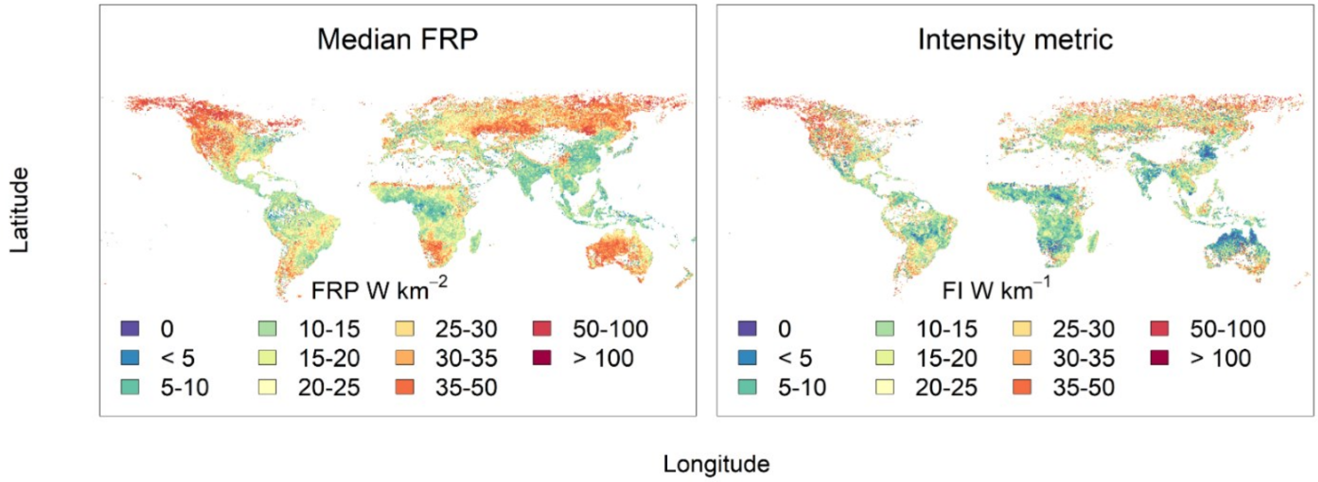

Figure 19. Global distribution of observed median FRP values (in W.km^{-2}) from MCD14ML (Giglio et al., 2006) (left) and the fire intensity metric used in this analysis (in W.km^{-1}) (right)

The relationships fitted between this weighted metric and the sixteen predictors were equally more consistent with the general understanding of fire intensity that when only considering FRP values. The final fire intensity model (using the weighted metric) showed a negative relationship with grass cover, an insignificant relationship with shrub cover and cropland density and a positive relationship with roads whereas median FRP values showed a strong positive relationship with both grass and shrub cover and a strong negative relationship with roads. The positive relationship with roads in the final model is in line with previous research that shows a positive relationship between human activity and burnt area in regions which are predominantly fire-free (Harrison et al., 2021). In these regions, road creation for deforestation and commercial activities creates new forest edges, which promote drying and increase wind speed as well as providing the probability of a human-caused ignition (Armenteras et al 2013, Cano-Crespo et al 2015, Pausas and Keeley 2021). These forested, fire-free ecosystems are more likely to have high fuel loads which can promote intense wildfires. In contrast, the negative relationship between fire intensity and grass cover is consistent with rapidly spreading but low intensity fires in grassdominated ecosystems. When fitting statistical relationships between the burnt area and median FRP and the fire intensity metric globally, the relationship between burnt area and median FRP is monotonically positive ($R^2 = 0.18$) and a very weak negative correlation ($r=-0.07$), however the relationship between burnt area and the fire intensity metric is monotonically negative ($R^2 = 0.11$) and a stronger negative correlation ($r=-0.16$). This second relationship is also more consistent with the negative correlation we would expect between burnt area and fire intensity given their opposite distributions (Luo et al., 2013). The spatial correlations also make more sense when considering the fire intensity metric values, with burnt area and fire intensity positively correlated in much of the United States for example, where we expect large and intense wildfires but negatively in regions of frequent fire activity (such as African savannas and Australia). Although this metric is simple, it represents a consistent way of mapping for fire intensity. This thesis provides the first standalone model for fire intensity and established its independent global controls.

Wildfire regimes and global change

The aim of this thesis was to explore the impacts of changes in climate, atmospheric CO_2 levels and human activity on the spatial distribution of global burnt area, fire size and fire intensity. Here, I consider these individual influences on fire properties.

Climate impact on global wildfire regimes

Most of the research into modelling the direct effect of climate on global wildfires has focused on short-term climate effects, and specifically how instantaneous weather conditions influence the probability of burning. These questions have been explored by quantifying the effect of fire weather (instantaneous air temperature, relative humidity, and wind speeds) on the flammability of vegetation (Jones et al., 2022). Originally, indices of fire weather, such as the FWI, were developed to aid in the establishment of daily fire risk at fine scales and were used in an operational setting. Since then, such indices have been used to project global fire risk (e,g, Abatzoglou et al., 2018; Jain et al., 2021; Jones et al., 2022) and the components of fire weather indices (and their relationship to fire spread) are incorporated into empirical schemes and models (e.g. Pechony and Shindell, 2010; Mangeon, 2016) and process based models (e.g. Venevsky et al., 2002; Thonicke et al., 2010) fire models. Nevertheless, fire weather indices were designed for a fine temporal and spatial scale and may not necessarily be expected to scale up globally (Lasslop et al., 2015). In my models the key components of fire weather do not appear globally significant for fire intensity, which had a negative relationship with VPD and an insignificant relationship with DTR and wind speed. Furthermore, although VPD and DTR were significant for burnt area, the t-values were much smaller than for other variables, and the relationship was negative with wind, in line with previous work showing the limited impact of wind speeds on burnt area globally for wind speeds above 2–3 m s^{1} (Lasslop et al., 2015). However, for the fire size model, DTR and wind speed (as well as VPD to a lesser extent) were key drivers. This makes intuitive sense as we would expect fire spread to be most important in predicting fire size. These results highlight that the climate components of fire weather are essential control on global fire size distribution. As such, fire weather indices may provide useful information on fire sizes at a global scale. Nevertheless, fire weather does not appear to provide additional or useful information on the global distribution of fire intensity. This is an important result for global modelling efforts: it suggests that the components of fire weather should be included when modelling fire regimes, but they should relate to the estimation of fire size and to a lesser extent burnt area but should not necessarily be considered for fire intensity. It calls for the current linear coupling of fire size and fire intensity that is built-in to global fire models such as SPITFIRE (Thonickle et al., 2010) to be revisited.

Furthermore, my results also show that wildfire regimes are highly sensitive to the interactions between different climate variables. Atmospheric dryness, as measured by VPD, is particularly important. The amplitude of changes of VPD in relation to other climate variables had a non-trivial impact on total burnt area estimates, with small changes in VPD leading to large changes in modelled outputs. This effect varied geographically with a stronger sensitivity in northern latitude. At the Last Glacial Maximum, under the climate only sensitivity experiment the magnitude of change in VPD was responsible for very large fluctuations in overall trends. Burnt area increased by 48% compared to modern under slightly warmer and wetter conditions when the magnitude of change in VPD values was not as large, compared to a 42% decrease in the coldest LGM climate where VPD values were very low. Furthermore, the response of fire size to wind and DTR changes was not as sensitive as the response to changes in VPD values and low values of VPD strongly inhibited fire size (and fire spread) at the LGM. One reason for this strong sensitivity to VPD relative to other climate variables may be its role on long-term plant growth (Grossiord et al., 2020), and thus on fuel loads. Whilst low VPD values inhibited fire spread under LGM conditions, it still allowed for long-term fuel build-up, thus enabling high-intensity fires to burn when conditions were favorable. Furthermore, increases in fire intensity compared to modern-day conditions were much larger at the LGM than under future conditions, which may appear counter-intuitive given the increased temperatures and burnt area under future conditions. However, given that fire intensity is very sensitive to VPD, high values of VPD become a limiting factor on fuel build up. This sensitivity also explains why fire intensity is reduced under the low mitigation scenario compared to the high mitigation scenario, since increased dryness (VPD but also dry days and dry day seasonality) prevents fuel build-up. The different impact of VPD, and its interaction with temperature and dryness, on fire intensity under cold and warm climates suggests trade-offs exist between different climate variables and that these trade-offs may be decoupled. Taken together, these results suggest that atmospheric dryness has a stronger effect on limiting fuel loads under warmer conditions, in line with previous work (Williams et al., 2013; Grossiord et al., 2020; Rao et al., 2022). The effect of VPD on plant growth has been shown to affect fuel loading and is expected to reduce fuel loading in boreal regions in the future due to warming (Foster et al., 2022; Gaboriau et al.,2023). Furthermore, it has been shown to influence forest resilience to burning (Stevens-Rumann et al., 2017). The relationship between VPD and other climate variables such as dryness has also been shown to be an important influence on burnt area (Rao et al., 2020). Future trajectories in wildfire regimes will depend on these variables' interactions and relative change to each other. This finding is demonstrated in the future simulation in which the high-mitigation scenario saw a much smaller increase in burning compared to the low-mitigation scenario. Under high-mitigation, climate only sensitivity experiment, burnt area decreased in three of the four models (solely driven by climate changes as there are no changes in human activity in this experiment), but one model did see a global increase (IPSL-CM5A-LR). Under the low-mitigation scenario, one of the models (MIROC5) showed decreasing burnt area, whilst another (HADGEM2-ES) simulated an increase of over 25% globally. These results emphasize that considering the effect of climate only through short-term fire weather conditions is not sufficient. Climate variables should not only serve as predictors for fuel flammability and fire spread but also as predictors of fuel load and fuel build-up. These processes operate on different time scales and may be decoupled from each other. There is a growing awareness that better understanding of how vegetation properties affect fuel build-up is needed to accurately predict fire regimes (Forkel et al., 2019a; Hantson et al., 2020) and research has shown the importance of accounting for antecedent vegetation conditions (which are in part controlled by climate) to improve burnt area predictions (van der Werf et al. 2008; Krawchuck and Moritz, 2011; O et al., 2020; Kuhn-Régnier et al., 2021). These results add to this by highlighting the importance of VPD (and its control on plant growth) as a control not just on burnt area but also fire intensity and to a less extent, fire size and call for its effect on long term fuel accumulation and fuel load to be explicitly included in modelling efforts, and for this effect to be decoupled from its effect on fire spread.

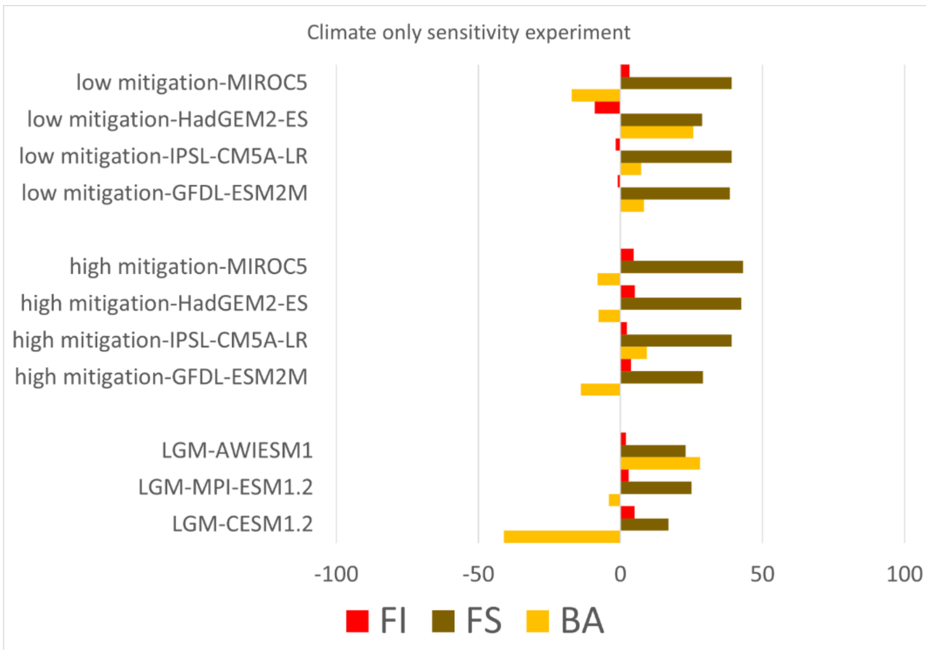

Figure 20. Percentage change in global total BA, median FS, and median FI between the modern, low mitigation 2100CE, high mitigation 2100CE and LGM experiments for the climate only sensitivity experiment.

CO_2 impact on global wildfire regimes

The impact of atmospheric CO_2 concentrations on global wildfire regimes is significant and operates through increasing fuel loads and hence increasing burning under future conditions and reducing fuel loads and burning at the LGM. The amplitude of the CO_2 effect on burnt area was large in both directions under the CO_2 only sensitivity experiment (~70% reduction at the LGM, a ~10% increase in BA with CO_2 levels at 421 ppm compared to present and a ~70%

increase in BA with CO_2 levels at 670 ppm compared to present). These results make a strong case for atmospheric CO_2 levels on fuel loads to be explicitly considered in global fire models. This work also provides a method through which to directly quantify the effect of CO_2 fertilization. However, this requires vegetation models and earth system models to get the response of vegetation to changes in CO_2 right which has proved difficult. The largest uncertainty between DGVM simulations of historical trends in GPP have been attributed to different treatments of CO_2 fertilization (Yang et al., 2022). This uncertainty is not limited to the modelling community. A study reporting a sharp decline in global CO_2 fertilization (Wang et al., 2020) raised concerns of inconsistent datasets (Frankenberg et al., 2021; Zhu et al., 2021) and there has since been disagreement in methods (Sang et al., 2021; Cortés et al., 2021; Jeong et al., 2023 (pre-print)). Given the significance of this effect on global wildfire regimes, it is essential to correctly capture the response of vegetation to changing CO_2 levels. Recent work has shown that it is possible to constrain CO_2 fertilization and estimate it quantitatively (Keenan et al., 2023; Ruehr et al., 2023). As such, the next step is to incorporate the effect of CO2 fertilization explicitly into modelling efforts. In the long-run, this would require PFT-specific vegetation inputs of fire models to be replaced by vegetation properties which can be predicted from environmental conditions and can flexibly respond to changing conditions in climate and CO2. Whilst this thesis has demonstrated that this can be achieved for GPP, through using the P Model, some parameters remain distinct such as tree cover, grass cover and shrub cover. Future steps could be taken to explore which vegetation properties influence vegetation flammability, survivability and recovery, ultimately enabling such inputs to also be replaced.

Fire intensity also showed a response to the CO_2 effect on fuel loads, though it was in the opposite direction to the impact on burnt area and had a much smaller effect under future conditions (warming) than at the LGM (cooling). This finding appears counter-intuitive since increased fuel loads might be expected to increase fire intensity. One explanation is that, with more frequent burning under warming conditions, there is an indirect limitation of fuel build-up and hence less intense fires whereas reduced burning at the LGM allowed fuel to build up over a longer period and thus promoted more intense fires when they did occur. This is in line with the point made about the controls of fire size, burnt area and fire intensity operating on different timescales. My results also show that the sensitivity of wildfire regimes to CO_2-enduced changes on vegetation is spatially heterogeneous. Increasing CO_2 (CO_2 –fertilization) has a consistent effect globally on GPP and is responsible for increases over the last decades (Yang et al., 2022). This increase in productivity uniformly increases fuel loads (or decreasing them in the case of decreasing CO_2). However, the relative sensitivity of global fire regimes to changes in CO_2 varies spatially and may be outweighed by other factors (climate, human activity). My results identify key regions in which the CO_2 effect is most influential on fire regimes and where the effects of increasing CO_2 may either amplify the current future projections or dampen them. Furthermore, they also show that the regions of high sensitivity to CO_2 are not the same for burnt area, fire size and fire intensity. For burnt area and fire size, under LGM conditions, the regions that were most sensitive to low CO_2 were concentrated in the tropics, Alaska and across Europe and Eurasia above 50°N. Fire intensity was sensitive to changes in CO_2 in these regions, with the addition of North America also showing strong a strong sensitivity to CO_2. Under future conditions, the regions with the largest sensitivity were concentrated in tropical regions and in latitudes below 50°N for burnt area. For fire size and fire intensity the most sensitive regions were concentrated in the northern-high latitudes. This spatially heterogenous sensitivity between burnt area on the one hand and fire size and intensity on the other has important management implications. Even in regions where burnt area is expected to increase under increasing CO_2, fire size and fire intensity may be reduced due to CO_2-enduced changes in vegetation. This reduction is notably the case in North America, the Amazon and inland southern-hemisphere Africa in the future CO_2 sensitivity experiment. This is important to consider, as many integrated fire management strategies promote fuel load management through vegetation clearance or prescribed burning. Given that vegetation is not adapted to fire but to fire regimes, altering for fire regimes can make species vulnerable, and thus the impact of such management strategies needs to be carefully considered (Keeley et al., 2011). If fuel loads are increased in the future due to a high sensitivity to CO2-enduced changes in vegetation this must be considered when designing fire management schemes. There is a growing argument that, through active fire suppression, usually high fuel loads have accumulated, increasing the risk of large and intense wildfires in fuel-limited regions (Miller et al. 2012, Mallek et al. 2013; Steel et al., 2015). This argument has been made in many regions in North America for example and as a response there has been a growing call for prescribed burning and managed wildfires as part of a move towards integrated fire management (Forest Climate Action Team, 2018, USDA, 2023). Given that this is a region in which CO_2-enduced changes in vegetation are predicted to reduce fire size and intensity, this should be considered when developing such strategies.

Human impact on global wildfire regimes

This work shows the significant impact of human activity on global wildfire regimes under both modern day and future conditions. When setting all human activity (population density, road density and cropland) to zero in the models, global burnt area increased by 63% and mean fire size increased by 60%. The effect on fire intensity was negligible (0.15% decrease). Under the low-mitigation future scenario, keeping human activity constant increased burnt area by 35-62%, fire size by 20-33% and fire intensity by 4% for three models, and 30% for the fourth model. Given that the overall trend is one of declining burnt area and smaller increases in both fire size and fire intensity when all factors are included, this highlights the role human activity plays in overriding changes in wildfire regimes as a response to a warming climate and increasing atmospheric CO_2 concentrations.

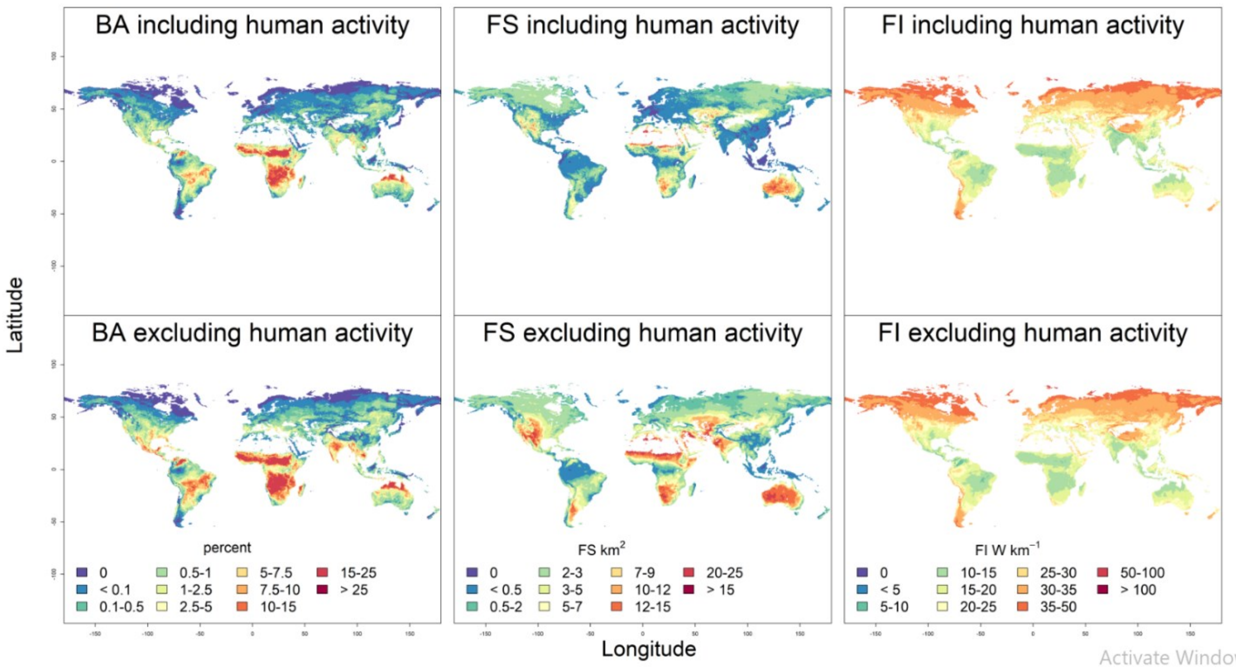

Figure 21. Global distribution of modelled burnt area (BA) in km^2, fire size (FS) in km^2, and fire intensity (FI) in W.km^{-1} for the original model (including human activity) (top) and for the sensitivity analysis in which all human predictors are set to zero (excluding human activity) (bottom)

These results show that the influence of current human activity on global wildfires is one of suppression, through landscape fragmentation, which is expected to continue. Whilst this suppression effect is not a new finding (Bistinas et al., 2014; Knorr et al., 2014; 2016; Andela et al., 2017), this understanding of human activity's effect on wildfire regimes has yet successfully to make it into global fire models. Most global fire models use human population density to calculate human ignition rates, with increasing ignitions as population density increases up to a threshold, after which no more ignitions occur (Hantson et al., 2016; Rabin et al., 2017). This assumption directly contradicts findings that globally the relationship between population density and burnt area is negative (Bistinas et al., 2014). One of the reasons for this negative relationship is that, although humans are responsible for ignitions, their effect is overwhelmingly one of suppression through agricultural and urban expansion (Andela et al., 2017; Harrison et al., 2021). To account for this double effect of humans on ignition and suppression, some global fire models simulate the fire suppression by humans either explicitly or implicitly through GDP (LM3-FINAL; CLM-Li) and population density (LM3-FINAL; CLM-Li; CTEM; JSBACH-SPITFIRE). Many models assume also that no fires occur on agricultural land, which indirectly captures the effect of cropland expansion and agricultural intensification on burnt area (Rabin et al., 2017). However, these relationships rely on simplistic assumptions about human influence on fire regimes (Ford et al., 2021) and itthat fire models have not been able to accurately predict the magnitude of the recent decline in burnt area due to inadequate representation of human activity (Andela et al., 2017).

The inclusion of road density in addition to the most common human predictors usually included in global fire models (cropland and population density) proved a significant improvement in my models. It allowed for the interactions between human activity and fire regimes to be capture as it provided a way for the effect of both human ignitions and human suppression on burnt area to be accounted for. Only when road density was included did the relationship between burnt area and population density become positive. Furthermore, for fire size, the inclusion of road density led the population density predictor to become insignificant, showing in the case of fire size, ignitions were not important, but that landscape fragmentation was key. On a regional scale, information about roads has proved to have a much more spatially diverse relationship with fire than other anthropogenic variables such as population density (Parisien et al., 2016).

Running the models with and without including human activity under modern day conditions also highlighted that the sensitivity of global fire regimes to human population varied between biomes. Sensitivity to human activity was largest in tropical xeric and temperate shrublands. This is in line with research showing that the effect of human activity on burnt area is strongest in intermediate productivity ecosystems, since fire is limited neither by moisture nor fuel availability (Lasslop et al., 2017). Furthermore, even within the same biome, different socioeconomic activities, cultural practices, and rural population trends also influence fire regimes (Chergui et al., 2018; Mancini et al., 2018). My models were able to capture this, with, for example, much larger decreases in burnt area under future conditions in tropical Africa and India than in South America and South-East Asia. These regional differences most likely reflects the difference between human-fire relationship in these regions, with crop related fire use (field preparation, and residue burning) across Africa and India but vegetation clearance fires in the Amazon and South-East Asia. Given that my models can identify these regions of varying sensitivity to human influence, future work could consist of comparing these regions with current knowledge about human fire use globally (Millington et al., 2022). Increased collaboration is needed between the global fire modelling community, predominantly based in physical modelling, and other human-fire research based in different modelling perspectives, such as people-centric models for example (Ford et al., 2021). Such collaboration would lead to greater understanding of our human-fire interactions, ultimately providing improved representation of human activity in global fire models.

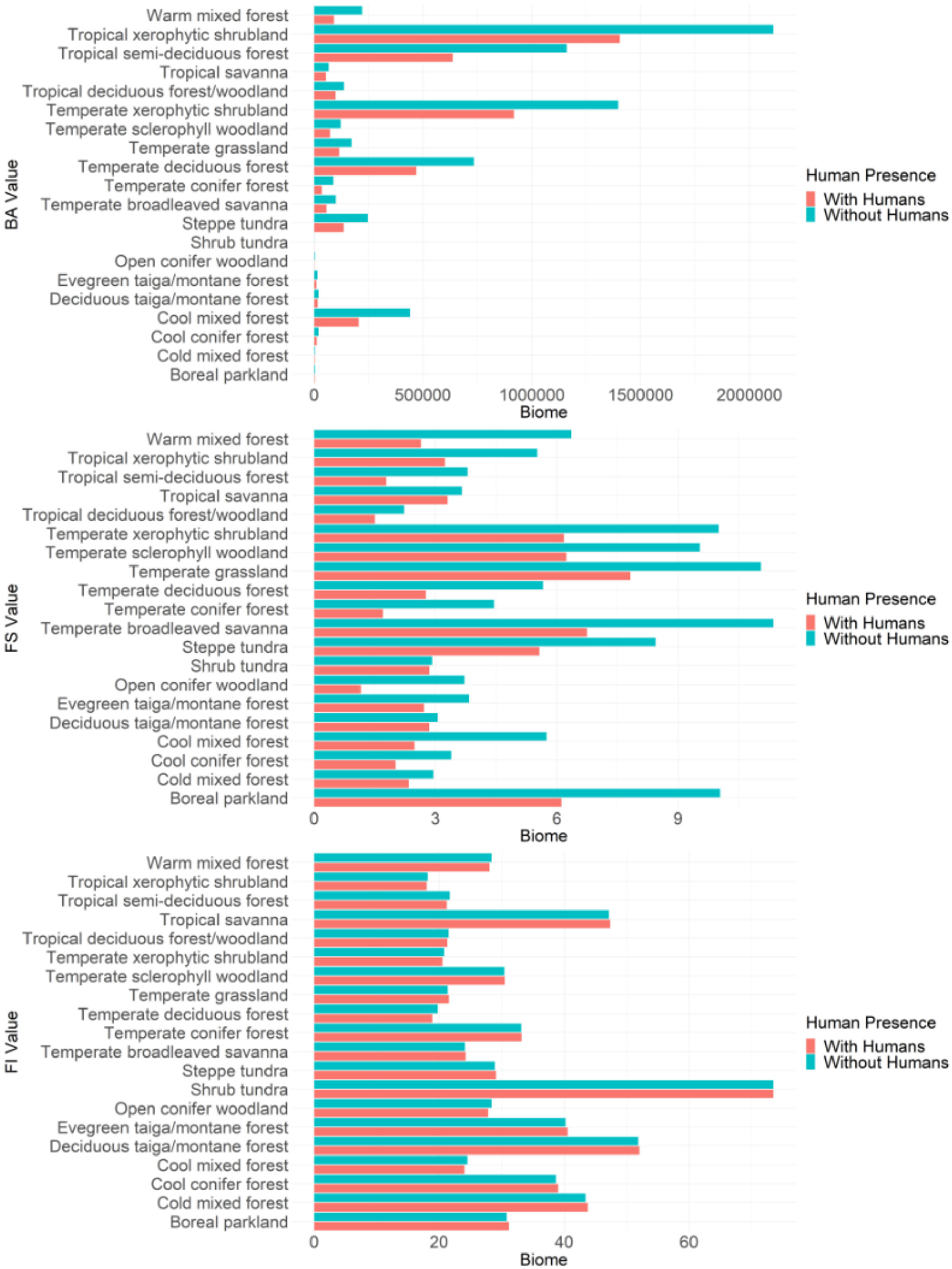

Figure 22. Breakdown per biome of total annual burnt area (in km^2), mean fire size (in km^2) and mean fire intensity (W.km^{-1}) for the modelled values with and without human presence

Finally, though the effect of human activity on wildfire regimes today is significant, debate remains within the literature about when humans started having a noticeable impact on global fire regimes (Moreno et al., 2000; Pinter and Anderson, 2006; Power et al., 2008; Pausas and Keeley, 2009; Archibald et al., 2012; McDonald et al., 2017; Gowlett, 2016). Claims have been made that their effect dates back many millennia, at least from the advent of landscape management associated with the adoption of agriculture (e.g. Vanniere et al., 2016; Dietze et al., 2018). Hunter-gather communities used fire during the LGM, however the impact on the landscape is not clear (Gott et al., 2005; Kaplan et al., 2016; Constantine IV et al., 2023) There is evidence that humans were already using fire at this time for land management, to facilitate hunting and promote vegetation (Gott, 2005). However, others have argued that the impact of humans on fire regimes was negligible before the Holocene (Black et al., 2007; Fuller et al., 2014; Portenga et al., 2016). My models addressed the question of human influence on global fire regimes at the LGM. The sensitivity analysis showed that, at this time, the impact of humans on a large-scale wildfire was negligible. Including human activity made no significant difference in either Europe, Africa or Australia, regions where estimates of LGM human populations have been made (Gautney and Holliday, 2015). The changes in wildfire regimes compared to present can be explained solely by changes in climate and atmospheric CO_2 levels. This is to be expected as much of the world would have been inhabitable for humans under LGM conditions (A.N. Williams et al., 2013; Blinkhorn et al., 2022). Given that I successfully ran this analysis for the LGM, the next step could be to conduct a transient simulation running these models from the Holocene onwards to establish when the impact of humans first becomes visible on a global and regional scale.

Conclusion

Given the short-time frame of satellite data available that the global wildfire modelling community must build empirical models from, it remains challenging to assess how robust our current state-of-the art models are at simulating fire regimes under conditions dramatically different to the ones they were trained on. This difficulty in assessing model robustness is more concerning since diverging historical trends between models show that, although there is relatively good agreement on the patterns of burning today, the underlying process assume to capture those patterns differ. Furthermore, until now empirical fire modelling effort have remained focused on burnt area, with no global empirical models for fire intensity and very few for fire size. This focus on burnt area has proved a major limitation in understanding the independent global drivers of these fire properties, which process-based models still struggle to simulate accurately.

This thesis has provided a roadmap on how to develop robust empirical fire models beyond burnt area and use the past to ensure their robustness in the future. It has presented three standalone empirical models for burnt area, fire size and fire intensity and offered insights into (1) their independent global controls (2) their individual responses to changes in climate, atmospheric CO_2 levels and human activity, both in the past and future. A key strength of this work is the use of sensitivity analysis to isolate out the independent effects of climate, CO_2 levels and human activity on fire regimes. By using a first-principle productivity model and a coupled biogeography, biochemistry model allowed for effect of climate and CO_2 levels to be decoupled. This separation could not have been achieved based only on data analysis alone.

I have shown that whereas burnt area is controlled primarily by fuel availability and dryness, fire intensity is controlled by fuel-build up. Fire size is primarily controlled by fuel continuity and fire weather which promote fire spread. The availability of fuel, one of the four conditions for a fire to start, is a key control for all three properties. However, considering them separately allowed for new insights. The availability of fuel needs to be considered along two dimensions: fuel continuity and fuel load. Both these factors act as separate controls, and they affect different aspects of global wildfire regimes differently. Fuel continuity does not appear to be as limiting for fire intensity and fuel load does not appear to be as limiting for fire size. Moving forward, these two dimensions of fuel availability need to be considered separately and decoupled from each other; whereas fuel continuity is primarily controlled by human activity, fuel load is driven by VPD, the seasonality of dryness and CO_2 levels (through its control on productivity). VPD and CO_2 levels play especially important role on fuel-build up and appear essential for modelling fire intensity and burnt area. Both their effects need to be considered to capture how changing conditions will affect fuel-loading. Furthermore, although fire weather and human activity played the most significant role in determining the distribution of fire size, the long-term effect of VPD and CO_2 levels on fuels also proved to be a limiting factor for fire size both under LGM and future conditions. My results also showed that even when fire properties shared the same predictors, their effect operated in different directions and on different timescales. This finding was most apparent for burnt area and fire intensity. Whereas the highest fire intensity occurs at low dryness seasonality to provide the conditions for long-term fuel build-up, the largest burnt area required high dryness seasonality to provide drying out of fuels. These differences in the timescale are a further explanation of the IOFI hypothesis.

From a methodological perspective my results have also shown the value of using out-of-sample experiments for the evaluation of global fire models and calls for this practice to be adopted by the greater wildfire modelling community. More cross-collaboration is needed between the fire modelling community and the palaeo community if we want to ensure greater robustness in our models. This thesis has also demonstrated the power of sensitivity analysis and counter-factual experiments as a strong explanatory tool. Applying sensitivity analysis under LGM conditions allowed me to highlight the importance of considering both climate and CO_2 levels to correctly capture the magnitude of burning. Furthermore, running the same set of sensitivity analysis under future conditions allowed me to identify regions that were sensitive to climate, CO_2 or human activity changes, which can help inform management decisions. In the case of climate and CO_2, having identified sensitive regions (and the effect of different variables in those regions) under both LGM and future conditions also provides a way in which to identify regions that are sensitive to change in both directions regardless of warming or cooling as well as regions that only demonstrate a strong sensitivity in one direction (either under warming conditions or cooling conditions). The identification of these different regions will help direct future explanatory work. In the case of human activity, identifying regions in which the sensitivity was greatest also provides useful information for the wider community working on human-fire interactions. The simplicity of the models does not appear to have reduced its performance and they were able to outperform many of the process-based models in FireMIP. but provided strong explanatory power. The models require very little computational power, and this is what allowed for the volume of sensitivity analysis that were able to be run. The simplicity of the models also means that they can easily be shared and quickly applied for the use of new academic research questions, such as transient runs during the Holocene, but also during the next century. Furthermore, their use is not limited to academic circle. These models can easily be shared with a wider community of fire practitioners and policy makers to be used as a dynamic research tool which supports policymaking. For example, experiments could be designed with relevant stakeholders to study the response of fire regimes to different management strategies such as vegetation thinning or prescribed burning. This provides the opportunity for knowledge exchange and collaboration, going beyond only providing policy makers with finalized and fixed projections.

Empirical models such as the ones developed here are not without their disadvantages. For one, they require a large amount of training data, and given the short-time frame of available satellite imagery, large uncertainties on the fitted relationships remain. Furthermore, these models remain probabilistic and cannot be coupled directly with land surface models. As such questions of feedback between climate, vegetation and fire (including the effect of each fire property on the others) cannot be explored directly. This remains a major limitation of these types of models. The long-term aim for the fire modelling community should be the improvement of process-based fire models able to address these limitations. These process-based models should be able to reproduce historical trends and capture the effect of large-scale changes in climate, CO_2 and human activity on wildfires. However, this is not yet the case, and given that our understanding of the processes driving global fire distribution is currently incomplete, empirical models provide an essential tool from which new hypotheses can be developed and tested. In turn, new insights, such as the ones presented in this thesis, will provide the building blocks from which to develop a new generation of empirically informed process-based fire models. Given the growing concerns over changing fire regimes in larger society and our inability to provide robust projections as a global modelling community, explanatory tools and analysis such as these are crucial.

References

Abatzoglou J.T., A.P. Williams, R. Barbero, Global emergence of anthropogenic climate change in fire weather indices. *Geophysical Research Letters* **46(1)**, pp.326-336 (2019).

Abatzoglou, J.T., Kolden, C.A., Balch, J.K. and Bradley, B.A., Controls on interannual variability in lightning-caused fire activity in the western US. *Environmental Research Letters,* **11(4)**, p.045005 (2016).

Albani, S., Balkanski, Y., Mahowald, N., Winckler, G., Maggi, V.,and Delmonte, B.: Aerosol-climate interactions during the Last Glacial Maximum*, Current Climate Change Reports*, **4**, 99–114 (2018).

Amatulli, G., Domisch, S., Tuanmu, M.N., Parmentier, B., Ranipeta, A., Malczyk, J. and Jetz, W., A suite of global, cross-scale topographic variables for environmental and biodiversity modeling. *Scientific data*, **5(1)**, pp.1-15 (2018).

Andela N., D.C. Morton, L. Giglio,Y. Chen, G.R. van der Werf, P.S. Kasibhatla, R.S. DeFries, G.J. Collatz, S. Hantson, S. Kloster, D. Bachelet, A human-driven decline in global burned area. *Science* **356(6345)**, pp.1356-1362 (2017).

Andela, N. and Van Der Werf, G.R., Recent trends in African fires driven by cropland expansion and El Niño to La Niña transition. *Nature Climate Change* **4(9)**, pp.791-795 (2014).

Andela, N., Morton, D.C., Giglio, L., Paugam, R., Chen, Y., Hantson, S., Van Der Werf, G.R. and Randerson, J.T., The Global Fire Atlas of individual fire size, duration, speed and direction. *Earth System Science Data* **11(2)**, pp.529-552 (2019).

Archibald, S., Lehmann, C.E., Belcher, C.M., Bond, W.J., Bradstock, R.A., Daniau, A.L., Dexter, K.G., Forrestel, E.J., Greve, M., He, T. and Higgins, S.I., Biological and geophysical feedbacks with fire in the Earth system. *Environmental Research Letters* **13(3)**, p.033003 (2018).

Archibald, S., Lehmann, C.E., Gómez-Dans, J.L. and Bradstock, R.A., Defining pyromes and global syndromes of fire regimes. *Proceedings of the National Academy of Sciences* **110(16)**, pp.6442-6447 (2013).

Archibald, S., Staver, A.C. and Levin, S.A. Evolution of human-driven fire regimes in Africa. *Proceedings of the National Academy of Sciences* **109(3)**, pp.847-852 (2012).

Armenteras D, Barreto J S, Tabor K, Molowny-Horas R and Retana J. Changing patterns of fire occurrence in proximity to forest edges, roads and rivers between NW Amazonian countries *Biogeosciences* **14** 2755–65 (2017).

Artés, T., Oom, D., De Rigo, D., Durrant, T.H., Maianti, P., Libertà, G. and San-Miguel-Ayanz, J., A global wildfire dataset for the analysis of fire regimes and fire behaviour. *Scientific data* ***6*(1)**, p.296 (2019).

Bachelet, D., Ferschweiler, K., Sheehan, T. J., Sleeter, B. M., and Zhu, Z., Projected carbon stocks in the conterminous USA with land use and variable fire regimes. *Global Change Biology* **21**, 4548– 4560 (2015).

Bak, P., Tang, C. and Wiesenfeld, K., Self-organized criticality: An explanation of the 1/f noise. *Physical review letters* **59(4)**, p.381 (1987).

Balch, J. K., Abatzoglou, J. T., Joseph, M. B., Koontz, M. J., Mahood, A. L., McGlinchy, J., Cattau, M. E., and Williams, A.P.: Warming weakens the night-time barrier to global fire, *Nature*, **602**, 442–448, (2022).

Barrett, K. and Kasischke, E.S., Controls on variations in MODIS fire radiative power in Alaskan boreal forests: Implications for fire severity conditions. *Remote sensing of Environment* **130**, pp.171-181 (2013)

Bastin, J.F., Finegold, Y., Garcia, C., Mollicone, D., Rezende, M., Routh, D., Zohner, C.M. and Crowther, T.W., The global tree restoration potential. *Science* ***365*****(6448)**, pp.76-79 (2019)

Basuki. I., W.C. Adinugroho, N.A. Utomo, A. Syaugi, D.H. Tryanto, H. Krisnawati, S.C. Cook-Patton, M. Novita, Reforestation opportunities in Indonesia: mitigating climate change and achieving sustainable development goals. *Forests*, **13(3)**, p.447 (2022).

Beerling, D.J. and Osborne, C.P., The origin of the savanna biome. *Global change biology* ***12*****(11)**, pp.2023-2031 (2006).

Betts, R. A., Golding, N., Gonzalez, P., Gornall, J., Kahana, R.,Kay, G., Mitchell, L., and Wiltshire, A.: Climate and land use change impacts on global terrestrial ecosystems and river flows in the HadGEM2-ES Earth system model using the representative concentration pathways, *Biogeosciences*, **12**, 1317–1338 (2015).

Bistinas, I., Harrison, S.P., Prentice, I.C. and Pereira, J.M.C., Causal relationships versus emergent patterns in the global controls of fire frequency. *Biogeosciences* **11(18)**, pp.5087-5101 (2014).

Bistinas, I., Oom, D., Sá, A.C., Harrison, S.P., Prentice, I.C. and Pereira, J.M., Relationships between human population density and burned area at continental and global scales, *PLoS One* **8(12)**, p.e81188 (2013).

Black, M.P., Mooney, S.D. and Haberle, S.G., The fire, human and climate nexus in the Sydney Basin, eastern Australia. *The Holocene* **17(4)**, pp.469-480 (2007).

Blarquez, O., Vannière, B., Marlon, J. R., Daniau, A.-L., Power, M. J., Brewer, S., and Bartlein, P. J.: paleofire: An R package to analyse sedimentary charcoal records from the Global Charcoal Database to reconstruct past biomass burning, *Comput. Geosci.* **72**, 255–261 (2014).

Blinkhorn, J., Timbrell, L., Grove, M. and Scerri, E.M., Evaluating refugia in recent human evolution in Africa. *Philosophical Transactions of the Royal Society B* **377(1849)**, p.20200485 (2022).

Boer, M.M., De Dios, V.R., Stefaniak, E.Z. and Bradstock, R.A., A hydroclimatic model for the distribution of fire on Earth. *Environmental Research Communications* **3(3)**, p.035001 (2021).

Bond, W. J. and Midgley, G. F.: Carbon dioxide and the uneasy interactions of trees and savannah grasses, *Philos. T. R. Soc. B*, **367**, 601–612 (2012).

Bond, W. J., Midgley, G. F., and Woodward, F. I.: The importance of low atmospheric CO2 and fire in promoting the spread of grasslands and savannas, *Glob. Change Biol.*, **9**, 973–998 (2003).

Bond, W.J., Woodward, F.I. and Midgley, G.F., The global distribution of ecosystems in a world without fire. *New Phytologist* **165(2)**, pp.525-538 (2005).

Bowman D.M., Balch J., Artaxo P., Bond W.J., Cochrane M.A., D'antonio C.M., DeFries R., Johnston F.H., Keeley J.E., Krawchuk M.A., Kull C.A., The human dimension of fire regimes on Earth. *Journal of biogeography* **38(12)** pp.2223-2236 (2011).

Bowman, D. M. J. S.: The impact of Aboriginal landscape burning on the Australian biota, *New Phytol*., **140**, 385–410 (1998).

Bowman, D. Wildfire science is at a loss for comprehensive data. *Nature*. **560** (7716), 7–8 (2018).

Bowman, D.M., Balch, J.K., Artaxo, P., Bond, W.J., Carlson, J.M., Cochrane, M.A., D'Antonio, C.M., DeFries, R.S., Doyle, J.C., Harrison, S.P. and Johnston, F.H., Fire in the Earth system. *Science* **324(5926)**, pp.481-484. (2009).

Bowman, D.M., Kolden, C.A., Abatzoglou, J.T., Johnston, F.H., van der Werf, G.R. and Flannigan, M., Vegetation fires in the Anthropocene. *Nature Reviews Earth & Environment* **1(10)**, pp.500-515 (2020).

Braconnot, P., Otto-Bliesner, B., Harrison, S., Joussaume, S., Peterchmitt, J.Y., Abe-Ouchi, A., Crucifix, M., Driesschaert, E., Fichefet, T., Hewitt, C.D. and Kageyama, M., Results of PMIP2 coupled simulations of the Mid-Holocene and Last Glacial Maximum–Part 1: experiments and large-scale features. *Climate of the Past* **3(2)**, pp.261-277 (2007).

Bradstock, R.A., A biogeographic model of fire regimes in Australia: current and future implications. *Global Ecology and Biogeography* **19(2)**, pp.145-158 (2010).

Bragg, F. J., Prentice, I. C., Harrison, S. P., Eglinton, G., Foster, P. N., Rommerskirchen, F., and Rullkötter, J.: Stable isotope and modelling evidence for CO2 as a driver of glacial–interglacial vegetation shifts in southern Africa, *Biogeosciences*, 10, 2001–2010 (2013).

Brancalion P.H., K.D. Holl, Guidance for successful tree planting initiatives. *Journal of Applied Ecology* **57(12)** pp.2349-2361 (2020).

Brierley, C., Zhao, A., Harrison, S.P., Braconnot, P., Williams, C., Thornalley, D., Shi, X., Peterschmitt, J-Y., Ohgaito, R., Kaufman, D.S., Kagayama, M., Hargreaves, J.C., Erb, M., Emile-Geay, J., D'Agostino, R., Chandan, D., Carré, M., Bartlein, P.J., Zheng, W., Zhang, Z., Zhang, Q., Yang, H., Volodin, E.M., Routsen, C., Peltier, W.R., Otto-Bliesner, B., Morozova, P.A., McKay, N.P., Lohmann, G., LeGrande, A.N., Guo, C., Cao, J., Brady, E., Annan, J.D., Abe-Ouchi, A., Large-scale features and evaluation of the PMIP4-CMIP6 midHolocene simulations. *Climate of the Past* **16**: 1847-1872 (2020).

Bring, J. A geometric approach to compare variables in a regression model. *The American Statistician*. **50 (1)**, 57–62 (1996).

Buitenwerf, R., Bond, W. J., Stevens, N., and Trollope, W. S. W, Increased tree densities in South African savannas: > 50 years of data suggests CO2 as a driver, *Glob. Change Biol*., **18**, 675–684 (2012).

Bukovsky, M.S., Gao, J., Mearns, L.O. and O'Neill, B.C., SSP-based land-use change scenarios: A critical uncertainty in future regional climate change projections. *Earth's Future* **9(3)**, p.e2020EF001782. (2021).

Burls, N. and Sagoo, N., Increasingly Sophisticated Climate Models Need the Out-Of-Sample Tests Paleoclimates Provide. *Journal of Advances in Modeling Earth Systems* **14(12)**, p.e2022MS003389 (2022).

Calder, W.J., Stefanova, I. and Shuman, B., Climate–fire–vegetation interactions and the rise of novel landscape patterns in subalpine ecosystems, Colorado. *Journal of Ecology* **107(4)**, pp.1689-1703 (2019).

Cano-Crespo A, Oliveira P J C, Boit A, Cardoso M and Thonicke K, Forest edge burning in the Brazilian Amazon promoted by escaping fires from managed pastures J. *Geophys. Res. Biogeosci*. **120** 2095–107 (2015).

Carmona-Moreno, C., Belward, A., Malingreau, J.P., Hartley, A., Garcia-Alegre, M., Antonovskiy, M., Buchshtaber, V. and Pivovarov, V., Characterizing interannual variations in global fire calendar using data from Earth observing satellites. *Global Change Biology* **11(9)**, pp.1537-1555 (2005).

Charles-Dominique, T., Midgley, G.F. and Bond, W.J., Fire frequency filters species by bark traits in a savanna–forest mosaic. *Journal of Vegetation Science* **28(4)**, pp.728-735 (2017).

Chen Y., D.M. Romps, J.T. Seeley, S. Veraverbeke, W.J. Riley, Z.A. Mekonnen, J.T. Randerson, Future increases in Arctic lightning and fire risk for permafrost carbon. *Nature Climate Change*, **11(5)**, pp.404-410 (2021).

Chen Y., J. Hall, D. van Wees, N. Andela, S. Hantson, L. Giglio, G.R. van der Werf, D.C. Morton, J.T. Randerson, Multi-decadal trends and variability in burned area from the 5th version of the Global Fire Emissions Database (GFED5). *Earth System Science Data*, pp.1-52 (2023).

Chergui, B., Fahd, S., Santos, X. and Pausas, J.G., Socioeconomic factors drive fire-regime variability in the Mediterranean Basin. *Ecosystems*, **21**, pp.619-628 (2018).

Chuvieco, E., Giglio, L. and Justice, C., Global characterization of fire activity: toward defining fire regimes from Earth observation data. *Global change biology* **14(7)**, pp.1488-1502 (2008).

Chuvieco, E., Lizundia-Loiola, J., Pettinari, M.L., Ramo, R., Padilla, M., Tansey, K., Mouillot, F., Laurent, P., Storm, T., Heil, A. and Plummer, S. Generation and analysis of a new global burned area product based on MODIS 250 m reflectance bands and thermal anomalies. *Earth System Science Data* ***10*(4)**, pp.2015-2031 (2018).

Chuvieco, E., Mouillot, F., Van der Werf, G.R., San Miguel, J., Tanase, M., Koutsias, N., García, M., Yebra, M., Padilla, M., Gitas, I. and Heil, A., Historical background and current developments for mapping burned area from satellite Earth observation. *Remote Sensing of Environment* **225**, pp.45-64 (2019).

Chuvieco, E., Pettinari, M.L., Koutsias, N., Forkel, M., Hantson, S. and Turco, M., Human and climate drivers of global biomass burning variability. *Science of the Total Environment* **779**, p.146361 (2021).

Chuvieco, E., Yue, C., Heil, A., Mouillot, F., Alonso-Canas, I., Padilla, M., Pereira, J. M., Oom, D., and Tansey, K.: A new global burned area product for climate assessment of fire impacts, *Global Ecol. Biogeogr.* **25**, 619–629 (2016).

Clarke, H., Nolan, R. H., de Dios, V. R., Bradstock, R., Griebel, A. Khanal, S., and Boer, M. M.: Forest fire threatens global carbon sinks and population centres under rising atmospheric water demand, *Nat. Commun*., **13**, 7161 (2022).

Clarke, P.J., Lawes, M.J., Murphy, B.P., Russell-Smith, J., Nano, C.E., Bradstock, R., Enright, N.J., Fontaine, J.B., Gosper, C.R., Radford, I. and Midgley, J.J., A synthesis of postfire recovery traits of woody plants in Australian ecosystems. *Science of the Total Environment* **534**, pp.31-42 (2015).

Commission, E. & Centre, J., 2020. *European wildfire danger and vulnerability in a changing climate : towards integrating risk dimensions : JRC PESETA IV project : Task 9 - forest fires.*, Publications Office of the European Union. Belgium. Retrieved from https://policycommons.net/artifacts/295120/european-wildfire-danger-and-vulnerability-in-a-changing-climate/1189733/ on 20 Nov 2023. CID: 20.500.12592/6hhnmh.

Constantine IV, M., Williams, A. N., Francke, A., Cadd, H.,Forbes, M., Cohen, T. J., Zhu, X., and Mooney, S. D.: Exploration of the burning question: a long history of fire in eastern Australia with and without people, *Fire*, **6**, 152 (2023).

Cortés, J., Mahecha, M.D., Reichstein, M., Myneni, R.B., Chen, C. and Brenning, A., 2021. Where are global vegetation greening and browning trends significant?. *Geophysical Research Letters* **48(6)**, p.e2020GL091496 (2021).

Countryman, C. M. The Fire Environment Concept (U.S. Department of Agriculture Forest Service Pacific Southwest Forest and Range Experiment Station, Berkeley, CA) (1972).
Cucchi, M., Weedon, G.P., Amici, A., Bellouin, N., Lange, S., Müller Schmied, H., Hersbach, H. & Buontempo, C. WFDE5: bias-adjusted ERA5 reanalysis data for impact studies. *Earth System Science Data*. **12 (3)**, 2097–2120 (2020).

D'Anjou, Robert M., Raymond S. Bradley, Nicholas L. Balascio, and David B. Finkelstein, Climate impacts on human settlement and agricultural activities in northern Norway revealed through sediment biogeochemistry. *Proceedings of the National Academy of Sciences* **109, no. 50**, 20332-20337 (2012).

Daniau, A.L., Harrison, S.P. and Bartlein, P.J., 2010. Fire regimes during the Last Glacial. *Quaternary Science Reviews* **29(21-22)**, pp.2918-2930 (2010).
Darlington, R.B. Multiple regression in psychological research and practice. *Psychological bulletin*. **69 (3)**, 161 (1968).

De Dios, V. R., Hedo, J., Camprubí, À. C., Thapa, P., Del Castillo, E.M., de Aragón, J. M., Bonet, J. A., Balaguer-Romano, R., DíazSierra, R., Yebra, M., and Boer, M. M.: Climate change induced declines in fuel moisture may turn currently fire-free Pyrenean mountain forests into fire-prone ecosystems, *Sci. Total Environ.,* **797**, 149104 (2021).

De Faria, B. L., Brando, P. M., Macedo, M. N., Panday, P. K., Soares-Filho, B. S., and Coe, M. T.: Current and future patterns of fire-induced forest degradation in Amazonia, *Environ. Res. Lett.,* **12**, 095005 (2017).

DellaSala, D.A., Baker, B.C., Hanson, C.T., Ruediger, L. and Baker, W., Have western USA fire suppression and megafire active management approaches become a contemporary Sisyphus?. *Biological Conservation* **268**, p.109499 (2022).

Denis, Elizabeth H., Jaime L. Toney, Rafael Tarozo, R. Scott Anderson, Lydia D. Roach, and Yongsong Huang, Polycyclic aromatic hydrocarbons (PAHs) in lake sediments record historic fire events: Validation using HPLC-fluorescence detection. *Organic Geochemistry* **45** 7-17 (2012).

Dial, R. J., Maher, C. T., Hewitt, R. E., and Sullivan, P. F.: Sufficient conditions for rapid range expansion of a boreal conifer, *Nature*, **608**, 546–551 (2022).

Dickman, L.T., Jonko, A.K., Linn, R.R., Altintas, I., Atchley, A.L., Bär, A., Collins, A.D., Dupuy, J.L., Gallagher, M.R., Hiers, J.K. and Hoffman, C.M., Integrating plant physiology into simulation of fire behavior and effects. *New Phytologist*, **238(3)**, pp.952-970 (2023).

Dietze, E., Theuerkauf, M., Bloom, K., Brauer, A., Dörfler, W., Feeser, I., Feurdean, A., Gedminienė, L., Giesecke, T., Jahns, S. and Karpińska-Kołaczek, M., Holocene fire activity during low-natural flammability periods reveals scale-dependent cultural human-fire relationships in Europe. *Quaternary Science Reviews*, **201**, pp.44-56 (2018).

Diffenbaugh, N. S., Konings, A. G., and Field, C. B.: Atmospheric variability contributes to increasing wildfire weather but not as much as global warming, *P. Natl. Acad. Sci. USA*, **118** e2117876118 (2021).

Donohue, R. J., Roderick, M. L., McVicar, T. R., and Farquhar, G.D.: Impact of CO2 fertilization on maximum foliage cover across the globe's warm, arid environments, *Geophys. Res. Lett.,* **40**,3031–3035 (2013).

Drossel, B. and Schwabl, F., Self organization in a forest-fire model. *Fractals* **1(04)**, pp.1022-102 (1993).

Duane A., M. Castellnou, L. Brotons, Towards a comprehensive look at global drivers of novel extreme wildfire events. *Climatic Change* **165(3-4)**, p.43 (2021).

Duffin, K. I.: The representation of rainfall and fire intensity in fossil pollen and charcoal records from a South African savanna, *Rev. Palaeobot. Palyno*., **151**, 59–71 (2008).

Dupuy J.L., H. Fargeon, N. Martin-StPaul, F. Pimont, J. Ruffault, M. Guijarro, C. Hernando, J. Madrigal, P. Fernandes, Climate change impact on future wildfire danger and activity in southern Europe: a review. *Annals of Forest Science* **77(2)**, pp.1-24 (2020).

Dwomoh F.K., M.C. Wimberly, Fire regimes and their drivers in the Upper Guinean Region of West Africa. *Remote Sensing* **9(11)**, p.1117 (2017).

Ellis, E.C., Anthropogenic transformation of the terrestrial biosphere. *Philosophical Transactions of the Royal Society A: Mathematical, Physical and Engineering Sciences*, **369(1938)**, pp.1010-1035 (2011).

Edwards, E.J., Osborne, C.P., Strömberg, C.A., Smith, S.A., C4 Grasses Consortium, Bond, W.J., Christin, P.A., Cousins, A.B., Duvall, M.R., Fox, D.L. and Freckleton, R.P., The origins of C4 grasslands: integrating evolutionary and ecosystem science. *Science*, **328(5978)**, pp.587-591 (2010).

Eloy. L., B.A. Bilbao, J. Mistry, I.B. Schmidt, From fire suppression to fire management: Advances and resistances to changes in fire policy in the savannas of Brazil and Venezuela. *The Geographical Journal* **185(1)** pp.10-22 (2019).

Enright, N.J., Fontaine, J.B., Lamont, B.B., Miller, B.P. and Westcott, V.C., 2014. Resistance and resilience to changing climate and fire regime depend on plant functional traits. *Journal of Ecology* **102(6)**, pp.1572-1581 (2014).

Essen M., S. McCaffrey, J. Abrams, T. Paveglio, Improving wildfire management outcomes: shifting the paradigm of wildfire from simple to complex risk. *Journal of Environmental Planning and Management* **66(5)** pp.909-927 (2023).

European Commission, Directorate-General for Environment, Nuijten, D., Onida, M., Lelouvier, R. (2021) Land-based wildfire prevention: principles and experiences on managing landscapes, forests and woodlands for safety and resilience in Europe. Publications Office of the European Union. https://data.europa.eu/doi/10.2779/695867

Fady B., H. Davi, N. Martin-StPaul, J. Ruffault, Caution needed with the EU forest plantation strategy for offsetting carbon emissions. *New Forests* **52** pp.733-735 (2021).

Falk, D.A., Miller, C., McKenzie, D. and Black, A.E., Cross-scale analysis of fire regimes. *Ecosystems* **10**, pp.809-823 (2007).

Falster, D., Gallagher, R., Wenk, E.H., Wright, I.J., Indiarto, D., Andrew, S.C., Baxter, C., Lawson, J., Allen, S. & Fuchs, A. AusTraits, a curated plant trait database for the Australian flora. *Scientific data*. **8 (1)**, 1–20 (2021).

Farquhar, G.D. and Sharkey, T.D., Stomatal conductance and photosynthesis. *Annual review of plant physiology*, **33(1)**, pp.317-345 (1982).

Field, R.D., Spessa, A.C., Aziz, N.A., Camia, A., Cantin, A., Carr, R., De Groot, W.J., Dowdy, A.J., Flannigan, M.D., Manomaiphiboon, K. and Pappenberger, F., Development of a global fire weather database. *Natural Hazards and Earth System Sciences* **15(6)**, pp.1407-1423 (2015).
Finney D.L., R.M. Doherty, O. Wild, D.S. Stevenson, I.A. MacKenzie, A.M. Blyth, A projected decrease in lightning under climate change. *Nature Climate Change* **8(3)** pp.210-213 (2018).

Flannigan, M.D., Krawchuk, M.A., de Groot, W.J., Wotton, B.M. and Gowman, L.M., Implications of changing climate for global wildland fire. *International journal of wildland fire* **18(5)**, pp.483-507 (2009).

Flatley, W.T., Lafon, C.W. and Grissino-Mayer, H.D., Climatic and topographic controls on patterns of fire in the southern and central Appalachian Mountains, USA. *Landscape Ecology*, **26(2)**, pp.195-209 (2011).

Foley, J.A., Prentice, I.C., Ramankutty, N., Levis, S., Pollard, D., Sitch, S. and Haxeltine, A., An integrated biosphere model of land surface processes, terrestrial carbon balance, and vegetation dynamics. *Global biogeochemical cycles,* **10(4)**, pp.603-628 (1996).

Ford, A.E., Harrison, S.P., Kountouris, Y., Millington, J.D., Mistry, J., Perkins, O., Rabin, S.S., Rein, G., Schreckenberg, K., Smith, C. and Smith, T.E., Modelling human-fire interactions: combining alternative perspectives and approaches. *Frontiers in Environmental Science* **9**, p.649835 (2021).

Forkel, M., Andela, N., Harrison, S.P., Lasslop, G., Van Marle, M., Chuvieco, E., Dorigo, W., Forrest, M., Hantson, S., Heil, A. and Li, F., Emergent relationships with respect to burned area in global satellite observations and fire-enabled vegetation models, *Biogeosciences* **16(1)**, pp.57-76 (2019a).

Forkel, M., Dorigo, W., Lasslop, G., Chuvieco, E., Hantson, S., Heil, A., Teubner, I., Thonicke, K. and Harrison, S.P., 2019b. Recent global and regional trends in burned area and their compensating environmental controls. *Environmental research communications*, **1(5)**, p.051005 (2019b).

Forkel, M., Dorigo, W., Lasslop, G., Teubner, I., Chuvieco, E. & Thonicke, K. A data-driven approach to identify controls on global fire activity from satellite and climate observations (SOFIA V1). *Geoscientific Model Development*. **10 (12)**, 4443–4476. doi:10.5194/gmd-10-4443-2017 (2017).

Foster, A.C., Shuman, J.K., Rogers, B.M., Walker, X.J., Mack, M.C., Bourgeau-Chavez, L.L., Veraverbeke, S. and Goetz, S.J., 2022. Bottom-up drivers of future fire regimes in western boreal North America. *Environmental Research Letters*, **17(2)**, p.025006 (2022).

Foster, C.N., Barton, P.S., MacGregor, C.I., Catford, J.A., Blanchard, W. and Lindenmayer, D.B., Effects of fire regime on plant species richness and composition differ among forest, woodland and heath vegetation. *Applied vegetation science* **21(1)**, pp.132-143 (2018).

Frankenberg, C., Yin, Y., Byrne, B., He, L. and Gentine, P., Comment on “Recent global decline of CO2 fertilization effects on vegetation photosynthesis”. *Science*, **373(6562)**, p.eabg2947(2021).

Fu, Z., Ciais, P., Prentice, I.C., Gentine, P., Makowski, D., Bastos, A., Luo, X., Green, J.K., Stoy, P.C. & Yang, H., Atmospheric dryness reduces photosynthesis along a large range of soil water deficits. *Nature communications* **13 (1)**, 1–10 (2022).

Fuchs G., R. Noebel, The role of ecosystem restoration for the UNFCCC and the Paris Agreement (2022).

Fuller, D. Q., Denham, T., Arroyo-Kalin, M., Lucas, L., Stevens, C. J., Qin, L., Allaby, R. G., and Purugganan, M. D.: Convergent evolution and parallelism in plant domestication revealed by an expanding archaeological record, *P. Natl. Acad. Sci. USA*, **111**, 6147–6152 (2014).

Gaboriau, D.M., Chaste, É., Girardin, M.P., Asselin, H., Ali, A.A., Bergeron, Y. and Hély, C., Interactions within the climate-vegetation-fire nexus may transform 21st century boreal forests in northwestern Canada. *Iscience*, **26(6)** (2023).

García, M., Pettinari, M.L., Chuvieco, E., Salas, J., Mouillot, F., Chen, W. and Aguado, I.,Characterizing global fire regimes from satellite-derived products. *Forests*, **13(5)**, p.699 (2022).

Gautney, J.R. and Holliday, T.W., New estimations of habitable land area and human population size at the Last Glacial Maximum. *Journal of Archaeological Science*, **58**, pp.103-112 (2015).

Giglio, L. and Roy, D.P., On the outstanding need for a long-term, multi-decadal, validated and quality assessed record of global burned area: Caution in the use of Advanced Very High Resolution Radiometer data. *Science of Remote Sensing* **2**, p.100007 (2020).

Giglio, L., Boschetti, L., Roy, D.P., Humber, M.L. and Justice, C.O., The Collection 6 MODIS burned area mapping algorithm and product. *Remote sensing of environment* **217**, pp.72-85 (2018).

Giglio, L., Csiszar, I. and Justice, C.O., Global distribution and seasonality of active fires as observed with the Terra and Aqua Moderate Resolution Imaging Spectroradiometer (MODIS) sensors. *Journal of geophysical research: Biogeosciences*, **111**(G2) (2006).

Giglio, L., Randerson, J.T. and Van Der Werf, G.R., Analysis of daily, monthly, and annual burned area using the fourth-generation global fire emissions database (GFED4). *Journal of Geophysical Research: Biogeosciences* **118(1)**, pp.317-328 (2013).

Giglio, L., Randerson, J.T., Van der Werf, G.R., Kasibhatla, P.S., Collatz, G.J., Morton, D.C. and DeFries, R.S., Assessing variability and long-term trends in burned area by merging multiple satellite fire products. *Biogeosciences* **7(3)**, pp.1171-1186 (2010).

Giglio, L., Schroeder, W. and Justice, C.O., The collection 6 MODIS active fire detection algorithm and fire products. *Remote sensing of environment*, *178*, pp.31-41. (2016).

Gillson L., C. Whitlock, G. Humphrey, Resilience and fire management in the Anthropocene. *Ecology and Society* **24(3)** (2019).

Goldewkuijk K., A. Beusen, J. Doelman E.Stehfest E, Anthropogenic land use estimates for the Holocene–HYDE 3.2 *Earth System Science Data* **9**, 927–53 (2017).

Gonsamo, A., Ciais, P., Miralles, D.G., Sitch, S., Dorigo, W., Lombardozzi, D., Friedlingstein, P., Nabel, J.E., Goll, D.S., O'Sullivan, M. and Arneth, A., Greening drylands despite warming consistent with carbon dioxide fertilization effect. *Global change biology*, *27*(14), pp.3336-3349 (2021).

Goss, M., Swain, D.L., Abatzoglou, J.T., Sarhadi, A., Kolden, C.A., Williams, A.P. and Diffenbaugh, N.S., Climate change is increasing the likelihood of extreme autumn wildfire conditions across California. *Environmental Research Letters* ***15*****(9)**, p.094016 (2020).

Gott, B., Aboriginal fire management in south-eastern Australia: aims and frequency. *Journal of biogeography*, pp.1203-1208 (2005).

Grillakis, M., Voulgarakis, A., Rovithakis, A., Seiradakis, K. D.,Koutroulis, A., Field, R. D., Kasoar, M., Papadopoulos, A., and Lazaridis, M.: Climate drivers of global wildfire burnedarea,*Environ. Res. Lett*., **17**, 045021 (2022).

Grömping, U. Variable importance in regression models. *Wiley interdisciplinary reviews: Computational statistics*. **7 (2)**, 137–152 (2015).

Grossiord, C., Buckley, T.N., Cernusak, L.A., Novick, K.A., Poulter, B., Siegwolf, R.T., Sperry, J.S. and McDowell, N.G., Plant responses to rising vapor pressure deficit. *New Phytologist* ***226*****(6)**, pp.1550-1566 (2020).

Haas, O., Prentice, I.C. and Harrison, S.P., 2023. The response of wildfire regimes to Last Glacial Maximum carbon dioxide and climate. *Biogeosciences* **20(18)**, pp.3981-3995 (2023).

Haas, O., Prentice, I.C. and Harrison, S.P., Global environmental controls on wildfire burnt area, size, and intensity. *Environmental Research Letters* **17(6)**, p.065004 (2022).

Hantson, S., Arneth, A., Harrison, S.P., Kelley, D.I., Prentice, I.C., Rabin, S.S., Archibald, S., Mouillot, F., Arnold, S.R., Artaxo, P. and Bachelet, D., The status and challenge of global fire modelling. *Biogeosciences* **13(11)**, pp.3359-3375 (2016).

Hantson, S., Kelley, D. I., Arneth, A., Harrison, S. P., Archibald, S., Bachelet, D., Forrest, M., Hickler, T., Lasslop, G., Li, F., Mangeon, S., Melton, J. R., Nieradzik, L., Rabin, S. S., Prentice, I. C., Sheehan, T., Sitch, S., Teckentrup, L., Voulgarakis, A., and Yue, C.: Quantitative assessment of fire and vegetation properties in simulations with fire-enabled vegetation models from the Fire Model Intercomparison Project, *Geosci. Model Dev*., **13**, 3299–3318 (2020).

Hantson, S., Padilla, M., Corti, D. and Chuvieco, E., Strengths and weaknesses of MODIS hotspots to characterize global fire occurrence. *Remote sensing of Environment*, **131**, pp.152-159 (2013).

Hantson, S., Pueyo, S. and Chuvieco, E., Global fire size distribution is driven by human impact and climate. *Global Ecology and Biogeography* **24(1)**, pp.77-86 (2015).

Harrison S.P., I.C. Prentice, K.J Bloomfield, N. Dong, M. Forkel, M. Forrest, R.K. Ningthoujam, A. Pellegrini, Y Shen, M Baudena, A.W. Cardoso, Understanding and modelling wildfire regimes: an ecological perspective. *Environmental Research Letters* **16(12)**, 125008 (2021).

Harrison, S.P. and Prentice, C.I., Climate and CO2 controls on global vegetation distribution at the last glacial maximum: analysis based on palaeovegetation data, biome modelling and palaeoclimate simulations. *Global Change Biology* **9(7)**, pp.983-1004 (2003).

Harrison, S.P., Bartlein, P.J., Izumi, K., Li, G., Annan, J., Hargreaves, J., Braconnot, P.B., and Kageyama, M., Evaluation of CMIP5 palaeo-simulations to improve climate projections. *Nature Climate Change* **5** 735-74(2015).

Harrison, S.P., Marlon, J.R. and Bartlein, P.J. *Fire in the Earth system* (pp. 21-48) (2010).

Harrison, S.P., Villegas-Diaz, R., Cruz-Silva, E., Gallagher, D., Kesner, D., Lincoln, P., Shen, Y., Sweeney, L., Colombaroli, D., Ali, A. and Barhoumi, C., The Reading Palaeofire Database: an expanded global resource to document changes in fire regimes from sedimentary charcoal records. *Earth system science data* **14(3)**, pp.1109-1124 (2022).

He, T., Lamont, B.B. and Pausas, J.G., Fire as a key driver of Earth's biodiversity. *Biological Reviews* **94(6)**, pp.1983-2010 (2019).

Hermoso V., A. Regos, A. Morán-Ordóñez, A. Duane, L. Brotons., Tree planting: A double-edged sword to fight climate change in an era of megafires. *Global Change Biology* **27(13)** pp.3001-3003 (2021).

Hessilt T.D., J.T. Abatzoglou, J.T., Y. Chen, J.T. Randerson, R.C. Scholten, G. Van Der Werf, S. Veraverbeke, Future increases in lightning ignition efficiency and wildfire occurrence expected from drier fuels in boreal forest ecosystems of western North America. *Environmental Research Letters*, **17(5)**, p.054008 (2022).

Heward, H., Smith, A.M., Roy, D.P., Tinkham, W.T., Hoffman, C.M., Morgan, P. and Lannom, K.O., Is burn severity related to fire intensity? Observations from landscape scale remote sensing. *International Journal of Wildland Fire*, **22(7)**, pp.910-918 (2013).

Hickler, T., Smith, B., Prentice, I.C., Mjöfors, K., Miller, P., Arneth, A. and Sykes, M.T., CO2 fertilization in temperate FACE experiments not representative of boreal and tropical forests. *Global Change Biology* **14(7)**, pp.1531-1542 (2008).

Higuera, P., 2009. CharAnalysis 0.9: Diagnostic and analytical tools for sediment-charcoal analysis. *User's Guide, Montana State University, Bozeman, MT.*

Higuera, P.E., Briles, C.E. and Whitlock, C., Fire-regime complacency and sensitivity to centennial-through millennial-scale climate change in Rocky Mountain subalpine forests, C olorado, USA. *Journal of Ecology*, **102(6)**, pp.1429-1441 (2014).

Higuera, P.E., Brubaker, L.B., Anderson, P.M., Hu, F.S. and Brown, T.A., Vegetatihaon mediated the impacts of postglacial climate change on fire regimes in the south-central Brooks Range, Alaska. *Ecological Monographs* **79(2)**, pp.201-219 (2009).

Hoegh-Guldberg O.D., Jacob, M. Taylor, M. Bindi, S. Brown, I. Camilloni, A. Diedhiou, R. Djalante, K.L. Ebi, F. Engelbrecht, J. Guiot, Y. Hijioka, S. Mehrotra, A. Payne, S.I. Seneviratne, A. Thomas, R. Warren, and G. Zhou, Impacts of 1.5ºC Global Warming on Natural and Human Systems. In: Global Warming of 1.5°C. An IPCC Special Report on the impacts of global warming of 1.5°C above pre-industrial levels and related global greenhouse gas emission pathways, in the context of strengthening the global response to the threat of climate change, sustainable development, and efforts to eradicate poverty [Masson-Delmotte, V., P. Zhai, H.-O. Pörtner, D. Roberts, J. Skea, P.R. Shukla, A. Pirani, W. Moufouma-Okia, C. Péan, R. Pidcock, S. Connors, J.B.R. Matthews, Y. Chen, X. Zhou, M.I. Gomis, E. Lonnoy, T. Maycock, M. Tignor, and T. Waterfield (eds.)]. *Cambridge University Press, Cambridge*, UK and New York, NY, USA, pp. 175-312 (2018).

Holl K.D., P.H. Brancalion, Tree planting is not a simple solution. *Science* **368(6491)** pp.580-581 (2020).

Hollingsworth, T.N., Johnstone, J.F., Bernhardt, E.L. & Chapin III, F.S. Fire severity filters regeneration traits to shape community assembly in Alaska's boreal forest. *PloS one*. **8 (2)**, e56033 (2013).

Holsinger, L., Parks, S.A. and Miller, C., Weather, fuels, and topography impede wildland fire spread in western US landscapes. *Forest ecology and management,* **380**, pp.59-69 (2016).

Hou O, S., X., and Orth, R., Observational Evidence of Wildfire Promoting Soil Moisture Anomalies, *Sci. Rep.,* **10**, 11008 (2020).

Huang, Y., Wu, S. and Kaplan, J.O., Sensitivity of global wildfire occurrences to various factors in the context of global change. *Atmospheric Environment*, **121**, pp.86-92 (2015).

Humber, M. L., Boschetti, L., Giglio, L., and Justice, C. O.: Spatial and temporal intercomparison of four global burned area products, *Int. J. Digit. Earth*, **12**, 460–484 (2019).

Humphrey G.L., G. Lindsey, G. Ziervogel, How changing fire management policies affect fire seasonality and livelihoods. *Ambio* **50** 475-491 (2021).

Ichoku, C., Giglio, L., Wooster, M.J. and Remer, L.A., Global characterization of biomass-burning patterns using satellite measurements of fire radiative energy. *Remote sensing of Environment* **112(6),** pp.2950-2962 (2008).

Iglesias, M.C., Hermoso, V., Campos, J.C., Carvalho-Santos, C., Fernandes, P.M., Freitas, T.R., Honrado, J.P., Santos, J.A., Sil, Â., Regos, A. and Azevedo, J.C., Climate-and fire-smart landscape scenarios call for redesigning protection regimes to achieve multiple management goals. *Journal of Environmental Management*, **322**, p.116045 (2022).

Ingalsbee T., Whither the paradigm shift? Large wildland fires and the wildfire paradox offer opportunities for a new paradigm of ecological fire management. *International Journal of Wildland Fire* **26(7)** pp.557-561 (2017).

Janssen, T.A., Jones, M.W., Finney, D., van der Werf, G.R., van Wees, D., Xu, W. and Veraverbeke, S., Extratropical forests increasingly at risk due to lightning fires. *Nature Geoscience*, pp.1-9 (2023).

Jeong, S., Ryu, Y., Gentine, P., Lian, X., Fang, J., Li, X., Kong, J., Choi, W., Jiang, C., Keenan, T. and Harrison, S.P., Persistent Global Greening Over the Last Four Decades Using Novel Long-term Vegetation Index Data with Enhanced Temporal Consistency (2023) (pre-print).

Jolly, W.M., Cochrane, M.A., Freeborn, P.H., Holden, Z.A., Brown, T.J., Williamson, G.J. and Bowman, D.M., Climate-induced variations in global wildfire danger from 1979 to 2013. *Nature communications* ***6*(1)**, p.7537 (2015).

Jones M.W., J.T. Abatzoglou, S. Veraverbeke, N. Andela, G. Lasslop, M. Forkel, A.J. Smith, C. Burton, R.A. Betts, G.R. van der Werf, S. Sitch, Global and regional trends and drivers of fire under climate change. *Reviews of Geophysics* **60(3)**, p.e2020RG000726 (2022).

Jones, M.W., Smith, A., Betts, R., Canadell, J.G., Prentice, I.C. and Le Quéré, C., Climate change increases the risk of wildfires. *ScienceBrief Review* **116**, p.117 (2020).

Joussaume, S., Taylor, K.E., Braconnot, P., Mitchell, J.F.B., Kutzbach, J.E., Harrison, S.P., Prentice, I.C., Broccoli, A.J., Abe-Ouchi, A., Bartlein, P.J., Bonfils, C., Dong, B., Guiot, J., Herterich, K., Hewitt, C.D., Jolly, D., Kim, J.W., Kislov, A., Kitoh, A., Loutre, M.F., Masson, V., McAvaney, B., McFarlane, N., de Noblet, N., Peltier, W.R., Peterschmitt, J.Y., Pollard, D., Rind, D., Royer, J.F., Schlesinger, M.E., Syktus, J., Thompson, S., Valdes, P., Vettoretti, G., Webb, R.S. and Wyputta, U, Monsoon changes for 6000 years ago: results of 18 simulations from the Paleoclimate Modeling Intercomparison Project (PMIP). *Geophysical Research Letters* **26**: 859-862 (1999).

Juszczak, P., Tax, D. & Duin, R.P.W. Feature scaling in support vector data description. In: *Proc. asci*. 2002 Citeseer. pp. 95–102 (2002).

Kageyama, M., Braconnot, P., Harrison, S.P., Haywood, A., Jungclaus, J., Otto-Bliesner, B., Peterschmitt, J.-Y., Abe-Ouchi, A., Albani, S., Bartlein, P., Brierley, C., Crucifix, M., Dolan, A., Fernandez-Donado, L., Fischer, H., Hopcroft, P., Ivanovic, R., Lambert, F., Lunt, D., Mahowald, N., Peltier, W.R., Phipps, S., Roche, D., Schmidt, G., Tarasov, L., Valdes, P., Zhang, Q., and Zhou, T., The PMIP4 contribution to CMIP6 – Part 1: Overview and over-arching analysis plan. *Geoscientific Model Development* **11**: 1033-1057 (2018).

Kageyama, M., Braconnot, P., Harrison, S.P., Haywood, A.M., Jungclaus, J., Otto-Bliesner, B.L., Peterschmitt, J.Y., Abe-Ouchi, A., Albani, S., Bartlein, P.J. and Brierley, C., PMIP4-CMIP6: the contribution of the Paleoclimate Modelling Intercomparison Project to CMIP6. *Geoscientific Model Development Discussions*, **11(3)**, pp.1033-1057 (2018).

Kageyama, M., Harrison, S.P., Kapsch, M.L., Lofverstrom, M., Lora, J.M., Mikolajewicz, U., Sherriff-Tadano, S., Vadsaria, T., Abe-Ouchi, A., Bouttes, N. and Chandan, D., The PMIP4 Last Glacial Maximum experiments: preliminary results and comparison with the PMIP3 simulations. *Climate of the Past*, **17(3)**, pp.1065-1089 (2021).

Kaplan J.O., K.H.K. Lau, The WGLC global gridded lightning climatology and time series. *Earth System Science Data* **13(7)** pp.3219-3237 (2021).

Kaplan, J. O., Bigelow, N. H., Prentice, I. C., Harrison, S. P., Bartlein, P. J., Christensen, T. R., Cramer, W., Matveyeva, N. V., McGuire, A. D., Murray, D. F., Razzhivin, V. Y., Smith, B., Walker, D. A., Anderson, P. M., Andreev, A. A., Brubaker, L. B., Edwards, M. E., and Lozhkin, A. V.: Climate change and Arctic ecosystems II: Modeling, palaeodata-model comparisons, and future projections, *J. Geophys. Res.-Atmos*., **108**, 8171 (2003).

Kaplan, J. O.: jedokaplan/BIOME4: BIOME4 public release (1999) (v4.2.2), Zenodo [code], https://doi.org/10.5281/zenodo.8368294, 2023.

Kaplan, J.O. & Lau, K.H.-K. The WGLC global gridded lightning climatology and timeseries. *Earth System Science Data Discussions*. 1–25 (2021).

Kaplan, J.O., Pfeiffer, M., Kolen, J.C. and Davis, B.A., Large scale anthropogenic reduction of forest cover in Last Glacial Maximum Europe *PLoS One* **11(11)**, p.e0166726 (2016).

Keeley, J.E. & Syphard, A.D., Large California wildfires: 2020 fires in historical context. *Fire Ecology* **17 (1)**, 1–11 (2021).

Keeley, J.E. and Pausas, J.G., Evolutionary ecology of fire. *Annual Review of Ecology, Evolution, and Systematics* **53**, pp.203-225 (2022).

Keeley, J.E. and Syphard, A.D., Different historical fire–climate patterns in California. *International Journal of Wildland Fire*, **26(4)**, pp.253-268 (2017).

Keeley, J.E. and Syphard, A.D., Twenty-first century California, USA, wildfires: Fuel-dominated vs. wind-dominated fires. *Fire Ecol.*, **15**, 24 (2019).

Keeley, J.E. Fire intensity, fire severity and burn severity: a brief review and suggested usage. *International journal of wildland fire*. **18 (1)**, 116–126 (2009).

Keeley, J.E., Pausas, J.G., Rundel, P.W., Bond, W.J. & Bradstock, R.A. Fire as an evolutionary pressure shaping plant traits. *Trends in plant science*. **16 (8)**, 406–411 (2011).
Kelley, D. I., Prentice, I. C., Harrison, S. P., Wang, H., Simard, M., Fisher, J. B., and Willis, K. O.: A comprehensive benchmarking system for evaluating global vegetation models, *Biogeosciences*, **10**, 3313–3340 (2013).

Keenan, T.F., Luo, X., Stocker, B.D., De Kauwe, M.G., Medlyn, B.E., Prentice, I.C., Smith, N.G., Terrer, C., Wang, H., Zhang, Y. and Zhou, S., A constraint on historic growth in global photosynthesis due to rising CO2. *Nature Climate Change*, **13(12)**, pp.1376-1381 (2023).

Kelley, D.I., Bistinas, I., Whitley, R., Burton, C., Marthews, T.R. and Dong, N., How contemporary bioclimatic and human controls change global fire regimes. *Nature Climate Change* **9(9)**, pp.690-696 (2019).

Kelley, D.I., Harrison, S.P. and Prentice, I.C., Improved simulation of fire–vegetation interactions in the Land surface Processes and eXchanges dynamic global vegetation model (LPX-Mv1). Geoscientific Model Development, **7(5)**, pp.2411-2433 (2014).

Kelley, D.I., Prentice, I.C., Harrison, S.P., Wang, H., Simard, M., Fisher, J.B. and Willis, K.O, A comprehensive benchmarking system for evaluating global vegetation models. *Biogeosciences*, **10(5)**, pp.3313-3340 (2013).

Kgope, B. S., Bond, W. J., and Midgley, G. F.: Growth responses of African savanna trees implicate atmospheric [CO2] as a driver of past and current changes in savanna tree cover, *Austral Ecol.,* **35**, 451–463(2010).

Klein Goldewijk, K., Beusen, A. and Janssen, P., Long-term dynamic modeling of global population and built-up area in a spatially explicit way: HYDE 3.1. *The Holocene*, **20(4)**, pp.565-573 (2010).

Klein Goldewijk, K., Beusen, A., Doelman, J. & Stehfest, E. Anthropogenic land use estimates for the Holocene–HYDE 3.2. *Earth System Science Data*. **9 (2)**, 927–953 (2017).

Kloster S., G. Lasslop, Historical and future fire occurrence (1850 to 2100) simulated in CMIP5 Earth System Models. *Global and Planetary Change*, **150**, pp.58-69 (2017).
Kloster, S., Mahowald, N.M., Randerson, J.T. & Lawrence, P.J. The impacts of climate, land use, and demography on fires during the 21st century simulated by CLM-CN. *Biogeosciences*. **9 (1)**, 509–525 (2012).

Knorr W., L. Jiang, A. Arneth, Climate, CO_2 and human population impacts on global wildfire emissions. *Biogeosciences* **13(1)** pp.267-282 (2016).

Knorr, W., Arneth, A. and Jiang, L., Demographic controls of future global fire risk. *Nature Climate Change* **6(8)**, pp.781-785 (2016).

Knorr, W., Kaminski, T., Arneth, A. and Weber, U., Impact of human population density on fire frequency at the global scale. *Biogeosciences* **11(4)**, pp.1085-1102 (2014).

Kobayashi Y., R. Seidl, W. Rammer, K.F. Suzuki, A.S. Mori, Identifying effective tree planting schemes to restore forest carbon and biodiversity in Shiretoko National Park, Japan. *Restoration Ecology*, **31(1)**, p.e13681. (2023).

Krause A., S. Kloster, S. Wilkenskjeld, H. Paeth, The sensitivity of global wildfires to simulated past, present, and future lightning frequency. *Journal of Geophysical Research: Biogeosciences*, **119(3)**, pp.312-322 (2014).

Krawchuk M.A., M.A. Moritz, M.A. Parisien, J. Van Dorn, K. Hayhoe, Global pyrogeography: the current and future distribution of wildfire. *PloS one* **4(4)**, p.e5102 (2009).

Krawchuk, M. A. and Moritz, M. A.: Constraints on Global Fire Activity Vary across a Resource Gradient, *Ecology*, **92**, 121–132 (2011).

Krebs, P., Pezzatti, G.B., Mazzoleni, S., Talbot, L.M. and Conedera, M., fire regime: history and definition of a key concept in disturbance ecology. *Theory in Biosciences* **129**, pp.53-69 (2010).

Kuhn-Régnier A., A. Voulgarakis, Nowack, P., M. Forkel, I.C. Prentice, S.P. Harrison, The importance of antecedent vegetation and drought conditions as global drivers of burnt area. *Biogeosciences* **18(12)** pp.3861-3879 (2021).

Kumar, S.S., Roy, D.P., Boschetti, L. & Kremens, R. Exploiting the power law distribution properties of satellite fire radiative power retrievals: A method to estimate fire radiative energy and biomass burned from sparse satellite observations. *Journal of Geophysical Research: Atmospheres*. **116** (D19) (2011).

Lamont, B.B., Historical links between climate and fire on species dispersion and trait evolution. *Plant Ecology*, **223(7)**, pp.711-732 (2022).

Lamont, B.B., Pausas, J.G., He, T., Witkowski, E.T. and Hanley, M.E., Fire as a selective agent for both serotiny and nonserotiny over space and time. *Critical Reviews in Plant Sciences*, **39(2)**, pp.140-172 (2020).

Lange S., M. Büchner, ISIMIP2b bias-adjusted atmospheric climate input data, version 1.0, ISIMIP. Repository (2017); https://doi.org/10.48364/ISIMIP.208515.

Larsen, W.A. & McCleary, S.J. (1972) The use of partial residual plots in regression analysis. *Technometrics*. 14 (3), 781–790.

Lasslop, G. and Kloster, S., Human impact on wildfires varies between regions and with vegetation productivity. *Environmental Research Letters*, **12(11)**, p.115011 (2017).

Lasslop, G., Hantson, S. and Kloster, S., Influence of wind speed on the global variability of burned fraction: a global fire model's perspective. *International Journal of Wildland Fire,* **24(7)**, pp.989-1000 (2015).

Lasslop, G., Thonicke, K., and Kloster, S., SPITFIRE within the MPI Earth system model: Model development and evaluation. *J Adv. Model. Earth Sy.* **6** 740–755 (2014).

Lasslop, G., Hantson, S., Harrison, S.P., Bachelet, D., Burton, C., Forkel, M., Forrest, M., Li, F., Melton, J.R., Yue, C. and Archibald, S., Global ecosystems and fire: Multi-model assessment of fire-induced tree-cover and carbon storage reduction. *Global Change Biology*, **26(9)**, pp.5027-5041 (2020).

Laurent, P., Mouillot, F., Moreno, M.V., Yue, C. and Ciais, P., Varying relationships between fire radiative power and fire size at a global scale. *Biogeosciences* **16(2)**, pp.275-288 (2019).

Laurent, P., Mouillot, F., Yue, C., Ciais, P., Moreno, M.V. and Nogueira, J.M., FRY, a global database of fire patch functional traits derived from space-borne burned area products. *Scientific Data* **5(1)**, pp.1-12 (2018).

Lavorel, S., Flannigan, M.D., Lambin, E.F. and Scholes, M.C., Vulnerability of land systems to fire: Interactions among humans, climate, the atmosphere, and ecosystems. *Mitigation and Adaptation Strategies for Global Change*, **12**, pp.33-53 (2007).

Lehndorff, E., Jörg Linstädter, J., Kehl, M., and Weniger, G.-C. Fire history reconstruction from Black Carbon analysis in Holocene cave sediments at Ifri Oudadane, Northeastern Morocco. *Holocene* **25**, 398–402 (2014).

Lehsten, V., Harmand, P., Palumbo, I. & Arneth, A. Modelling burned area in Africa. *Biogeosciences*. **7 (10)**, 3199–3214 (2010)

Lehsten, V., Tansey, K., Balzter, H., Thonicke, K., Spessa, A., Weber, U., Smith, B., and Arnrabeth, A., Estimating carbon emissions from African wildfires. *Biogeosciences* **6**, 349–360 (2009).

Lelouvier, R., Nuijten, D., Onida, M. and Stoof, C.R., 2021. *Land-based wildfire prevention: principles and experiences on managing landscapes, forests and woodlands for safety and resilience in Europe*. Publications Office of the European Union.

Lenihan, J. M. and Neilson, R. P.: Simulating Broad-Scale Fire Severity in a Dynamic Global Vegetation Model, *Northwest Sci*., **72**, 91–103 (1998).

Li W., N. MacBean, P. Ciais, P. Defourny, C. Lamarche, S.Bontemps, R.A. Houghton, S. Peng, Gross and net land cover changes in the main plant functional types derived from the annual ESA CCI land cover maps (1992–2015), *Earth Syst. Sci. Dat*a, **10,** 219–34 (2018).

Li, F., Levis, S., and Ward, D. S., Quantifying the role of fire in the Earth system – Part 1: Improved global fire modeling in the Community Earth System Model (CESM1). *Biogeosciences* **10**, 2293–2314 (2013).

Li, F., Levis, S., and Ward, D. S.: Quantifying the role of fire in the Earth system – Part 1: Improved global fire modeling in the Community Earth System Model (CESM1), *Biogeosciences*, **10**, 2293–2314 (2013).

Li, W., MacBean, N., Ciais, P., Defourny, P., Lamarche, C., Bontemps, S., Houghton, R.A. & Peng, S. Gross and net land cover changes in the main plant functional types derived from the annual ESA CCI land cover maps (1992–2015). *Earth System Science Data*. **10 (1)**, 219–234 (2018).

Lindenmayer D.B., M. Yebra, G.J. Cary, Better managing fire in flammable tree plantations. *Forest Ecology and Management* **528** p.120641 (2023).

Liu, L., Bestel, S., Shi, J., Song, Y., and Chen, X.: Paleolithic human exploitation of plant foods during the last glacial maximum in North China, *P. Natl. Acad. Sci. USA*, **110**, 5380–5385 (2013).

Liu, M., Prentice, I.C., Menviel, L., Harrison, S.P., 2022. Past rapid warmings as a constraint on greenhouse-gas climate feedbacks. *Nature, Communications Earth and Environment* **3**: 196 (2022).

Liu, Y., Stanturf, J. and Goodrick, S., 2010. Trends in global wildfire potential in a changing climate. *Forest ecology and management*, **259(4)**, pp.685-697 (2010).

Lohmann, G., Butzin, M., Eissner, N., Shi, X., and Stepanek,C.: Abrupt climate and weather changes across time scales, *Paleoceanogr. Paleocl*., **35**, e2019PA003782 (2020).

Lund, M.T., Nordling, K., Gjelsvik, A.B. and Samset, B.H., The influence of variability on fire weather conditions in high latitude regions under present and future global warming. *Environmental Research Communications* (2023).

Luo, R., Hui, D., Miao, N., Liang, C. and Wells, N., Global relationship of fire occurrence and fire intensity: A test of intermediate fire occurrence-intensity hypothesis. *Journal of Geophysical Research: Biogeosciences*, **122(5)**, pp.1123-1136 (2017).

Luo, R., L. Wu, Z. Yu, Z. Shen, H. Xu, K. Wang, and J. Deng Global analysis of fire regimes: Burnt area and fire intensity, *Life Sci. J.,* **10(2)**, 86–94 (2013).

Luvuno L., R. Biggs, N. Stevens, K. Esler, Woody encroachment as a social-ecological regime shift. *Sustainability* **10(7)** p.2221 (2018).

Malamud, B.D. and Turcotte, D.L., Self-organized criticality applied to natural hazards. *Natural Hazards* **20**, pp.93-116 (1999).

Mallek, C., H. Safford, J. Viers, and J. Miller, Modern departures in fire severity and area vary by forest type, Sierra Nevada and southern Cascades, California, USA. *Ecosphere* **4**:153 (2013).

Malmierca-Vallet, I., Sime, L.C., Abe-Ouchi, A., Bouttes, N., Ditlevsen, P., Erb, M.P., Gregoire, L., Guo, C., Harrison, S.P., Kageyama, M., Klockmann, M., Lambert, F., Nisancioglu, K.H., Oliver, K., Peltier, R., Rehfeld, K., Robinson, A.J., Tarasov, L., Valdes, P.J., Vettoretti, G., Weitzel, N., Zhang, X., Dansgaard-Oeschger events in climate models: Review and baseline MIS3 protocol. *Climate of the Past* **19**: 915-942 9 (2022).

Mancini, L.D., Corona, P. and Salvati, L., Ranking the importance of Wildfires' human drivers through a multi-model regression approach. *Environmental Impact Assessment Review*, **72**, pp.177-186 (2018).

Mangeon, S., Voulgarakis, A., Gilham, R., Harper, A., Sitch, S., and Folberth, G., INFERNO: a fire and emissions scheme for the UK Met Office's Unified Model. *Geosci. Model Dev* **9**, 2685–2700 (2016).

Mansoor S., I. Farooq, M.M. Kachroo, A.E.D. Mahmoud, M. Fawzy, S.M. Popescu, M.N. Alyemeni, C. Sonne, J. Rinklebe, P. Ahmad, P, Elevation in wildfire frequencies with respect to the climate change. *Journal of Environmental Management* **301**, p.113769 (2022).

Marlon, J.R., Bartlein, P.J., Carcaillet, C., Gavin, D.G., Harrison, S.P., Higuera, P.E., Joos, F.knorr, Power, M.J. and Prentice, I.C., Climate and human influences on global biomass burning over the past two millennia. *Nature geoscience* **1(10)**, pp.697-702 (2008).

Marlon, J.R., Bartlein, P.J., Daniau, A.L., Harrison, S.P., Maezumi, S.Y., Power, M.J., Tinner, W. and Vanniére, B., Global biomass burning: a synthesis and review of Holocene paleofire records and their controls. *Quaternary Science Reviews* **65**, pp.5-25 (2013).

Marlon, J.R., Bartlein, P.J., Walsh, M.K., Harrison, S.P., Brown, K.J., Edwards, M.E., Higuera, P.E., Power, M.J., Anderson, R.S., Briles, C. and Brunelle, A., Wildfire responses to abrupt climate change in North America. *Proceedings of the National Academy of Sciences* **106(8)**, pp.2519-2524 (2009).

Marlon, J.R., Kelly, R., Daniau, A.L., Vannière, B., Power, M.J., Bartlein, P., Higuera, P., Blarquez, O., Brewer, S., Brücher, T. and Feurdean, A., Reconstructions of biomass burning from sediment-charcoal records to improve data–model comparisons. *Biogeosciences*, **13(11)**, pp.3225-3244 (2016).

Marlon, J.R., What the past can say about the present and future of fire. *Quaternary Research* **96**, pp.66-87 (2020).

Martin Calvo, M. and Prentice, I.C., Effects of fire and CO 2 on biogeography and primary production in glacial and modern climates. *New Phytologist* **208(3)**, pp.987-994 (2015).

Martin Calvo, M., Prentice, I.C. and Harrison, S.P., Climate versus carbon dioxide controls on biomass burning: a model analysis of the glacial–interglacial contrast. *Biogeosciences* **11(21)**, pp.6017-6027 (2014).

Mauritsen, T., Bader, J., Becker, T., Behrens, J., Bittner, M.,Brokopf, R., Brovkin, V.,Claussen, M., Crueger, T., Esch, M.,Fast, I., Fiedler, S., Fläschner, D., Gayler, V.,Giorgetta, M.,Goll, D. S., Haak, H., Hagemann, S., Hedemann, C., Hohenegger, C., Ilyina, T., Jahns, T.,Jimenéz-de-la-Cuesta, D., Jungclaus,J., Kleinen, T., Kloster, S., Kracher, D., Kinne, S.,Kleberg, D.,Lasslop, G., Kornblueh, L., Marotzke, J., Matei, D., Meraner,K.,Mikolajewicz, U., Modali, K., Möbis, B., Müller, A. W., Julia,E. M. S., Nabel, J. E. M. S., Nam, C. C. W.,Notz, D., Nyawira,S., Paulsen, H., Peters, K., Pincus, R., Pohlmann, H., PongratzJ., Popp, M., Jürgen Raddatz, T., Rast, S., Redler, R., Reick, C. H., Rohrschneider, T., Schemann, V.,Schmidt, H., Schnur, R.,Schulzweida, U., Six, K. D., Stein, L., Stemmler, I.,Stevens,B.,Storch, J.-S. V., Tian, F., Voigt, A., Vrese, P., Wieners, K., Wilkenskjeld, S., Winkler, A., and Roeckner, E.: Developments in the MPI-M Earth System Model version 1.2 (MPI-ESM1.2) and its response to increasing CO2, J. *Adv. Model. Earth Sy.,* **11**,998–1038 (2019).

Maximum and terminal Pleistocene: A geospatial analysis of the McCullagh, P. & Nelder, J.A. *Generalized Linear Models 2nd ed. Chapman and Hall, New York* (1989).

McFadden, D.*Conditional Logit Analysis of Qualitative Choice Behavior" in P. Zarembka Eds. Frontiers in Econometrics, New York Acedemic press* (1974).

McLauchlan, K.K., Higuera, P.E., Miesel, J., Rogers, B.M., Schweitzer, J., Shuman, J.K., Tepley, A.J., Varner, J.M., Veblen, T.T., Adalsteinsson, S.A. and Balch, J.K., Fire as a fundamental ecological process: Research advances and frontiers. *Journal of Ecology* **108(5)**, pp.2047-2069 (2020).

Meek D.W., J.L. Hatfield, T.A. Howell, S.B. Idso, R.J. Reginato, A generalized relationship between photosynthetically active radiation and solar radiation, *Agronomy journal*, **76(6)**, pp.939-945 (1984).

Meijer, J.R., Huijbregts, M.A., Schotten, K.C. and Schipper, A.M., 2018. Global patterns of current and future road infrastructure. *Environmental Research Letters*, **13(6)**, p.064006.

Melton, J. R. and Arora, V. K.: Competition between plant functional types in the Canadian Terrestrial Ecosystem Model (CTEM) v. 2.0. *Geosci. Model Dev* **9**, 323–361 (2016).

Meng, M., Harrison, S.P., Jie, D., Li, N., Liu, B., Li, D., Gao, G. and Niu, H., Climate and fire drivers of forest composition and openness in the Changbai Mountains since the Late Glacial. *Forest Ecosystems*, **10**, p.100127 (2023).

Miller, J. D., and H. Safford. Trends in wildfire severity: 1984 to 2010 in the Sierra Nevada, Modoc Plateau, and southern Cascades, California, USA. *Fire Ecology* **8**:41–57 (2012).

Millington J.D., O. Perkins, C. Smith, Human fire use and management: a global database of anthropogenic fire impacts for modelling. *Fire* **5(4)** p.87 (2022).

Mistry J., I.B. Schmidt, L. Eloy, B. Bilbao, New perspectives in fire management in South American savannas: The importance of intercultural governance. *Ambio* **48** pp.172-179 (2019).

Mooney, S.D., Harrison, S.P., Bartlein, P.J., Daniau, A.L., Stevenson, J., Brownlie, K.C., Buckman, S., Cupper, M., Luly, J., Black, M. and Colhoun, E., Late Quaternary fire regimes of Australasia. *Quaternary Science Reviews*, **30(1-2)**, pp.28-46 (2011).

Moreira F., D. Ascoli, H. Safford, M.A. Adams, J.M. Moreno, J.M. Pereira, F.X. Catry, J. Armesto, W. Bond, M.E. González, T. Curt,Wildfire management in Mediterranean-type regions: paradigm change needed. *Environmental Research Letters* **15(1)** p.011001 (2020).

Moreno, P. I., Videla, J., Valero-Garcés, B., Alloway, B. V., and Heusser, L. E.: A continuous record of vegetation, fireregime and climatic changes in northwestern Patagonia spanning the last 25,000 years, *Quaternary Sci. Rev*., **198**, 15–36 (2018).

Morford S.L., B.W. Allred, D Twidwell, M.O. Jones, J.D. Maestas, C.P. Roberts, D.E. Naugle, Herbaceous production lost to tree encroachment in United States rangelands. *Journal of Applied Ecology*, **59(12)**, pp.2971-2982 (2022).

Moritz M.A., M.A. Parisien, E. Batllori, M.A. Krawchuk, J. Van Dorn, D.J. Ganz, K. Hayhoe, Climate change and disruptions to global fire activity. *Ecosphere* **3(6)** pp.1-22 (2012).

Moritz, M.A., Morais, M.E., Summerell, L.A., Carlson, J.M. and Doyle, J., Wildfires, complexity, and highly optimized tolerance. *Proceedings of the National Academy of Sciences,* **102(50)**, pp.17912-17917 (2005).

Mouillot, F. and Field, C.B., Fire history and the global carbon budget: a 1× 1 fire history reconstruction for the 20th century. *Global Change Biology* **11(3)**, pp.398-420 (2005).

Mouillot, F., Schultz, M.G., Yue, C., Cadule, P., Tansey, K., Ciais, P. and Chuvieco, E., Ten years of global burned area products from spaceborne remote sensing—A review: Analysis of user needs and recommendations for future developments. *International Journal of Applied Earth Observation and Geoinformation,* **26**, pp.64-79 (2014).

Mucina, L., Biome: evolution of a crucial ecological and biogeographical concept. *New Phytologist*, **222(1)**, pp.97-114 (2019).

Mueller S.E., A.E. Thode, E.Q Margolis, L.L. Yocom, J.D. Young, J.M. Iniguez, Climate relationships with increasing wildfire in the southwestern US from 1984 to 2015. *Forest Ecology and Management* **460**, p.117861 (2020).

Murray L.T., An uncertain future for lightning. *Nature Climate Change* **8(3)** pp.191-192 (2018).

Nelder, J.A. & Wedderburn, R.W.M. (1972) Generalized linear models. *Journal of the Royal Statistical Society: Series A (General)*. 135 (3), 370–384.

O’brien, R.M. (2007) A caution regarding rules of thumb for variance inflation factors. *Quality & quantity*. 41 (5), 673–690.

Ogunkoya, A., Kaplan, J., Whitlock, C., Nanavati, W., Roberts, D.W. and Poulter, B., Drivers of recent forest cover change in southern South America are linked to climate and CO2. *Landscape Ecology* **36(12)**, pp.3591-3606 (2021).

Parisien, M.A., Miller, C., Parks, S.A., DeLancey, E.R., Robinne, F.N. and Flannigan, M.D., The spatially varying influence of humans on fire probability in North America. *Environmental Research Letters*, **11(7)**, p.075005 (2016).

Parisien, Marc-André, Sean A. Parks, Meg A. Krawchuk, John M. Little, Mike D. Flannigan, Lynn M. Gowman, and Max A. Moritz, An analysis of controls on fire activity in boreal Canada: comparing models built with different temporal resolutions. *Ecological Applications* **24**, no. 6 (2014): 1341-1356 (2014).

Park Williams, A., Allen, C.D., Macalady, A.K., Griffin, D., Woodhouse, C.A., Meko, D.M., Swetnam, T.W., Rauscher, S.A., Seager, R., Grissino-Mayer, H.D. and Dean, J.S., Temperature as a potent driver of regional forest drought stress and tree mortality. *Nature climate change*, **3(3)**, pp.292-297 (2013).

Pausas J.G., J.E. Keeley, Wildfires and global change. *Frontiers in Ecology and the Environment* **19(7)**, pp.387-395 (2021).

Pausas, J.G. and Bradstock, R.A., Fire persistence traits of plants along a productivity and disturbance gradient in mediterranean shrublands of south-east Australia. *Global Ecology and Biogeography*, **16(3)**, pp.330-340 (2007).

Pausas, J.G. and Keeley, J.E., A burning story: the role of fire in the history of life. *BioScience* ***59(7)***, pp.593-601 (2009).

Pausas, J.G. and Keeley, J.E., Wildfires and global change. *Frontiers in Ecology and the Environment* **19(7)**, pp.387-395 (2021).

Pausas, J.G. and Ribeiro, E., The global fire–productivity relationship. *Global Ecology and Biogeography* **22(6)**, pp.728-736 (2013).

Pausas, J.G., Bark thickness and fire regime. *Functional Ecology*, **29(3)**, pp.315-327 (2015).

Pausas, J.G., Bark thickness and fire regime: another twist (2017).

Pausas, J.G., Changes in fire and climate in the eastern Iberian Peninsula (Mediterranean basin). *Climatic change,* **63(3)**, pp.337-350 (2004).

Pausas, J.G., Keeley, J.E. and Schwilk, D.W., Flammability as an ecological and evolutionary driver. *Journal of Ecology*, **105(2)**, pp.289-297 (2017).

Pausas, J.G., Pratt, R.B., Keeley, J.E., Jacobsen, A.L., Ramirez, A.R., Vilagrosa, A., Paula, S., Kaneakua-Pia, I.N. & Davis, S.D. Towards understanding resprouting at the global scale. *New Phytologist*. **209 (3)**, 945–954 (2016).

Pechony, O. and Shindell, D.T., Driving forces of global wildfires over the past millennium and the forthcoming century. *Proceedings of the National Academy of Sciences* **107(45)**, pp.19167-19170 (2010).

Peltier, W. R., Argus, D. F., and Drummond, R.: Space geodesy constrains ice age terminal deglaciation: The global ICE-6G_C (VM5a) model, J. *Geophys. Res.-Sol*. Ea., **120**, 450–487 (2015).

Pérez-Invernón, F.J., Gordillo-Vázquez, F.J., Huntrieser, H. and Jöckel, P., 2023. Variation of lightning-ignited wildfire patterns under climate change. *Nature communications*, **14(1)**, p.739 (2023).

Pfeiffer, M., Spessa, A. and Kaplan, J.O., A model for global biomass burning in preindustrial time: LPJ-LMfire (v1. 0). *Geoscientific Model Development*, **6(3)**, pp.643-685 (2013).

Piao, S., Wang, X., Park, T., Chen, C., Lian, X.U., He, Y., Bjerke, J.W., Chen, A., Ciais, P., Tømmervik, H. and Nemani, R.R., Characteristics, drivers and feedbacks of global greening. *Nature Reviews Earth & Environment* **1(1)**, pp.14-27 (2020).

Plummer, S., Arino, O., Simon, M. and Steffen, W., Establishing a earth observation product service for the terrestrial carbon community: The globcarbon initiative. *Mitigation and adaptation strategies for global change*, **11**, pp.97-111 (2006).

Popović, Z., Bojović, S., Marković, M. and Cerdà, A., Tree species flammability based on plant traits: A synthesis. *Science of the Total Environment*, **800**, p.149625 (2021).

Portenga, E. W., Rood, D. H., Bishop, P., and Bierman, P. R.: A late Holocene onset of Aboriginal burning in southeastern Australia, *Geology*, **44**, 131–134 (2016).

Poulter, B., MacBean, N., Hartley, A., Khlystova, I., Arino, O., Betts, R., Bontemps, S., Boettcher, M., Brockmann, C. & Defourny, P. Plant functional type classification for earth system models: results from the European Space Agency's Land Cover Climate Change Initiative. *Geoscientific Model Development*. **8 (7)**, 2315–2328 (2015).

Povak, N.A., Hessburg, P.F. and Salter, R.B., Evidence for scale-dependent topographic controls on wildfire spread. *Ecosphere*, **9(10)**, p.e02443 (2018).

Power, M. J., Marlon, J. R., Bartlein, P. J., and Harrison, S. P.: Fire history and the Global Charcoal Database: a new tool for hypothesis testing and data exploration, *Palaeogeogr. Palaeoclim*., **291**, 52–59, (2010).

Power, M. J., Ortiz, N., Marlon, J., Bartlein, P. J., Harrison, S. P., Mayle, F., Ballouche, A., Bradshaw, R., Carcaillet, C., Cordova, C., Mooney, S., Moreno, P., Prentice, I. C., Thonicke, K., Tinner, W., Whitlock, C., Zhang, Y., Zhao, Y., Anderson, R. S., Beer, R., Behling, H., Briles, C., Brown, K, Brunelle A., Bush, M., Clark, J., Colombaroli, D., Chu, C. Q., Daniels, M., Dodson, J., Edwards, M. E., Fisinger, W., Gavin, D. G., Gobet, E., Hallett, D. J., Higuera, P., Horn, S., Inoue, J., Kaltenrieder, P., Kennedy, L., Kong, Z. C., Long, C., Lynch, J., Lynch, B., McGlone, M., Meeks, S., Meyer, G., Minckley, T., Mohr, J., Noti, R., Pierce, J., Richard, P., Shuman, B. J., Takahara, H., Toney, J., Turney, C., Umbanhower, C., Vandergoes, M., Vanniere, B., Vescovi, E., Walsh, M., Wang, X., Williams, N., Wilmshurst, J., and Zhang, J. H.: Changes in fire activity since the LGM: an assessment based on a global synthesis and analysis of charcoal data, *Clim. Dynam.,* **30**, 887–907, (2008).

Prentice, I.C., Kelley, D.I., Foster, P.N., Friedlingstein, P., Harrison, S.P. and Bartlein, P.J., Modeling fire and the terrestrial carbon balance. *Global Biogeochemical Cycles* ***25(3)*** (2011).
Pyne, S. J., Andrews, P. A. & Laven, R. D. *Introduction to Wildland Fire* (Wiley, New York), p. 769 (1996).

Rabin, S.S., Melton, J.R., Lasslop, G., Bachelet, D., Forrest, M., Hantson, S., Kaplan, J.O., Li, F., Mangeon, S., Ward, D.S. and Yue, C., 2017. The Fire Modeling Intercomparison Project (FireMIP), phase 1: experimental and analytical protocols with detailed model descriptions. *Geoscientific Model Development*, **10(3)**, pp.1175-1197 (2017).

Randerson, J. T., G. R. Van Der Werf, L. Giglio, G. J. Collatz, and P. S. Kasibhatla, Global Fire Emissions Database, Version 4.1 (GFEDv4), ORNL DAAC, Oak Ridge, Tennessee, USA (2018).

Rao, K., Williams, A.P., Diffenbaugh, N.S., Yebra, M. and Konings, A.G., Plant-water sensitivity regulates wildfire vulnerability, *Nat. Ecol. Evol*., **6**, 332–339 (2022).

Regos, A., Campos, J. C., Lecina-Diaz, J., Pais, S., Sil, Â., Cánibe-Iglesias, M., Freitas, T., Aquilué, N., Gonçalves, J., Carvalho-Santos, C., Lomba, Â., Moreira, F., Hermoso, V., Brotons, L., Chas-Amil, M. L., Touza, J., Santos, J. A., Fernandes, P., Azevedo, ., & Horando, J. P. Final Report of the FirESmart -Nature-based solutions for preventive fire management and sustained supply of ecosystem services. Zenodo. https://doi.org/10.5281/zenodo.7829308 (2023).

Riley, K.L., Williams, A.P., Urbanski, S.P., Calkin, D.E., Short, K.C. and O'Connor, C.D., Will landscape fire increase in the future? A systems approach to climate, fire, fuel, and human drivers. *Current Pollution Reports* **5**, pp.9-24 (2019).

Ripley, Brad S., Sarah L. Raubenheimer, Lavinia Perumal, Maurice Anderson, Emma Mostert, Barney S. Kgope, Guy F. Midgley, and Kimberley J. Simpson, CO2-fertilisation enhances resilience to browsing in the recruitment phase of an encroaching savanna tree. *Functional Ecology* **36**, no. 12 3223-3233 (2022).

Rodrigues, M., Costafreda-Aumedes, S., Comas, C. & Vega-García, C. Spatial stratification of wildfire drivers towards enhanced definition of large-fire regime zoning and fire seasons. *Science of the total environment*. **689**, 634–644. (2019)

Rogers, B.M., Balch, J.K., Goetz, S.J., Lehmann, C.E.R. & Turetsky, M., Focus on changing fire regimes: interactions with climate, ecosystems, and society. *Environmental Research Letters*.**15 (3)** (2020).

Rothermel, R.C., *A mathematical model for predicting fire spread in wildland fuels* (Vol. 115). Intermountain Forest & Range Experiment Station, Forest Service, US Department of Agriculture (1972).

Rowe, C., Wurster, C. M., Zwart, C., Brand, M., Hutley, L. B., Levchenko, V., and Bird, M. I.: Vegetation over the last glacial maximum at Girraween Lagoon, monsoonal northern Australia, *Quaternary Res.,* **102**, 39–52 (2021).

Roy, D., Justice, C. and Boschetti, L., 2006, July. Global mapping of fire-affected areas using multitemporal MODIS data: The MCD45 product. In 2006 IEEE International Symposium on Geoscience and Remote Sensing (pp. 4165-4168). IEEE.

Ruan, Y., Mohtadi, M., Dupont, L. M., Hebbeln, D., van der Kaars, S., Hopmans, E. C., Schouten, S., Hyer, E. J., and Schefuß, E.: Interaction of fire, vegetation, and climate in tropical ecosystems: A multiproxy study over the past 22,000 years, *Global Biogeochem. Cy*., **34**, e2020GB006677 (2020).

Rubino, M., D'Onofrio, A., Seki, O., and Bendle, J. A.: Ice-core records of biomass burning, *Anthropocene Review*, **3**, 140–162 (2015).

Safford, H.D. and Van de Water, K.M., *Using fire return interval departure (FRID) analysis to map spatial and temporal changes in fire frequency on national forest lands in California* (p. 59). Albany, CA, USA: United States Department of Agriculture, Forest Service, Pacific Southwest Research Station (2014).

Saitoh T. M., S. Nagai, H. M. Noda, H. Muraoka, K.N. Nasahara, Examination of the extinction coefficient in the Beer–Lambert law for an accurate estimation of the forest canopy leaf area index. *Forest Science and Technology* **8(2)** 67–76 (2012).

Sang, Y., Huang, L., Wang, X., Keenan, T.F., Wang, C. and He, Y., Comment on "Recent global decline of CO2 fertilization effects on vegetation photosynthesis". *Science*, **373(6562)**, p.eabg4420 (2021).

Santín, C. and Doerr, S.H., Fire effects on soils: the human dimension. *Philosophical Transactions of the Royal Society B: Biological Sciences* **371(1696)**, p.20150171 (2016).

Sappington, J.M., Longshore, K.M. and Thompson, D.B., Quantifying landscape ruggedness for animal habitat analysis: a case study using bighorn sheep in the Mojave Desert. *The Journal of wildlife management,* **71(5)**, pp.1419-1426 (2007).

Sato, H., Kelley, D.I., Mayor, S.J., Martin Calvo, M., Cowling, S.A. and Prentice, I.C., Dry corridors opened by fire and low CO2 in Amazonian rainforest during the Last Glacial Maximum. *Naturep Geoscience* **14(8)**, pp.578-585 (2021).

Scheiter, S., Kumar, D., Corlett, R. T., Gaillard, C., Langan, L.,Schertzer, E., Staver, A. C., and Levin, S. A.: Implications of the spatial dynamics of fire spread for the bistability of savanna and forest, *J. Math. Biol*., **70**, 329–341 (2015).

Scheiter, Simon, Dushyant Kumar, Richard T. Corlett, Camille Gaillard, Liam Langan, Ralph Sedricke Lapuz, Carola Martens, Mirjam Pfeiffer, and Kyle W. Tomlinson, Climate change promotes transitions to tall evergreen vegetation in tropical Asia. *Global Change Biology* **26**, no. 9 5106-5124 (2020).

Schielzeth, H. Simple means to improve the interpretability of regression coefficients. *Methods in Ecology and Evolution*. **1 (2)**, 103–113(2010).

Scholtz R., V.M. Donovan, T. Strydom, C. Wonkka, U.P. Kreuter, W.E. Rogers, C. Taylor, I.P. Smit, N. Govender, W. Trollope, D.T. Fogarty, High-intensity fire experiments to manage shrub encroachment: lessons learned in South Africa and the United States. *African Journal of Range & Forage Science* **39(1)**, pp.148-159 (2022).

Scott, A.C. and Glasspool, I.J., The diversification of Paleozoic fire systems and fluctuations in atmospheric oxygen concentration. *Proceedings of the National Academy of Sciences* **103(29)**, pp.10861-10865 (2006).

Scott, A.C., Chaloner, W.G., Belcher, C.M. and Roos, C.I., The interaction of fire and mankind: Introduction. *Philosophical Transactions of the Royal Society B: Biological Sciences* **371(1696)**, p.20150162 (2016).

Sedano, F. and Randerson, J. T.: Multi-scale influence of vapor pressure deficit on fire ignition and spread in boreal forest ecosystems, *Biogeosciences*, **11**, 3739–3755 (2014).

Seddon N., Harnessing the potential of nature-based solutions for mitigating and adapting to climate change. *Science*, **376(6600)**, pp.1410-1416 (2022).

Sheehan, T., Bachelet, D. & Ferschweiler, K., Projected major fire and vegetation changes in the Pacific Northwest of the conterminous United States under selected CMIP5 climate futures. *Ecological Modelling*. **317**, 16–29 (2015).

Shen, Y., Cai, W., Prentice, I.C. and Harrison, S.P., Community abundance of resprouting in woody plants reflects fire return time, intensity, and type. *Forests* **14(5)**, p.878 (2023).

Shiffler, R.E. Maximum Z scores and outliers. *The American Statistician*. **42 (1)**, 79–80 (1998).

Sidorenko, D., Rackow, T., Jung, T., Semmler, T., Barbi, D.,Danilov, S., Dethloff, K., Dorn, W., Fieg, K., Gößling, H.F., Handorf, D., Harig, S., Hiller, W., Juricke, S., Losch, M., Schröter, J., Sein, D. V., and Wang, Q.: Towards multi-resolution global climate modeling with ECHAM6–FESOM. Part I: model formulation and mean climate, *Clim. Dynam.,* **44**, 757–780 (2015).

Simon, M., Plummer, S., Fierens, F., Hoelzemann, J.J. and Arino, O., Burnt area detection at global scale using ATSR-2: The GLOBSCAR products and their qualification. *Journal of Geophysical Research: Atmospheres*, 109(D14) (2004).

Simpson, K.J., Archibald, S. and Osborne, C.P., Savanna fire regimes depend on grass trait diversity. *Trends in Ecology & Evolution* (2022).

Simpson, K.J., Jardine, E.C., Archibald, S., Forrestel, E.J., Lehmann, C.E., Thomas, G.H. and Osborne, C.P., Resprouting grasses are associated with less frequent fire than seeders. *New Phytologist* **230(2)**, pp.832-844 (2021).

Sitnov, S.A. and Mokhov, I.I., A comparative analysis of the characteristics of active fires in the boreal forests of Eurasia and North America based on satellite data. *Izvestiya, Atmospheric and Oceanic Physics* **54**, pp.966-978 (2018).

Smith, A.M. and Wooster, M.J., Remote classification of head and backfire types from MODIS fire radiative power and smoke plume observations. *International Journal of Wildland Fire*, **14(3)**, pp.249-254 (2005).

Smith, B., Wårlind, D., Arneth, A., Hickler, T., Leadley, P., Siltberg, J., and Zaehle, S., Implications of incorporating N cycling and N limitations on primary production in an individual based dynamic vegetation model. *Biogeosciences* **11**, 2027- 2054 (2014).

Snitker, G.: Identifying natural and anthropogenic drivers of prehistoric fire regimes through simulated charcoal records, *J. Archaeol. Sci.,* **95**, 1–15 (2018).

Song, M., Dodson, J., Lu, F., Shi, G., and Yan, H.: A continuous paleorecord of vegetation and environmental change from Erxianyan Wetland over the past 60,000 years in central China, *Palaeogeogr. Palaeocl*., **613**, 111399 (2023).

Song, Y. & Wang, Y. Global Wildfire Outlook Forecast with Neural Networks. *Remote Sensing*. **12 (14)**, 2246 (2020).

Song, Y., Jiao, W., Wang, J., and Wang, L.: Increased global vegetation productivity despite rising atmospheric dryness over the last two decades, *Earth's Future*, **10**, e2021EF002634 (2022).

Srock, A.F., Charney, J.J., Potter, B.E. and Goodrick, S.L.,The hot-dry-windy index: A new fire weather index. *Atmosphere* **9(7)**, p.279 (2018).

Steel, Z.L., Safford, H.D. and Viers, J.H., The fire frequency-severity relationship and the legacy of fire suppression in California forests. *Ecosphere*, **6(1)**, pp.1-23 (2015).

Stevens-Rumann, C.S., Kemp, K.B., Higuera, P.E., Harvey, B.J., Rother, M.T., Donato, D.C., Morgan, P. and Veblen, T.T., Evidence for declining forest resilience to wildfires under climate change. *Ecology letters*, **21(2)**, pp.243-252 (2018).

Stocker, B.D., Wang, H., Smith, N.G., Harrison, S.P., Keenan, T.F., Sandoval, D., Davis, T. and Prentice, I.C., P-model v1. 0: an optimality-based light use efficiency model for simulating ecosystem gross primary production. *Geoscientific Model Development* **13(3)**, pp.1545-1581 (2020).

Stocks, B.J., Lawson, B.D., Alexander, M.E., Wagner, C.V., McAlpine, R.S., Lynham, T.J. and Dube, D.E.,The Canadian forest fire danger rating system: an overview. *The Forestry Chronicle* **65(6)**, pp.450-457 (1989).

Sitch, S., Smith, B., Prentice, I.C., Arneth, A., Bondeau, A., Cramer, W., Kaplan, J.O., Levis, S., Lucht, W., Sykes, M.T. and Thonicke, K., Evaluation of ecosystem dynamics, plant geography and terrestrial carbon cycling in the LPJ dynamic global vegetation model. *Global change biology*, **9(2)**, pp.161-185 (2003).

Sitch, S., Prentice, I.C., Smith, B., Kaplan, W.C.J., Lucht, W., Sykes, M., Thonicke, K. and Venevsky, S., LPJ-A Coupled Model of Vegetation Dynamics and the Terrestrial Carbon Cycle (2000).

Strydom T., I.P. Smit, hantN. Govender, C. Coetsee, J. Singh, A.B. Davies, B.W. van Wilgen, High-intensity fires may have limited medium-term effectiveness for reversing woody plant encroachment in an African savanna. *Journal of Applied Ecology*, **60(4)**, pp.661-672 (2023).

Sugihara, N.G., van Wagtendonk, J.W. & Fites-Kaufman, J. Fire as an ecological process. *Fire in California's ecosystems*. 58–74 (2006),

Sweeney, L., Harrison, S.P. and Vander Linden, M., Assessing anthropogenic influence on fire history during the Holocene in the Iberian Peninsula. *Quaternary Science Reviews*, **287**, p.107562 (2022).

Syphard A. D., T. Sheehan, H. Rustigian-Romsos, K. Ferschweiler, Mapping future fire probability under climate change: does vegetation matter? *PLoS ONE* **13(8)**, p.e0201680 (2018).

Syphard A.D, J.E. Keeley, A.H. Pfaff, K. Ferschweiler, Human presence diminishes the importance of climate in driving fire activity across the United States. *Proceedings of the National Academy of Sciences* **114(52)** pp.13750-13755 (2017).

Tallavaara, M., Luoto, M., Korhonen, N., Järvinen, H., and Seppä,H.: Human population dynamics in Europe over the Last Glacial Maximum, *P. Natl. Acad. Sci. USA*, **112**, 8232–8237 (2015).

Tang, R., Mao, J., Jin, M., Chen, A., Yu, Y., Shi, X., Zhang, Y., Hoffman, F.M., Xu, M. and Wang, Y., 2021. Interannual variability and climatic sensitivity of global wildfire activity. *Advances in Climate Change Research*, **12(5)**, pp.686-695 (2021).

Tansey, K., Grégoire, J.M., Stroppiana, D., Sousa, A., Silva, J., Pereira, J.M., Boschetti, L., Maggi, M., Brivio, P.A., Fraser, R. and Flasse, S., Vegetation burning in the year 2000: Global burned area estimates from SPOT VEGETATION data. *Journal of Geophysical Research: Atmospheres*, **109**(D14) (2004).

Tavşanoğlu, Ç. & Pausas, J.G. A functional trait database for Mediterranean Basin plants. *Scientific Data*. **5 (1)**, 1–18 (2018).

Teckentrup L., S.P. Harrison, S. Hantson, A. Heil, J.R. Melton, M. Forrest, F. Li, C. Yue, A. Arneth, T. Hickler, S. Sitch, Response of simulated burned area to historical changes in environmental and anthropogenic factors: a comparison of seven fire models. *Biogeosciences* **16(19)** pp.3883-3910 (2019).

Tedim, F. and Leone, V., The dilemma of wildfire definition: What it reveals and what it implies. *Frontiers in Forests and Global Change* **3**, p.553116 (2020).

Thonicke, K., Spessa, A., Prentice, I.C., Harrison, S.P., Dong, L. and Carmona-Moreno, C., The influence of vegetation, fire spread and fire behaviour on biomass burning and trace gas emissions: results from a process-based model. *Biogeosciences*, **7(6)**, pp.1991-2011 (2010).

Thonicke, K., Venevsky, S., Sitch, S. and Cramer, W., The role of fire disturbance for global vegetation dynamics: coupling fire into a Dynamic Global Vegetation Model. *Global Ecology and Biogeography*, **10(6)**, pp.661-677 (2001).

Tierney, J.E., Poulsen, C.J., Montañez, I.P., Bhattacharya, T., Feng, R., Ford, H.L., Hönisch, B., Inglis, G.N., Petersen, S.V., Sagoo, N. and Tabor, C.R., Past climates inform our future. *Science*, **370(6517)**, p.eaay3701 (2020).

Tinner W., Andrič M., Atanassova J., Behling H., Black M., Blarquez O., Brown K. J., Carcaillet C., Colhoun E. A., Colombaroli D., Davis B. A. S., D'Costa D., Dodson J., Dupont L., Eshetu Z., Gavin D. G., Genries A., Haberle S., Hallett D. J., Hope G., Horn S. P., Kassa T. G., Katamura., F., Kennedy L. M., Kershaw P., Krivonogov S., Long C., Magri D., Marinova E., McKenzie G. M., Moreno P. I., Moss P., Neumann F. H., Norström E., Paitre C., Rius D., Roberts N., Robinson G. S., Sasaki N., Scott L., Takahara H., Terwilliger V., Thevenon F., Turner R., Valsecchi V. G., Vannière B., Walsh M., Williams N., Zhang Y., Predictability of biomass burning in response to climate changes, *Global Biogeochemical Cycles* **26**, no. 4 (2012).

UNEP, "Spreading like Wildfire – The Rising Threat of Extraordinary Landscape Fires. A UNEP Rapid Response Assessment. Nairobi", (UNEP, 2022); https://www.unep.org/resources/report/spreading-wildfire-rising-threat-extraordinary-landscape-fires

Valdez, M.C., Chang, K.T., Chen, C.F., Chiang, S.H. and Santos, J.L., Modelling the spatial variability of wildfire susceptibility in Honduras using remote sensing and geographical information systems. *Geomatics, Natural Hazards and Risk* **8(2)**, pp.876-892 (2017).

Van Der Sleen, P., Groenendijk, P., Vlam, M., Anten, N.P., Boom, A., Bongers, F., Pons, T.L., Terburg, G. and Zuidema, P.A., No growth stimulation of tropical trees by 150 years of CO2 fertilization but water-use efficiency increased. *Nature geoscience*, ***8*****(1)**, pp.24-28 (2015).

van der Werf G.R, J.T. Randerson, L. Giglio, T.T. van Leeuwen, Y. Chen, B.M. Rogers, M. Mu, M.J.E. van Marle, D.C. Morton, G.J. Collatz, R.J. Yokelson, P.S. Kasibhatla, Global fire emissions estimates during 1997–2016, *Earth System Science Data*, **9(2)**, p697–720 (2017).

Van Der Werf, G.R., Randerson, J.T., Giglio, L., Gobron, N. and Dolman, A.J., Climate controls on the variability of fires in the tropics and subtropics. *Global Biogeochemical Cycles* **22(3)** (2008).

Van Der Werf, G.R., Randerson, J.T., Giglio, L., Van Leeuwen, T.T., Chen, Y., Rogers, B.M., Mu, M., Van Marle, M.J., Morton, D.C., Collatz, G.J. and Yokelson, R.J., Global fire emissions estimates during 1997–2016. *Earth System Science Data* **9(2)**, pp.697-720 (2017).

Van Wagner, C.E.,*Structure of the Canadian forest fire weather index* (Vol. 1333). Alberta, Canada: Environment Canada, Forestry Service (1974).

Vannière, B., Blarquez, O., Rius, D., Doyen, E., Brücher, T., Colombaroli, D., Connor, S., Feurdean, A., Hickler, T., Kaltenrieder, P. and Lemmen, C. 7000-year human legacy of elevation-dependent European fire regimes. *Quaternary Science Reviews*, **132**, pp.206-212 (2016).

Venevsky, S., Thonicke, K., Sitch, S. and Cramer, W., Simulating fire regimes in human-dominated ecosystems: Iberian Peninsula case study. *Global Change Biology*, **8(10)**, pp.984-998 (2002).

Venter, Z. S., M. D. Cramer, and H-J. Hawkins, Drivers of woody plant encroachment over Africa. *Nature communications* **9**, no. 1 2272 (2018).

Viedma, O., Angeler, D.G. & Moreno, J.M., Landscape structural features control fire size in a Mediterranean forested area of central Spain. *International Journal of Wildland Fire*. 18 (5), 575–583 (2009).

Vitolo, C., Di Giuseppe, F., Krzeminski, B. and San-Miguel-Ayanz, J., A 1980–2018 global fire danger re-analysis dataset for the Canadian Fire Weather Indices. *Scientific data* **6(1)**, pp.1-10 (2019).

W.: Climate change promotes transitions to tall evergreen vegetation in tropical Asia, Glob. Change Biol., 26, 5106–5124,

Wang, H., Prentice, I. C., Keenan, T. F., Davis, T. W., Wright, I. J., Cornwell, W. K., Evans, B. J., and Peng, C.: Towards a universal model for carbon dioxide uptake by plants, *Nature Plants*, **3**, 734– 741 (2017).

Wang, H., Prentice, I.C., Keenan, T.F., Davis, T.W., Wright, I.J., Cornwell, W.K., Evans, B.J. and Peng, C., Towards a universal model for carbon dioxide uptake by plants. *Nature plants* **3(9)**, pp.734-741 (2017).

Wang, S., Zhang, Y., Ju, W., Chen, J.M., Ciais, P., Cescatti, A., Sardans, J., Janssens, I.A., Wu, M., Berry, J.A. and Campbell, E., Recent global decline of CO2 fertilization effects on vegetation photosynthesis. *Science*, **370(6522)**, pp.1295-1300 (2020).

Wang, Z., Chappellaz, J., Park, K. and Mak, J.E., Large variations in Southern Hemisphere biomass burning during the last 650 years. *Science* **330(6011)**, pp.1663-1666 (2010).

Williams, A. P., Allen, C. D., Macalady, A. K., Griffin, D., Woodhouse, C. A., Meko, D. M., Swetnam, T. W., Rauscher, S. A., Seager, R., Grissino-Mayer, H. D., Dean, J. S., Cook, E.

R.,Gangodagamage, C., Cai, M., and McDowell, N. G.: Temperature as a potent driver of regional forest drought stress and tree mortality, *Nature Climate Change Change*, **3**, 292–297 (2013).

Williams, A.N., Ulm, S., Cook, A.R., Langley, M.C. and Collard, M., Human refugia in Australia during the Last Glacial Maximum and Terminal Pleistocene: a geospatial analysis of the 25–12 ka Australian archaeological record. *Journal of archaeological science*, **40(12)**, pp.4612-4625 (2013).

Williams, A.P., Abatzoglou, J.T., Gershunov, A., Guzman-Morales, J., Bishop, D.A., Balch, J.K. and Lettenmaier, D.P., Observed impacts of anthropogenic climate change on wildfire in California. *Earth's Future* **7(8)**, pp.892-910 (2019).

Wirth, C., fire regime and tree diversity in boreal forests: implications for the carbon cycle. *Forest diversity and function: temperate and boreal systems* (pp. 309-344) (2005).

Wollstein, K., Creutzburg, M.K., Dunn, C., Johnson, D.D., O'Connor, C. and Boyd, C.S., Toward integrated fire management to promote ecosystem resilience. *Rangelands*, **44(3)**, pp.227-234 (2022).

Wooster, M.J. and Zhang, Y.H., Boreal forest fires burn less intensely in Russia than in North America. *Geophysical Research Letters* **31(20)** (2004).

Wooster, M.J., Roberts, G., Perry, G.L.W. & Kaufman, Y.J. Retrieval of biomass combustion rates and totals from fire radiative power observations: FRP derivation and calibration relationships between biomass consumption and fire radiative energy release. *Journal of Geophysical Research: Atmospheres*. **110** (D24) (2005).

Wooster, M.J., Roberts, G.J., Giglio, L., Roy, D.P., Freeborn, P.H., Boschetti, L., Jusatice, C., Ichoku, C., Schroeder, W., Davies, D. and Smith, A.M., Satellite remote sensing of active fires: History and current status, applications and future requirements. *Remote Sensing of Environment*, **267**, p.112694 (2021).

Wotton B.M., M.D. Flannigan, G.A. Marshall, Potential climate change impacts on fire intensity and key wildfire suppression thresholds in Canada. *Environmental Research Letters* **12(9)**, p.095003 (2017).

Wu C., S. Venevsky, S. Sitch, L.M. Mercado, C. Huntingford, A.C. Staver, Historical and future global burned area with changing climate and human demography. *One Earth* **4(4)**, pp.517-530 (2021).

Yang, J., Tian, H., Tao, B., Ren, W., Kush, J., Liu, Y. and Wang, Y., Spatial and temporal patterns of global burned area in response to anthropogenic and environmental factors: Reconstructing global fire history for the 20th and early 21st centuries. *Journal of Geophysical Research: Biogeosciences* **119(3)**, pp.249-263 (2014).

Yang, R., Wang, J., Zeng, N., Sitch, S., Tang, W., McGrath, M.J., Cai, Q., Liu, D., Lombardozzi, D., Tian, H. and Jain, A.K., 2022. Divergent historical GPP trends among state-of-the-art multi-model simulations and satellite-based products. Earth System Dynamics, **13(2)**, pp.833-849 (2022).

Yue, C., Ciais, P., Cadule, P., Thonicke, K., Archibald, S., Poulter, B., Hao, W. M., Hantson, S., Mouillot, F., Friedlingstein, P., Maignan, F., and Viovy, N., Modelling the role of fires in the terrestrial carbon balance by incorporating SPITFIRE into the global vegetation model ORCHIDEE – Part 1: simulating historical global burned area and fire regimes. *Geosci. Model Dev.* **7**, 2747–2767 (2014).

Zhai, H., Gu, B. and Wang, Y., Evaluation of policies and actions for nature-based solutions in nationally determined contributions. *Land Use Policy*, **131**, p.106710 (2023).

Zhu, J., Otto-Bliesner, B.L., Brady, E.C., Gettelman, A., Bacmeister, J.T., Neale, R.B., Poulsen, C.J., Shaw, J.K., McGraw, Z.S. and Kay, J.E., LGM paleoclimate constraints inform cloud parameterizations and equilibrium climate sensitivity in CESM2. *Journal of Advances in Modeling Earth Systems*, **14(4)**, p.e2021MS002776 (2022).

Annexes

Supplementary information for Chapter 2

This section contains supplementary information for Chapter 2. It contains information on (a) the derivation of the climate data, (b) the motivation for estimating fire intensity, (c) the parameters of gross primary production (GPP), (d) statistics and partial residual plots for the models made using all 16 predictor variables, and (e) statistics and partial residual plots for models excluding road density, population density, VPD and GPP respectively.

Derivation of the climate data

Some of the climate data were not directly available and required some calculations, the description of which is presented here.

Mean Daily Vapour Pressure Deficit

Vapour Pressure Deficit was derived from the specific humidity, pressure, and temperature data from the WFDE5 bias-adjusted ERA5 dataset (Cucchi et al., 2020) from January 2010 to December 2015. Hourly temperature data were converted from Kelvin to Celsius. Hourly specific humidity (q) was converted to actual vapour pressure (ea) as follows:

$$\mathrm{ea} = \frac{q * P_{loc}}{0.622 + (1 - 0.622)q} \qquad (8)$$

, where P_{loc} is the local atmosphere pressure. Hourly saturated vapour pressure (es) was then calculated following the FAO's methodology such that:

$$\mathrm{es} = 610.8^{\frac{17.27T}{T+237.3}} \qquad (9)$$

, where T is the hourly temperature in degrees Celsius. Vapour pressure deficit was then derived:

$$\mathrm{VPD} = \mathrm{es} - \mathrm{ea} \qquad (10)$$

Monthly Number of Dry Days

The monthly number of dry days was derived from the WFDE5 bias-adjusted ERA5 dataset (Cucchi et al., 2020). The hourly rain speed was summed to get total daily precipitation and converted from kg m^{-2} s^{-1} to mm day^{-1}. The sum of the days with precipitation levels lower than 1 mm was then calculated.

Mean Daily Diurnal Temperature Range

The monthly mean daily diurnal temperature range was calculated by taking the difference between the maximum and the minimum daily temperature the WFDE5 bias-adjusted ERA5 dataset (Cucchi et al., 2020) from January 2010 to December 2015 such that:

$$DTR_{daily} = \max(temp_{daily}) - \min(temp_{daily}),$$

where DTR represents diurnal temperature range, *temp* represents hourly temperature and n represents the number of days in the month.

Mean Daily Wind Speeds

The monthly mean daily wind speed was calculated from the hourly daily mean from WFDE5 bias-adjusted ERA5 dataset (Cucchi et al., 2020) from January 2010 to December 2015 and then averaged over each month.

Motivation for estimating fire intensity

Fire intensity has been represented in multiple ways. Some studies have simply used measures of fire radiative power (FRP) (Wooster & Zhang, 2004; Wooster et al., 2005) whilst others have used monthly fire pixel counts to weight FRP (Luo et al., 2017) and others yet have performed spatial-temporal matching between fire patches and FRP values (Laurent et al., 2019). The potential issue with using FRP values directly from the MCD14ML dataset is that it represents instantaneous energy emitted by fire over the whole 1km x 1km MODIS pixel, therefore picking up not just on the energy emitted from the fire front but also any potential smoldering. Rothermel's (1972) equation represents reaction intensity, the energy emitted per unit volume multiplied by the speed the energy is moving at, in W m^{-2}. However, a measure of the rate of energy emitted per unit length of the fire line, in W m^{-1} (Byram, 1959) has become a common indicator of fire intensity (Keeley, 2009). As such, an estimation of this fire line intensity was used in this study. This was done using the following equation:

$$FI_i = \frac{FRP_i}{\sqrt{FS_i}}, \qquad (11)$$

, where FI_i is the fire intensity of a specific grid cell *i, FS_i* is the median fire size of specific grid cell *i* and FRP_i is the median fire radiative power of a specific grid cell *i.*

Parameters used for the calculation of gross primary production

Table S1. Inputs used for the calculation of GPP in the p-model (Wang et al., 2017; Stocker et al., 2020)

Input parameters	**Source**	**Derivation**
Mean daily temperature (°C)	Cucchi et al., 2020	Monthly daily mean temperature calculated from hourly data
Fractional fAPAR	NASA/GIMMS fAPAR 3g	Monthly mean of daily fAPAR
Photosynthetic Photon Flux Density (PPFD)	Cucchi et al., 2020	$PPFD = 60 * 60 * 24 * 10^{-6} * k_{EC} R_{SW}$, where k_{EC}=*2.04* µmol J^{-1} and R_{SW} is incoming shortwave radiation (Meek et al., 1984).(Meek et al., 1984).
Atmospheric CO_2 Concentrations (ppm)	Ed Dlugokencky and Pieter Tans, NOAA/GML (gml.noaa.gov/ccgg/trends/)	Global averaged monthly CO_2
Atmospheric pressure	Cucchi et al., 2020	Monthly daily mean atmospheric pressure calculated from hourly data
Vapour pressure deficit (Pa)	Cucchi et al., 2020	Monthly daily mean of VPD, calculated from hourly specific humidity, pressure and temperature

Results of models with all sixteen predictors

Table S2. Summary table of results of for all three models when all predictors are included with regression coefficients (where *** ($p<0.001$), ** ($p<0.01$), * ($p<0.05$),. ($p<0.1$) and results in brackets represent ($p\geq0.05$)), t-values and variance inflation factors (VIF).

Predictors	**Burnt area**			**Fire size**			**Fire intensity**		
	Coefficient	*t*-value	VIF	Coefficient	*t*-value	VIF	Coefficient	*t*-value	VIF
(intercept)	-48.25 ***	-103.6		-13.49 ***	-17.187		5.77 ***	25.228	
Gross primary production (g C m^{-2} a^{-1})	1.76 ***	63.00	4.13	(0.04)	(0.79)	(4.78)	-0.19 ***	-13.92	4.37
Seasonality of gross primary production	0.59 ***	14.78	2.43	0.32 ***	4.64	4.46	0.07 ***	3.32	4.79
Fractional tree cover	-0.93 ***	-18.74	2.92	-0.45 ***	-4.52	3.46	0.20 ***	7.52	3.24
Fractional shrubland cover	1.39 ***	26.35	1.70	0.66 ***	7.55	1.41	-0.13 ***	-3.76	1.33
Fractional grassland cover	2.93 ***	52.91	1.56	(0.13)	(1.45)	(1.22)	-0.34 ***	-10.50	1.39
Road density (km^{-2})	-0.05 ***	-37.32	1.44	-0.04 ***	-15.44	1.60	0.00 ***	8.16	1.83
Fractional cropland cover	-0.79 ***	-10.05	2.15	-3.45 ***	-18.99	1.89	(0.04)	(0.95)	(2.48)
Vector Ruggedness Measure	-188.70 ***	-21.39	1.55	-66.53 ***	-5.17	2.13	6.06 **	2.82	2.16
Topographic Position Index	0.43 ***	18.86	1.33	(-0.04)	(-0.86)	(1.69)	(0.00)	(-0.07)	(1.56)
Mean monthly number of dry days	4.54 ***	70.23	2.89	0.97 ***	8.08	3.22	-0.30 ***	-11.64	2.80
Seasonality of monthly number of dry days	1.33 ***	59.26	2.57	-0.10 **	-3.06	2.34	-0.14 ***	-14.48	2.21
Maximum mean monthly vapour pressure deficit (Pa)	1.35 ***	39.11	1.78	0.36 ***	5.70	3.98	-0.62 ***	-32.84	3.72
Maximum mean monthly diurnal temperature range (K)	0.87 ***	19.82	1.78	1.25 ***	13.90	2.08	(0.02)	(0.93)	(1.87)
Mean wind speed of the hottest month (m s^{-1})	-0.20 ***	-6.80	1.93	0.75 ***	12.37	2.64	(0.02)	(1.15)	(2.43)
Mean monthly lightning ground-strikes (km^{-2})	0.94 ***	12.35	1.66	0.83 ***	5.24	2.28	-0.26 ***	-5.87	2.35
Population density (km^{-2})	0.02 ***	10.64	1.71	(0.00)	(-0.94)	(1.71)	-0.01 ***	-13.36	1.86
R^2 (McFadden, 1974)	0.685			0.290			0.267		

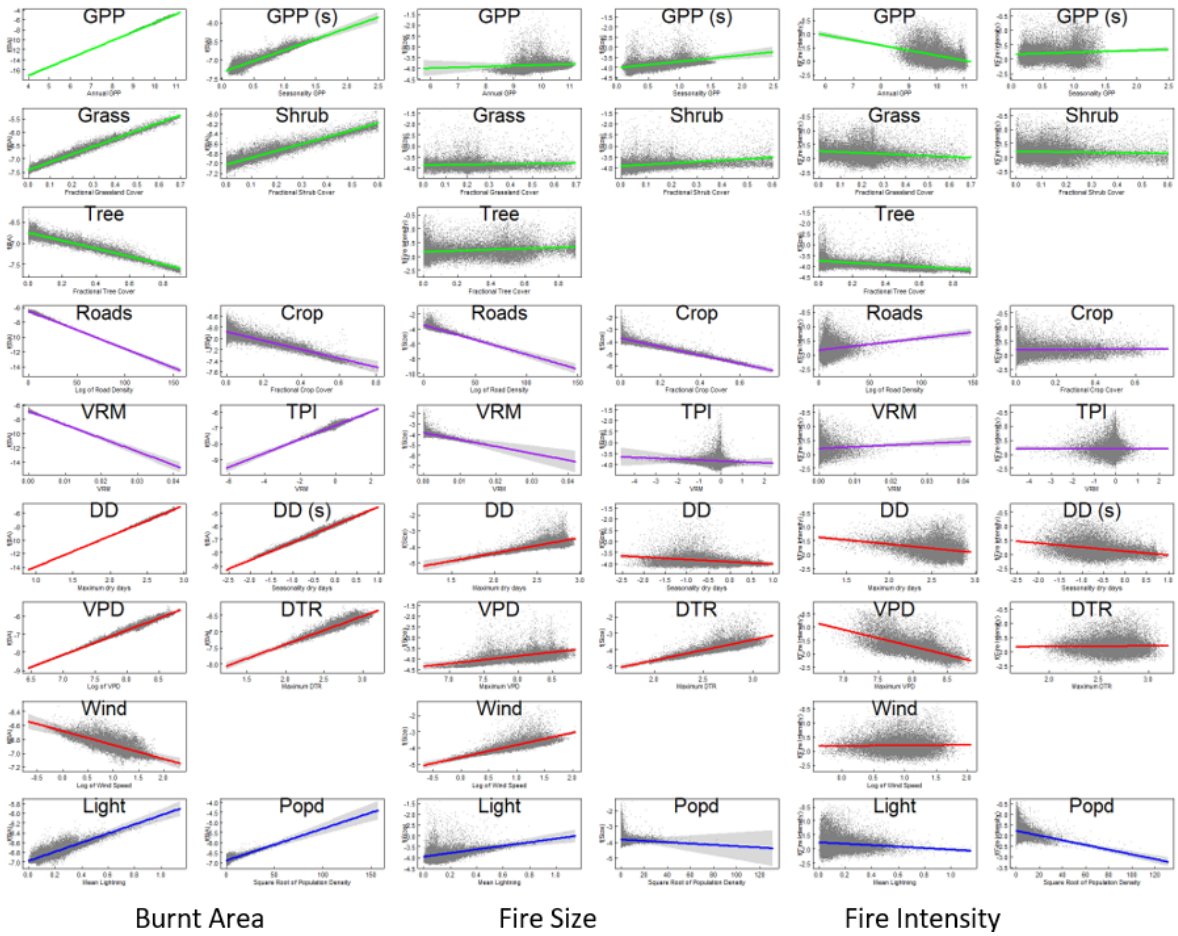

Figure S1. Partials residual plots for burnt area, fire size and fire intensity as functions of (GPP) gross primary production, (GPP (s)) seasonality of GPP, (shrub) shrubland cover, (grass) grassland cover, (tree) tree cover, (roads) road density, (crop) cropland, (VRM) vector ruggedness measure, (TPI) topographic position index, (DD) dry days, (DD (s)) dry days seasonality, (VPD) vapour pressure deficit, (DTR) diurnal temperature range, (wind) wind speed, (popd) population density and (light) lightning ground-strikes . Green represents vegetation and land cover predictors; purple represents fragmentation predictors; red represents climate predictors; blue represents ignition source predictors.

Results of models with all predictors excluding road density

Table S3 Summary table of results of for all three models when all predictors are included with regression coefficients (where *** (p<0.001), ** (p<0.01), * (p<0.05). (p<0.1) and results in brackets represent (p≥0.05)), t-values and variance inflation factors (VIF).

Predictors	**Burnt area**			**Fire size**			**Fire intensity**		
	Coefficient	*t*-value	VIF	Coefficient	*t*-value	VIF	Coefficient	*t*-value	VIF
(intercept)	-48.12 ***	-98.93		-12.18 ***	-15.66		5.65 ***	24.70	
Gross primary production (g C m^{-2} a^{-1})	1.64 ***	56.86	3.98	-0.10 *	-2.11	4.56	-0.17 ***	-12.50	4.20
Seasonality of gross primary production	0.62 ***	14.73	2.34	0.33 ***	4.80	4.31	0.06 **	3.08	4.81
Fractional tree cover	-0.51 ***	-10.26	2.68	-0.18 .	-1.81	3.27	0.14 ***	5.66	3.03
Fractional shrubland cover	1.65 ***	30.21	1.68	0.59 ***	6.86	1.39	-0.15 ***	-4.27	1.33
Fractional grassland cover	3.07 ***	53.76	1.52	0.17 .	1.88	1.22	-0.35 ***	-10.89	1.39
Fractional cropland cover	-1.03 ***	-12.68	2.06	-3.83 ***	-21.05	1.78	(0.04)	(1.10)	(2.49)
Vector Ruggedness Measure	-220.10 ***	-23.22	1.54	-73.79 ***	-5.68	2.12	6.62 **	3.08	2.16
Topographic Position Index	0.45 ***	18.80	1.33	(-0.04)	(-0.89)	(1.69)	(0.00)	(-0.02)	(1.56)
Mean monthly number of dry days	4.67 ***	68.89	2.90	0.91 ***	7.58	3.24	-0.30 ***	-11.47	2.80
Seasonality of monthly number of dry days	1.49 ***	64.67	2.53	(-0.03)	(-0.77)	(2.25)	-0.15 ***	-15.76	2.17
Maximum mean monthly vapour pressure deficit (Pa)	1.36 ***	38.18	1.71	0.31 ***	5.05	3.77	-0.63 ***	-32.97	3.75
Maximum mean monthly diurnal temperature range (K)	0.97 ***	21.37	1.77	1.35 ***	15.04	2.08	(0.01)	(0.31)	(1.86)
Mean wind speed of the hottest month (m s^{-1})	-0.23 ***	-7.63	1.88	0.75 ***	12.39	2.61	(0.02)	(1.36)	(2.43)
Mean monthly lightning ground-strikes (km^{-2})	0.53 ***	6.94	1.60	0.70 ***	4.52	2.21	-0.23 ***	-5.28	2.35
Population density (km^{-2})	0.00 .	-1.96	1.60	-0.03 ***	-6.52	1.52	-0.01 ***	-11.26	1.61
R^2 (McFadden, 1974)	0.668			0.276			0.265		

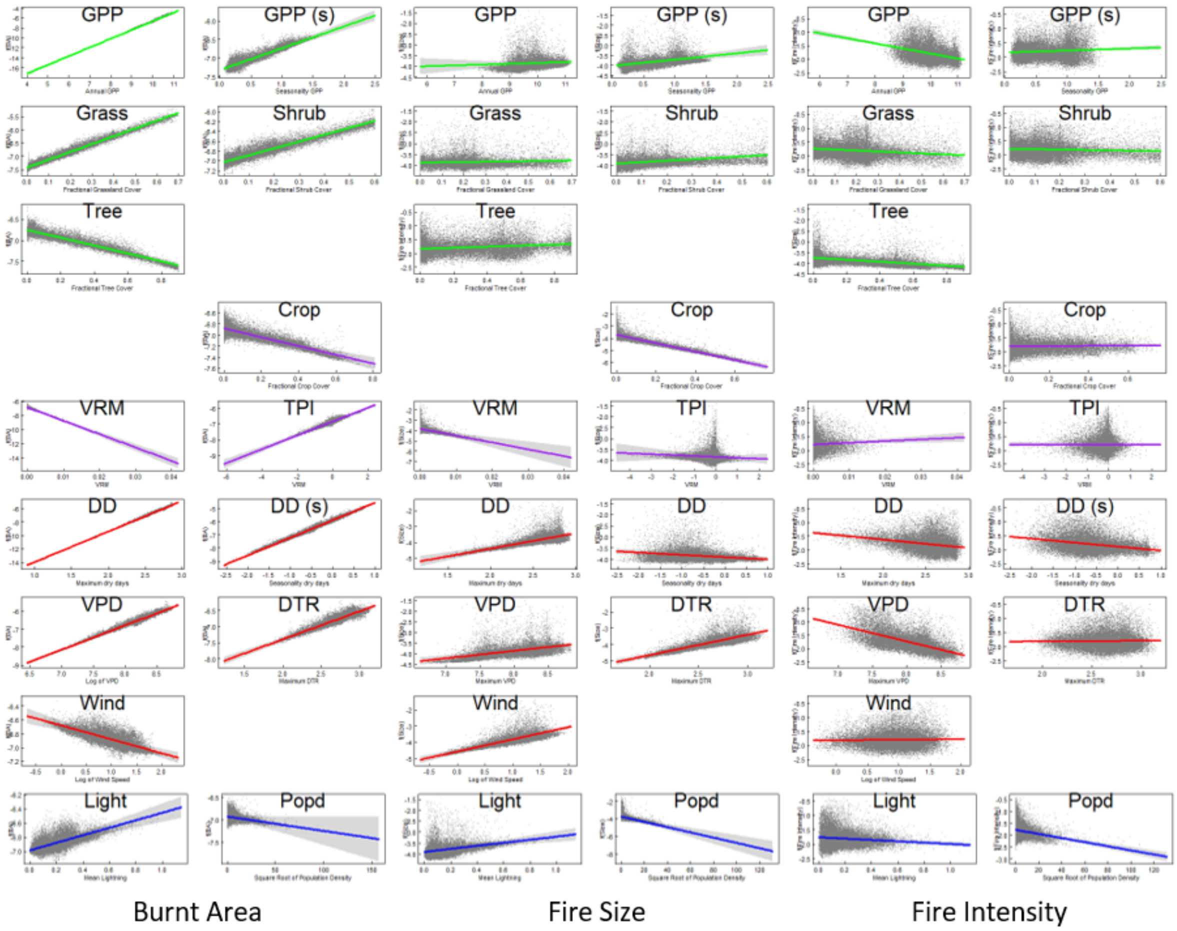

Figure S2. Partial residual plots for burnt area, fire size and fire intensity as functions of (GPP) gross primary production, (GPP (s)) seasonality of GPP, (shrub) shrubland cover, (grass) grassland cover, (tree) tree cove (crop) cropland, (VRM) vector ruggedness measure, (TPI) topographic position index, (DD) dry days, (DD (s)) dry days seasonality, (VPD) vapour pressure deficit, (DTR) diurnal temperature range, (wind) wind speed, (popd) population density and (light) lightning ground-strikes . Green represents vegetation and land cover predictors; purple represents fragmentation predictors; red represents climate predictors; blue represents ignition source predictors.

Results of models with all predictors excluding population density

Table S4 Summary table of results of for all three models when all predictors are included with regression coefficients (where *** (p<0.001), ** (p<0.01), * (p<0.05). (p<0.1) and results in brackets represent (p≥0.05)), t-values and variance inflation factors (VIF).

Predictors	**Burnt area**			**Fire size**			**Fire intensity**		
	Coefficient	*t*-value	VIF	Coefficient	*t*-value	VIF	Coefficient	*t*-value	VIF
(intercept)	-48.59 ***	-103.65		-13.45 ***	-17.18		5.82 ***	25.39	
Gross primary production (g C m^{-2} a^{-1})	1.77 ***	63.24	4.11	(0.04)	(0.78)	(4.78)	-0.18 ***	-13.47	4.37
Seasonality of gross primary production	0.59 ***	14.69	2.43	0.32 ***	4.66	4.45	0.08 ***	3.63	4.79
Fractional tree cover	-0.95 ***	-19.13	2.89	-0.45 ***	-4.51	3.46	0.19 ***	7.26	3.24
Fractional shrubland cover	1.36 ***	25.69	1.68	0.66 ***	7.61	1.41	-0.12 ***	-3.39	1.34
Fractional grassland cover	2.92 ***	52.57	1.55	(0.13)	(1.45)	(1.22)	-0.34 ***	-10.44	1.39
Road density (km^{-2})	-0.05 ***	-35.60	1.34	-0.04 ***	-16.47	1.46	0.00 **	3.01	1.58
Fractional cropland cover	-0.51 ***	-6.92	1.88	-3.51 ***	-20.50	1.68	-0.11 **	-2.89	2.31
Vector Ruggedness Measure	-186.80 ***	-21.12	1.55	-66.60 ***	-5.18	2.13	6.07 **	2.81	2.16
Topographic Position Index	0.43 ***	18.66	1.33	(-0.04)	(-0.84)	(1.69)	(0.00)	(0.38)	(1.55)
Mean monthly number of dry days	4.63 ***	71.73	2.83	0.96 ***	8.03	3.19	-0.34 ***	-13.19	2.76
Seasonality of monthly number of dry days	1.35 ***	59.84	2.56	-0.11 **	-3.20	2.30	-0.16 ***	-16.07	2.18
Maximum mean monthly vapour pressure deficit (Pa)	1.37 ***	39.47	1.77	0.35 ***	5.63	3.91	-0.65 ***	-34.42	3.68
Maximum mean monthly diurnal temperature range (K)	0.81 ***	18.56	1.74	1.26 ***	14.25	2.03	0.08 ***	3.53	1.81
Mean wind speed of the hottest month (m s^{-1})	-0.24 ***	-7.97	1.91	0.76 ***	12.70	2.57	0.05 ***	3.40	2.36
Mean monthly lightning ground-strikes (km^{-2})	0.84 ***	11.05	1.63	0.85 ***	5.44	2.23	-0.18 ***	-4.02	2.30
R^2 (McFadden, 1974)	0.684			0.289			0.262		

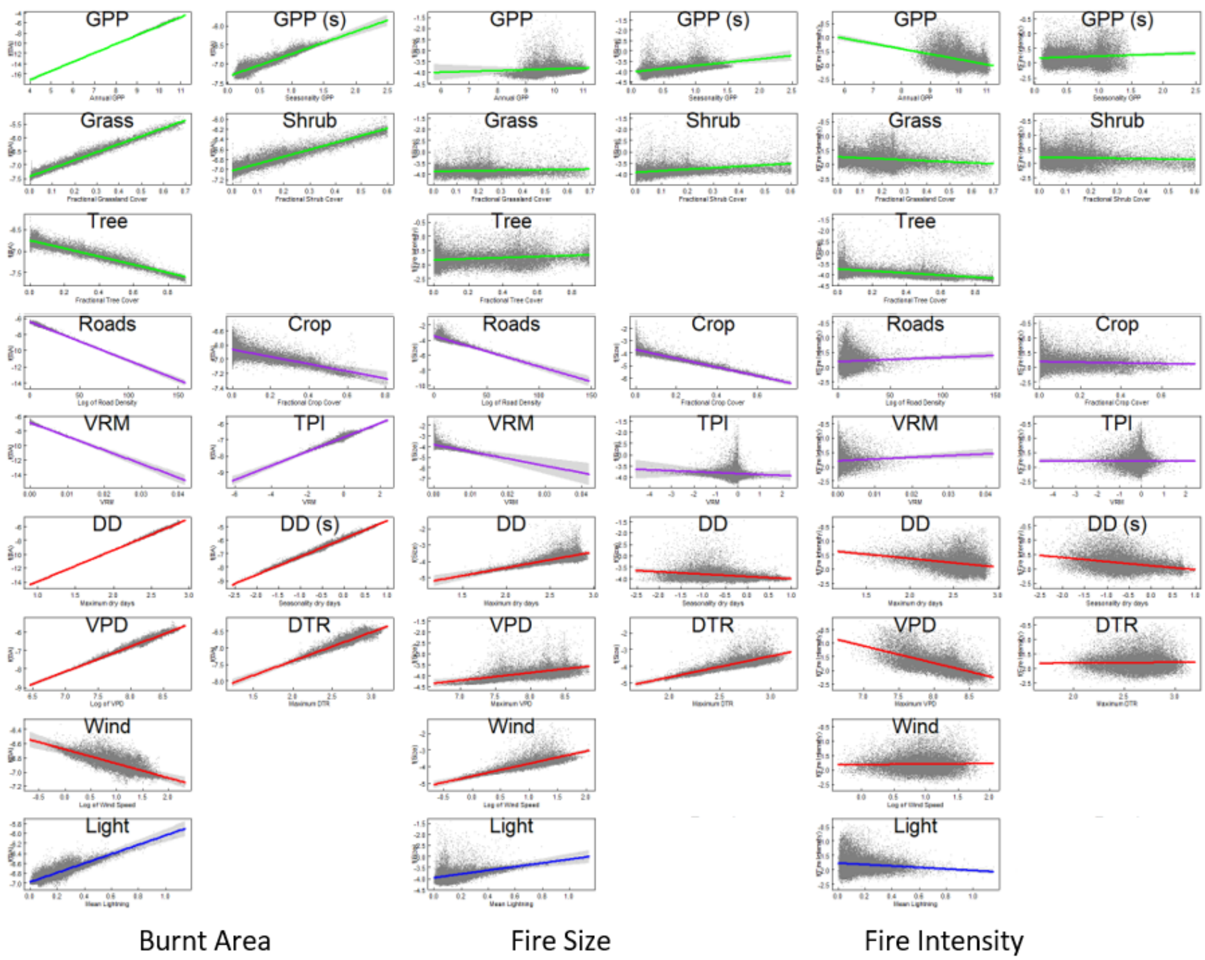

Figure S3. Partial residual plots for burnt area, fire size and fire intensity as functions of (GPP) gross primary production, (GPP (s)) seasonality of GPP, (shrub) shrubland cover, (grass) grassland cover, (tree) tree cover, (roads) road density, (crop) cropland, (VRM) vector ruggedness measure, (TPI) topographic position index, (DD) dry days, (DD (s)) dry days seasonality, (VPD) vapour pressure deficit, (DTR) diurnal temperature range, (wind) wind speed, and (light) lightning ground-strikes . Green represents vegetation and land cover predictors; purple represents fragmentation predictors; red represents climate predictors; blue represents ignition source predictors.

Results of models with all predictors excluding VPD

Table S5 Summary table of results of for all three models when all predictors are included with regression coefficients (where *** ($p<0.001$), ** ($p<0.01$), * ($p<0.05$). ($p<0.1$) and results in brackets represent ($p\geq0.05$)), t-values and variance inflation factors (VIF).

Predictors	**Burnt area**			**Fire size**			**Fire intensity**		
	Coefficient	*t*-value	VIF	Coefficient	*t*-value	VIF	Coefficient	*t*-value	VIF
(intercept)	-36.28 ***	-105.11		-10.60 ***	-17.77		0.37 *	2.26	
Gross primary production (g C m^{-2} a^{-1})	1.59 ***	57.19	3.92	0.00	-0.01	4.69	-0.12 ***	-8.69	4.30
Seasonality of gross primary production	(0.00)	(0.05)	(2.39)	0.11 .	1.90	3.29	0.47 ***	27.67	3.07
Fractional tree cover	-1.05 ***	-20.64	2.86	-0.50 ***	-5.03	3.41	0.21 ***	7.75	3.28
Fractional shrubland cover	1.69 ***	31.17	1.68	0.62 ***	7.10	1.39	-0.06 .	-1.65	1.34
Fractional grassland cover	2.60 ***	45.33	1.53	(0.10)	(1.05)	(1.22)	-0.26 ***	-7.88	1.39
Road density (km^{-2})	-0.05 ***	-36.85	1.47	-0.04 ***	-15.27	1.61	0.00 ***	8.64	1.80
Fractional cropland cover	-0.21 ***	-2.63	2.07	-3.35 ***	-18.64	1.87	-0.18 ***	-4.47	2.42
Vector Ruggedness Measure	-288.80 ***	-29.64	1.49	-84.42 ***	-6.65	2.02	24.67 ***	11.89	1.98
Topographic Position Index	0.33 ***	13.98	1.37	(-0.03)	(-0.72)	(1.69)	0.00 .	0.06	1.55
Mean monthly number of dry days	4.75 ***	71.37	2.72	1.06 ***	8.91	3.10	-0.42 ***	-15.76	2.84
Seasonality of monthly number of dry days	1.41 ***	61.72	2.47	-0.08 *	-2.35	2.29	-0.17 ***	-16.83	2.22
Maximum mean monthly diurnal temperature range (K)	1.03 ***	23.43	1.73	1.33 ***	15.13	2.03	-0.04 .	-1.75	1.88
Mean wind speed of the hottest month (m s^{-1})	-0.14 ***	-4.85	1.83	0.78 ***	13.01	2.60	-0.06 ***	-3.84	2.40
Mean monthly lightning ground-strikes (km^{-2})	1.43 ***	18.73	1.67	1.00 ***	6.48	2.20	-0.57 ***	-12.80	2.24
Population density (km^{-2})	0.02 ***	13.03	1.65	(0.00)	(-0.26)	(1.66)	-0.01 ***	-16.36	1.86
R^2 (McFadden, 1974)	0.668			0.290			0.239		

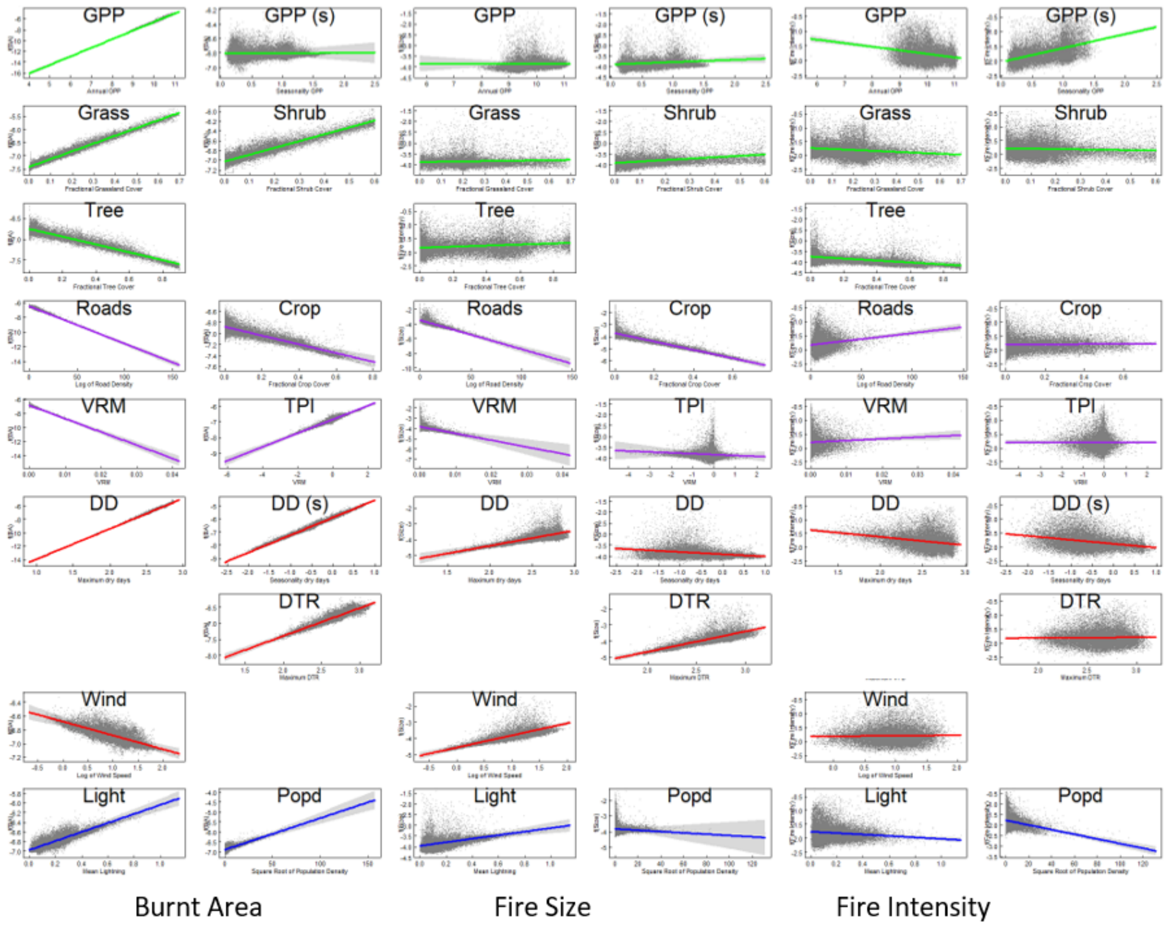

Figure S4. Figure 1. Partial residual plots for burnt area, fire size and fire intensity as functions of (GPP) gross primary production, (GPP (s)) seasonality of GPP, (shrub) shrubland cover, (grass) grassland cover, (tree) tree cover, (crop) cropland, (VRM) vector ruggedness measure, (TPI) topographic position index, (DD) dry days, (DD (s)) dry days seasonality, (DTR) diurnal temperature range, (wind) wind speed, (popd) population density and (light) lightning ground-strikes . Green represents vegetation and land cover predictors; purple represents fragmentation predictors; red represents climate predictors; blue represents ignition source predictors.

Results of models with all predictors excluding GPP seasonality

Table S6. Summary table of results of for all three models when all predictors are included with regression coefficients (where *** (p<0.001), ** (p<0.01), * (p<0.05). (p<0.1) and results in brackets represent (p≥0.05)), t-values and variance inflation factors (VIF).

	Burnt area			**Fire size**			**Fire intensity**		
	Coefficient	*t*-value	VIF	Coefficient	*t*-value	VIF	Coefficient	*t*-value	VIF
(intercept)	-44.22 ***	-116.14		-10.77 ***	-20.73		6.35 ***	42.61	
Gross primary production (g C m^{-2} a^{-1})	1.56 ***	64.28	3.17	-0.07 .	-1.82	3.59	-0.21 ***	-17.84	3.33
Fractional tree cover	-0.81 ***	-16.41	2.90	-0.34 ***	-3.48	3.26	0.22 ***	8.84	2.98
Fractional shrubland cover	1.47 ***	27.79	1.67	0.69 ***	7.92	1.40	-0.14 ***	-3.95	1.33
Fractional grassland cover	2.93 ***	52.65	1.57	0.21 *	2.36	1.18	-0.32 ***	-10.18	1.37
Road density (km^{-2})	-0.05 ***	-37.33	1.43	-0.04 ***	-15.51	1.60	0.00 ***	8.06	1.83
Fractional cropland cover	-0.59 ***	-7.57	2.10	-3.19 ***	-18.53	1.72	0.08 *	2.05	2.25
Vector Ruggedness Measure	-193.20 ***	-21.80	1.55	-74.69 ***	-5.85	2.08	4.66 *	2.21	2.08
Topographic Position Index	0.42 ***	18.18	1.33	(-0.03)	(-0.56)	(1.67)	0.00	0.10	1.55
Mean monthly number of dry days	4.45 ***	69.45	2.90	0.95 ***	8.05	3.21	-0.30 ***	-11.71	2.80
Seasonality of monthly number of dry days	1.32 ***	58.76	2.63	-0.08 *	-2.41	2.32	-0.14 ***	-14.60	2.21
Maximum mean monthly vapour pressure deficit (Pa)	1.18 ***	35.72	1.52	0.20 ***	3.83	2.84	-0.66 ***	-43.06	2.44
Maximum mean monthly diurnal temperature range (K)	0.87 ***	19.86	1.77	1.21 ***	13.61	2.05	0.01	0.63	1.86
Mean wind speed of the hottest month (m s^{-1})	-0.23 ***	-7.64	1.96	0.70 ***	11.89	2.58	0.02	1.15	2.43
Mean monthly lightning ground-strikes (km^{-2})	0.65 ***	8.65	1.54	0.65 ***	4.22	2.15	-0.29 ***	-6.79	2.23
Population density (km^{-2})	0.02 ***	10.60	1.72	(0.00)	(-0.99)	(1.72)	-0.01 ***	-13.44	1.86
R^2 (McFadden, 1974)	0.682			0.288			0.267		

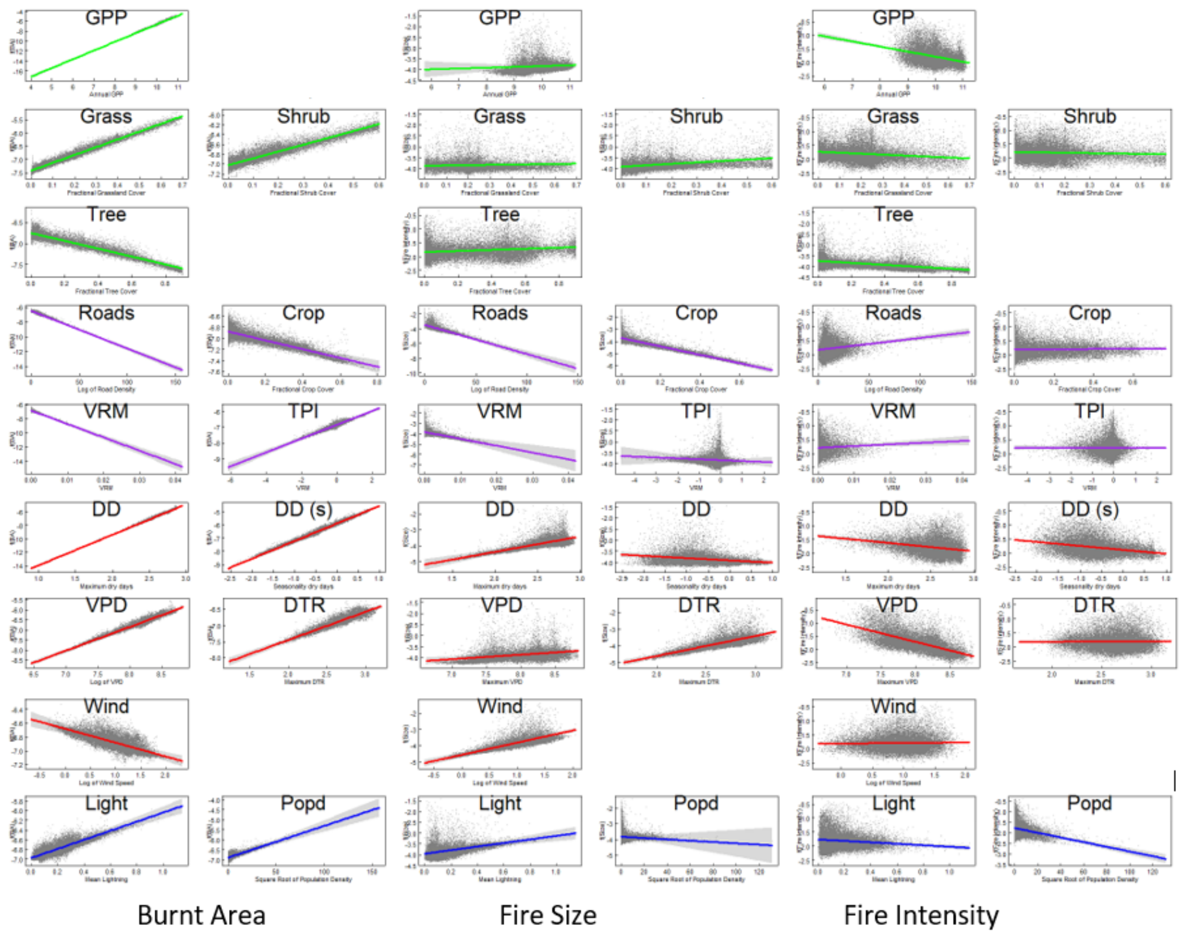

Figure S5. Partial residual plots for burnt area, fire size and fire intensity as functions of (GPP) gross primary production, (shrub) shrubland cover, (grass) grassland cover, (tree) tree cover, (roads) road density, (crop) cropland, (VRM) vector ruggedness measure, (TPI) topographic position index, (DD) dry days, (DD (s)) dry days seasonality, (VPD) vapour pressure deficit, (DTR) diurnal temperature range, (wind) wind speed, (popd) population density and (light) lightning ground-strikes . Green represents vegetation and land cover predictors; purple represents fragmentation predictors; red represents climate predictors; blue represents ignition source predictors.

Supplementary information for Chapter 3

This section contains supplementary information for Chapter 3. It contains information on (a) obtaining fAPAR from BIOME4, (b) obtaining an ignition threshold mask, (c) the mapped results for all experiments for all three of the LGM scenarios, and (d) the comparisons of the experiment outputs with the Reading Palaeofire Database for burnt area, fire size and fire intensity.

Obtaining Fraction of Absorbed Photosynthetically Active Radiation (fAPAR) from BIOME4

BIOME4 (Kaplan et al., 2003) is a coupled biogeography and biogeochemistry with which we can simulate the equilibrium distribution of biomes from latitude, atmospheric CO_2 concentration, mean monthly precipitation, temperature, and cloud cover. On of the outputs provided by the model is monthly leaf area index (LAI), which we can convert to Fraction of Absorbed Photosynthetically Active Radiation (fAPAR) using Beer-Lamberth law:

$$\text{fAPAR} = 1 - \exp(-k.\ \text{LAI}) \qquad (5)$$

where k ≈ 0..5, a constant extinction coefficient (Saitoh et al., 2012).

fAPAR simulated from BIOME4 under modern-day conditions (2010-2015 seasonal climatology; Cucchi et al., 2020) overestimated fAPAR compared to observed fAPAR from NASA/GIMMS fAPAR 3g from the same period. As such, we rescaled the simulated BIOME fAPAR for each experiment such that:

$$fAPAR_{rescaled} = fAPAR_{exp}\frac{fAPAR_{obs}}{fAPAR_{sim}}) \qquad (6),$$

where $fAPAR_{rescaled}$ is the monthly rescaled fAPAR for that experiment, $fAPAR_{exp}$ is the original fAPAR output from BIOME4 for that experiment and $\frac{fAPAR_{obs}}{fAPAR_{sim}}$ is a constant scaling factor, determined for each biome, where $fAPAR_{obs}$ is the monthly NASA/GIMMS fAPAR 3g median value for that biome, and $fAPAR_{sim}$ is the monthly fAPAR median value simulated by BIOME4 for that biome. This method provided a rescaled fAPAR for the modern day that was correlated at 0.63 with the observational data, compared to 0.13 for the original BIOME4 fAPAR output for the same period, a reasonable estimation of fAPAR for each of the experiments.

Obtaining burnt area mask for fire size and fire intensity experiments

In this analysis, we were interested in how the global pattern of burnt area (BA), fire size (FS) and fire intensity (FI) change under different climate and CO_2 scenarios. Both the GLM models for FS and FI return values of estimated FS and FI assuming a fire occurs since the models were fitted to observed data for FS and FI. When no fire occurred, there was no data for either FS or FI. As such, these models cannot determine themselves if an ignition occurred.

To study changes in FS and FI, it is necessary to apply an ignition threshold, which we obtained from the BA model. The burnt area (BA) generalized linear model (GLM) provides a robust reconstruction of BA under the model training conditions with a 0.8 correlation between the observational data and the fitted values. There are no systematic biases evident from plotting the residuals of the model but there is a compression of the range of reconstructed values, leading to apparent over- (under-) prediction at the low (high) extremes. This is to be expected, as the observational values reflect what really happened over the study period. Whilst some exceptionally large/intense wildfires occurred, many grid-cells also had no fire activity whilst the fitted values represent the probability of burning in each grid-cell, regardless of what happened during the study period. We obtained the ignition threshold value by studying the distribution of reconstructed BA values under the original model training period (2010-2015) when the observed BA value is 0, representing 26% of the grid-cells (a total of 14,816 data points and associated fitted values). We then took the median value of these fitted values as a threshold for ignition.

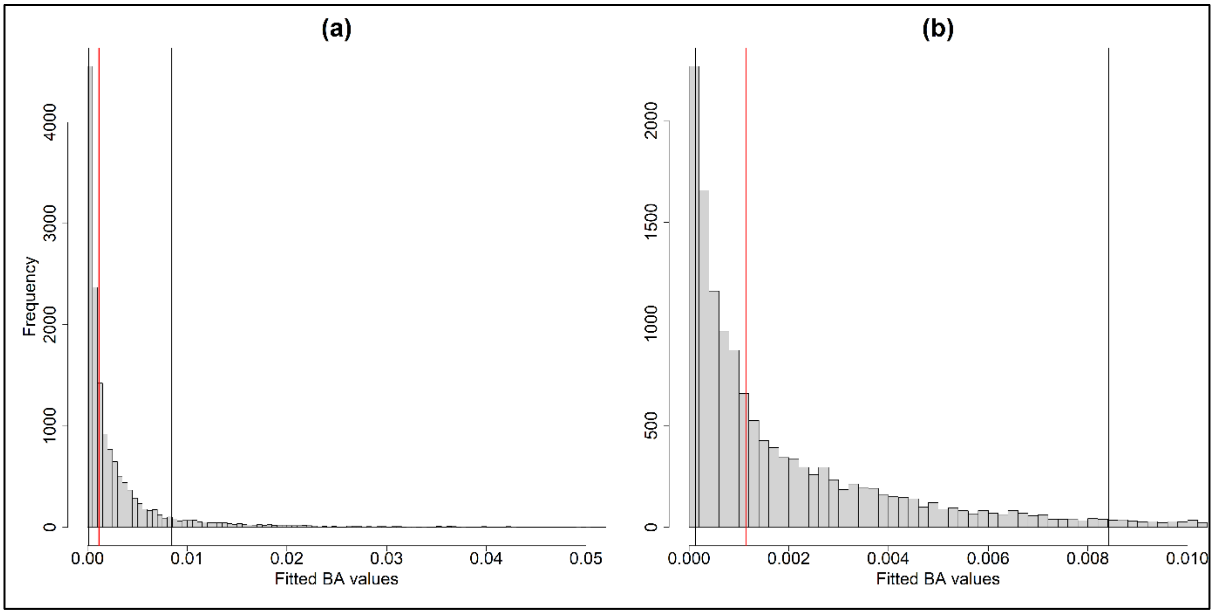

Figure S6. Histograms showing the distribution of the fitted values by the GLM BA model when observed BA values are 0 in the 2010-2015 climatology for (a) the whole range and (b) the range up to the 95th percentile. The red line shows the median value, and the black lines show the 10th and 90th percentile values.

Table S7. Statistics for the fitted BA distribution when observed BA is 0 for the 2010-2015 climatology.

	10th percentile	50th percentile	90th percentile
Fitted BA	0.0001	0.0011	0.0084

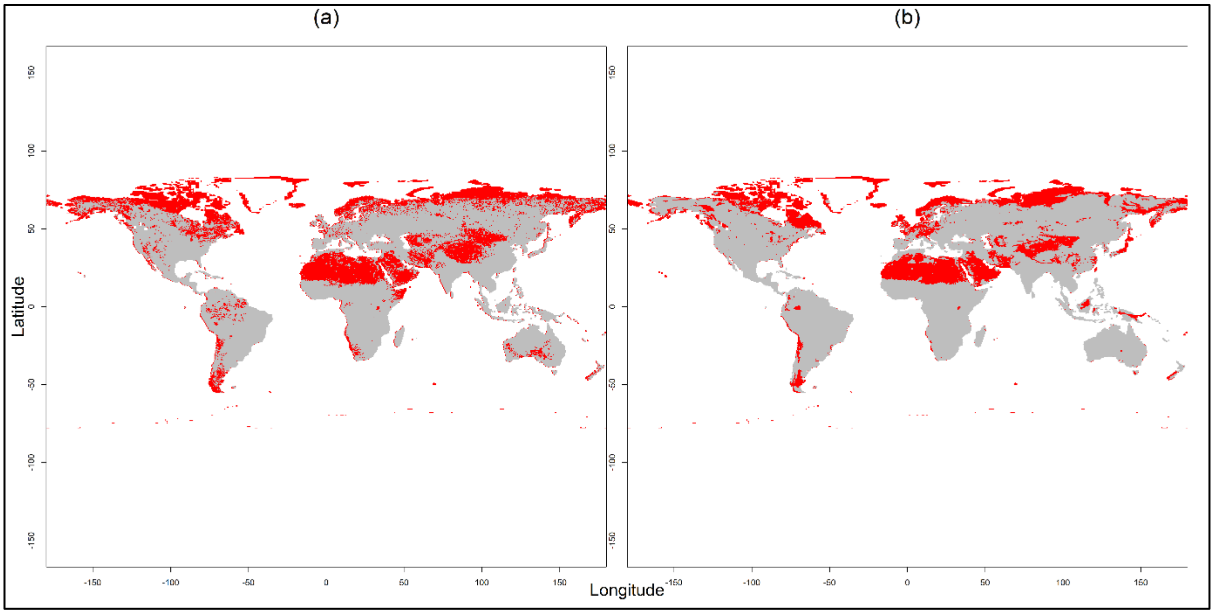

Figure S.7 Maps of BA ignition mask (where no burning is assumed to occur) under modern-day conditions (2010-2015 climatology) showing in red (a) where the observational BA values are 0 and (b) where the fitted BA values are equal or lower to 0.0011.

Mapped results from the 12 experiments for all three LGM scenarios

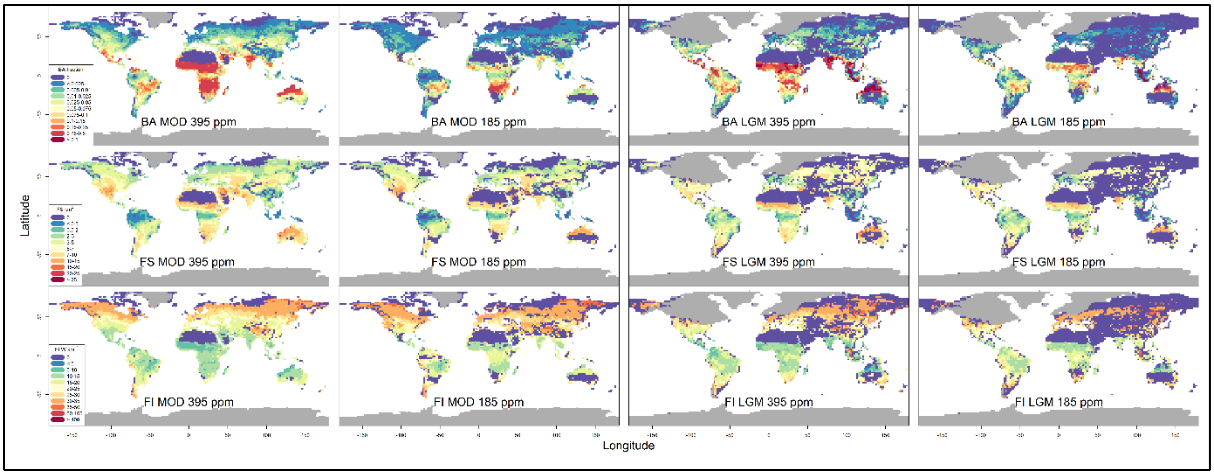

Figure S8. Changes in burnt area (BA), fire size (FS) and fire intensity (FI) using modern day climate (MOD) or Last Glacial Maximum (LGM) climate from the MPI-ESM1.2 simulation with either modern (395 ppm) or LGM (185 ppm) CO_2.

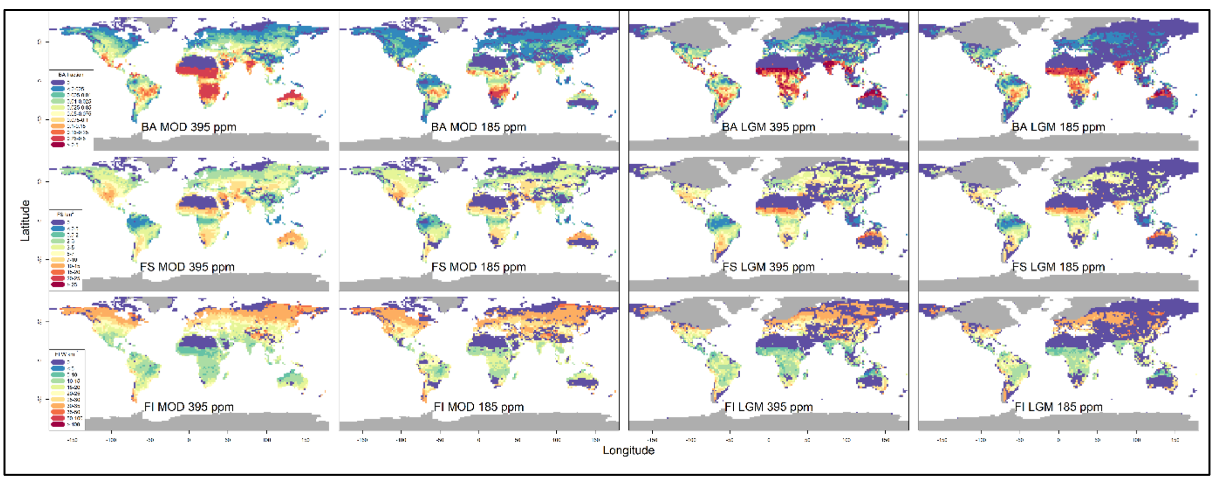

Figure S9. Changes in burnt area (BA), fire size (FS) and fire intensity (FI) using modern day climate (MOD) or Last Glacial Maximum (LGM) climate from the AWIESM1 simulation with either modern (395 ppm) or LGM (185 ppm) CO_2.

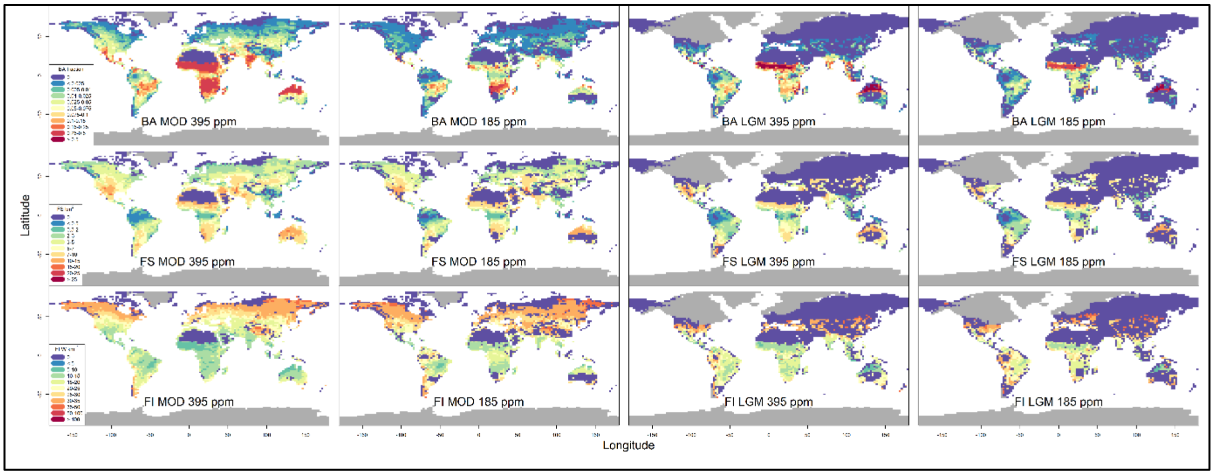

Figure S10. Changes in burnt area (BA), fire size (FS) and fire intensity (FI) using modern day climate (MOD) or Last Glacial Maximum (LGM) climate CESM1.2 simulation with either modern (395 ppm) or LGM (185 ppm) CO_2.

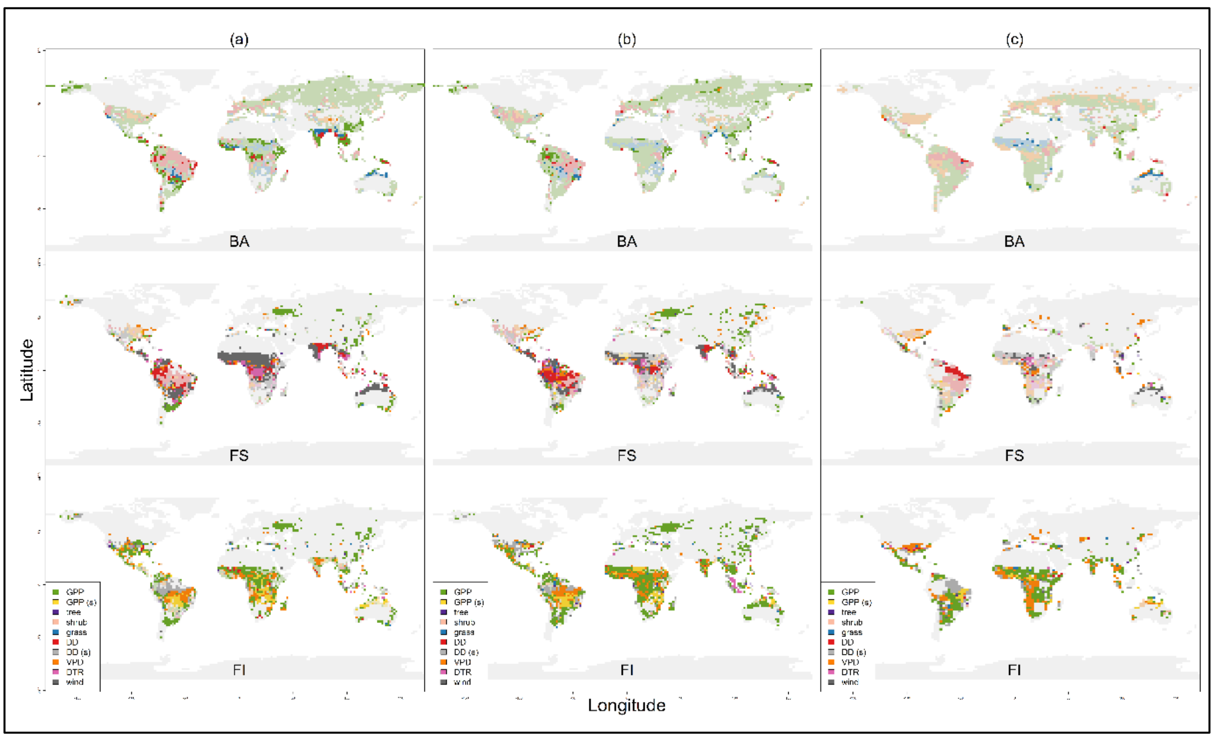

Figure S11. Map showing which model variable was responsible for some of the most important grid-cell changes between the realistic modern-day climate (MOD) 395 ppm experiment and the realistic Last Glacial Maximum (LGM) 190 ppm scenarios for BA, FS and FI for (a) the AWIESM1 LGM scenario, (b) the MPI-ESM1.2 LGM scenario and (c) the CESM1.2 LGM scenarios. Faded colors represent that the effect was a negative one, leading to a decrease in the wildfire property at the LGM whilst full colors represent an increase in the wildfire property at the LGM.

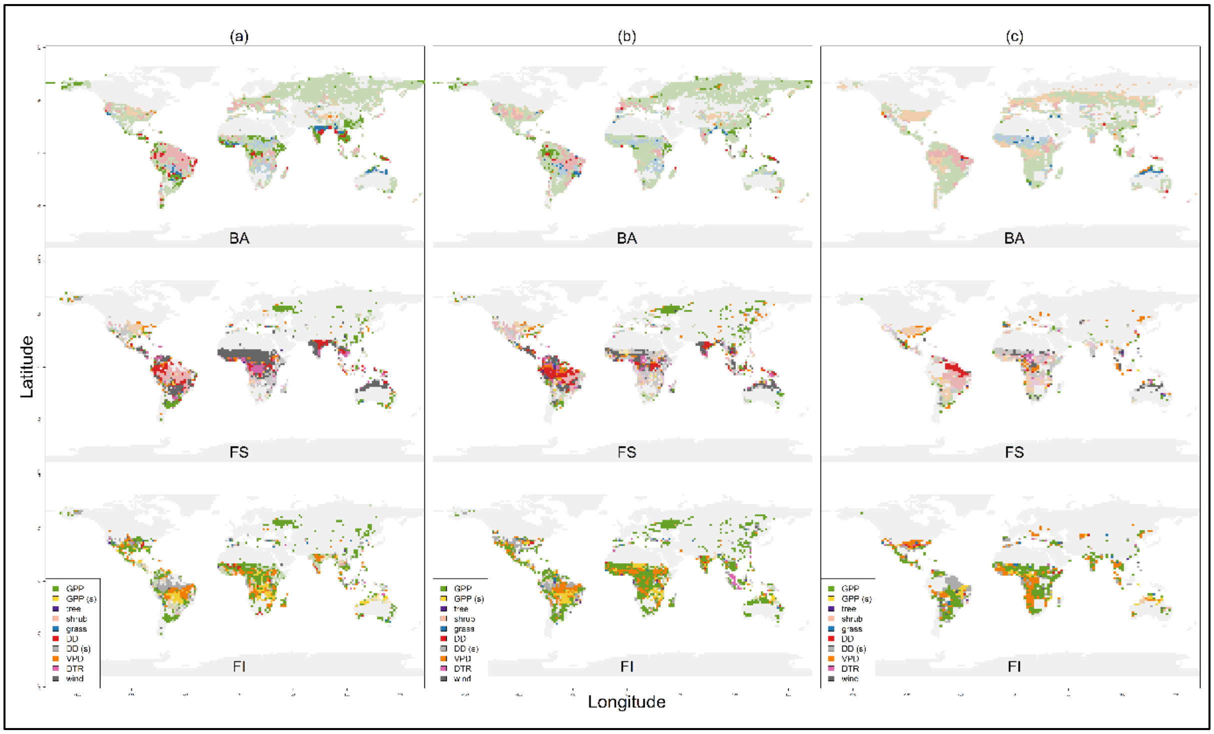

Figure S12. Map showing which model variable was responsible for some of the most important grid-cell changes between the MOD 395 ppm and LGM 395 ppm experiment (LGM climate/MOD CO_2) for BA, FS and FI for (a) the AWIESM1 LGM scenario, (b) the MPI-ESM1.2 LGM scenario and (c) the CESM1.2 LGM scenarios. Faded colors represent that the effect was a negative one, leading to a decrease in the wildfire property at the LGM whilst full colors represent an increase in the wildfire property at the LGM.

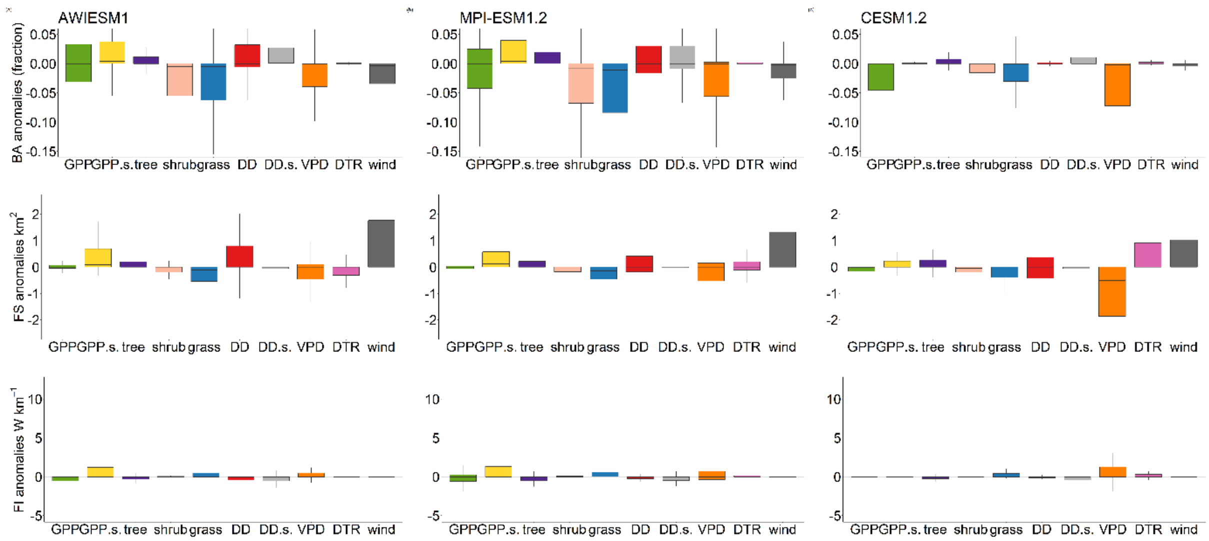

Figure S13. Boxplots showing relative importance of each predictor (GPP; gross primary production, GPP.s.; GPP seasonality, tree; tree cover, shrub; shrub cover, grass; grass cover, DD; dry days, DD.s.; dry days seasonality, VPD; vapour pressure deficit, DTR; diurnal temperature range, wind; wind speed) in driving the anomaly between the MOD 395 ppm and LGM 395 ppm experiment. For each grid cell common to both experiments (on modern-day continental shelves and masking the LGM ice sheets), the predictor which cause the largest change in the anomaly between the two experiments when it was excluded from the GLM model was retained, it is the change in anomaly that is shown here. This was taken as an indicator of relative importance of that predictor in driving the observed change for (a) the AWIESM1 LGM scenario, (b) the MPI-ESM-1.2 LGM scenario and (c) the CESM1.2 LGM scenario. A positive anomaly represents the variable driving an increase in BA, FS or FI at the LGM and a negative anomaly represents the variable driving a decrease in BA, FS or FI at the LGM.

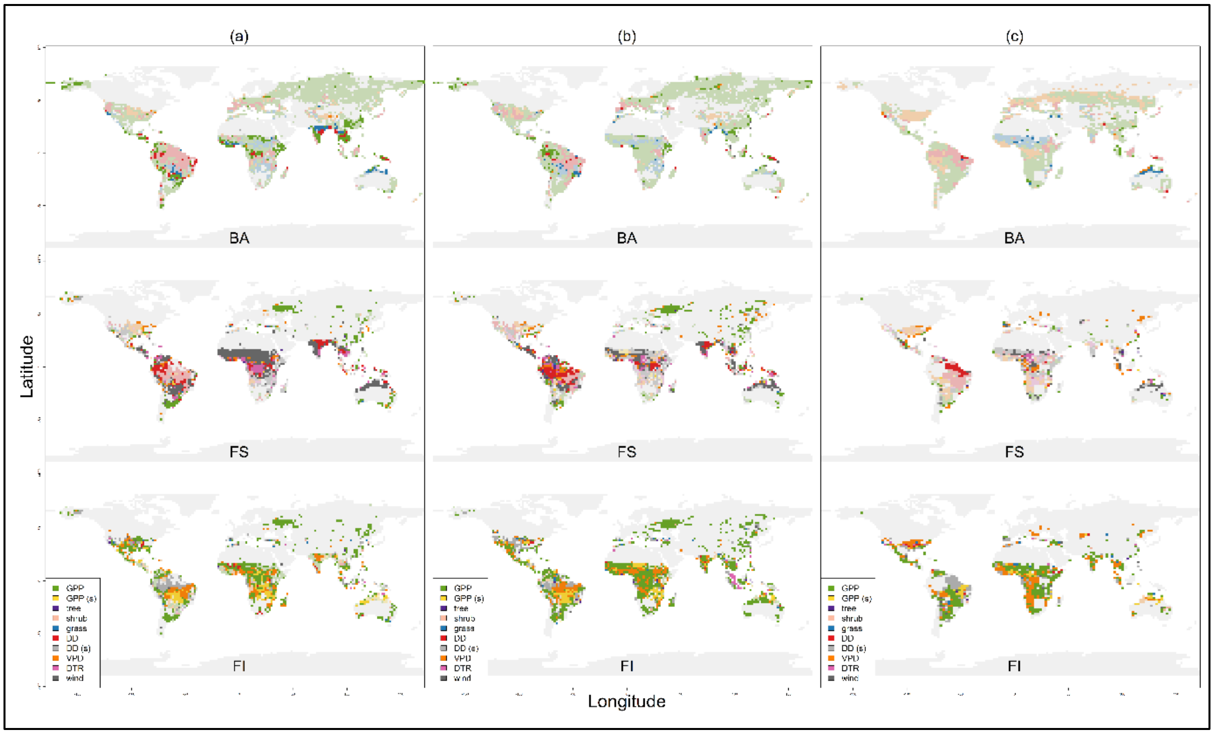

Figure S14. Map showing which model variable was responsible for some of the most important grid-cell changes between the realistic MOD 395 ppm and MOD 190 ppm experiment (MOD climate/LGM CO_2) for BA, FS and FI for (a) the AWIESM1 LGM scenario, (b) the MPI-ESM1.2 LGM scenario and (c) the CESM1.2 LGM scenarios. Faded colors represent that the effect was a negative one, leading to a decrease in the wildfire property at the LGM whilst full colors represent an increase in the wildfire property at the LGM.

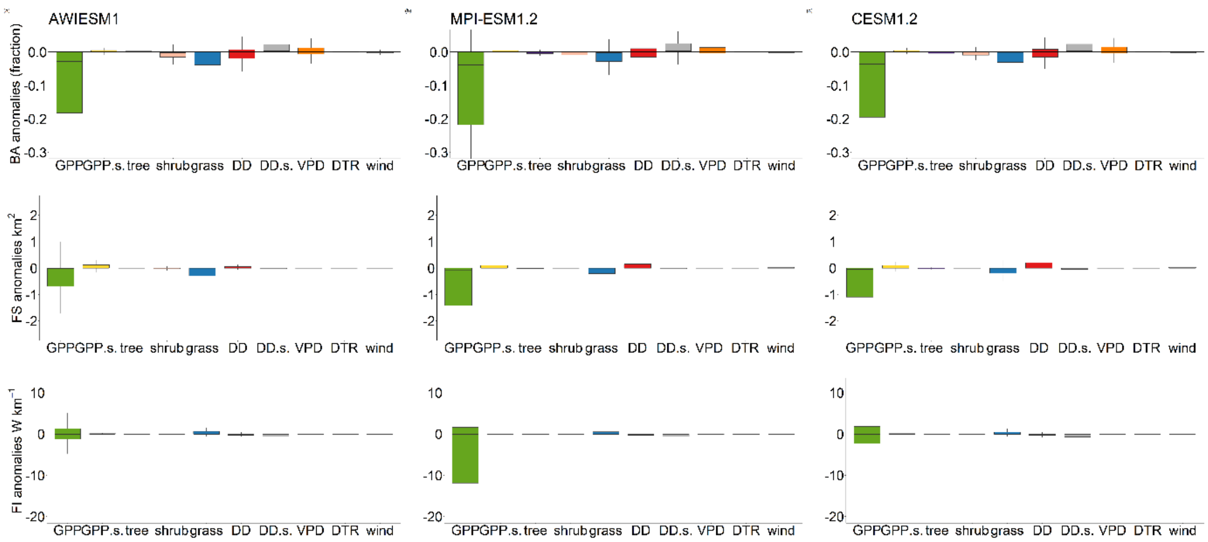

Figure S15. Boxplots showing relative importance of each predictor (GPP; gross primary production, GPP.s.; GPP seasonality, tree; tree cover, shrub; shrub cover, grass; grass cover, DD; dry days, DD.s.; dry days seasonality, VPD; vapour pressure deficit, DTR; diurnal temperature range, wind; wind speed) in driving the anomaly between the MOD 395 ppm and MOD 190 ppm experiment. For each grid cell common to both experiments (on modern-day continental shelves and masking the LGM ice sheets), the predictor which cause the largest change in the anomaly between the two experiments when it was excluded from the GLM model was retained, it is the change in anomaly that is shown here. This was taken as an indicator of relative importance of that predictor in driving the observed change for (a) the AWIESM1 LGM scenario, (b) the MPI-ESM-1.2 LGM scenario and (c) the CESM1.2 LGM scenario. A positive anomaly represents the variable driving an increase in BA, FS or FI at the LGM and a negative anomaly represents the variable driving a decrease in BA, FS or FI at the LGM.

Comparison of experiments with charcoal records from the Reading Palaeofire Database (RPD)

Table S8. Comparison of sign in BA anomalies (between the MOD climate/MOD CO_2 experiment and other three experiments respectively) at the location of each RDP (Harrison et al., 2022) charcoal-based reconstructions record. A positive anomaly represents increased biomass burning, and a negative anomaly represents decreased biomass burning. Successful identification means that the sign of the experiment anomaly and the sign of the RPD charcoal-based reconstructions are the same.

BA experiments		**MPI_ESM1.2**			**AWIESM1**			**CESM1.2 LGM**		
Scenario	RPD	LGM 190	MOD 190	LGM 395	LGM 190	MOD 190	LGM 395	LGM 190	MOD 190	LGM 395
Negative RPD anomalies										
Number of records	35	20	21	13	17	21	10	20	20	17
Successful identification (percentage)		57	60	37	49	60	29	57	57	49
Positive RPD anomalies										
Number of records	16	3	0	8	6	0	5	0	0	3
Successful identification (percentage)		19	0	50	38	0	31	0	0	19
Total RPD anomalies										
Number of records	51	23	21	21	23	21	15	20	20	20
Successful identification (percentage)		45	41	41	45	41	29	39	39	39

Table S9. Comparison of sign in FS anomalies (between the MOD climate/MOD CO_2 experiment and other three experiments respectively) at the location of each RDP (Harrison et al., 2022) charcoal-based reconstructions record. A positive anomaly represents increased biomass burning, and a negative anomaly represents decreased biomass burning. Successful identification means that the sign of the experiment anomaly and the sign of the RPD charcoal-based reconstructions are the same.

FS experiments		**MPI_ESM1.2**			**AWIESM1**			**CESM1.2 LGM**		
Scenario	RPD	LGM 190	MOD 190	LGM 395	LGM 190	MOD 190	LGM 395	LGM 190	MOD 190	LGM 395
Negative RPD anomalies										
Number records showing reduced burning	35	10	15	7	11	9	8	10	14	11
Successful identification (percentage)		29	43	20	31	26	23	29	40	31
Positive RPD anomalies										
Number records showing increased burning	16	6	2	7	8	8	9	4	2	4
Successful identification (percentage)		38	13	44	50	50	56	25	13	25
Total RPD anomalies										
Total number of records	51	16	17	14	19	17	17	14	16	15
Successful identification (percentage)		31	33	27	37	33	33	27	31	29

Table S10. Comparison of sign in FI anomalies (between the MOD climate/MOD CO_2 experiment and other three experiments respectively) at the location of each RDP (Harrison et al., 2022) charcoal-based reconstructions record. A positive anomaly represents increased biomass burning, and a negative anomaly represents decreased biomass burning. Successful identification means that the sign of the experiment anomaly and the sign of the RPD charcoal-based reconstructions are the same.

FI experiments		**MPI_ESM1.2**			**AWIESM1**			**CESM1.2 LGM**		
Scenario	RPD	LGM 190	MOD 190	LGM 395	LGM 190	MOD 190	LGM 395	LGM 190	MOD 190	LGM 395
Negative RPD anomalies										
Number records showing reduced burning	35	5	7	9	7	7	11	3	5	4
Successful identification (percentage)		14	20	26	20	20	31	9	14	11
Positive RPD anomalies										
Number records showing increased burning	16	10	12	7	10	12	8	9	11	8
Successful identification (percentage)		63	75	44	63	75	50	56	69	50
Total RPD anomalies										
Total number of records	51	15	19	16	17	19	19	12	16	12
Successful identification (percentage)		30	37	31	33	37	37	24	31	24

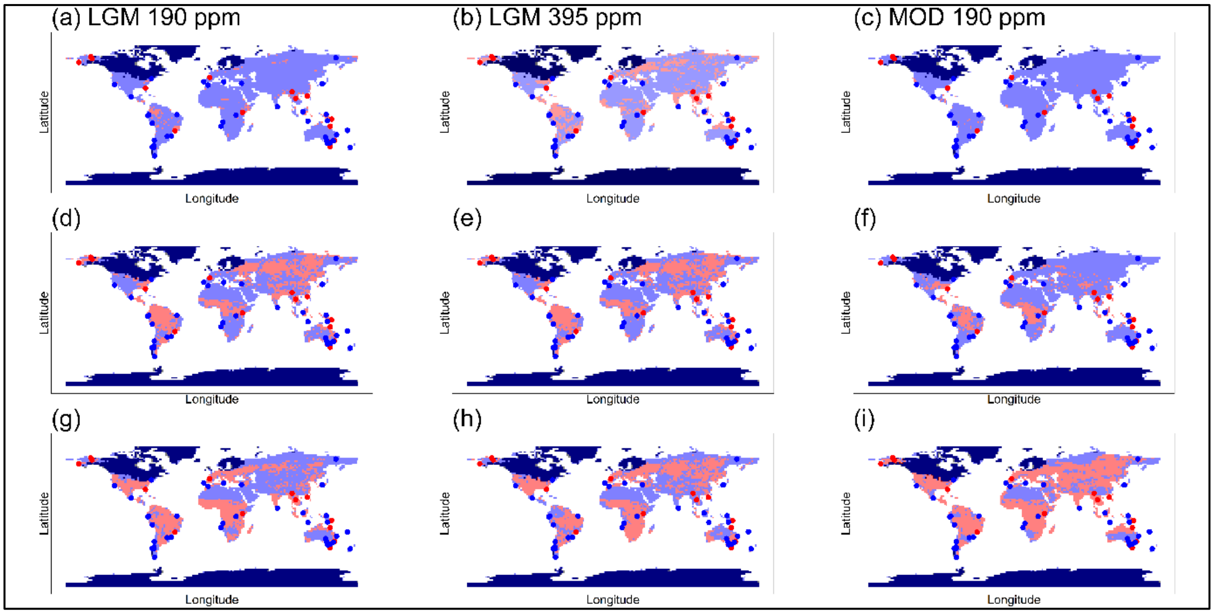

Figure S16. Comparison of anomalies between the experiment outputs from the MPI-ESM1.2 LGM scenario with charcoal records from the Reading Palaeofire Database (RPD) for (a) the relatistic BA LGM experiment (b) the BA LGM climate/MOD CO_2 sensitivity experiment and (c) the BA MOD climate/LGM CO_2 sensitivity experiment (d) the relatistic FS LGM experiment (e) the FS LGM climate/MOD CO_2 sensitivity experiment and (f) the FS MOD, (g) the relatistic FI LGM experiment (h) the FI LGM climate/MOD CO_2 sensitivity experiment and (i) the FI MOD climate/LGM CO_2 sensitivity experiment climate/LGM CO_2 sensitivity experiment. The modeled positive LGM-MOD anomalies are shown in red and LGM-MOD negative anomalies in blue. Dotted red (positive anomaly) and blue (negative anomaly) points show the location of the RPD records for the LGM. The LGM ice sheets are shown in dark blue.

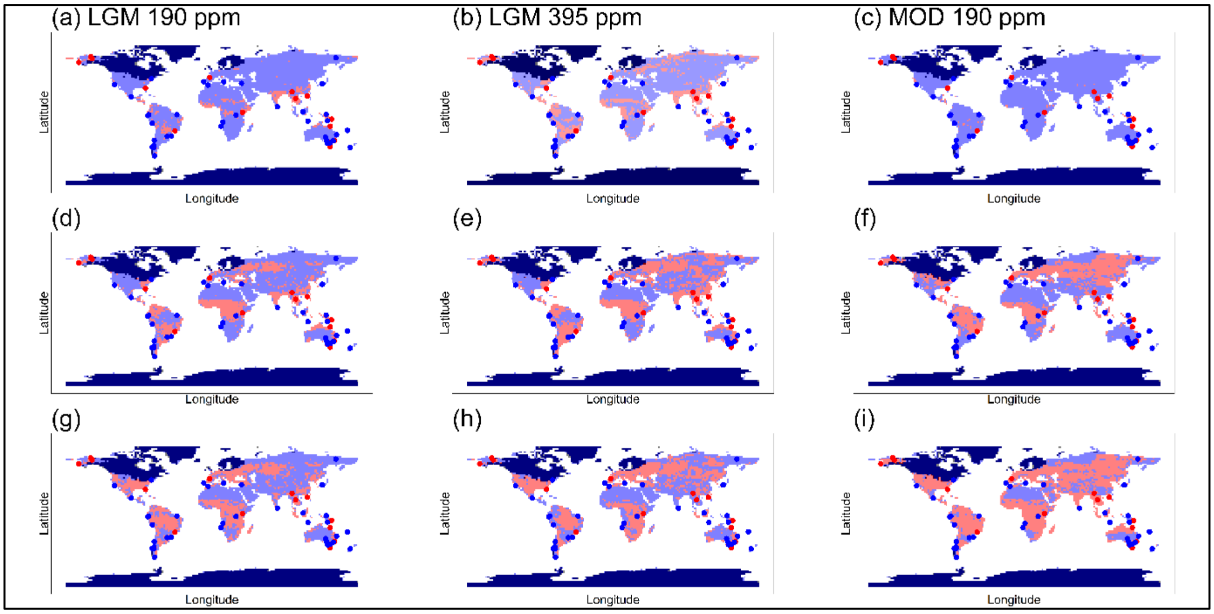

Figure S17. Comparison of anomalies between the experiment outputs from the AWIESM1 LGM scenario with charcoal records from the Reading Palaeofire Database (RPD) for (a) the relatistic BA LGM experiment (b) the BA LGM climate/MOD CO_2 sensitivity experiment and (c) the BA MOD climate/LGM CO_2 sensitivity experiment (d) the relatistic FS LGM experiment (e) the FS LGM climate/MOD CO_2 sensitivity experiment and (f) the FS MOD, (g) the relatistic FI LGM experiment (h) the FI LGM climate/MOD CO_2 sensitivity experiment and (i) the FI MOD climate/LGM CO_2 sensitivity experiment climate/LGM CO_2 sensitivity experiment. The modeled positive LGM-MOD anomalies are shown in red and LGM-MOD negative anomalies in blue. Dotted red (positive anomaly) and blue (negative anomaly) points show the location of the RPD records for the LGM. The LGM ice sheets are shown in dark blue.

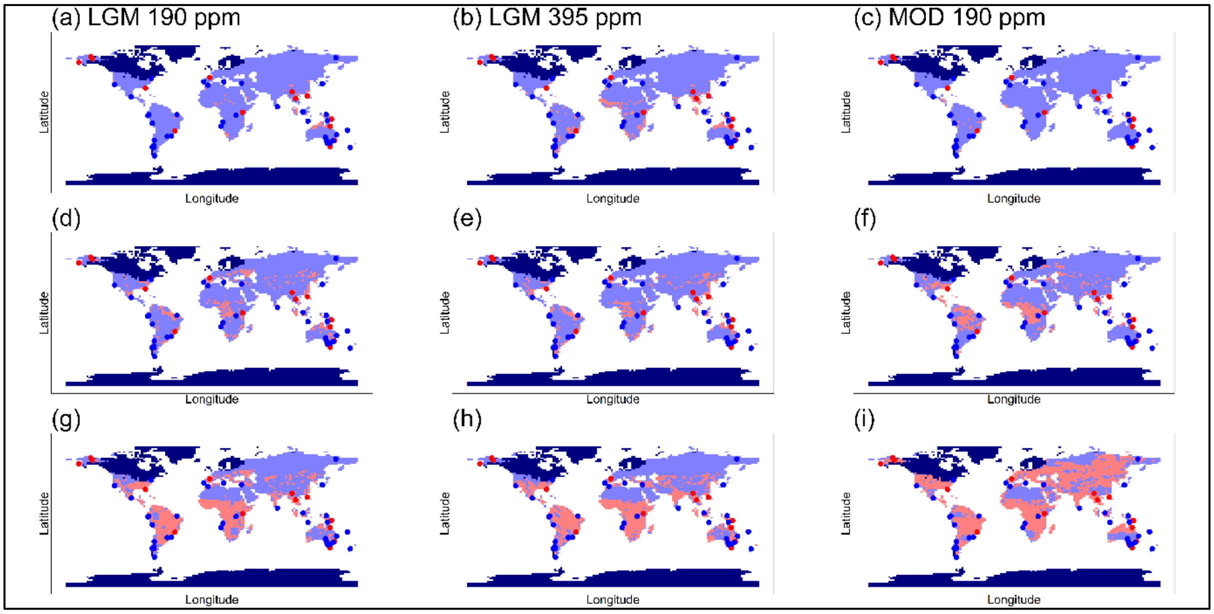

Figure S18. Comparison of anomalies between the experiment outputs from the CESM1.2 LGM scenario with charcoal records from the Reading Palaeofire Database (RPD) for (a) the relatistic BA LGM experiment (b) the BA LGM climate/MOD CO_2 sensitivity experiment and (c) the BA MOD climate/LGM CO_2 sensitivity experiment (d) the relatistic FS LGM experiment (e) the FS LGM climate/MOD CO_2 sensitivity experiment and (f) the FS MOD, (g) the relatistic FI LGM experiment (h) the FI LGM climate/MOD CO_2 sensitivity experiment and (i) the FI MOD climate/LGM CO_2 sensitivity experiment climate/LGM CO_2 sensitivity experiment. The modeled positive LGM-MOD anomalies are shown in red and LGM-MOD negative anomalies in blue. Dotted red (positive anomaly) and blue (negative anomaly) points show the location of the RPD records for the LGM. The LGM ice sheets are shown in dark blue.

Supplementary information for Chapter 4

This section contains supplementary information for Chapter 4. It contains information on (a) the performance of the burnt area model for inter-annual variability, (b) the results from the future realistic experiments for all four of the climate models, (c) the results from the future climate only sensitivity experiments for all four of the climate models, (d) the results from the future CO_2 only sensitivity experiments for all four of the climate models, (e) the results from the future climate and CO_2 only sensitivity experiments for all four of the climate models, and (f) the results from the human activity only sensitivity experiments for all four of the climate models.

BA inter-annual variability performance and trends

We ran the burnt area GLM model for the 10-year period from 2006-2015, with lightning held constant to be consistent with the future scenario experiment. The same roads model was also used for consistency. We set burnt area fractional values lower than 0.0011 to zero and we also excluded burning is regions where the ESA CCI land cover bare soil fraction > 95%. We compared the simulated BA trend with both the observations (van der Werf et al., 2017; Chen et al., 2023) and simulated burnt area fraction from the FireMIP models (CLM: Li et al., 2013, CLASS–CTEM: Melton and Arora, 2016, JULES–INFERNO: Mangeon et al., 2016, JSBACH–SPITFIRE: Lasslop et al., 2014, LPJ–GUESS–SIMFIRE–BLAZE: Knorr et al., 2016, LPJ-GUESS-SPITFIRE: Lehsten et al., 2009, LPJ–GUESS–GlobFIRM: Smith et al., 2014, ORCHIDEE–SPITFIRE: Yue et al., 2014). We did not include the MC2 model, as there were only 3 years overlapping. We used normalized mean error (step 3) to assess performance Kelley et al., 2013s; Hantson et al., 2020)

Table S11. Burnt area correlations and benchmarking scores of modelled burnt area and the global fire models included in the first Fire Modeling Intercomparaison Project (FireMIP) compared to GFED4(s) and GFED5. The normalized mean error (NME) scores for the spatial patterns (Kelley et al., 2013; Hantson et al., 2020) are for the overlapping period (2006-2013). A perfect score is 0, and a score below 1 is better than the mean model. The mean value and the range (in brackets) are given for the FireMIP models.

Fire product and model	***NME score (Spatial)***		***Global correlation***		***Mean annual BA (km²)***
	Dataset		*Dataset*		
	GFED4(s)	GFED5	GFED4(s)	GFED5	
GFED4(s)		0.520		0.883	4,497,908
GFED5	0.520		0.883		7,641,454
Observed mean					6,069,681
Modelled BA	0.628	0.658	0.727	0.673	6,229,255
FireMIP models	0.758 [0.682-0.862]	0.760 [0.686-0.855]	0.464 [0.260-0.606]	0.445 [0.246-0.613]	3,972,677 [3,020,070-4,817,958]

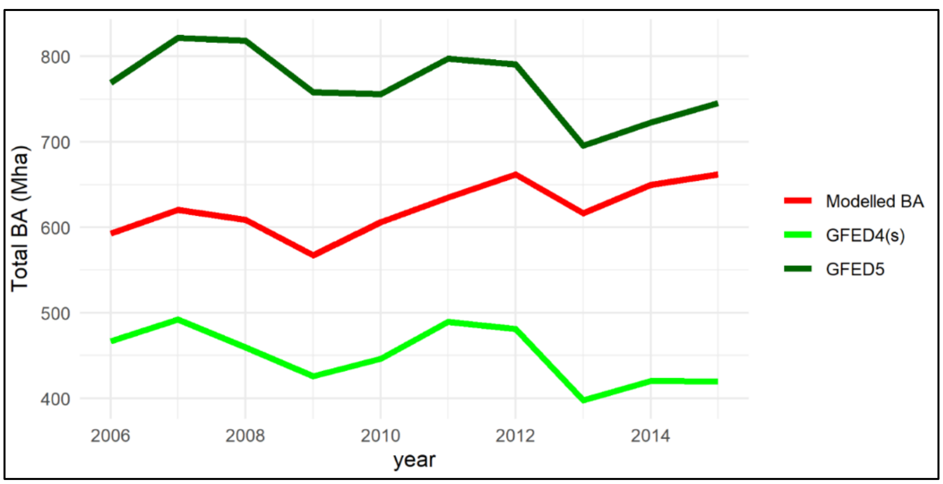

Figure S19. Global 10-year trend in burnt area (BA) from 2006-2015 in Mha from the model (red), GFED4(s) (light green) and GFED5 (dark green).

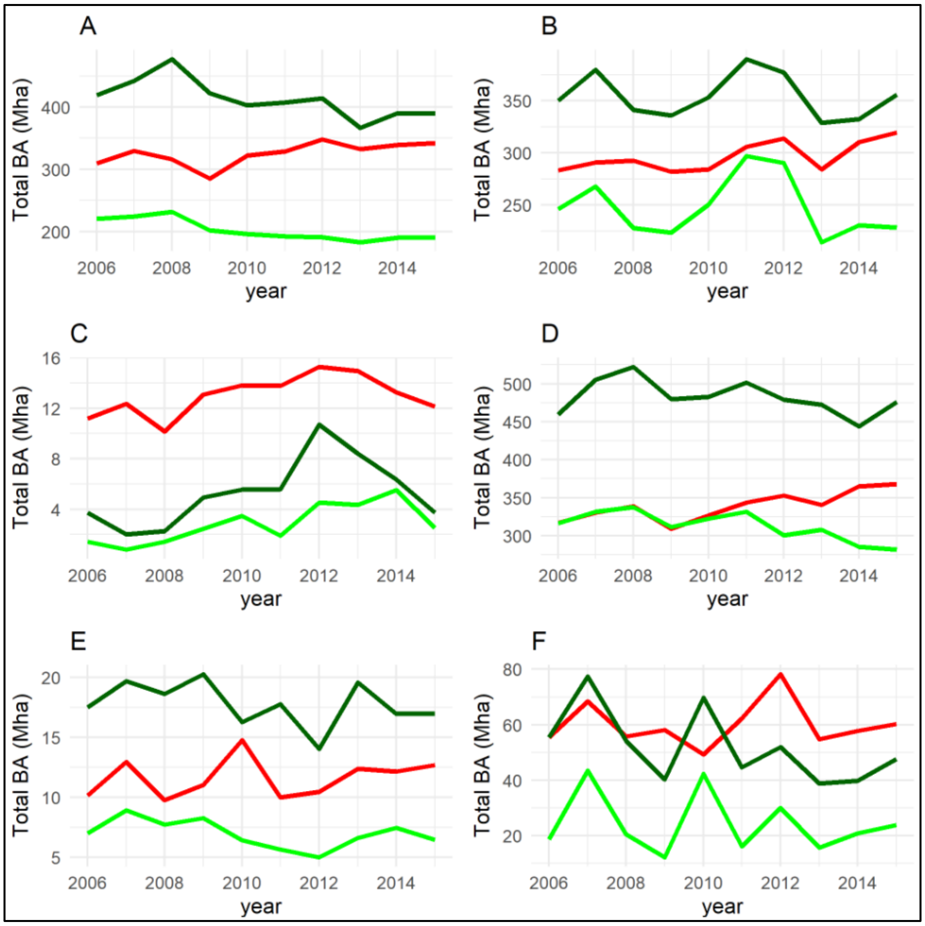

Figure S20. Global 10-year trend in burnt area (BA) for the (A) northern hemisphere, (B) southern hemisphere, (C) above 60°N, (D) Africa, (E) northern hemisphere America and (F) southern hemisphere America from the model (in red), GFED4(s) (in light green) and GFED5 (in dark green)

Realistic experiments

All figures presented below are from the realistic experiments where changes occurred in climate inputs, CO_2 levels (affecting vegetation) and human activity under high (SPP2-RCP2.6) and low (SSP2-RCP6.0) climate change mitigation efforts.

Table S12. Global annual burnt area (BA), mean fire size (FS) and mean fire intensity (FI) values for the realistic experiments.

BA (km^2)	**Modern-day (realistic)**	**High mitigation**	**Percentage change**	**Low mitigation**	**Percentage change**
GFDL-ESM2M	4,059,433	3,159,178	-22.18	6,323,332	55.77
IPSL-CM5A-LR	4,059,433	4,057,701	-0.04	6,620,413	63.09
HadGEM2-ES	4,059,433	3,353,882	-17.38	6,714,088	65.40
MIROC5	4,059,433	3,349,281	-17.49	4,785,615	17.89
FS (km^2)	**Modern-day (realistic)**	**High mitigation**	**Percentage change**	**Low mitigation**	**Percentage change**
GFDL-ESM2M	2.84	3.496252	23.29	3.761441	32.64
IPSL-CM5A-LR	2.84	3.760604	32.61	3.696352	30.34
HadGEM2-ES	2.84	3.853699	35.89	3.392539	19.63
MIROC5	2.84	3.868113	36.40	3.710909	30.86
FI ($W.km^{-1}$)	**Modern-day (realistic)**	**High mitigation**	**Percentage change**	**Low mitigation**	**Percentage change**
GFDL-ESM2M	26.42	27.33	3.42	25.08	-5.09
IPSL-CM5A-LR	26.42	26.98	2.12	24.62	-6.84
HadGEM2-ES	26.42	27.73	4.95	23.04	-12.83
MIROC5	26.42	27.75	5.00	26.11	-1.19

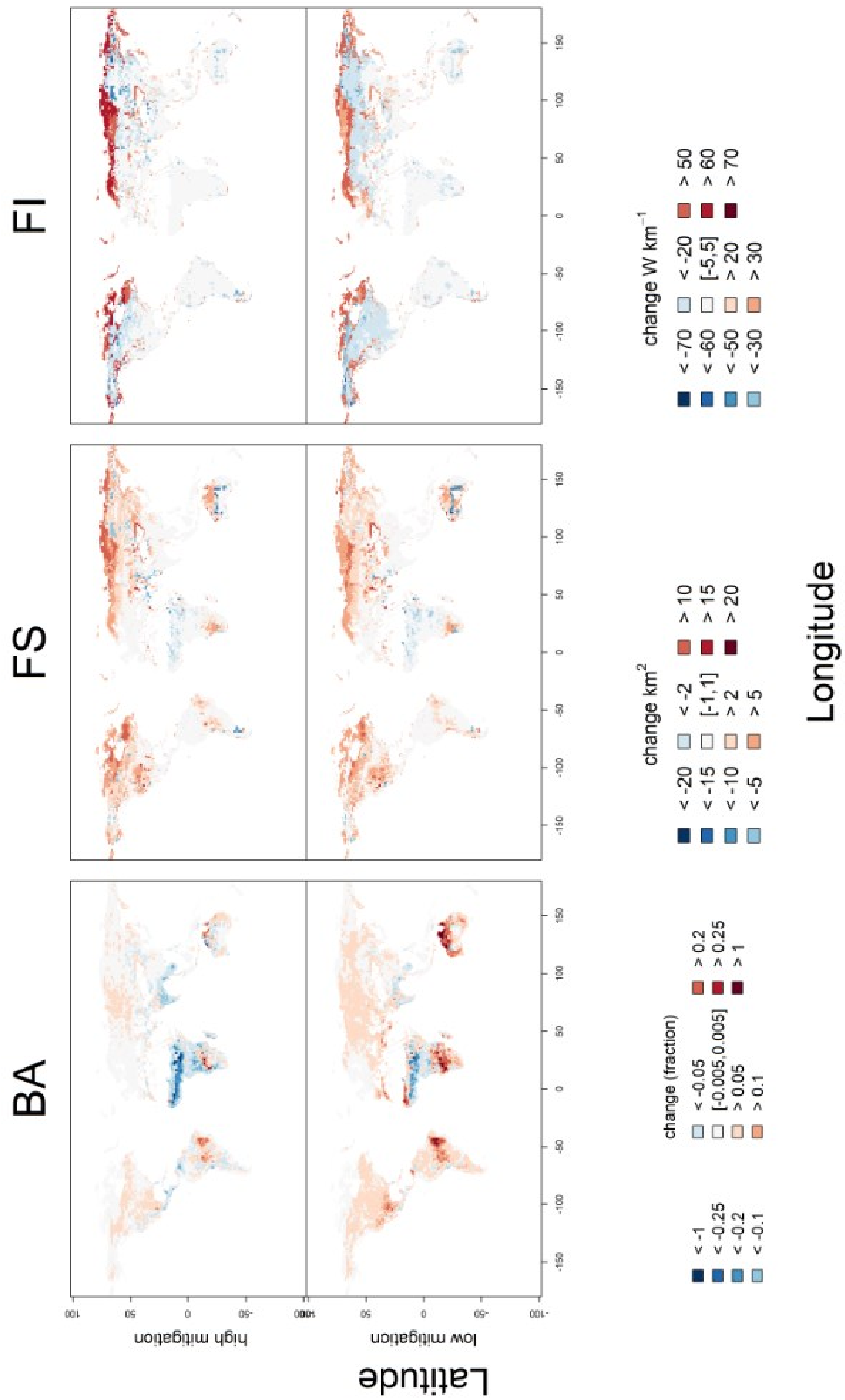

Figure S21. Anomalies for burnt area (BA), fire size (FS) and fire intensity (FI) between the modern-day experiment and the high mitigation experiment (top) and low mitigation experiment (bottom) for the mean of the experiments driven by the outputs of all four climate models in which CO_2 levels are 424ppm and 651ppm respectively and human activity follows a SSP2 trajectory. Red represents an increase in the fire property by the end of the century and blue represents a decrease.

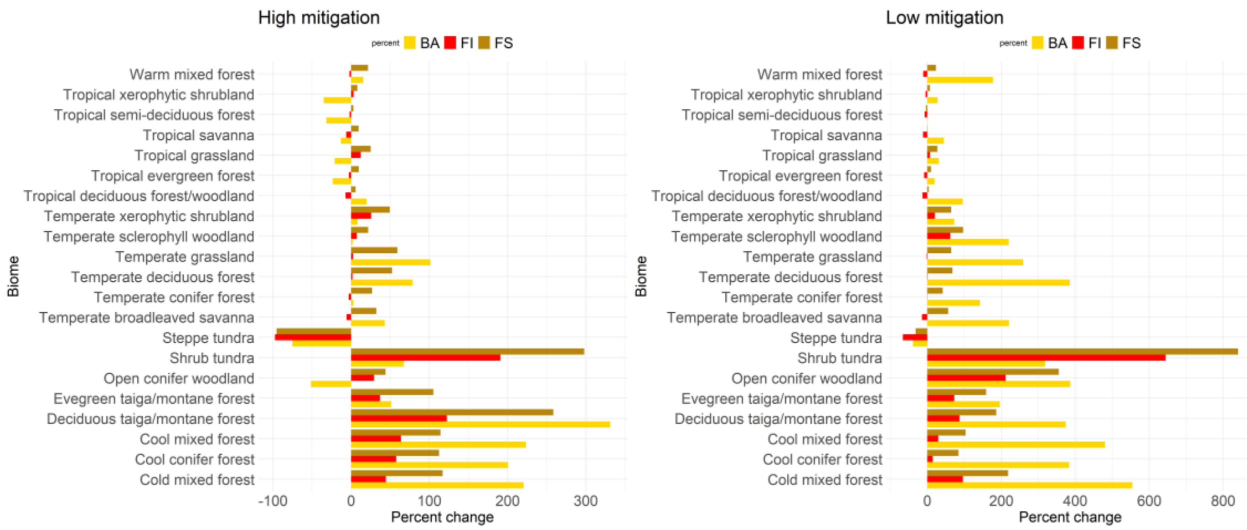

Figure S22. Percentage change for all three fire properties between realistic modern-day conditions and the realistic future experiments broken down by biome type. The mean is across all four of the climate model experiments for each scenario.

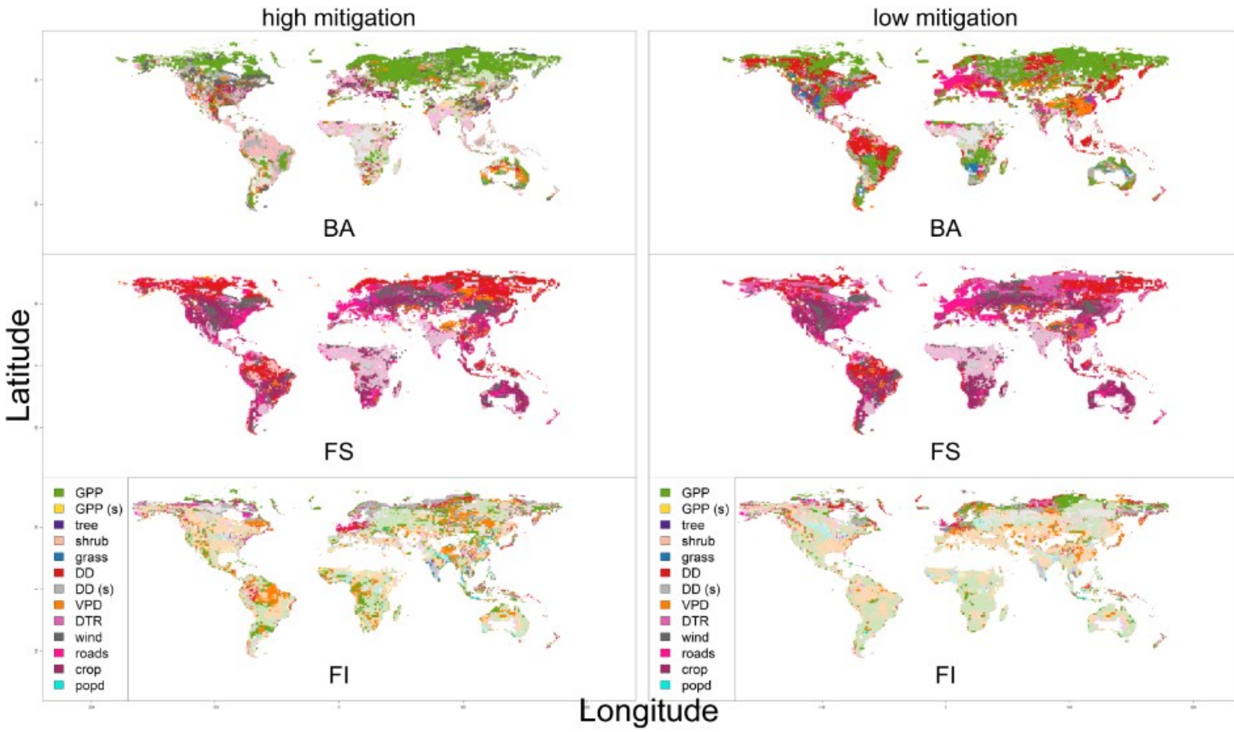

Figure S23. Map showing which GLM model variable was responsible for the most important grid-cell changes between the realistic modern-day experiment and the realistic future high mitigation (left) and low mitigation (right) experiment for the GFDL-ESM2M climate model outputs. Muted colours show that the effect was negative, leading to a decrease in the wildfire property at under future conditions, whilst full colours represent an increase in the wildfire property under future conditions.

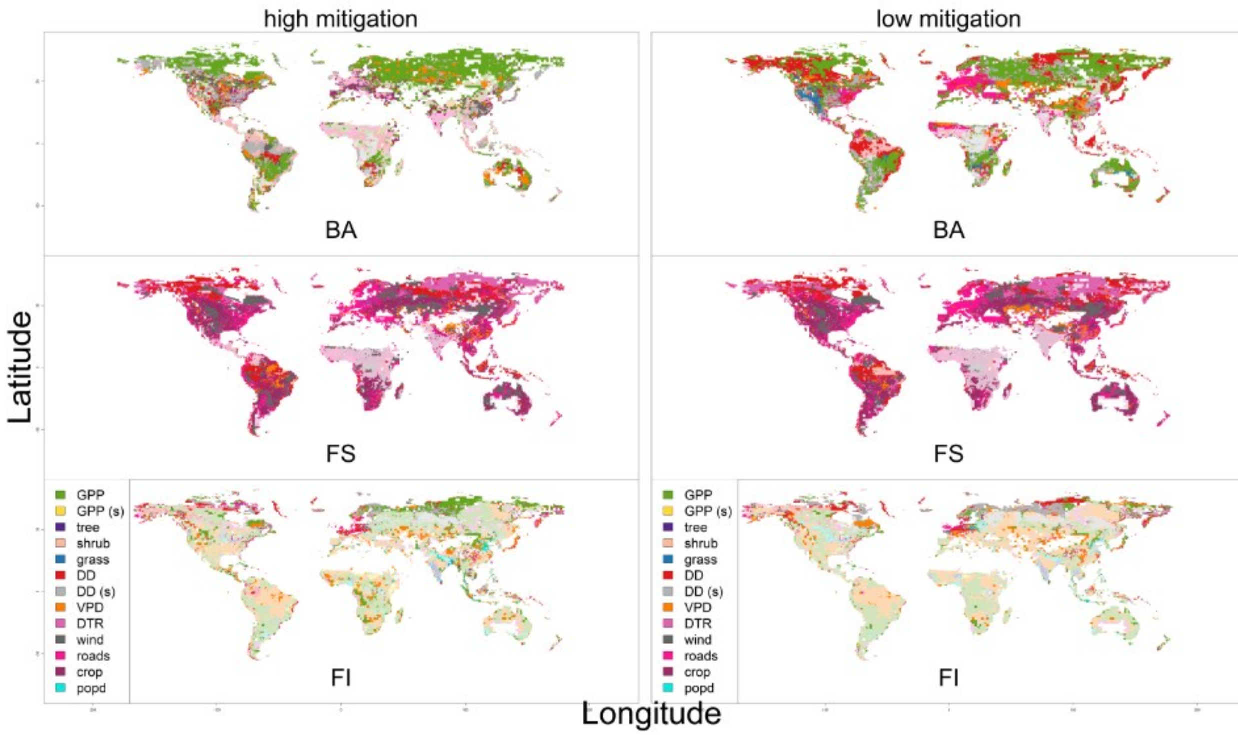

Figure S24. Map showing which GLM model variable was responsible for the most important grid-cell changes between the realistic modern-day experiment and realistic future high mitigation (left) and low mitigation (right) experiments for the IPSL-CM5A-LR climate model outputs. Muted colours show that the effect was negative, leading to a decrease in the wildfire property at under future conditions, whilst full colours represent an increase in the wildfire property under future conditions.

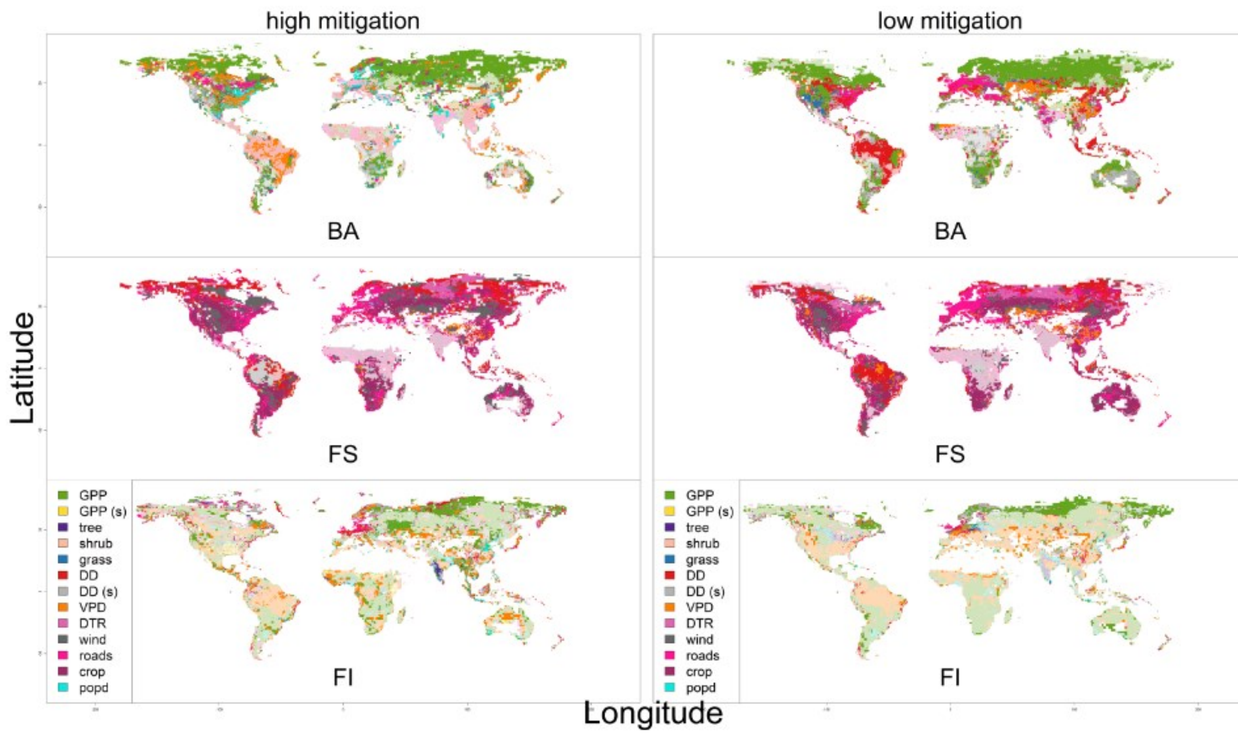

Figure S25. Map showing which GLM model variable was responsible for the most important grid-cell changes between the realistic modern-day experiment realistic future high mitigation (left) and low mitigation (right) experiment for the HadGEM2-ES climate model outputs. Muted colours show that the effect was negative, leading to a decrease in the wildfire property at under future conditions, whilst full colours represent an increase in the wildfire property under future conditions.

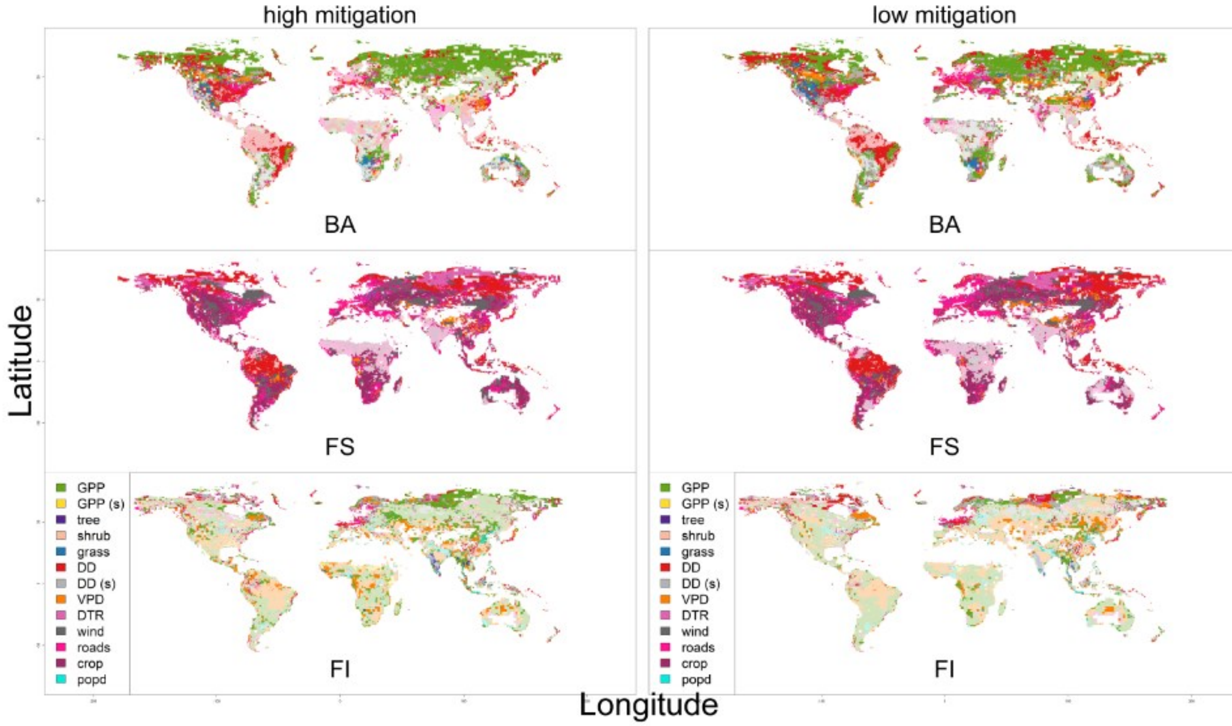

Figure S26. Map showing which GLM model variable was responsible for the most important grid-cell changes between the realistic modern-day experiment realistic future high mitigation (left) and low mitigation (right) experiment for the MIROC5 climate model outputs. Muted colours show that the effect was negative, leading to a decrease in the wildfire property at under future conditions, whilst full colours represent an increase in the wildfire property under future conditions.

Climate only sensitivity experiments

All figures presented below are from the sensitivity experiments where only climate inputs were changed, while CO_2 levels (affecting vegetation) and human activity held constant under modern-day conditions.

Table S13. Global for annual burnt area (BA), mean fire size (FS) and mean fire intensity (FI) values for the climate only experiments.

BA (km^2)	**Modern-day (realistic)**	**High mitigation**	**Percentage change**	**Low mitigation**	**Percentage change**
GFDL-ESM2M	4,059,433	3,493,071	-13.95	4,396,259	8.30
IPSL-CM5A-LR	4,059,433	4,436,700	9.30	4,359,014	7.38
HadGEM2-ES	4,059,433	3,748,743	-7.65	5,102,338	25.69
MIROC5	4,059,433	3,733,911	-8.02	3,360,245	-17.22
FS (km^2)	**Modern-day (realistic)**	**High mitigation**	**Percentage change**	**Low mitigation**	**Percentage change**
GFDL-ESM2M	2.84	3.66	29.04	3.93	38.53
IPSL-CM5A-LR	2.84	3.95	39.19	3.95	39.19
HadGEM2-ES	2.84	4.04	42.61	3.65	28.79
MIROC5	2.84	4.00	43.18	3.95	39.17
FI ($W.km^{-1}$)	**Modern-day (realistic)**	**High mitigation**	**Percentage change**	**Low mitigation**	**Percentage change**
GFDL-ESM2M	26.42	27.41	3.73	26.18	-0.94
IPSL-CM5A-LR	26.42	27.03	2.31	25.98	-1.67
HadGEM2-ES	26.42	27.76	5.06	24.03	-9.06
MIROC5	26.42	27.66	4.67	27.28	3.24

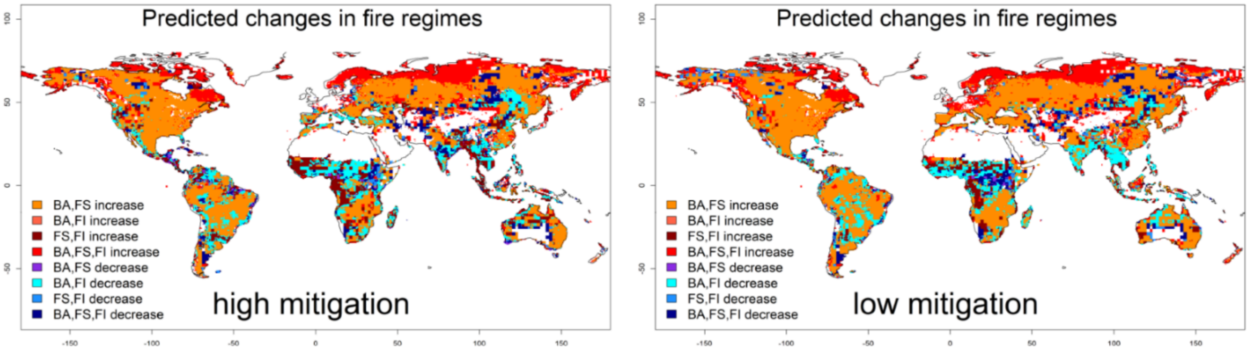

Figure S27. Regions of change in burnt area (BA), fire size (FS) and fire intensity (FI) under the high mitigation scenario (left) and the low mitigation scenario (right) where CO_2 levels and human activity were held constant. Regions where all three properties increase are shown in red, regions where all three properties decrease are shown in dark blue.

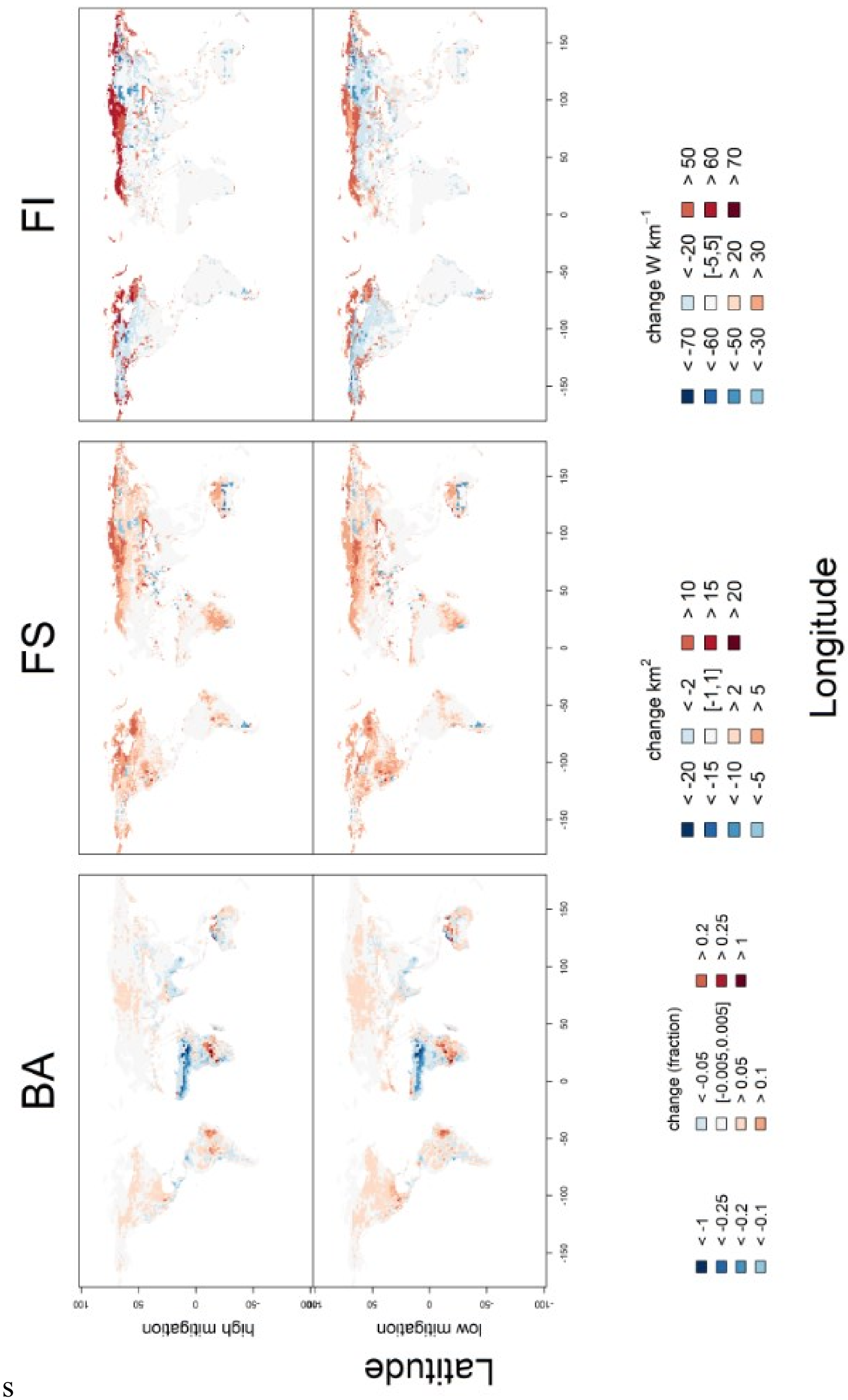

s

Figure S28. Anomalies for burnt area (BA), fire size (FS) and fire intensity (FI) between the modern-day experiment and the high mitigation experiment (top) and low mitigation experiment (bottom) for the mean of the experiments driven by the outputs of all four climate models in which CO_2 levels are held constant at 395ppm and human activity is held constant at the 2010-2015 baseline. Red represents an increase in the fire property by the end of the century and blue represents a decrease.

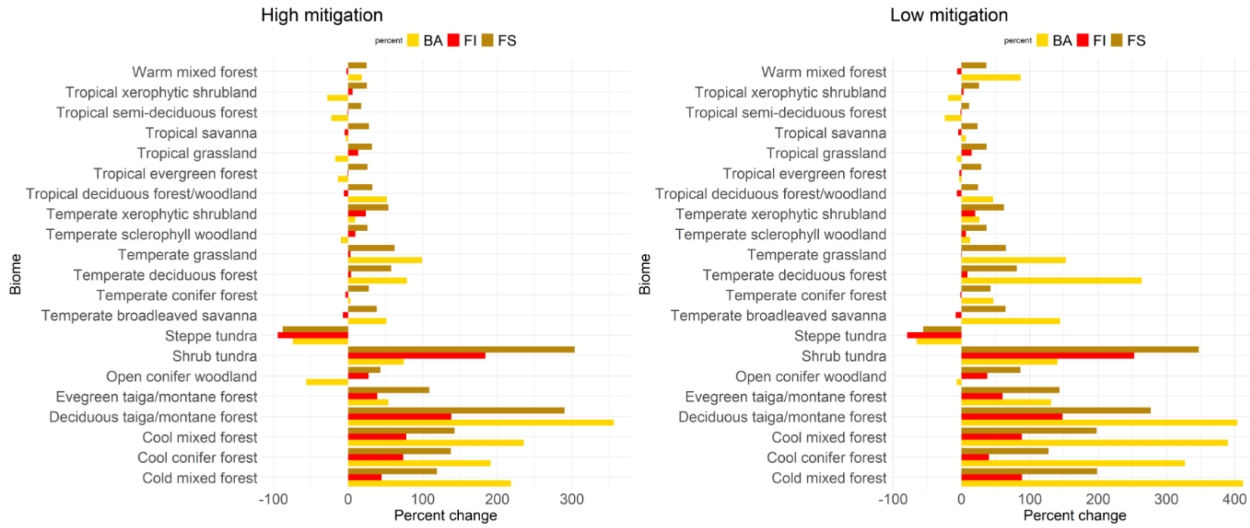

Figure S29. Percentage change for all three fire properties between realistic modern-day conditions and the climate only future experiments broken down by biome type. The mean is taken across all four climate-model experiments for each scenario.

CO_2 only sensitivity experiments

All figures presented below are from the sensitivity experiments where only changes were allowed in CO_2 levels (affecting vegetation; 424ppm under RCP2.6 and 651ppm under RCP6.0) and climate human activity held constant under modern-day conditions.

Table S14. Global annual burnt area (BA), mean fire size (FS) and mean fire intensity (FI) values for the CO_2 only experiments.

BA (km^2)	**Modern-day (realistic)**	**High mitigation**	**Percentage change**	**Low mitigation**	**Percentage change**
	4,059,433	4,466,470	10.03	6,997,835	72.89
FS (km^2)	**Modern-day (realistic)**	**High mitigation**	**Percentage change**	**Low mitigation**	**Percentage change**
	2.84	2.82	-0.66	2.80	-1.38
FI ($W.km^{-1}$)	**Modern-day (realistic)**	**High mitigation**	**Percentage change**	**Low mitigation**	**Percentage change**
	26.42	26.27	-0.58	25.43	-3.76

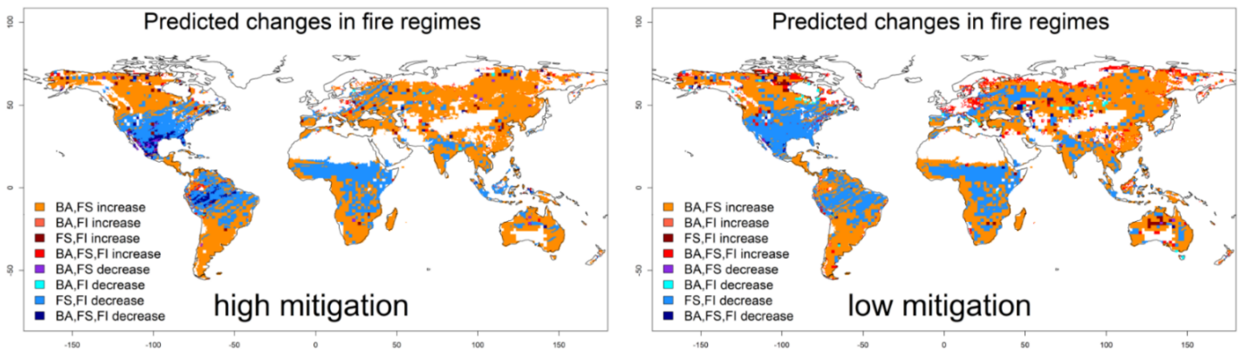

Figure S30. Regions of change in burnt area (BA), fire size (FS) and fire intensity (FI) under the high mitigation scenario (left) and the low mitigation scenario (right) where climate and human activity were held constant. Regions where all three properties increase are shown in red, regions where all three properties decrease are shown in dark blue.

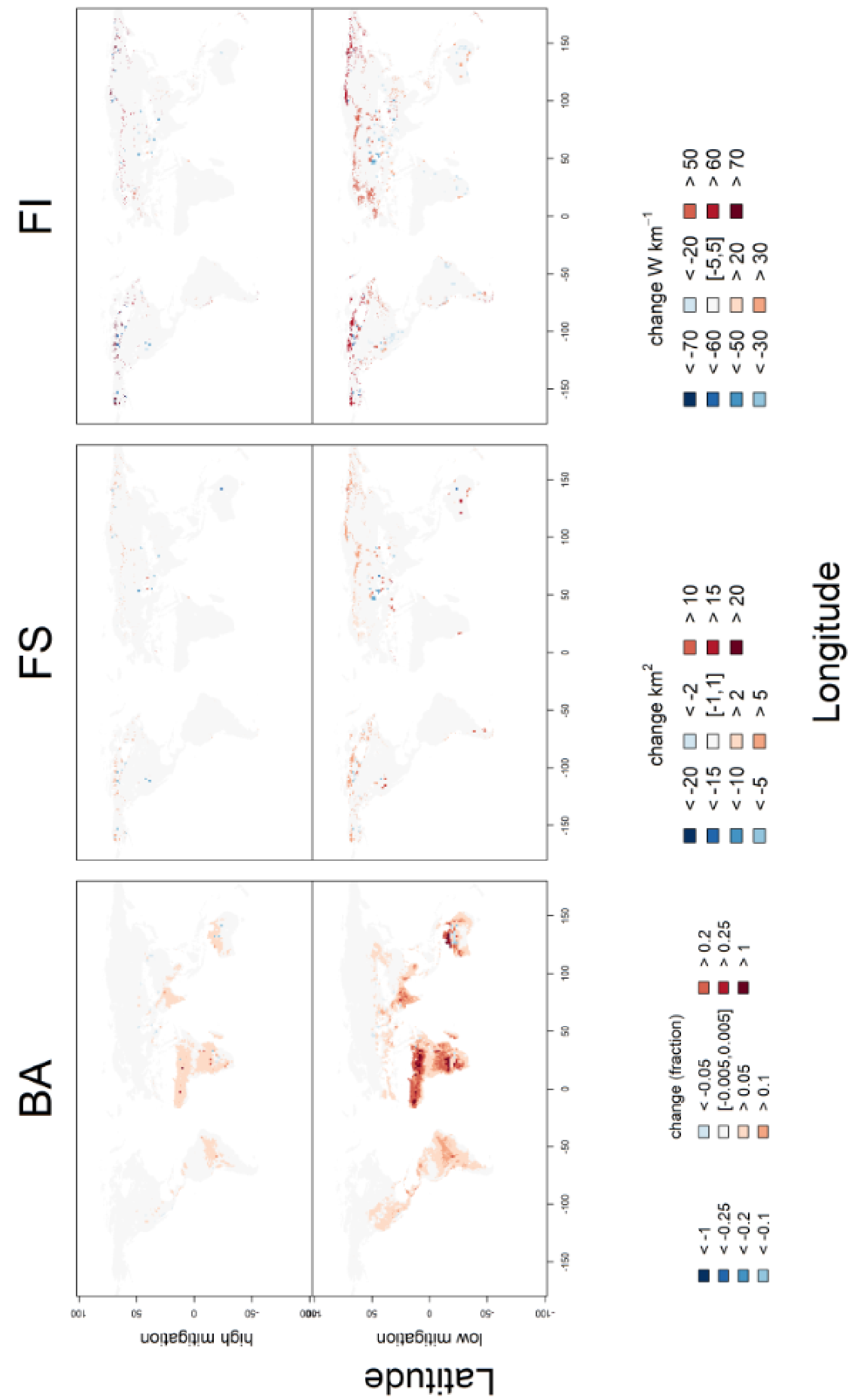

Figure S31. Anomalies for burnt area (BA), fire size (FS) and fire intensity (FI) between the modern-day experiment and the high mitigation experiment (top) and low mitigation experiment (bottom) for the mean of the experiments driven by the outputs of all four climate models in which CO_2 levels are 424ppm and 651ppm respectively and climate human activity are held constant at the 2010-2015 baseline. Red represents an increase in the fire property by the end of the century and blue represents a decrease.

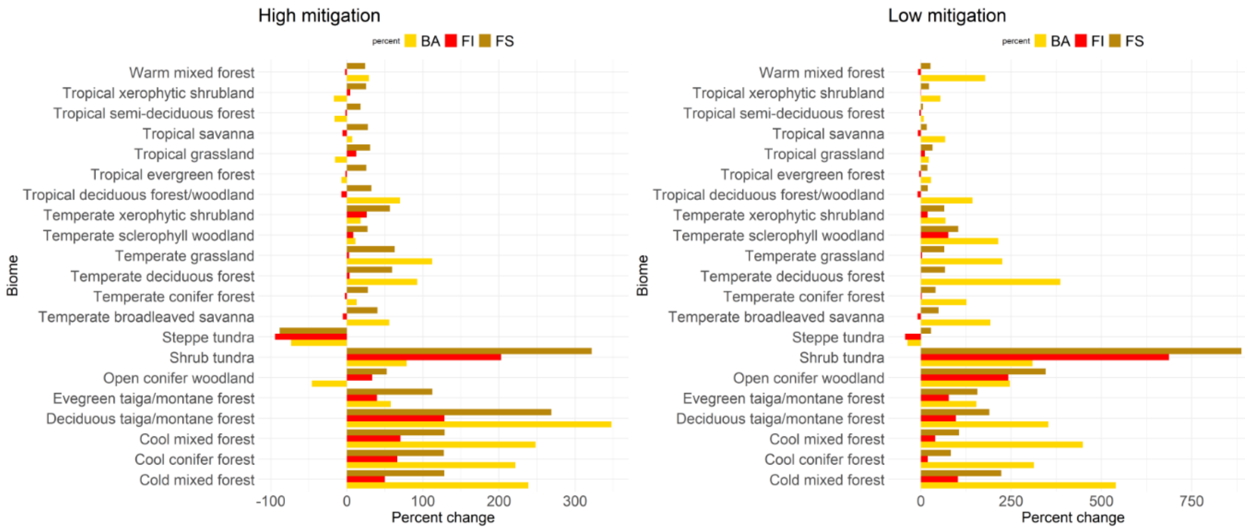

Figure S32. Percentage change for all three fire properties between realistic modern-day conditions and the CO_2 only future experiments broken down by biome type. The mean is taken across all four climate-model experiments for each scenario.

Climate and CO_2 only sensitivity experiments

All figures presented below are from the sensitivity experiments where climate inputs and CO_2 levels were changed, while human activity was held constant under modern-day conditions.

Table S15. Global annual burnt area (BA), mean fire size (FS) and mean fire intensity (FI) values for the climate and CO_2 only experiments.

BA (km^2)	Modern-day (realistic)	High mitigation	Percentage change	Low mitigation	Percentage change
GFDL-ESM2M	4,059,433	3856381	-5.001989	7692990	89.50898
IPSL-CM5A-LR	4,059,433	4876644	20.13116	8063178	98.62818
HadGEM2-ES	4,059,433	4156526	2.391791	8141939	100.5684
MIROC5	4,059,433	4123215	1.571191	5949635	46.56319
FS (km^2)	**Modern-day (realistic)**	**High mitigation**	**Percentage change**	**Low mitigation**	**Percentage change**
GFDL-ESM2M	2.84	3.66	28.94	3.96	39.74
IPSL-CM5A-LR	2.84	3.95	39.16	3.91	37.95
HadGEM2-ES	2.84	4.03	42.35	3.65	28.75
MIROC5	2.84	4.068125	43.45373	3.912421	37.96316
FI ($W.km^{-1}$)	**Modern-day (realistic)**	**High mitigation**	**Percentage change**	**Low mitigation**	**Percentage change**
GFDL-ESM2M	26.42	27.22	3.02	25.01	-5.34
IPSL-CM5A-LR	26.42	26.86	1.64	24.53	-7.17
HadGEM2-ES	26.42	27.62	4.54	22.88	-13.40
MIROC5	26.42	27.61	4.48	25.98	-1.69

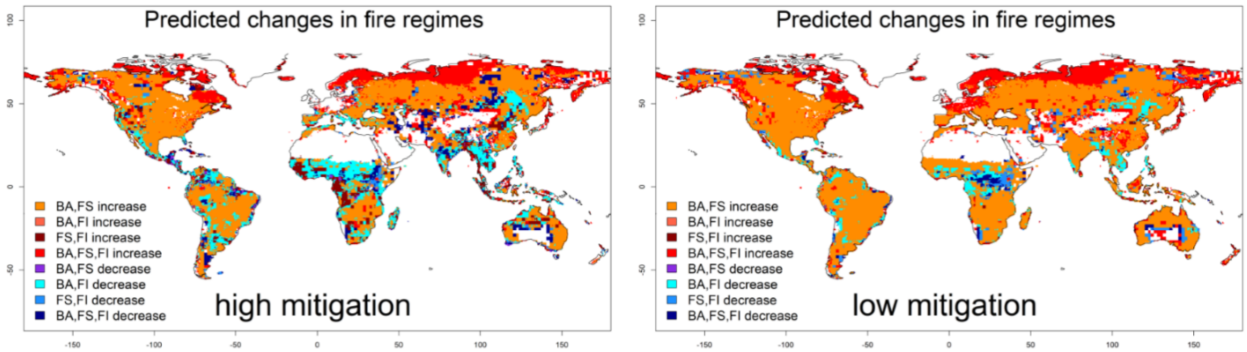

Figure S33. Regions of change in burnt area (BA), fire size (FS) and fire intensity (FI) under the high mitigation scenario (left) and the low mitigation scenario (right) where human activity were held constant. Regions where all three properties increase are shown in red, regions where all three properties decrease are shown in dark blue.

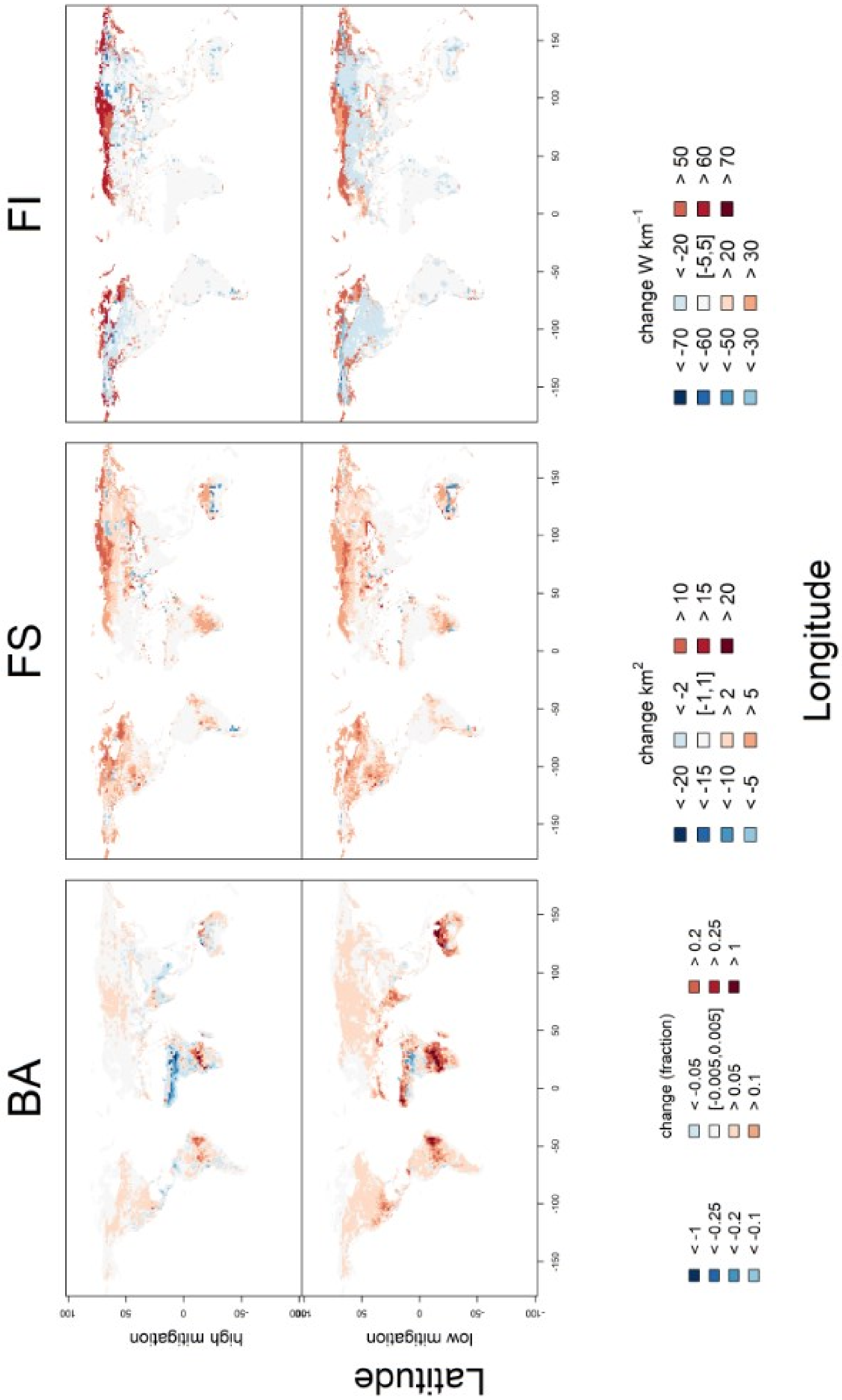

Figure S34. Anomalies for burnt area (BA), fire size (FS) and fire intensity (FI) between the modern-day experiment and the high mitigation experiment (top) and low mitigation experiment (bottom) for the mean of the experiments driven by the outputs of all four climate models in which CO_2 levels are 424ppm and 651ppm respectively and human activity are held constant at the 2010-2015 baseline. Red represents an increase in the fire property by the end of the century and blue represents a decrease.

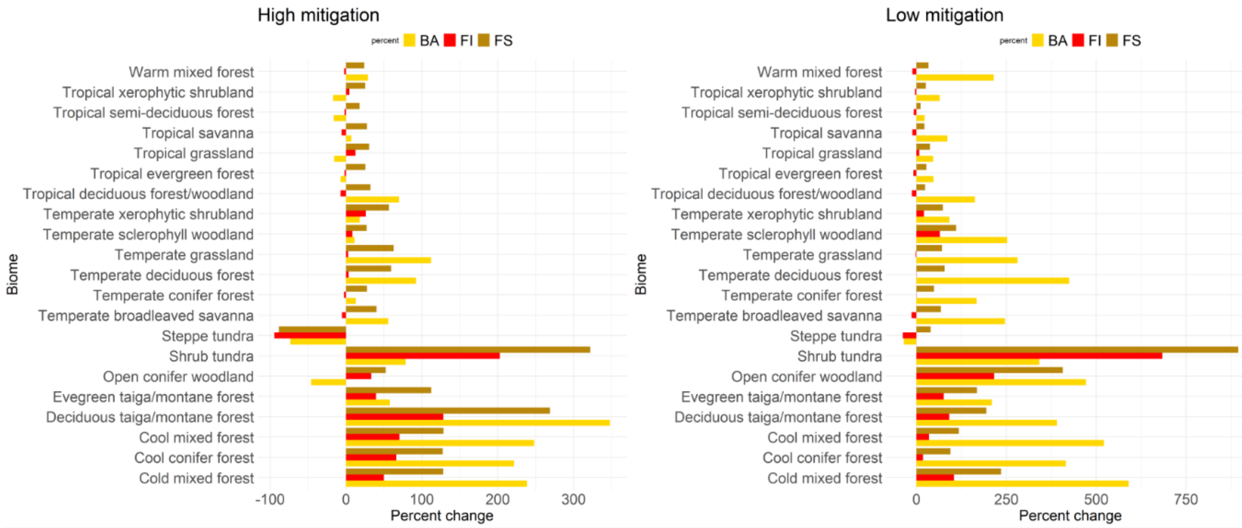

Figure S35. Percentage change for all three fire properties between realistic modern-day conditions and the climate and CO_2 and climate only future experiments broken down by biome type. The mean is taken across all four climate-model experiments for each scenario.

Human activity only sensitivity experiments

All figures presented below are from the sensitivity experiments where human activity (SSP2 scenario) was changed, while climate inputs and CO_2 levels (affecting vegetation) are held constant under modern-day conditions.

Table S15. Global annual burnt area (BA), mean fire size (FS) and mean fire intensity (FI) values for human only experiments.

BA (km^2)	**Modern-day (realistic)**	**High mitigation**	**Percentage change**	**Low mitigation**	**Percentage change**
GFDL-ESM2M	4,059,433	3245393	-20.05306	3219161	-20.69926
IPSL-CM5A-LR	4,059,433	3247321	20.00556	3215363	-20.79282
HadGEM2-ES	4,059,433	3242333	-20.12844	3206252	-21.01724
MIROC5	4,059,433	3246905	-20.01579	3228145	-20.47794
FS (km^2)	**Modern-day (realistic)**	**High mitigation**	**Percentage change**	**Low mitigation**	**Percentage change**
GFDL-ESM2M	2.84	2.67	-5.84	2.62	-7.69
IPSL-CM5A-LR	2.84	2.66	-6.10	2.61	-7.80
HadGEM2-ES	2.84	2.66	-6.02	2.61	-7.80
MIROC5	2.84	2.66	-6.22	2.62	-7.48
FI ($W.km^{-1}$)	**Modern-day (realistic)**	**High mitigation**	**Percentage change**	**Low mitigation**	**Percentage change**
GFDL-ESM2M	26.42	26.55	0.46	26.55	0.46
IPSL-CM5A-LR	26.42	26.55	0.46	26.55	0.47
HadGEM2-ES	26.42	26.55	0.47	26.55	0.47
MIROC5	26.42	26.55	0.46	26.55	0.46

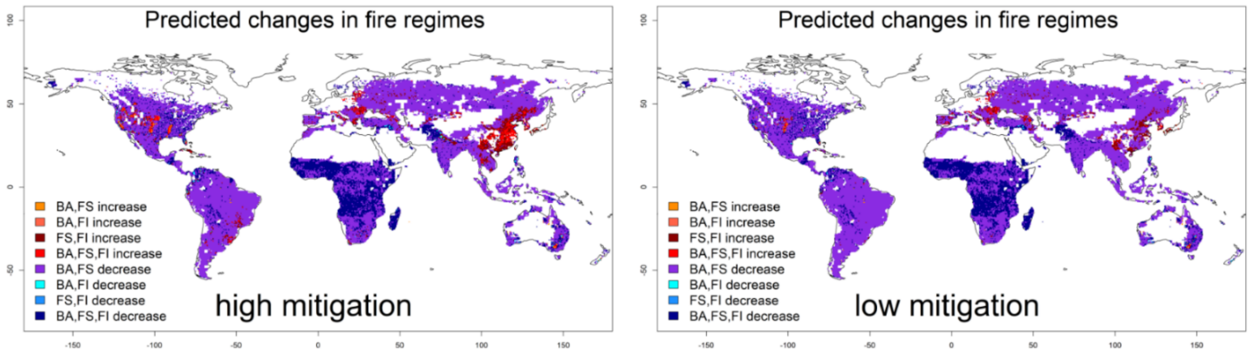

Figure S36. Regions of change in burnt area (BA), fire size (FS) and fire intensity (FI) under the high mitigation scenario (left) and the low mitigation scenario (right) where climate and CO_2 were held constant. Regions where all three properties increase are shown in red, regions where all three properties decrease are shown in dark blue.

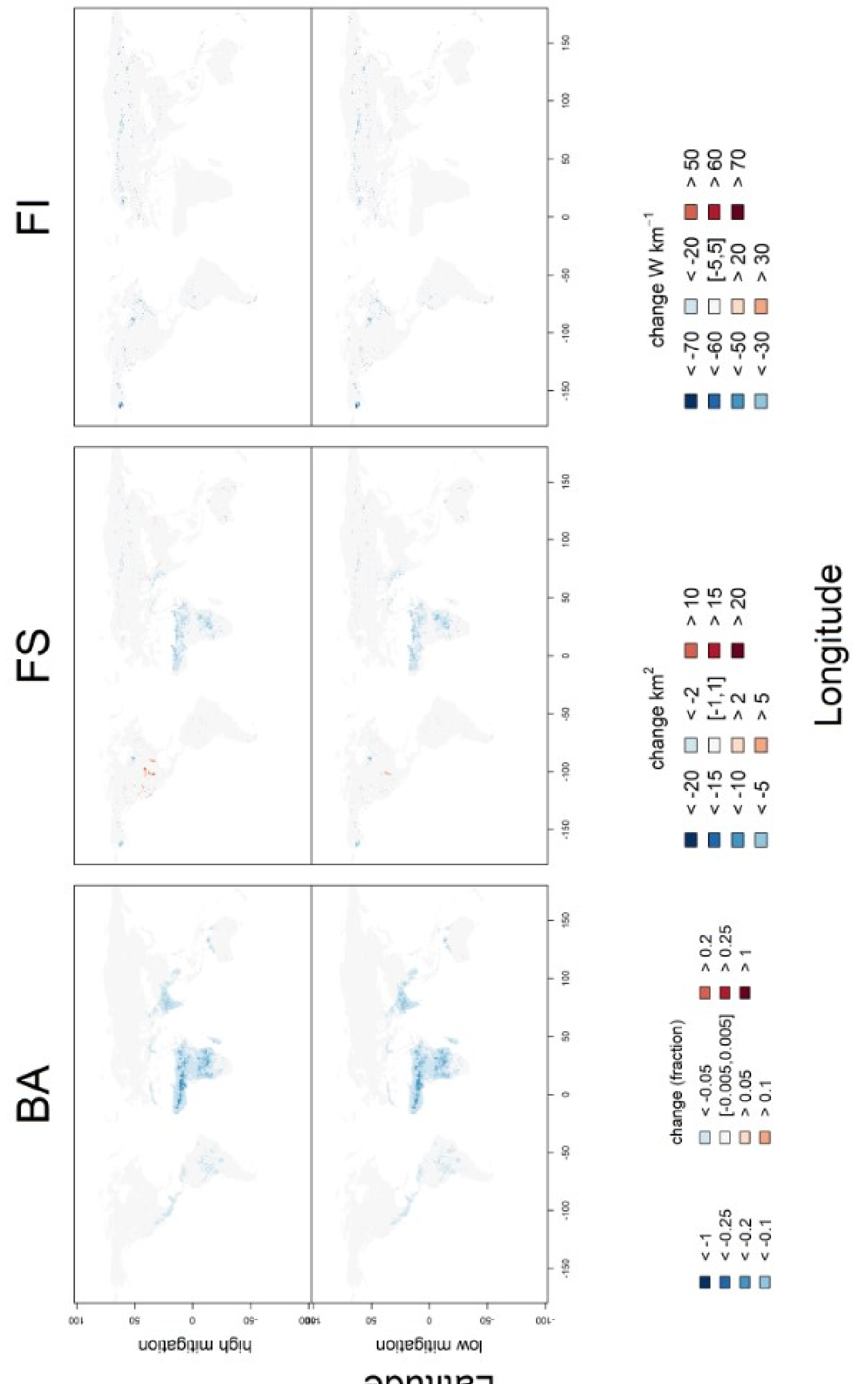

Figure S37. Anomalies for burnt area (BA), fire size (FS) and fire intensity (FI) between the modern-day experiment and the high mitigation experiment (top) and low mitigation experiment (bottom) for the mean of the experiments driven by the outputs of all four climate models in which only human activity changes (SSP2 scenario) and in which climate and CO_2 levels are held constant at the 2010-2015 baseline. Red represents an increase in the fire property by the end of the century and blue represents a decrease.

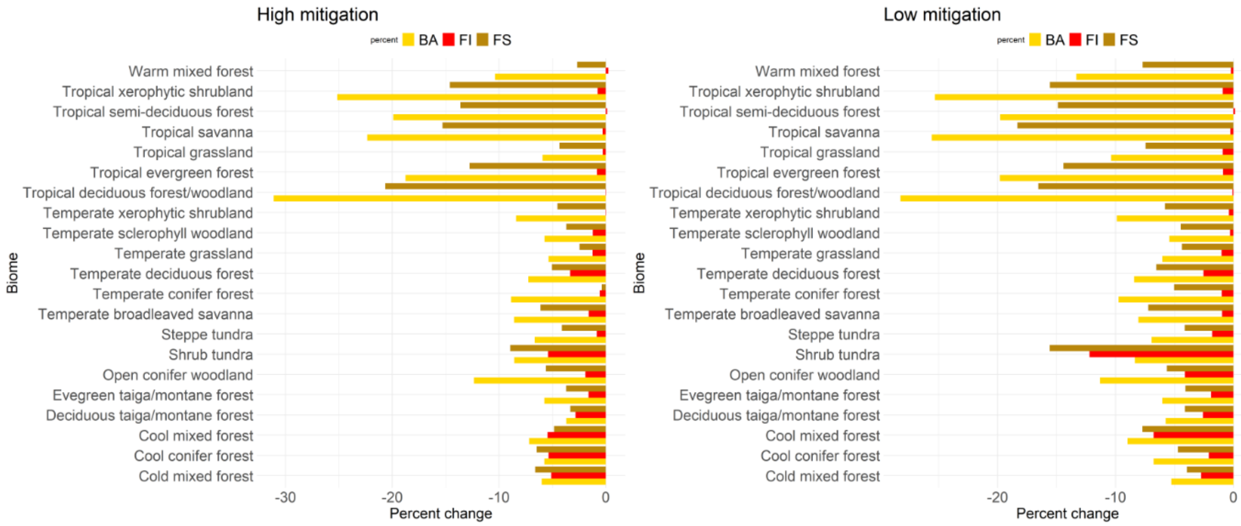

Figure S38. Percentage change for all three fire properties between realistic modern-day conditions and the human activity only future experiments broken down by biome type. The mean is taken across all four climate-model experiments for each scenario.

Sausset-les-Pins, France, summer 2023